THE UNIVERSITY
of ADELAIDE

Pharmacological Modulation of Inflammation, Bone Loss and Pain in a Murine Model
of Inflammatory Arthritis

A thesis submitted in fulfilment for degree of

DOCTOR OF PHILOSOPHY

In

The Discipline of Anatomy and Pathology

Adelaide Medical School

The University of Adelaide

By

Bonnie Williams

March 2019

TABLE OF CONTENTS

THESIS ABSTRACT

Rheumatoid arthritis (RA) is a chronic autoimmune condition, affecting approximately 1% of the population. RA is characterised by a chronic inflammatory response resulting in destruction of soft and hard tissues within the synovial joints. Disease progression in RA is complex, with multiple signalling pathways identified as crucial to T-cell mediated inflammation and increased osteoclastogenesis in the progression of joint destruction. Cell-adhesion molecules and alterations in apoptotic and autophagic pathways in cells located in the synovial joints have recently emerged as key components of the progression of inflammation and bone destruction in RA. Despite the growing knowledge of these mechanisms, control of bone destruction is still challenging and the prognosis of joint pain is often poor despite optimal control of inflammation. For this reason, it is imperative to utilise appropriate cell culture and *in vivo* models to identify key signalling pathways and develop targeted therapeutics that may inhibit inflammation, bone destruction and pain concomitantly upon diagnosis or prior to the onset of visible symptoms. The aim of this research was to use *in vitro* human osteoclast assays in conjunction with a modified collagen-antibody induced arthritis (CAIA) murine model of inflammatory arthritis to determine the effects of emerging novel compounds on inflammation, bone loss and pain-like behaviour. These studies also explored the pathology and progression of pain in a mild and moderate form of the CAIA model whilst extending micro-computed tomography analysis to include assessment of local inflammation and bone volume in the hind paws. The results of these studies support that novel compounds targeting cell adhesion molecules and NF-κB intracellular signalling have the potential to treat inflammatory induced bone loss. The findings presented also highlight the complex mechanisms associated with progression of joint destruction and pain-like behaviour in inflammatory arthritis. Further studies are necessary to elucidate the specific roles of each novel compound and further test the effectiveness of these compounds as potential therapies for RA.

DECLARATION

I certify that this work contains no material which has been accepted for the award of any other degree or diploma in my name, in any university or other tertiary institution and, to the best of my knowledge and belief, contains no material previously published or written by another person, except where due reference has been made in the text. In addition, I certify that no part of this work will, in the future, be used in a submission in my name, for any other degree or diploma in any university or other tertiary institution without the prior approval of the University of Adelaide and where applicable, any partner institution responsible for the joint-award of this degree.

I acknowledge that copyright of published works contained within this thesis resides with the copyright holder(s) of those works.

I also give permission for the digital version of my thesis to be made available on the web, via the University's digital research repository, the Library Search and also through web search engines, unless permission has been granted by the University to restrict access for a period of time.

Bonnie Williams

ACKNOWLEDGMENTS

First and foremost, I wish to thank my primary PhD supervisor Associate Professor Tania Crotti, along with Dr Kencana Dharmapatni and Dr Egon Perilli for being my co-supervisors. Your ideas, guidance and encouragement have been invaluable throughout my candidature. Thank you for your constant support and the opportunities you have provided me to grow as a researcher.

I would like to express my sincere gratitude to Helen Tsangari who was instrumental in conducting the animal models and ongoing tissue analysis for each study. Thank you for your patience in the lab, continuous support and friendship.

I also wish to thank Kent Algate for his ongoing friendship and guidance throughout my candidature, and the other members of the Bone and Joint Research Laboratory.

I also extend my thanks to the staff of Adelaide Microscopy, the University of Adelaide Laboratory Animal Services and the University of Adelaide Histology Services for their help and expertise with the animal models, imaging, tissue processing and analysis.

I acknowledge the support of my PhD through an Australian Government Research Training Program Scholarship and Cedric Stanton Hicks Supplementary Scholarship. I also acknowledge funding from Arthritis Australia for the projects conducted throughout my candidature within the Bone and Joint Research Laboratory.

To all my family and friends, without whom all my achievements to date would not have been possible, thank you for your continuous patience, encouragement and support over the past 4 years, this would not have been possible without you all.

TABLE OF ABBREVIATIONS

28-joint disease activity score	DAS28	Interleukin	IL
Adjuvant induced arthritis	AIA	Macrophage-colony stimulating factor	M-CSF
Alpha-minimum essential medium	α-MEM	Magnetic resonance imaging	MRI
Antigen induced arthritis	AIA	Micro-computed tomography	Micro-CT
Apoptosis inducing factor	AIF	Matrix metalloproteinase	MMP
Autophagy related genes	Atgs	Non-steroidal anti-inflammatory drugs	NSAIDs
Avidin-Biotin complex	ABC	Nuclear factor kappa B	NF-κB
Baculovirus inhibitor of apoptotic protein repeats 1-3	BIR1-3	Nuclear factor kappa B essential modulator	NEMO
Bone morphogenetic protein	BMP	Nuclear factor kappa B inducing kinase	NIK
Bone volume	BV	Nuclear factor of activated T cell cytoplasmic 1	NFATc1
Cadherin-11	CDH11	Nuclear factor of activated T cells	NFAT
Calcitonin receptor	CTR	Osteoclast-associated immunoglobulin-like receptor	OSCAR
Carboxy-terminal collagen crosslinks	CTX	Parthenolide	PAR
Caspase activated DNase	CAD	Paw volume	PV
C-jun N-terminal kinases	JNK	Peripheral blood mononuclear cells	PBMC
Collagen antibody induced arthritis	CAIA	Phosphate buffered saline	PBS
Collagen induced arthritis	CIA	Phosphatidylethanolamine	PE
Complementary DNA	cDNA	Phosphoinositide 3-kinase/protein kinase B	PI-3 kinase/Akt
Conventional radiography	CR	Quantitative real time polymerase chain reaction	qRT-PCR
CT Analyser	CTAn	Receptor activator of NF-κB	RANK
Cytochrome c	Cyt c	Receptor activator of NF-κB ligand	RANKL
Deoxyribonucleic acid	DNA	Recombinant human	rh
Dimethyl sulfoxide	DMSO	Rheumatoid arthritis	RA
Disease modifying anti-rheumatic drugs	DMARDs	Scanning electron microscopy	SEM
E.coli lipopolysaccharide	LPS	Second mitochondrial activator of caspases	SMAC
Enzyme linked immunosorbent assay	ELISA	Standard error of mean	SEM
Ethylene diamineteraacetic acid	EDTA	Tartrate resistant acid phosphatase	TRAP
European League against Rheumatism	EULAR	Terminal deoxynucleotidyl transferase nick-end labelling	TUNEL
Fas associated death domain	FADD	Three dimensional	3D
Fas ligand	Fas-L	Tissue volume	TV
Fibroblast growth factor	FGF	Transmission electron microscopy	TEM
Fibroblast growth factor receptor	FGFR	Tumour necrosis factor receptor	TNFR
Fibroblast-like synoviocytes	FLS	Tumour necrosis factor receptor associated factors	TRAF
FLICE-like inhibitory protein	FLIP	Tumour necrosis factor alpha	TNF-α
Human acid ribosomal protein	hARP	Tumour necrosis factor-receptor type-I associated death domain protein	TRADD
Haematoxylin and eosin	HE	Tumour necrosis factor-related apoptosis inducing ligand	TRAIL
Hydroxychloroquine	HCQ	Volume of interest	VOI
Inhibitor of kappa B	IκB	Wingless-type MMTV integration site	Wnt
Inhibitor of kappa B kinase complex	IKK	X linked inhibitory apoptosis protein	XIAP
Inhibitory apoptotic proteins	IAP		

PUBLICATIONS ARISING FROM THIS THESIS

<u>**B. Williams,**</u> A. Dharmapatni, T.N. Crotti (2018). Intracellular apoptotic pathways: A potential target for reducing joint damage in rheumatoid arthritis. *Inflammation Research.* 67(3):219-231.

PDF of manuscript in press can be found in Appendix II.

ADDITIONAL PUBLICATIONS ARISING FROM OUTSIDE THIS THESIS

<u>**B. Williams,**</u> E. Tsangari, R. Stansborough, V. Marino, M. Cantley, A. Dharmapatni, R. Gibson, E. Perilli, T.N. Crotti (2017). Mixed effects of caffeic acid phenethyl ester (CAPE) on joint inflammation, bone loss and gastrointestinal inflammation in a murine model of collagen antibody-induced arthritis. *Inflammopharmacology.* 25(1):55-68.

PDF of manuscript in press can be found in Appendix III.

CHAPTER 1: POTENTIAL THERAPEUTIC TARGETS FOR REDUCING JOINT DAMAGE IN RHEUMATOID ARTHRITIS

B. Williams, A. Dharmapatni, T.N. Crotti

Chapter 1 is an introductory chapter, setting the premise of this thesis. It incorporates a published review paper: Intracellular apoptotic pathways: a potential target for reducing joint damage in rheumatoid arthritis. **B. Williams**, A. Dharmapatni, T.N. Crotti. Inflammation Research 2018; 67:219-231.

1.1. Abstract

Rheumatoid arthritis (RA) is a chronic autoimmune inflammatory disease that results in significant bone erosion. Progressive joint destruction is a hallmark feature of RA and ultimately leads to severe pain, even when disease progression is maintained through disease-modifying anti-rheumatic drugs. The chronic inflammatory response involving pro-inflammatory cytokines, cell adhesion molecules and intracellular signalling pathways significantly influence the physiological bone remodelling processes within synovial joints of RA patients. In this chapter, the process of RA disease progression will be discussed in conjunction with the current understanding of the role of osteoclasts in inflammatory induced bone loss. Furthermore, murine models are extensively used to elucidate the pathogenesis of RA, however, limited studies evaluate the effect of disease progression on pain-like behaviour in preclinical animal models. Evidence published to date recognises the immense therapeutic potential of modulating cell proliferation or death, particularly apoptosis, in the synovial joints of RA patients. However, the aim of most pharmacological therapies in RA is to resolve inflammation, thus control of bone destruction is still a challenging problem and pain-like behaviour persists. Nonetheless, it is evident that novel therapeutics that manage the chronic inflammatory response, in addition to the altered bone remodelling process and progression of pain-like behaviour is needed to improve RA disease outcomes.

1.2. Statement of Authorship

Statement of Authorship

Title of Paper	Intracellular apoptotic pathways: a potential target for reducing joint damage in rheumatoid arthritis.
Publication Status	☑ Published ☐ Accepted for Publication ☐ Submitted for Publication ☐ Unpublished and Unsubmitted work written in manuscript style
Publication Details	Williams, B., Dharmapatni, A., Crotti, T.N. (2018). Intracellular apoptotic pathways: a potential target for reducing joint damage in rheumatoid arthritis. Inflammation Research; 67:219-231.

Principal Author

Name of Principal Author (Candidate)	Bonnie Williams
Contribution to the Paper	First author and main contributor; Concept design, investigation of literature, formulation of primary draft, in addition to reviewing and incorporating co-author comments and suggestions.
Overall percentage (%)	90
Certification:	This paper reports on original research I conducted during the period of my Higher Degree by Research candidature and is not subject to any obligations or contractual agreements with a third party that would constrain its inclusion in this thesis. I am the primary author of this paper.
Signature	Date 22 / 2 / 19

Co-Author Contributions

By signing the Statement of Authorship, each author certifies that:

    i.   the candidate's stated contribution to the publication is accurate (as detailed above);

    ii.   permission is granted for the candidate in include the publication in the thesis; and

    iii.   the sum of all co-author contributions is equal to 100% less the candidate's stated contribution.

Name of Co-Author	Kencana Dharmapatni
Contribution to the Paper	Conceptualisation, supervision and manuscript review.
Signature	Date 22/2/2019

Name of Co-Author	Tania Crotti
Contribution to the Paper	Conceptualisation, supervision and manuscript review.
Signature	Date 22\2\19

1.3. Introduction

Rheumatoid arthritis (RA) is a common, chronic autoimmune condition that demonstrates an exuberant chronic inflammatory reaction resulting in destruction of both soft and hard tissues within the synovial joints (1, 2). Specifically the metacarpo-phalangeal, proximal interphalangeal, mid-carpal, radiocarpal, intertarsal and metatarso-phalangeal joints are affected, leading to chronic pain, progressive functional disability and greater morbidity (3).

Globally, the prevalence of RA is estimated to be 0.24%, with prevalence being 2 times higher in females than males (4). Interestingly, data on the prevalence and incidence of RA display high variability among different geographic areas, possibly due to genetic or epigenetic conditions, as well as environmental factors (5-9). Despite this, many population-based studies have reported a prevalence rate of RA closer to 1% (5-9). Within Australia, RA is the second most common form of arthritis (5), affecting almost 2% of the national population and comprising 10.8% of the total arthritis population in 2015 (5). The prevalence of RA is expected to increase substantially over the coming decades, with the number of people affected in Australia projected to increase from 422, 309 in 2015 to 579, 915 in 2030 (5).

The aetiology of RA still remains unknown, however, activation of the immune system is fundamental to the pathological changes within the synovial joints and the development of characteristic hallmark features, including synovial hyperplasia, formation of invasive pannus tissue and progressive joint destruction (10). Activation of the immune response leads to the generation of autoantibodies, such as rheumatoid factor and antibodies against citrullinated peptides/protein (11-13). Progressive joint destruction in RA is dominated by activated cells of fibroblast and macrophage origin, creating an environment with increased pro-inflammatory cytokine production, specifically interleukin (IL)-6 and -1β, and tumour necrosis factor-alpha (TNF-α) (14-16). This array of pro-inflammatory cytokines continuously released by T cells, B cells, fibroblastic stromal cells, macrophages and fibroblast-like synoviocytes (FLS) ultimately causes the recruitment, differentiation and activation of bone resorbing osteoclasts leading to cartilage and bone destruction at the site of pannus invasion (1, 17-21).

RA patients identify pain as the most-debilitating symptom that they experience. The prognosis of pain for RA patients is often poor despite optimal control of disease progression and remission, suggesting a greater understanding of pain is needed in RA (22, 23). Within the synovial joint, all structures, excluding cartilage are innovated by nociceptive (pain sensing) neurons. During RA disease progression, when physical and biochemical changes occur in the joint, the threshold for activation of these peripheral nociceptive neurons is lowered resulting in allodynia, where an innocuous stimuli produces pain, and hyperalgesia, where responses to noxious stimuli are enhanced (24). Pain at the inflamed joints may also arise spontaneously in the absence of an external trigger (25). Due to the chronic course of RA disease progression, prolonged excitation of the peripheral nociceptive neurons leads to sensitisation of these neurons, enabling them to respond more easily to stimuli in a non-inflamed state, resulting in pain even with optimal control of inflammation or remission (26). Studies also indicate that central pain processing is augmented in RA patients as they display increased pain sensitivity at remote non-articular sites as well as at inflamed joints (27-29). RA associated pain is therefore no longer considered to be solely a consequence of inflammation and joint destruction. Recent studies have identified that pain can arise prior to disease manifestations and does not necessarily correlate with the degree of inflammation or pharmacological management (22, 30-33). Thus, detailed clinical assessment is required and further research in pre-clinical phases, including animal models of inflammatory arthritis, is necessary to understand the complex mechanisms that initiate and contribute to pain progression in RA.

1.4. Rheumatoid arthritis in the clinical setting: Assessment of pain and inflammation

Currently disease activity is assessed in patients using composite scoring methods such as the 28-joint disease activity score (DAS 28). The DAS 28 combines patient reported outcomes on the visual analogue scale of patient assessment of their general health, with observed and laboratory measured components (34). Based on the current characterisation and assessment of RA, the aim of most pharmacological therapies is to resolve the inflammation of the affected synovial joints. Despite major progress in the treatment of RA, strong unmet medical need remains, as only a minor proportion of patients reach sustained clinical remission and symptoms of pain persist (22, 35, 36). Over

time joint erosion also becomes progressive and can continue despite suppression of inflammation (37, 38), thus contributing to the aetiology of RA associated pain (30, 36, 39, 40). Therefore, effective management of RA should involve therapies that target inflammation, bone destruction and the mechanisms behind pain development concurrently. This editorial will discuss the effects of the chronic inflammatory response in RA on synovial joint destruction. In addition, novel therapeutic treatments that target these destructive mechanisms in RA will be introduced.

1.5. Pathophysiology of rheumatoid arthritis

Joint biology has been researched extensively over the past decades and there is growing knowledge in the structure and composition of synovial joints (41, 42). The synovial joint comprises a collection of different tissue types including, synovial membrane and fluid, articular cartilage and bone, enclosed within a fibrous capsule, allowing the stable articulation between two or more skeletal elements (42). It is imperative to understand the development, structure and function of these tissues as damage within the joint can have debilitating effects.

1.5.1. Synovium and fibroblast-like synoviocytes (FLS)

The synovium is a thin membrane residing between the joint cavity and the fibrous joint capsule, organised into a synovial lining layer, 1-3 cells thick, and loose connective tissue (Figure 1.1) (14). The synovial membrane is the main site of immune cell infiltration and proliferation in RA, resulting in inflammation of the membrane and formation of invasive pannus tissue (Figure 1.1) (14, 16). The synovial lining layer is comprised of macrophage-lining synoviocytes which express markers of haematopoietic origin (43, 44) and FLS which express markers common to mesenchymal cells and produce the molecular constituents of the synovial fluid (44). In RA, the synovial lining becomes hyperplastic and thickens to 10-15 cell layers due to the influx of inflammatory cells and increased proliferation and survival of resident FLS (45-48). Thus, the degree of synovial hyperplasia correlates with the severity of cartilage and bone destruction in the synovial joints of RA patients (20, 21). FLS in RA show an activated destructive phenotype, independent of the surrounding inflammatory environment (46), however, knowledge about the mechanisms underlying the permanent activation of FLS in RA is limited.

Activated FLS further enhance and actively contribute to the inflammatory cycle within RA by producing inflammatory cytokines such as TNF-α, IL-6 and IL-1β, as reviewed by Choy and Panayi 2001, and Firestein 2003 (49, 50). These cytokines stimulate the expression of receptor activator of nuclear factor-kappa B (RANK) ligand (RANKL) by fibroblasts to further enhance osteoclastogenesis within the joint (1, 19). Although inflammation and disease progression can be efficiently reduced by current therapies, permanent FLS activation is not completely suppressed, resulting in ongoing joint destruction and bone erosion in the synovial joints of RA patients.
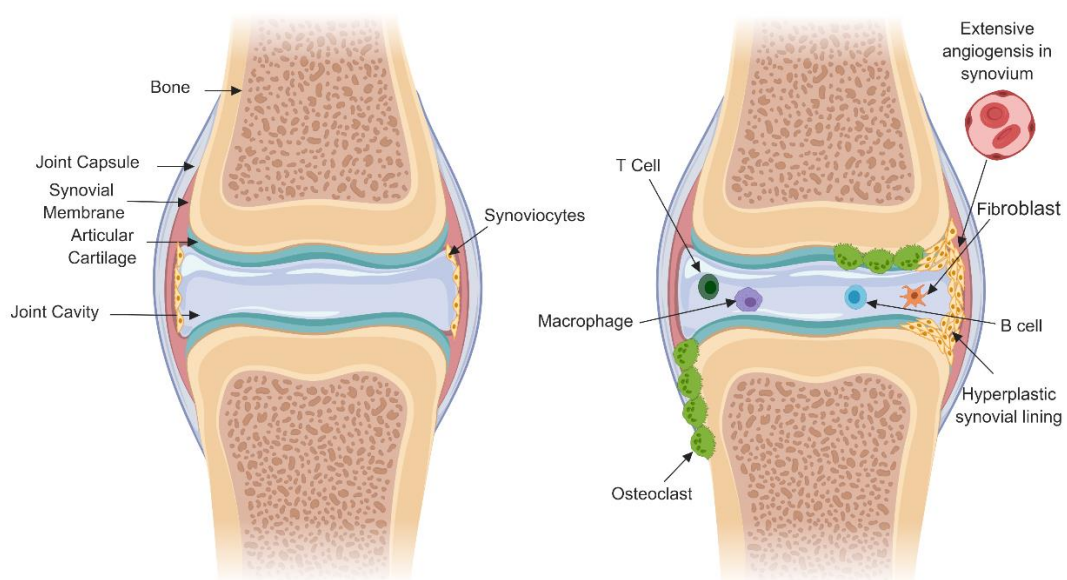
Figure 1.1. Schematic of the normal morphology of a synovial joint (left) and a synovial joint in rheumatoid arthritis (right). In a healthy joint, the thin (1-3 cells) synovial membrane lines the joint. In RA, the synovial membrane becomes hyperplastic and the joint becomes infiltrated with inflammatory cells. These cells form a pannus tissue which invades the articular cartilage and stimulates bone destruction by osteoclasts.

1.5.2. Bone remodelling in rheumatoid arthritis

Bone is a specialised type of connective tissue which undergoes continuous remodelling to ensure maintenance of constant bone mass and appropriate levels of calcium, phosphorous and proteins. In healthy adults, bone formation, by osteoblasts, and bone resorption, carried out by osteoclasts, occurs concurrently and balance exists, with no net change in bone volume occurring (51). If balance of bone resorption and formation is not maintained then pathological bone loss occurs (52). In RA, inflammation and treatment regimens alter bone turnover. As such, with chronic and recurrent disease activity, both local and systemic skeletal complications are observed, including focal bone erosions, juxta-articular osteopenia, periarticular osteoporosis and generalised bone loss.

1.5.2.1. Osteoblasts and osteoblastogenesis

Osteoblasts play a critical role in bone remodelling in normal physiological conditions by forming and depositing type I collagen, the primary organic component of bone. Osteoblasts originate from pluripotent mesenchymal stem cells derived from the neural crest during embryonic development (53, 54). Mesenchymal stem cells have the potential to differentiate into adipocytes, chondrocytes, myocytes and osteoblasts (53). Commitment of pluripotent mesenchymal stem cells to osteoprogenitors and the differentiation of these cells to osteoblasts is known as osteoblastogenesis. Osteoblastogenesis is a complex process and is dependent on several factors, including skeletal development, the presence of bone morphogenetic protein (BMP) and transcription factors, and the activation of signalling pathways (55-57). Activation of the wingless-type MMTV integration site (Wnt) signalling pathway promotes the differentiation of progenitor cells into the osteogenic lineage, through β-catenin activation which upregulates the necessary transcription factors crucial for osteoblast differentiation (57-60). Formation and activity of these differentiated osteoblasts is then stimulated through increased intracellular calcium levels via the activation of c-jun N-terminal kinases (JNKs) and transcription factors including Runt-related transcription factor 2, nuclear factor of activated T-cells (NFAT) and nuclear factor kappa B (NF-κB) (57, 61). Once differentiated, osteoblasts also play a critical role in supporting and stimulating osteoclast differentiation (62, 63). Thus, regulation of the signalling pathways and transcription factors required for osteoblast differentiation may also contribute to the development and exacerbation of generalised bone loss observed in RA.

1.5.2.2. *Osteoclasts and osteoclastogenesis*

Osteoclasts are giant multinucleated (6-12 nuclei) cells formed through the fusion of mononucleated cells derived from hematopoietic tissue. Osteoclasts are the primary cell responsible for bone resorption (51, 64-67). The differentiation and maturation of osteoclasts occurs in close vicinity of mineralised bone, and as such osteoclast precursor cells migrate from bone marrow into the blood stream to the site of intended bone resorption (51, 68). Macrophage colony stimulating factor (M-CSF) and RANKL are key factors for osteoclastic differentiation (69, 70). During osteoclastogenesis, M-CSF stimulation of osteoclast precursor cells enhances cell survival, promotes differentiation to the osteoclastic lineage and induces the expression of RANK on osteoclast precursor cells (69, 71). The RANK/RANKL signalling pathway is central to regulating osteoclast formation and bone resorption activity both in normal bone remodelling and in pathological conditions. RANKL is a cytokine in the TNF superfamily and is highly expressed in osteoblasts (64), bone marrow (72), lymphoid tissue (73), fibroblasts (18) and dendritic cells (74). RANKL is found both in membrane-bound and soluble forms released by osteoblasts, T cells and fibroblasts (75-77). Membrane-bound RANKL however, binds more efficiently to its receptor RANK, which is present on osteoclast precursor cells (75). The binding of RANKL to RANK on osteoclast precursor cells initiates a series of intracellular signalling pathways and promotes the expression of key osteoclast specific genes required to complete the formation, differentiation and activation of osteoclasts.

The importance of RANK/RANKL signalling in osteoclasts is well established *in vitro* (73, 78) and has been demonstrated *in vivo* in mutant, knockout and transgenic models. Mice with a disruption in RANK or RANKL show severe osteopetrosis, abnormally dense bone, due to the inability to produce osteoclasts (79). Consistent with this, RANK knock-out mice also exhibit severe bone sclerosis due to a lack of osteoclasts (80). Additionally, the involvement of RANKL in promoting osteoclast activation has been further shown in a serum transfer model of inflammatory arthritis where TNF-α transgenic RANKL knockout mice developed inflammation, however lacked osteoclasts and were resistant to arthritis induced bone destruction (81). This further supports the importance and role of RANK/RANKL signalling as a key factor in osteoclastogenesis in both normal physiological and pathological conditions, such as RA.

NF-κB is a widely encountered transcription factor which regulates the expression of genes that encode cytokines, chemokines, growth factors and cell adhesion molecules in physiological and pathological conditions (82). NF-κB signalling pathways are strictly regulated to maintain bone homeostasis by cytokines such as RANKL, TNF-α and IL-1β which differentially regulate classical (canonical) and/or alternative (non-canonical) NF-κB pathways in osteoclastic cells (Figure 1.2) (82, 83). In the classical NF-κB pathway, NF-κB activation causes inhibitor of kappa B (IκB) proteins to become phosphorylated by the macromolecular IκB kinase complex (IKK-α and IKK-β). This triggers the rapid ubiquitination and degradation of IκB proteins, allowing NF-κB proteins (p50 and p65) to translocate from the cytoplasm to the nucleus regulating the transcription of several downstream osteoclast target genes (Figure 1.2) (84). In contrast, the alternative NF-κB pathway involves phosphorylation of IKK-α by NF-κB inducing kinase (NIK), which leads to proteasomal processing of p100 to p52 (85, 86). P52 heterodimers then translocate into the nucleus to regulate its target genes (Figure 1.2) (85, 86). It is well established that RANKL activates both classical and alternative pathways of NF-κB in osteoclasts (87). However, the activation of NF-κB by TNF-α and IL-1β is restricted to the classical pathway (Figure 1.2) (87, 88). Thus, the expression of these cytokines and the resulting activation of NF-κB might manifest the outcome of osteoclast-mediated bone loss in different pathological conditions, including RA.
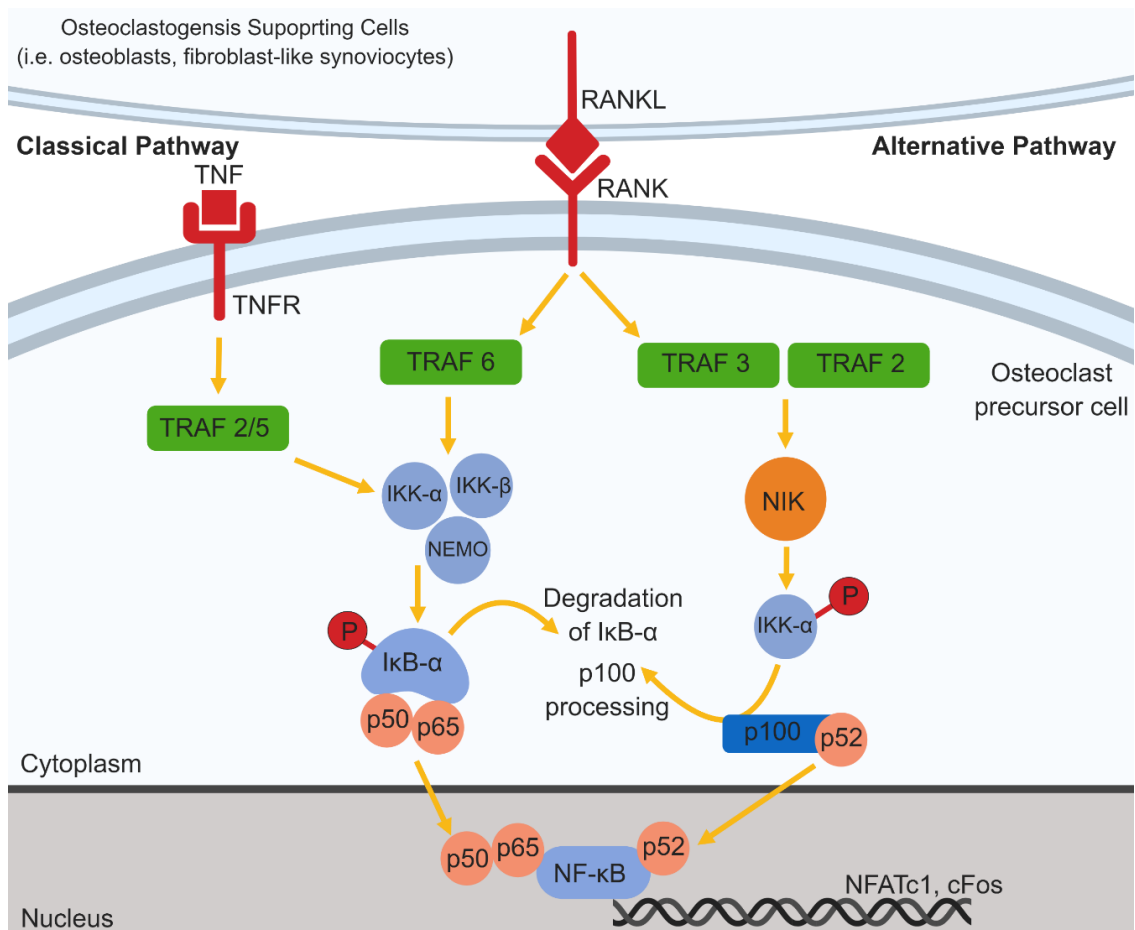
Figure 1.2. Nuclear factor-kappa B (NF-κB) signalling in osteoclastogenesis. NF-κB proteins reside in the cytoplasm of osteoclast precursor cells. NF-κB is activated by the binding of RANKL to RANK through the classical or alternative pathways and by binding of TNF to TNFR through the classical pathway (89). Binding of RANKL to RANK or TNF to TNFR (88) induces classical signalling by recruiting TNFR-associated factor (TRAF) 6, 2 or 5 to their receptors. This activates a complex consisting of IKK-α, IKK-β and NF-κB essential modulator (NEMO). This leads to phosphorylation of IκB-α and the release of p65/p50 heterodimers, which then translocate to the nucleus (84, 90). This induces the expression of other transcription factors (c-Fos and NFATc1) necessary for osteoclast differentiation. The alternative pathway can only be stimulated by binding of RANKL to RANK, which induces the lysosomal degradation of TRAF 3 through TRAF 2 and releases NIK to phosphorylate IKK-α and stimulate the proteasomal processing of p100 to p52 (91, 92). Similar to the classical pathway, p52 heterodimers translocate into the nucleus and regulate target gene expression necessary for osteoclast differentiation. IκB, Inhibitor of kappa B; IKK-α/β, Inhibitor of kappa B kinase complex alpha/beta; NEMO, Nuclear factor kappa B essential modulator; NFATc1, Nuclear factor

of activated T cell, cytoplasmic 1; NF-κB, Nuclear factor kappa B; NIK, Nuclear factor kappa B inducing kinase; P, Phosphorylation; RANK, Receptor activator of nuclear factor kappa B; RANKL, Receptor activator of nuclear factor kappa B ligand; TNF, Tumour necrosis factor; TNFR, Tumour necrosis factor receptor, TRAF, Tumour necrosis factor receptor associated factors.

1.5.2.3. *The role of osteoclasts in pathological bone loss in rheumatoid arthritis*

Osteoclasts are unique in their ability to resorb bone in both physiological and pathological conditions. Enhanced osteoclastic activity associated with inflammation is a common feature of many chronic inflammatory diseases, including RA, resulting in the rapid occurrence of bone loss preceding the development of an inflamed synovium (2, 17). At the synovial joint, the increased production of pro-inflammatory cytokines, TNF-α, IL-6, IL-1β and matrix metalloproteinases (MMPs) are involved in the destruction of the surrounding cartilage and soft tissue. In conjunction with this, the increase in pro-inflammatory cytokines drives the production of soluble RANKL produced by fibroblasts and activated T cells (Figure 1.3). This results in excessive binding of RANKL to RANK, increased activation of the classical NF-κB signalling pathway (Figure 1.2) and an increase in osteoclast number and activity (Figure 1.3).

Multiple human and animal studies provide strong evidence for increased bone resorbing osteoclasts in the subchondral bone at sites of bone loss where there is inflammatory arthritis (93, 94). More specifically, large numbers of mononuclear pre-osteoclastic cells and multinucleated osteoclasts found at the pannus-bone interface at sites of inflammatory arthritis, were found to express tartrate resistant acid phosphatase (TRAP; osteoclast-associated gene) mRNA and enzymatic activity (95). This identifies pre-osteoclastic cells at an intermediate stage of osteoclast differentiation, suggesting that the upregulation of pro-inflammatory cytokines in pannus tissue is capable of directly or indirectly stimulating osteoclastogenesis (95). This is further supported by animal studies which have identified increased NF-κB activity in osteoclasts present in the inflamed joints of arthritic mice (96). In contrast, in the serum transfer model of arthritis previously discussed, it was found that mice lacking osteoclasts through RANKL knockout were resistant to inflammatory arthritis induced bone loss (81). Thus, it is evident from these

studies that the RANK/RANKL regulated NF-κB signalling pathway may serve as a potential therapeutic target for osteoclast-associated bone loss in RA and will be discussed further in chapter four.
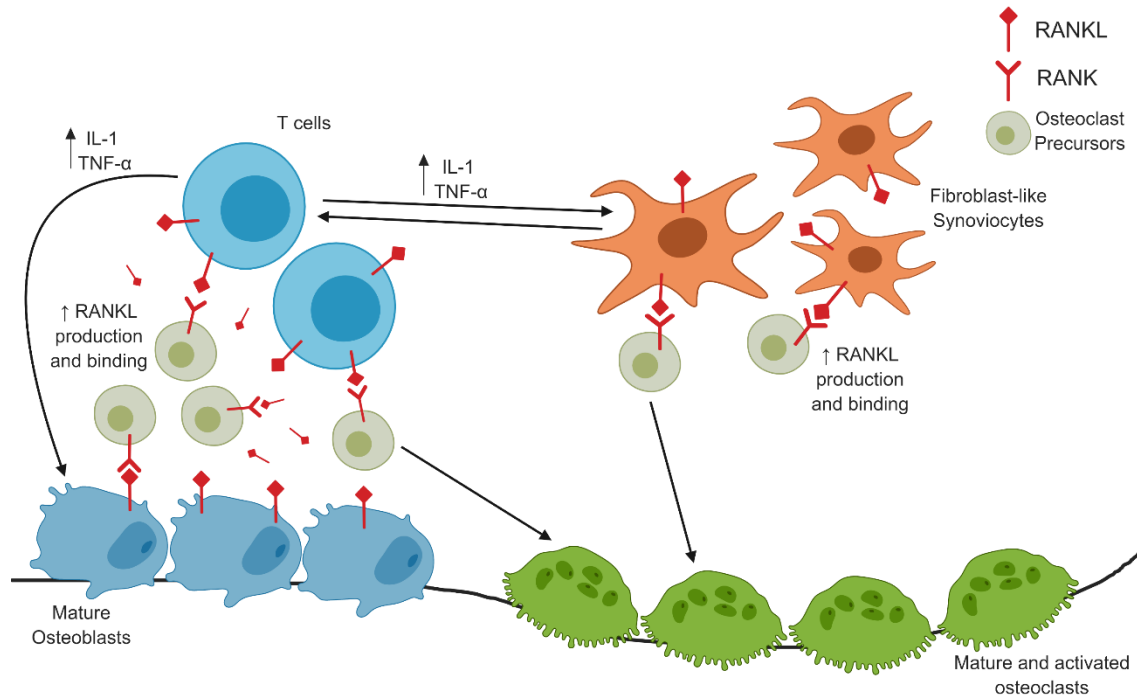
Figure 1.3. RANK/RANKL signalling involvement in rheumatoid arthritis. RANK/RANKL signalling is the key pathway involved in regulating osteoclast formation and activity in RA. RANKL expressed by osteoblasts, T cells and fibroblasts binds to its receptor RANK on pre-osteoclasts, causing differentiation and maturation into multinucleated osteoclasts (18, 64, 73, 74). In RA, the increase in immune cells and proliferation of fibroblast-like synoviocytes results in increased pro-inflammatory cytokine production. Inflammatory cytokines enhance the production of soluble RANKL produced by T cells, further driving NF-κB signalling (64, 97). Fibroblast-like synoviocytes also actively contribute to this process by increasing levels of soluble and membrane-bound RANKL (1, 19). This ultimately results in excessive binding of RANKL to RANK on pre-osteoclasts, increased activation of NF-κB signalling and maturation of bone resorbing osteoclasts. Thus, this signalling pathway could be a potential target for the development of new therapeutics in RA. IL-1, interleukin-1; TNF-α, Tumour necrosis factor alpha; RANK, Receptor activator of nuclear factor kappa B; RANKL, Receptor activator of nuclear factor kappa B ligand.

1.5.3. Cadherins and synovial joints

Direct cell to cell interactions are essential for the regulation of cell proliferation, differentiation and survival within the body and is mediated in part by cell adhesion molecules, known as cadherins (98). Cadherins are a family of single chain transmembrane glycoproteins that mediate calcium dependent homophilic cell-cell adhesion (99). These type I integral membrane proteins consist of five extracellular domains, a single transmembrane domain and a highly conserved cytoplasmic tail (99). The cytoplasmic tail interacts with β-catenin, linking cadherins to the actin cytoskeleton. As such, they are likely to be intimately involved in skeletal and joint tissue development (100, 101). Cadherins are expressed in a tissue-selective manner and different tissue types can express one or several types of cadherins (102). Thus, it is crucial to understand the role cadherins have in normal and pathological tissue architecture and development.

Previous studies have identified that RA-FLS express cadherin-11 (CDH11) and *in vivo* studies in CDH11-deficiant mice have demonstrated the importance of CDH11 in synovial lining architecture and inflammation (103-105). Pertinent to this, CDH11 may be crucial in the development of hyperplastic pannus tissue and cartilage destruction in RA, as mice deficient in CDH11 demonstrated a hypoplastic synovial lining and reduction in both the inflammatory response and cartilage destruction (105). As it is known that different tissue types express multiple types of cadherins, research has now focused on identifying whether other cadherins are expressed on cells located within the synovial joints. N-cadherin, a mesenchymal cadherin initially identified in chick retina (106-110), has now been identified on a broad repertoire of cells, including neural tissue, retina, endothelial cells, osteoblasts, myocytes and fibroblasts (106, 107, 109). N-cadherin is reported to be involved in normal cardiac and skeletal muscle development, as well as cartilage development and osteogenic differentiation (106-110). Thus, discussion of these overlapping, yet distinct roles, between N-cadherin and CDH11 within the skeletal system and synovial lining is emerging within the literature (101, 111). Currently, *in vivo* functional studies of N-cadherin are limited, as N-cadherin deletion is fatal to the mouse embryo (108). However, research is emerging on the role of N-cadherin in maintaining bone formation and tissue architecture within synovial joints and related structures (Figure 1.4), thus highlighting its potential involvement in inflammatory bone loss associated with RA.
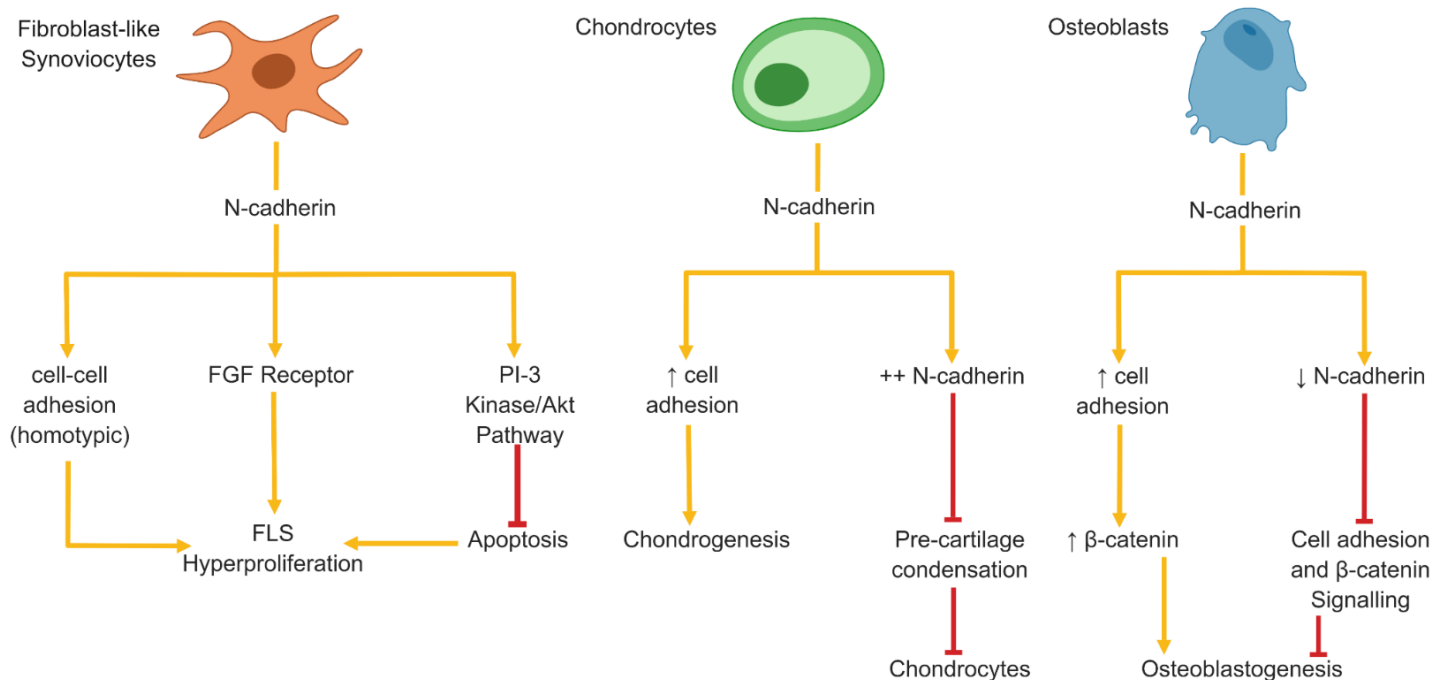
Figure 1.4. The role of N-cadherin in different cell types found within the synovial joint. Expression of N-cadherin in FLS causes cell-cell adhesion and modulation of the FGF receptor, thus stimulating FLS hyperproliferation (111, 112). N-cadherin in FLS also stimulates the PI-3 kinase/AKT pathway, increasing the presence of anti-apoptotic proteins, inhibiting apoptosis and perpetuating FLS proliferation (113, 114). N-cadherin expression in chondrocytes increases cell-cell adhesion and stimulates the differentiation of chondrocytes, while increased or persistent expression of N-cadherin results in inhibition of pre-cartilage condensation and decreased chondrocyte formation (115-117). Similar to chondrocytes, N-cadherin expression in osteoblasts increases cell-cell adhesion and stimulates Wnt/β-catenin signalling, resulting in osteoblast differentiation. When N-cadherin expression is decreased, osteoblastogenesis is inhibited (118-121). FGF, Fibroblast growth factor; FLS, Fibroblast-like synoviocyte; PI-3 kinase/Akt, Phosphoinositide 3-kinase/protein kinase B.

CDH11 expression in FLS has been demonstrated in human and mouse cultured FLS and *in vivo* in mouse synovial membranes (103, 111). However, the mechanisms by which N-cadherin acts on FLS to stimulate or inhibit FLS hyperproliferation in RA is still being investigated. Recent studies have demonstrated an association of N-cadherin with fibroblast growth factor (FGF) receptor (FGFR) through the fourth extracellular cadherin domain (112). Increased levels of FGF have been identified in the synovial fluid of RA patients (122) and increased expression of FGFR is linked to severe joint destruction in adjuvant induced arthritis in mice (123-125). Therefore, N-cadherin may play an important role in modulating FGF binding to FGFR and impact FLS activation and hyperproliferation in RA.

As discussed previously, osteoblastogenesis is a complex process involving the commitment of mesenchymal stem cells to osteoprogenitors and the differentiation of these cells into matrix producing osteoblasts. Direct cell-to-cell interactions during osteoblastogenesis are controlled by cadherins through the binding of β-catenin (101, 118, 126, 127). Cadherins can also modulate signal transduction in osteoprogenitors via Wnt/β-catenin signalling, thus ultimately stimulating osteoblastogenesis (Figure 1.4) (119, 120). Genetic ablation of N-cadherin causes a reduction in the expression of β-catenin and overall reduction in cell-cell adhesion of osteoblasts (121). Consequently, ablation of β-catenin impedes osteoblastogenesis and bone formation, resulting in impaired bone remodelling and skeletal defects (121).

N-cadherin is increased during early chondrogenic differentiation and progressively decreases at later stages, thus its role in mediating chondrogenesis has been confirmed in early chondroblast differentiation (117, 128, 129). Although, *in vitro* perturbation of N-cadherin inhibits chondrogenesis (130-132), it has also been identified that persistence of N-cadherin prevents further progression of chondrocyte development (115, 116). This suggests that either persistence or ablation of N-cadherin may impact chondrocyte differentiation (Figure 1.4). However, whether N-cadherin is upregulated in RA and thus preventing chondrocyte development is unknown. Models of N-cadherin inactivation in normal and RA chondrocytes are needed to further elucidate its role.

Despite the growing research surrounding N-cadherin, the role of N-cadherin in the formation of bone resorbing osteoclasts is not well understood. Recently, N-cadherin expression has been confirmed in mononuclear osteoclast precursors, suggesting that N-cadherin mediated cellular adhesion may contribute to the formation of osteoclasts (133). However, whether N-cadherin expression is altered in mature osteoclasts during RA disease progression is still unknown. Osteoclast precursor cells interact closely with osteoblasts to allow for the binding of RANKL to RANK during physiological and pathological osteoclastogenesis. N-cadherin in osteogenic cells could therefore modulate osteoclastogenesis through β-catenin dependent regulation of RANKL expression on osteoblasts (133). Further research is required to elucidate this relationship and the role of cadherins, specifically N-cadherin, in osteoclastogenesis and in the context of RA induced bone erosion. Studies have identified a range of roles for N-cadherin in synovial joints and illustrate that they could contribute to the overall joint structure and its destruction during RA disease progression. Thus, N-cadherin provides another target for the development of new therapies in the hope of targeting specific intracellular pathways in RA and will be investigated further in chapter three.

1.5.4. The role of apoptosis in rheumatoid arthritis

Recently, characteristic changes of the inflamed synovium in RA have been linked to an altered apoptotic response of synovial and inflammatory cells (134, 135). Apoptosis is a form of programmed cell death that plays pivotal roles in embryological cell development as well as in physiological cell turnover and homeostatic functioning of the body. Apoptosis is a highly complex process that involves a cascade of molecular events controlled by different genes and molecular mechanisms (136). The process of apoptosis occurs through two pathways, the extrinsic, death receptor, pathway and the intrinsic, mitochondrial, pathway (Figure 1.5).
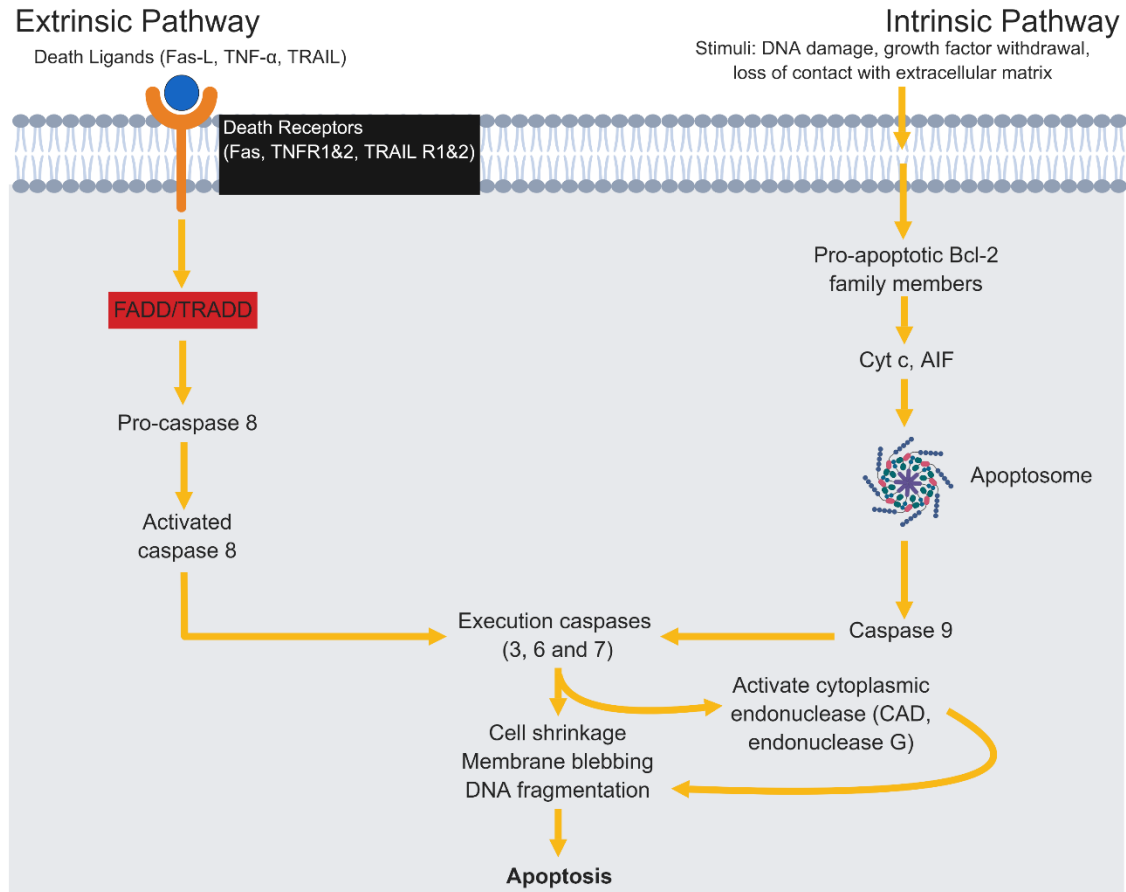
Figure 1.5. Extrinsic and intrinsic apoptotic pathways. Modified schematic diagram of the intrinsic and extrinsic apoptosis pathways (137). AIF, apoptosis-inducing factor; CAD, caspase-activated DNase; Cyt c, cytochrome c; FADD, Fas associated death domain; Fas-L, Fas ligand; TNF-α, tumour necrosis factor alpha; TRADD, TNF-receptor type-1 associated death domain protein; TRAIL, TNF-related apoptosis inducing ligand.

The extrinsic pathway initiates apoptosis through interaction between ligands (such as Fas ligand, TNF-α and tumour necrosis factor-related apoptosis-inducing ligand (TRAIL)) and their transmembrane receptors, which involve death receptors that are members of the TNF receptor gene superfamily (such as Fas, TNFR1 and TRAIL death receptor 1 and 2) (138). The sequence of events that characterise the extrinsic pathway include clustering of death receptors and binding with a homologous trimeric ligand. As a result, cytoplasmic adapter proteins, which exhibit corresponding death domains binding with the death receptors, are recruited (139, 140).

In contrast, the intrinsic pathway initiates apoptosis through non-receptor mediated stimuli including DNA damage, growth factor withdrawal or loss of contact with the extracellular matrix. These stimuli produce intracellular signals that act directly either positively or negatively on specific targets within the cell (141). Stimulation of this pathway leads to changes in the integrity of the mitochondrial membrane resulting in the loss of mitochondrial transmembrane potential and the release of several pro-apoptotic proteins such as cytochrome c, apoptosis inducing factor (AIF) and second mitochondrial activator of caspases (SMAC) (142). These proteins activate the caspase-dependent mitochondrial pathway (such as caspase 9) through different mechanisms and are summarised in Table 1.1.

Table 1.1. Intracellular pro-apoptotic proteins

Protein name	Mechanism to activate intrinsic pathway
Cytochrome C	Binds and activates pro-caspase 9 to form an apoptosome (143).
Bcl-2 family of pro-apoptotic proteins: *Bcl-10, BAX, BAk, Bid, Bad, Bim, Bik and Blk*	Regulation of cytochrome c release from mitochondria. Caspase 8 cleavage by Bid to regulate the Fas pathway (144). Bad heterodimerize with anti-apoptotic proteins Bcl-xL and Bcl-2 to neutralise their protective effect and promote apoptosis (145).
Second mitochondrial activator of caspase (SMAC)	Promotes apoptosis by inhibiting activity of inhibitor of apoptosis proteins (146).
Apoptosis inducing factor (AIF)	DNA fragmentation and condensation of peripheral nuclear chromatin (147).
Caspase-activated DNase (CAD)	Caspase-dependent cleavage of nuclear chromatin to produce oligonucleasomal DNA fragments (148).

These two pathways are linked, with molecules in one pathway influencing those of the other, and converge at the execution pathway (Figure 1.5) (141). The execution pathway is characterised by the activation of downstream caspases, such as caspase 3, 6 and 7 (149). Downstream caspases activate cytoplasmic endonuclease, leading to morphological changes characteristic of apoptosis, including DNA fragmentation, degradation of cytoskeletal and nuclear proteins and formation of apoptotic bodies. The uptake of apoptotic bodies by phagocytic cells is the last step of apoptosis (141).

An imbalance in apoptosis can be a major factor in the development of many human pathological conditions including cancer, neurodegenerative and autoimmune diseases (150-152). Currently, research in RA focuses on the theory that the chronic accumulation of inflammatory cells and osteoclasts in RA synovial joints is due to decreased apoptosis. Proteins involved in the apoptotic pathway have been identified as potential targets to modify the pathogenesis of RA. Additionally, these targets may also be involved in the

actions of existing medications or new therapeutics in RA that have not been fully elucidated (153).

1.5.4.1. *The role of intracellular anti-apoptotic molecules for rheumatoid arthritis pathogenesis*

There is growing research on the role of anti-apoptotic molecules in pathological conditions and it is now known that several of these anti-apoptotic molecules, including Bcl-2, FLICE-like inhibitory protein (FLIP) and inhibitory apoptotic proteins (IAP), are upregulated in RA (Table 1.2). The exact role of Bcl-2 proteins in RA pathogenesis remains unknown. However, previous studies have identified that the chronic inflammatory response in RA joints maintains high levels of Bcl-2 family proteins, specifically Bcl-xL (154), which results in inhibition of apoptosis in various cell types in the synovial joints of RA patients (155-157). FLIP is a naturally endogenous occurring anti-apoptotic protein. *In vitro* and *in vivo* studies have demonstrated that RA FLS and macrophages are resistant to Fas-mediated apoptosis due to increased levels of FLIP expression (Table 1.2) (158-160). It is evident that these intracellular molecules may play a large role in inhibiting apoptosis of various cell types in the synovial joints of RA patients (Table 1.2), however there are currently limited compounds which target Bcl-2 proteins, and more specifically, limited FLIP antagonists which have been identified and assessed in pre-clinical *in vitro* and *in vivo* models. Thus, current research has extended to the role of the IAP family of anti-apoptotic proteins in RA and how modulation of these molecules may be beneficial in reducing disease progression in RA.

Table 1.2. Intracellular anti-apoptotic proteins that are upregulated in rheumatoid arthritis joints

Anti-apoptotic Molecule	Mechanism of Apoptosis Inhibition	Upregulation in RA
Bcl-2 family of anti-apoptotic proteins: Bcl-2, Bcl-xL, BAG, Bcl-w, Mcl-1	Prevents apoptosis by maintaining mitochondrial homeostasis, inhibiting cytochrome c release and controlling activation of caspase proteases (161).	Increased expression of Bcl-2 in FLS correlates with synovial lining thickening and the progression of inflammation (157, 162). Increased expression of Bcl-xL in osteoclasts prolongs life span in erosive arthritis (163).
FLIP	Prevents association of procaspase 8 with FADD, inhibiting the extrinsic pathway.	Macrophages in active RA are resistant to Fas-induced apoptosis and have increased levels of FLIP (164). FLIP positive cells are predominantly present in the lining and sub lining of synovium in early RA (159, 160).
IAP family of proteins: XIAP	Prevents apoptosis by binding to active caspase 3, 7 and 9, inhibiting both the extrinsic and intrinsic pathways.	XIAP is highly expressed in the cytoplasm of CD68 positive cells in synovial joints of RA patients (135).
IAP family of proteins: Survivin	Downregulates directly or indirectly both the intrinsic and extrinsic pathways (165).	Highly expressed in cytoplasm of cells in the synovial tissue of active RA patients (135, 166).

1.5.4.2. *The role of inhibitory apoptotic proteins (IAP) in rheumatoid arthritis*

The IAP family of anti-apoptotic proteins, inhibits both upstream and downstream caspases throughout the apoptosis pathway. They are also involved in other cell processes such as cell cycle regulation, immune function and the activation of immune cells. Eight different IAPs have been identified and include X-linked IAP (XIAP), ILP-2, cIAP-1, cIAP-2, ML-IAP, NAIP, survivin and apollon (167). XIAP is the best characterised IAP as it has the most observable biological properties. XIAP has been shown to be a potent inhibitor of apoptosis by binding to active caspase 3, 7 or 9 and therefore can inhibit both extrinsic and intrinsic pathways of apoptosis (168). This is possible as XIAP has three conserved sequence motifs, the baculovirus IAP repeats (BIR 1-3), which are located at the amino terminal end of the protein and one zinc finger-like RING which is situated at the carboxyl terminus and mediates protein-protein interactions (168). XIAP can inhibit caspase activity through direct binding and this occurs as BIR 3 binds to caspase 9 and BIR 2 binds to caspase 3 and 7 (169). Dharmapatni *et al.* 2009 found XIAP to be highly expressed in the cytoplasm of cells in active RA (135). This elevated expression of XIAP was found to correlate with CD68 positive cells in the synovium, suggesting that XIAP is expressed by large numbers of macrophages (135). This supports the possibility that macrophage apoptosis may also be inhibited by XIAP in the active RA synovium. Thus, over-expression of XIAP has a major role in maintaining active RA disease progression through contributing to the inhibition of apoptosis of cells located within the synovial joints. Therefore, modulating XIAP may be essential for future treatment of RA and will be discussed in more detail below and in chapter two.

1.5.5. *Crosstalk between apoptosis and autophagy*

Autophagy is a process which occurs in normal physiological conditions to maintain homeostasis of a cell, by degradation of unused protein and turnover of damaged organelles (170). It is an adaptive cell survival mechanism that occurs in response to cellular stress or nutrition deprivation (170). Autophagy allows cells to sequester cytoplasmic contents through the formation of autophagosomes; a double membrane vesicle targeted for degradation by lysosomes (171). Previous research has identified increased levels of autophagy related genes (Atgs) in TRAP positive multinucleated cells from RA synovial tissues (172). Suggesting that osteoclasts may use mechanisms of

autophagy as a means of survival under inflammatory conditions, such as RA. Recently, TNF-α has also been identified as an inducer of Atgs and autophagy in mouse derived osteoclasts *in vivo* (172). Therefore, autophagy upregulation may contribute to both prolonged survival of osteoclasts and the stimulation of osteoclastogenesis when under inflammatory conditions. A crosstalk between apoptosis and autophagy has been demonstrated in recent studies whereby a reduction in apoptosis inversely correlated with an increase in autophagy in cancer cells (173) and RA synovial tissues (174). Although reduced apoptosis in the RA synovia has been reported extensively, a regulatory role for autophagy and its detailed relationship with apoptosis in RA has not been fully explored. Further investigation into the relationship between apoptosis and autophagy in RA could identify potential mediators for more targeted treatment of disease activity in RA and will be discussed further in chapter two.

1.6. Animal models of inflammatory arthritis

Animal models are essential in understanding the pathogenesis of RA as they enable the progression of local inflammation and joint destruction to be studied, along with other aspects of RA pathogenesis including pain and other co-morbidities. The development of RA can be characterised into three stages (20, 175). The initiation phase, which involves the initial activation of the immune system and inflammatory cascade, the transformation phase, where the inflammatory process perpetuates, and chronic pathology is established. The final stage is the effector phase which involves the destruction of the target tissues resulting in irreversible damage (20, 175). Thus, there are several well-established inducible and spontaneous animal models available to study the progression of RA through these key stages (as reviewed by Kannan *et al.* 2005; (176), Asquith *et al.* 2009; (177), and Caplazi *et al.* 2015; (178)).

Inflammatory arthritis animal models are commonly induced in rats or mice, as they can both spontaneously develop arthritis or disease can be provoked through the administration of an arthritogenic stimuli. The most common established models used to mimic pathogenic features of human RA are adjuvant-induced arthritis (AIA) in rats (179), collagen-induced arthritis (CIA) or antigen-induced arthritis in rats and mice (180-182) and spontaneous models, such as the K/BxN model in mice (183). There are

currently several comprehensive reviews which discuss these models and their pathogenic features in comparison to human RA disease progression (184-188). However, despite each model exhibiting the classical features of RA disease progression, including joint inflammation, synovitis, pannus formation and bone erosion, each model differs in speed of disease onset, chronicity, severity and resolution (186). Thus, ongoing comparisons are required to establish which model is most appropriate for the research question.

Recent studies have extensively used the collagen antibody-induced arthritis (CAIA) model over other models of inflammatory arthritis due to its speed of disease onset and high uptake rate in a wider spectrum of mouse strains (189, 190). The CAIA model is an extension to the classical CIA model, however the commercial availability of a cocktail of monoclonal antibodies that target type II collagen avoids the need for host generation of autoantibodies to type II collagen (190). Arthritis in this model is mediated by immune complex deposition in the joints, recruitment of inflammatory components and is B and T cell independent (191). This provides a straightforward, rapid and reproducible model of inflammatory arthritis, resulting in similar pathogenic features to human RA evident within the effector phase of the disease and is best suited for the study of subacute disease mechanisms (180, 192).

In the CAIA model, pathogenic features of RA are induced with the combination of a cocktail of monoclonal antibodies targeting type II collagen in combination with *E.coli* lipopolysaccharide (LPS) (190). The strong synergistic effect between the autoantibodies and LPS increases the incidence and severity of disease within the mice. As a result, studies modify the dose of autoantibodies and LPS to induce the desired pathogenic features and severity for their research. Due to this, there is currently a large range of variability in disease onset and severity within the CAIA mouse model. Recently the biological properties of RA associated pain have begun to be investigated in preclinical animal models of inflammatory arthritis (193, 194), as this is recognised by patients and clinicians as an important morbidity associated with RA, impacting overall wellbeing and function. However, not all animal models perfectly recapitulate all aspects of human RA and the correlation between clinical inflammation and RA associated pain requires further investigation. Thus, future studies are required specifically using the CAIA murine model of inflammatory arthritis to identify the optimal severity of pathogenic features, which

allows joint destruction, RA associated pain and potential novel therapeutics to be investigated concomitantly and will be discussed further in chapter five.

1.7.   Imaging techniques in rheumatoid arthritis

Imaging is routinely used in the management of RA and provides objective detection of disease activity that can predict subsequent bone erosion and disease progression. The widespread use of imaging in clinical practice supports the use of imaging in both clinical trials and *in vivo* animal models of inflammatory arthritis. The growing evidence of the impact of imaging on the management of RA has resulted in the publication of the European League against Rheumatism (EULAR) recommendations for the use of ultrasound, magnetic resonance imaging (MRI) and conventional radiography (CR) in the diagnosis and management of RA (195). Despite the potential benefits of using these imaging techniques in clinical RA management, diagnosis of early disease remains difficult due to their limited specificity (196). Presently, CR is only able to provide indirect information on synovial inflammation and the technique is insensitive to early inflammatory bone involvement and overall bone damage (197). Conversely, ultrasound and MRI are characterised by high sensitivity in depicting local inflammation (198) and synovitis detected through ultrasound can be more predictive of a therapeutic response than clinical features of disease activity (199, 200). MRI can also improve the certainty of a diagnosis in RA and predict disease progression (201-203), as well as, predict subsequent joint damage through the detection of inflammation even during clinical remission (204, 205). However, further research is needed to better characterise the appropriate use of this technology in clinical practice and there are still significant barriers in using imaging techniques in clinical practice, including cost and accessibility.

The growing understanding of RA pathogenesis and disease progression has recently been enhanced through novel imaging techniques, such as micro-computed tomography (CT) in clinical studies and in *in vivo* animal models of inflammatory arthritis. Micro-CT is more sensitive in detecting early bone erosions compared to routinely used ultrasound and MRI, and may be better in identifying bone erosion in the small joints of the hands and feet (206-209). Micro-CT has been extensively used in rodent models of inflammatory arthritis (94, 210-212), and has several advantages over ultrasound and MRI, including high resolution, short acquisition times and simultaneous acquisition of

all three planes (transverse, coronal and sagittal) (213). Recent studies, including those in our own laboratory, have utilised micro-CT for the quantification and visualisation of bone changes at the micrometre level in 3D, in the radiocarpal joints in murine models of inflammatory arthritis (94, 137, 214, 215). However, the precise measurement of paw swelling in these models remains limited and is commonly assessed through subjective methods, such as clinical grading of paw swelling by visual evaluation (216-219). Thus, our laboratory identified a novel 3D micro-CT image analysis protocol which is capable of visualising and quantifying both paw swelling and bone erosion in the radiocarpal joints of mice with inflammatory arthritis using the same micro-CT scan (214). As this is a non-destructive imaging and quantification technique, it can be used in murine models of inflammatory arthritis to assess the change of both bone erosion and paw swelling in 3D in the front paws when exposed to different therapeutics. However, the current method has not been adapted to the hind paws of mice. Thus, as RA effects both the small joints of the hands and feet, and the CAIA model is induced systemically resulting in all paws exhibiting pathogenic features of RA, the current 3D micro-CT image analysis protocol will be optimised throughout this thesis to quantify paw swelling and bone erosion in both the front and hind paws of mice.

1.8. Current therapies for rheumatoid arthritis

Current clinical guidelines define the overall goal of treatment for RA patients as remission, or low disease activity when remission is not possible (220, 221). Optimum disease management is thus important to prevent disease progression and to improve long term patient outcomes. The range of therapeutic options available for the treatment of RA has advanced tremendously over the past 30 years (222). Current treatments available and commonly used in the treatment of RA include non-steroidal anti-inflammatory drugs (NSAIDs), glucocorticoids, conventional disease modifying anti-rheumatic drugs (DMARDs) such as Methotrexate and DMARDs of biologic origin, such as TNF-α inhibitors (223). Although NSAIDs have anti-inflammatory properties, they have little to no effect on suppression of bone destruction (224). Glucocorticoids have been identified as having similar effects to NSAIDs in suppressing early inflammation. However, long term use of glucocorticoids may result in unwanted adverse effects, including osteoporosis (224, 225). Thus, it is evident that NSAIDs and glucocorticoids are unlikely to be useful in preventing joint destruction in RA.

Recently, the beneficial outcomes of conventional DMARD therapy for RA has been identified with evidence of improvements in joint inflammation and destruction in RA patients (226-229). Furthermore, studies provide evidence that DMARDs reduce the chronic inflammatory infiltrate in the synovial membrane by suppression of lymphocyte proliferation, suppression of neutrophil chemotaxis and inhibition of vascular endothelial proliferation (230, 231). Methotrexate is the most commonly used DMARD for RA patients and has been considerably beneficial as a first-line therapy due to it being relatively safe and well tolerated at therapeutic doses (232, 233). However, 50% of RA patients are still non-responsive to methotrexate treatment and do not achieve complete remission (232, 234). Randomised trials in early RA patients have also shown that monotherapy with methotrexate achieves the target outcome in only one in three patients (235-237).

A number of therapeutics have recently been developed to target the specific inflammatory cytokines known to be elevated and responsible for the up-regulation of osteoclasts in RA, as reviewed by Herman, Kronke and Schett 2008 (238). Biologic DMARDs, or anti-TNF-α therapy, has become an increasingly popular treatment option due to its rapid onset of action. There are currently five TNF-α antagonists approved for treatment of RA and include Adalimumab, Entanercept, Infliximab, Golimumab and Certolizuman pegol. Anti-TNF-α therapy has been found to reduce synovitis in RA, however its ability to halt or reduce bone erosion was not supported by studies involving 847 RA patients using biologic DMARDs (239). There are growing concerns around the development of adverse side effects to biologic DMARDS in addition to the high cost to patients and evidence that not all patients are responsive to treatment. Recent clinical data also suggests that bone damage can still occur during anti-TNF-α therapy (240). Of concern, patients may take time to respond to treatment and clinicians may take considerable time to identify the appropriate treatment. Meanwhile bone erosion may ensue. Although multiple animal models and RA patient studies demonstrate the positive effects of biologic DMARDs in reducing disease activity (235, 241-243) other evidence suggests biologic DMARDs may not directly inhibit osteoclast-mediated bone destruction (37, 38), as such bone and cartilage loss may continue. Recent advances in the understanding of RA pathogenesis has prompted the development of new therapeutic strategies to reduce inflammation and target osteoclast-mediated bone destruction

concurrently (244, 245). Thus, new targeted therapies such as XIAP, N-cadherin and NF-κB inhibitors, as discussed below, have the potential to greatly improve the management of disease progression in RA.

1.9. Novel therapeutic targets in rheumatoid arthritis

Despite many advances being made in the understanding of cellular and molecular processes of inflammation and bone destruction in RA, few safe and effective treatments target both pathological processes. Research into novel treatments to control joint inflammation and bone destruction in RA is now focused on natural and synthetic compounds that target apoptosis and specific cytokine-mediated processes.

1.9.1. XIAP as a therapeutic target of intracellular anti-apoptotic molecules in rheumatoid arthritis

Pro- or anti-apoptotic molecules have the potential to be novel targets for RA treatment, as promoting apoptosis may be beneficial in reducing RA pathogenic features. As several intracellular apoptotic inhibitory molecules have been found to be up regulated in RA (157, 162-164, 166, 215), research now focuses on small molecule forms of these inhibitors as potential compounds for RA treatment. XIAP is a potent suppressor of apoptosis, acting directly through the suppression of caspases 3, 7 and 9 (Figure 1.6) (246, 247). XIAP has therefore been identified as a new molecular target in the design of novel drugs to overcome apoptosis resistance of cells (Figure 1.6). Compounds developed to inhibit IAP actions are either in the form of normally occurring non-peptide small molecule inhibitors such as Embelin (Figure 1.6) (248), or synthetic antisense oligonucleotides and antagonist molecules such as AEG35156, which has been clinically tested for various cancer treatments (249). Extensive research has identified numerous anti-inflammatory benefits of Embelin, thus its potential use as a novel therapeutic for RA treatment will be discussed further.
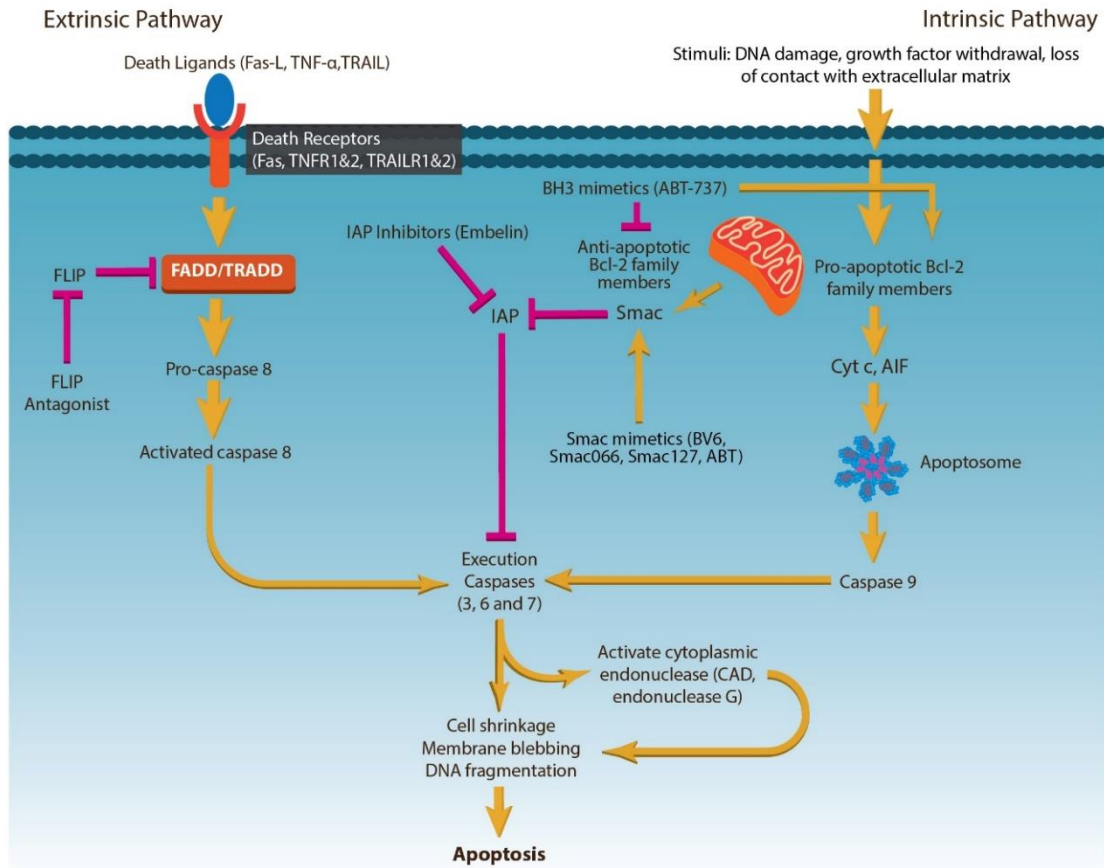
Figure 1.6. Proposed influence of antagonists of anti-apoptotic proteins on the extrinsic and intrinsic apoptotic pathways. Schematic diagram of the intrinsic and extrinsic apoptosis pathways. In RA, apoptosis is thought to be inhibited by FLIP, IAP and Bcl-2 proteins. Small molecule forms of these intracellular inhibitory molecules, such as FLIP antagonists, IAP inhibitors, BH3 mimetics and Smac mimetics are potential compounds for RA treatment as they can inhibit anti-apoptotic proteins to induce apoptosis. AIF, apoptosis-inducing factor; CAD, caspase-activated DNase; Cyt c, cytochrome c; FADD, Fas associated death domain; Fas-L, Fas ligand; FLIP, FLICE-like inhibitory protein; IAP, inhibitor of apoptosis protein; TNF-α, tumour necrosis factor alpha; TRADD, TNF receptor type-1 associated death domain protein; TRAIL, TNF-related apoptosis inducing ligand.

1.9.1.1. XIAP inhibition using Embelin for treatment in rheumatoid arthritis

Embelin (2, 5-dihydroxy-3-undecyl-1, 4-benzoquinone) is a naturally occurring alkyl substituted hydroxyl benzoquinone and is an active constituent of the fruit Embelia ribes BRUM (250). Embelin is a cell permeable non-peptide small molecule inhibitor of XIAP (251-253). Embelin has been found to have anti-inflammatory, anti-tumour and analgesic properties, however the precise mechanism underlying the different properties of Embelin is still unclear. The anti-inflammatory effects of Embelin have been investigated in several acute and chronic models of inflammation and are reviewed in detail by Williams, Dharmapatni and Crotti 2018 (see Appendix II) (254).

Extensive research has identified the benefits of Embelin by induction of growth inhibition and apoptosis in various types of human cancer cells (255-258). Embelin induces apoptosis in T98G glioma cells, pancreatic cancer, PC-3 prostate cancer and human leukaemia cell lines with high levels of XIAP and reduced levels of anti-apoptotic Bcl-2 family proteins (255-257, 259). As inflammatory cells and FLS in the RA synovium are thought to have similar properties to cancer cells, we propose Embelin may also be beneficial in the treatment of RA (47, 260).

There is now growing research on the anti-inflammatory and anti-apoptotic properties of Embelin in the context of RA and it is thought that Embelin may be beneficial in reducing chronic inflammation and bone erosion in the synovial joints. Embelin can suppress RANKL-induced osteoclastogenesis from RAW 264.7 cells *in vitro* (261). In this study, Embelin dose-dependently decreased the number of TRAP positive cells with almost complete inhibition post RANKL exposure (261). Embelin also induced apoptosis in mature osteoclasts, confirmed by increased activation of caspase 3 (261), suggesting that Embelin may be beneficial in both inhibiting the differentiation of osteoclasts and inducing apoptosis in mature and active osteoclasts. However, it is not clear if apoptosis of osteoclasts or inhibition of osteoclastogenesis is due to the inhibition of NF-κB, thus further research to elucidate the cross talk between NF-κB and the apoptosis pathway is required.

Recently, Embelin has been used to treat inflammation and bone erosion in a CAIA mouse model (215). In this study, Embelin at 30 mg/kg/day and 50 mg/kg/day suppressed inflammation clinically and microscopically, with the lower dose of Embelin significantly reducing inflammation, cartilage and bone degradation and pannus formation in the front paws of mice (215). This demonstrates that Embelin at a low dose can suppress joint inflammation and bone erosion in an acute inflammatory arthritis mouse model. Dharmapatni *et al.* 2015, also demonstrated that CAIA mice treated with low dose (30 mg/kg/day) Embelin had significantly increased numbers of apoptotic cells in the pannus of synovial joints as evidenced by increased terminal deoxynucleotidyl transferase nick-end labelling (TUNEL) staining (215). These mice also had reduced numbers of TRAP positive osteoclasts, suggesting that Embelin may be acting to suppress osteoclast activity as well as initiating apoptosis in these cells (215). However, the exact mechanism of action of Embelin to reduce bone erosion is still unclear. It is known that Embelin specifically inhibits XIAP, however, in this study there was no difference in XIAP protein expression within cells in the pannus, articular cartilage and bone marrow (215). Thus, the study could not conclude whether Embelin was completing its action by inhibition of XIAP expression. Although the beneficial effects of Embelin have been highlighted in an inflammatory arthritis mouse model, future research is required to further identify the specific mechanism of action and cell targets of Embelin.

Despite promising research into the effects of Embelin in RA, pre-clinical efforts have been hampered due to its poor aqueous solubility which leads to poor bioavailability via oral administration. As a result, new techniques and derivatives of Embelin have been trialled to improve solubility (262, 263). However, further research into these techniques or the use of Embelin derivatives for RA treatment and whether they will have the same mechanisms of action is required before clinical trials can be conducted. A possible alternative to overcome the poor solubility and bioavailability of Embelin is combining its use with a commonly used DMARD which suppresses autophagy, such as Hydroxychloroquine (HCQ). Importantly, recent studies have shown to reduce the occurrence and severity of inflammatory arthritis through suppression of the autophagy process *in vivo* (172). Similar to Embelin, the effectiveness of HCQ is limited by its slow onset of action to prevent bone erosion in RA. Thus, combination of the apoptosis inducer Embelin and autophagy inhibitor HCQ may enhance the effectiveness in reducing bone

erosion in RA by targeting both apoptosis and autophagy pathways and will be investigated further in chapter two.

1.9.2. Therapeutics targeting NF-kappa B in rheumatoid arthritis

An accumulating amount of evidence has shown that modulators of NF-κB signalling have a great therapeutic potential (85). Thus, there is growing interest in the generation of NF-κB inhibitors with a higher specificity and the effectiveness to treat human diseases. Several natural or synthetic NF-κB inhibitors have been identified and produced, including gliotoxin (264), Curcumin (265) and NEMO-binding peptide (266). These inhibitors interfere and exert their suppressive effects on NF-κB at different target sites and have successfully demonstrated effectiveness in inhibiting osteoclastogenesis and bone resorption *in vitro* and *in vivo* (82). The effects of selective inhibition of RANKL-induced NF-κB activation for the treatment of pathological bone disorders such as RA has recently been demonstrated with the compound Parthenolide (PAR).

PAR is a sesquiterpene lactone found in the Asteraceae family of medicinal plants, including Feverfew (267). PAR has been reported to have both anti-inflammatory and anti-tumorigenic actions (268, 269) and inhibits the activation of NF-κB transcriptional factors by preventing the degradation of the IκB kinase complex (270, 271). PAR has been found to block bacterial induced osteolysis in mice via inhibition of LPS-induced NF-κB activation (272) as well as inhibit ovariectomy-induced bone loss when administered at higher doses (3 and 10 mg/kg) (273). The inhibition of NF-κB activation by PAR also reduced methotrexate-induced osteoclastogenesis, in the associated pro-inflammatory cytokine production and NF-κB activation observed as a result of methotrexate chemotherapy (274). Recently, PAR was demonstrated to inhibit the effects of pro-inflammatory cytokines on cultured human chondrocytes, as well as attenuate the progression of CIA in rats (275). This was evident as PAR reduced inflammation and pannus formation in the proximal and distal interphalangeal joints in CIA rats (275). However, within this study there was no suppression of generalised osteopenia, nor clear anti-osteoclastic effects of PAR beyond its anti-inflammatory effect at the inflamed joint (275). The low PAR dosage (1 mg/kg) thus may not be sufficient to demonstrate a potential disconnect between synovitis and bone erosion. The recent reported qualities of

PAR as an anti-inflammatory, anti-osteoclastogenic and anti-tumorigenic compound thus make it appealing as a potential alternative therapeutic for RA. Preclinical studies for the application of PAR are currently lacking as further *in vivo* studies are required to identify the most suitable dose to reduce both inflammation and bone erosion concurrently. Thus, the effect of low dose PAR on inflammation, bone erosion and pain like-behaviour in an *in vivo* model of inflammatory arthritis will be investigated further in chapter four.

1.10. Conclusion

Significant advances have been made in the understanding of cellular and molecular processes of inflammation and bone destruction in RA through the extensive and complementary use of human and *in vivo* animal studies. Despite this, a strong unmet medical need remains. Only a minor portion of patients reach sustained clinical remission and few safe and effective treatments target both inflammation and bone destruction simultaneously, while also reducing RA associated pain. This has therefore prompted the development of new therapeutic strategies that can not only reduce inflammation and osteoclast-mediated bone destruction concurrently but also reduce RA associated pain. NF-κB signalling, cell adhesion molecules and anti-apoptotic proteins have emerged as new targets in the progression of bone destruction in RA. Further research is required to understand the specific role these molecules have in osteoclast mediated bone destruction both in physiological and pathological states. Overall, identification of safe and effective therapeutics that target inflammation, bone resorption and pain, will not only improve our treatment of RA, but also other bone loss pathologies.

1.11. Thesis Hypothesis and Aims

Three hypotheses were proposed. Firstly, that *targeting autophagy and apoptotic pathways individually and simultaneously through pharmacological modulation will reduce osteoclast activity in vitro and suppress bone resorption in inflammatory arthritis*. Secondly, that *topical antagonists targeting N-cadherin will reduce local inflammation and bone erosion in inflammatory arthritis*. The final hypothesis is that *inhibition of NF-κB will reduce local inflammation and bone erosion in inflammatory arthritis*. *In vitro* studies were carried out with human peripheral blood mononuclear cells (PBMC) with the addition of the inflammatory cytokine TNF-α to represent an inflammatory stimulus. *In vivo* studies were carried out using a mild collagen antibody-induced arthritis (CAIA) mouse model of inflammatory arthritis.

To test these hypotheses the following 4 aims were addressed:

1.

   a. To determine if targeted inhibition of autophagy with HCQ and induction of apoptosis with Embelin would reduce human osteoclast formation and bone resorption in osteoclasts derived from human PBMCs stimulated by the inflammatory cytokine TNF-α.

   b. To determine the effects of HCQ, Embelin and the combination of HCQ and Embelin on local inflammation and bone destruction in a CAIA mouse model.

2. To investigate the effects of a topical, cell adhesion molecule inhibitor on local inflammation, pannus formation and bone erosion in a CAIA mouse model.

3. To investigate the effect of the NF-κB inhibitor, Parthenolide, on inflammation, bone erosion and pain-like behaviour *in vivo*.

4. To optimise the severity of local inflammation and bone destruction and identify pain-like behaviour in the *in vivo* CAIA model with an increased dose of monoclonal antibodies and a low dose of *E. coli* lipopolysaccharide for more accurate use of the CAIA model in future investigations.

1.12. References

1. Romas E, Gillespie MT, Martin TJ. Involvement of receptor activator of NFkappaB ligand and tumor necrosis factor-alpha in bone destruction in rheumatoid arthritis. Bone. 2002;30(2):340-6.

2. Schett G. Erosive arthritis. Arthritis research & therapy. 2007;9 Suppl 1:S2.

3. Arnett FC, Edworthy SM, Bloch DA, McShane DJ, Fries JF, Cooper NS, et al. The American Rheumatism Association 1987 revised criteria for the classification of rheumatoid arthritis. Arthritis and rheumatism. 1988;31(3):315-24.

4. Cross M, Smith E, Hoy D, Carmona L, Wolfe F, Vos T, et al. The global burden of rheumatoid arthritis: estimates from the global burden of disease 2010 study. Annals of the rheumatic diseases. 2014;73(7):1316-22.

5. Ackerman IN, Pratt C, Gorelik A, Liew D. Projected Burden of Osteoarthritis and Rheumatoid Arthritis in Australia: A Population-Level Analysis. Arthritis care & research. 2018;70(6):877-83.

6. Hochberg MC. Changes in the incidence and prevalence of rheumatoid arthritis in England and Wales, 1970-1982. Seminars in arthritis and rheumatism. 1990;19(5):294-302.

7. Helmick CG, Felson DT, Lawrence RC, Gabriel S, Hirsch R, Kwoh CK, et al. Estimates of the prevalence of arthritis and other rheumatic conditions in the United States. Part I. Arthritis and rheumatism. 2008;58(1):15-25.

8. Hunter TM, Boytsov NN, Zhang X, Schroeder K, Michaud K, Araujo AB. Prevalence of rheumatoid arthritis in the United States adult population in healthcare claims databases, 2004-2014. Rheumatology international. 2017;37(9):1551-7.

9. Doran MF, Pond GR, Crowson CS, O'Fallon WM, Gabriel SE. Trends in incidence and mortality in rheumatoid arthritis in Rochester, Minnesota, over a forty-year period. Arthritis and rheumatism. 2002;46(3):625-31.

10. Burmester GR, Feist E, Dorner T. Emerging cell and cytokine targets in rheumatoid arthritis. Nature reviews Rheumatology. 2014;10(2):77-88.

11. Steiner G, Smolen J. Autoantibodies in rheumatoid arthritis and their clinical significance. Arthritis research. 2002;4 Suppl 2:S1-5.

12. Agrawal S, Misra R, Aggarwal A. Autoantibodies in rheumatoid arthritis: association with severity of disease in established RA. Clinical rheumatology. 2007;26(2):201-4.

13. Combe B, Eliaou JF, Daures JP, Meyer O, Clot J, Sany J. Prognostic factors in rheumatoid arthritis. Comparative study of two subsets of patients according to severity of articular damage. British journal of rheumatology. 1995;34(6):529-34.

14. Neumann E, Lefevre S, Zimmermann B, Gay S, Muller-Ladner U. Rheumatoid arthritis progression mediated by activated synovial fibroblasts. Trends in molecular medicine. 2010;16(10):458-68.

15. McInnes IB, Schett G. Cytokines in the pathogenesis of rheumatoid arthritis. Nature reviews Immunology. 2007;7(6):429-42.

16. Walsh NC, Crotti TN, Goldring SR, Gravallese EM. Rheumatic diseases: the effects of inflammation on bone. Immunological reviews. 2005;208:228-51.

17. Haynes DR, Barg E, Crotti TN, Holding C, Weedon H, Atkins GJ, et al. Osteoprotegerin expression in synovial tissue from patients with rheumatoid arthritis, spondyloarthropathies and osteoarthritis and normal controls. Rheumatology (Oxford, England). 2003;42(1):123-34.

18. Quinn JM, Horwood NJ, Elliott J, Gillespie MT, Martin TJ. Fibroblastic stromal cells express receptor activator of NF-kappa B ligand and support osteoclast differentiation. Journal of bone and mineral research : the official journal of the American Society for Bone and Mineral Research. 2000;15(8):1459-66.

19. Braun T, Zwerina J. Positive regulators of osteoclastogenesis and bone resorption in rheumatoid arthritis. Arthritis research & therapy. 2011;13(4):235.

20. McInnes IB, Schett G. The pathogenesis of rheumatoid arthritis. The New England journal of medicine. 2011;365(23):2205-19.

21. Redlich K, Smolen JS. Inflammatory bone loss: pathogenesis and therapeutic intervention. Nature reviews Drug discovery. 2012;11(3):234-50.

22. Lee YC, Cui J, Lu B, Frits ML, Iannaccone CK, Shadick NA, et al. Pain persists in DAS28 rheumatoid arthritis remission but not in ACR/EULAR remission: a longitudinal observational study. Arthritis research & therapy. 2011;13(3):R83.

23. Heiberg T, Kvien TK. Preferences for improved health examined in 1,024 patients with rheumatoid arthritis: pain has highest priority. Arthritis and rheumatism. 2002;47(4):391-7.

24. Schaible HG, Richter F, Ebersberger A, Boettger MK, Vanegas H, Natura G, et al. Joint pain. Experimental brain research. 2009;196(1):153-62.

25. Kidd BL, Urban LA. Mechanisms of inflammatory pain. British journal of anaesthesia. 2001;87(1):3-11.

26. Schaible HG, Ebersberger A, Von Banchet GS. Mechanisms of pain in arthritis. Annals of the New York Academy of Sciences. 2002;966:343-54.

27. Meeus M, Vervisch S, De Clerck LS, Moorkens G, Hans G, Nijs J. Central sensitization in patients with rheumatoid arthritis: a systematic literature review. Seminars in arthritis and rheumatism. 2012;41(4):556-67.

28. Edwards RR, Wasan AD, Bingham CO, 3rd, Bathon J, Haythornthwaite JA, Smith MT, et al. Enhanced reactivity to pain in patients with rheumatoid arthritis. Arthritis research & therapy. 2009;11(3):R61.

29. Pollard LC, Ibrahim F, Choy EH, Scott DL. Pain thresholds in rheumatoid arthritis: the effect of tender point counts and disease duration. The Journal of rheumatology. 2012;39(1):28-31.

30. Wolfe F, Michaud K. Assessment of pain in rheumatoid arthritis: minimal clinically significant difference, predictors, and the effect of anti-tumor necrosis factor therapy. The Journal of rheumatology. 2007;34(8):1674-83.

31. Bas DB, Su J, Sandor K, Agalave NM, Lundberg J, Codeluppi S, et al. Collagen antibody-induced arthritis evokes persistent pain with spinal glial involvement and transient prostaglandin dependency. Arthritis and rheumatism. 2012;64(12):3886-96.

32. Leffler AS, Kosek E, Lerndal T, Nordmark B, Hansson P. Somatosensory perception and function of diffuse noxious inhibitory controls (DNIC) in patients suffering from rheumatoid arthritis. European journal of pain (London, England). 2002;6(2):161-76.

33. McWilliams DF, Walsh DA. Pain mechanisms in rheumatoid arthritis. Clinical and experimental rheumatology. 2017;35 Suppl 107(5):94-101.

34. Leeb BF, Andel I, Sautner J, Nothnagl T, Rintelen B. The DAS28 in rheumatoid arthritis and fibromyalgia patients. Rheumatology (Oxford, England). 2004;43(12):1504-7.

35. Kukar M, Petryna O, Efthimiou P. Biological targets in the treatment of rheumatoid arthritis: a comprehensive review of current and in-development

biological disease modifying anti-rheumatic drugs. Biologics : targets & therapy. 2009;3:443-57.

36. McWilliams DF, Zhang W, Mansell JS, Kiely PD, Young A, Walsh DA. Predictors of change in bodily pain in early rheumatoid arthritis: an inception cohort study. Arthritis care & research. 2012;64(10):1505-13.

37. Smolen JS, Han C, van der Heijde DM, Emery P, Bathon JM, Keystone E, et al. Radiographic changes in rheumatoid arthritis patients attaining different disease activity states with methotrexate monotherapy and infliximab plus methotrexate: the impacts of remission and tumour necrosis factor blockade. Annals of the rheumatic diseases. 2009;68(6):823-7.

38. Landewe R, van der Heijde D, Klareskog L, van Vollenhoven R, Fatenejad S. Disconnect between inflammation and joint destruction after treatment with etanercept plus methotrexate: results from the trial of etanercept and methotrexate with radiographic and patient outcomes. Arthritis and rheumatism. 2006;54(10):3119-25.

39. Wiles NJ, Scott DG, Barrett EM, Merry P, Arie E, Gaffney K, et al. Benchmarking: the five year outcome of rheumatoid arthritis assessed using a pain score, the Health Assessment Questionnaire, and the Short Form-36 (SF-36) in a community and a clinic based sample. Annals of the rheumatic diseases. 2001;60(10):956-61.

40. Rupp I, Boshuizen HC, Roorda LD, Dinant HJ, Jacobi CE, van den Bos G. Course of patient-reported health outcomes in rheumatoid arthritis: comparison of longitudinal and cross-sectional approaches. The Journal of rheumatology. 2006;33(2):228-33.

41. Pacifici M, Koyama E, Iwamoto M. Mechanisms of synovial joint and articular cartilage formation: recent advances, but many lingering mysteries. Birth defects research Part C, Embryo today : reviews. 2005;75(3):237-48.

42. Archer CW, Dowthwaite GP, Francis-West P. Development of synovial joints. Birth defects research Part C, Embryo today : reviews. 2003;69(2):144-55.

43. Henderson B, Pettipher ER. The synovial lining cell: biology and pathobiology. Seminars in arthritis and rheumatism. 1985;15(1):1-32.

44. Revell PA. Synovial lining cells. Rheumatology international. 1989;9(2):49-51.

45.   Noss EH, Brenner MB. The role and therapeutic implications of fibroblast-like synoviocytes in inflammation and cartilage erosion in rheumatoid arthritis. Immunological reviews. 2008;223:252-70.

46.   Muller-Ladner U, Ospelt C, Gay S, Distler O, Pap T. Cells of the synovium in rheumatoid arthritis. Synovial fibroblasts. Arthritis research & therapy. 2007;9(6):223.

47.   Bartok B, Firestein GS. Fibroblast-like synoviocytes: key effector cells in rheumatoid arthritis. Immunological reviews. 2010;233(1):233-55.

48.   Perlman H, Pope RM. The synovial lining micromass system: toward rheumatoid arthritis in a dish? Arthritis and rheumatism. 2010;62(3):643-6.

49.   Choy EH, Panayi GS. Cytokine pathways and joint inflammation in rheumatoid arthritis. The New England journal of medicine. 2001;344(12):907-16.

50.   Firestein GS. Evolving concepts of rheumatoid arthritis. Nature. 2003;423(6937):356-61.

51.   Lerner UH. Osteoclast formation and resorption. Matrix biology : journal of the International Society for Matrix Biology. 2000;19(2):107-20.

52.   Parfitt AM. Osteonal and hemi-osteonal remodeling: the spatial and temporal framework for signal traffic in adult human bone. Journal of cellular biochemistry. 1994;55(3):273-86.

53.   Nuttall ME, Gimble JM. Controlling the balance between osteoblastogenesis and adipogenesis and the consequent therapeutic implications. Current opinion in pharmacology. 2004;4(3):290-4.

54.   Delfino-Machin M, Chipperfield TR, Rodrigues FS, Kelsh RN. The proliferating field of neural crest stem cells. Developmental dynamics : an official publication of the American Association of Anatomists. 2007;236(12):3242-54.

55.   Zuo C, Huang Y, Bajis R, Sahih M, Li YP, Dai K, et al. Osteoblastogenesis regulation signals in bone remodeling. Osteoporosis international : a journal established as result of cooperation between the European Foundation for Osteoporosis and the National Osteoporosis Foundation of the USA. 2012;23(6):1653-63.

56.   Cao X, Chen D. The BMP signaling and in vivo bone formation. Gene. 2005;357(1):1-8.

57.   Day TF, Guo X, Garrett-Beal L, Yang Y. Wnt/beta-catenin signaling in mesenchymal progenitors controls osteoblast and chondrocyte differentiation during vertebrate skeletogenesis. Developmental cell. 2005;8(5):739-50.

58.   Gaur T, Lengner CJ, Hovhannisyan H, Bhat RA, Bodine PV, Komm BS, et al. Canonical WNT signaling promotes osteogenesis by directly stimulating Runx2 gene expression. The Journal of biological chemistry. 2005;280(39):33132-40.

59.   Krishnan V, Bryant HU, Macdougald OA. Regulation of bone mass by Wnt signaling. The Journal of clinical investigation. 2006;116(5):1202-9.

60.   Yavropoulou MP, Yovos JG. The role of the Wnt signaling pathway in osteoblast commitment and differentiation. Hormones (Athens, Greece). 2007;6(4):279-94.

61.   Hill TP, Spater D, Taketo MM, Birchmeier W, Hartmann C. Canonical Wnt/beta-catenin signaling prevents osteoblasts from differentiating into chondrocytes. Developmental cell. 2005;8(5):727-38.

62.   Takahashi N, Akatsu T, Udagawa N, Sasaki T, Yamaguchi A, Moseley JM, et al. Osteoblastic cells are involved in osteoclast formation. Endocrinology. 1988;123(5):2600-2.

63.   Quinn JM, McGee JO, Athanasou NA. Cellular and hormonal factors influencing monocyte differentiation to osteoclastic bone-resorbing cells. Endocrinology. 1994;134(6):2416-23.

64.   Boyle WJ, Simonet WS, Lacey DL. Osteoclast differentiation and activation. Nature. 2003;423(6937):337-42.

65.   Suda T, Takahashi N, Martin TJ. Modulation of osteoclast differentiation. Endocrine reviews. 1992;13(1):66-80.

66.   Suda T, Nakamura I, Jimi E, Takahashi N. Regulation of osteoclast function. Journal of bone and mineral research : the official journal of the American Society for Bone and Mineral Research. 1997;12(6):869-79.

67.   Li Z, Kong K, Qi W. Osteoclast and its roles in calcium metabolism and bone development and remodeling. Biochemical and biophysical research communications. 2006;343(2):345-50.

68.   Takayanagi H. Osteoimmunology: shared mechanisms and crosstalk between the immune and bone systems. Nature reviews Immunology. 2007;7(4):292-304.

69.   Ross FP, Teitelbaum SL. alphavbeta3 and macrophage colony-stimulating factor: partners in osteoclast biology. Immunological reviews. 2005;208:88-105.

70. Theill LE, Boyle WJ, Penninger JM. RANK-L and RANK: T cells, bone loss, and mammalian evolution. Annual review of immunology. 2002;20:795-823.

71. Hodge JM, Collier FM, Pavlos NJ, Kirkland MA, Nicholson GC. M-CSF potently augments RANKL-induced resorption activation in mature human osteoclasts. PloS one. 2011;6(6):e21462.

72. Kearns AE, Khosla S, Kostenuik PJ. Receptor activator of nuclear factor kappaB ligand and osteoprotegerin regulation of bone remodeling in health and disease. Endocrine reviews. 2008;29(2):155-92.

73. Lacey DL, Timms E, Tan HL, Kelley MJ, Dunstan CR, Burgess T, et al. Osteoprotegerin ligand is a cytokine that regulates osteoclast differentiation and activation. Cell. 1998;93(2):165-76.

74. Wong BR, Josien R, Lee SY, Vologodskaia M, Steinman RM, Choi Y. The TRAF family of signal transducers mediates NF-kappaB activation by the TRANCE receptor. The Journal of biological chemistry. 1998;273(43):28355-9.

75. Nakashima T, Kobayashi Y, Yamasaki S, Kawakami A, Eguchi K, Sasaki H, et al. Protein expression and functional difference of membrane-bound and soluble receptor activator of NF-kappaB ligand: modulation of the expression by osteotropic factors and cytokines. Biochemical and biophysical research communications. 2000;275(3):768-75.

76. Kong YY, Feige U, Sarosi I, Bolon B, Tafuri A, Morony S, et al. Activated T cells regulate bone loss and joint destruction in adjuvant arthritis through osteoprotegerin ligand. Nature. 1999;402(6759):304-9.

77. Nakamichi Y, Udagawa N, Kobayashi Y, Nakamura M, Yamamoto Y, Yamashita T, et al. Osteoprotegerin reduces the serum level of receptor activator of NF-kappaB ligand derived from osteoblasts. Journal of immunology (Baltimore, Md : 1950). 2007;178(1):192-200.

78. Quinn JM, Elliott J, Gillespie MT, Martin TJ. A combination of osteoclast differentiation factor and macrophage-colony stimulating factor is sufficient for both human and mouse osteoclast formation in vitro. Endocrinology. 1998;139(10):4424-7.

79. Dougall WC, Glaccum M, Charrier K, Rohrbach K, Brasel K, De Smedt T, et al. RANK is essential for osteoclast and lymph node development. Genes & development. 1999;13(18):2412-24.

80.   Li J, Sarosi I, Yan XQ, Morony S, Capparelli C, Tan HL, et al. RANK is the intrinsic hematopoietic cell surface receptor that controls osteoclastogenesis and regulation of bone mass and calcium metabolism. Proceedings of the National Academy of Sciences of the United States of America. 2000;97(4):1566-71.

81.   Pettit AR, Ji H, von Stechow D, Muller R, Goldring SR, Choi Y, et al. TRANCE/RANKL knockout mice are protected from bone erosion in a serum transfer model of arthritis. The American journal of pathology. 2001;159(5):1689-99.

82.   Xu J, Wu HF, Ang ES, Yip K, Woloszyn M, Zheng MH, et al. NF-kappaB modulators in osteolytic bone diseases. Cytokine & growth factor reviews. 2009;20(1):7-17.

83.   Feng X. RANKing intracellular signaling in osteoclasts. IUBMB life. 2005;57(6):389-95.

84.   Dixit V, Mak TW. NF-kappaB signaling. Many roads lead to madrid. Cell. 2002;111(5):615-9.

85.   Karin M, Greten FR. NF-kappaB: linking inflammation and immunity to cancer development and progression. Nature reviews Immunology. 2005;5(10):749-59.

86.   Karin M, Yamamoto Y, Wang QM. The IKK NF-kappa B system: a treasure trove for drug development. Nature reviews Drug discovery. 2004;3(1):17-26.

87.   Novack DV, Yin L, Hagen-Stapleton A, Schreiber RD, Goeddel DV, Ross FP, et al. The IkappaB function of NF-kappaB2 p100 controls stimulated osteoclastogenesis. The Journal of experimental medicine. 2003;198(5):771-81.

88.   Jimi E, Ikebe T, Takahashi N, Hirata M, Suda T, Koga T. Interleukin-1 alpha activates an NF-kappaB-like factor in osteoclast-like cells. The Journal of biological chemistry. 1996;271(9):4605-8.

89.   Boyce BF, Xiu Y, Li J, Xing L, Yao Z. NF-kappaB-Mediated Regulation of Osteoclastogenesis. Endocrinology and metabolism (Seoul, Korea). 2015;30(1):35-44.

90.   Soysa NS, Alles N. NF-kappaB functions in osteoclasts. Biochemical and biophysical research communications. 2009;378(1):1-5.

91.   Bonizzi G, Karin M. The two NF-kappaB activation pathways and their role in innate and adaptive immunity. Trends in immunology. 2004;25(6):280-8.

92. Senftleben U, Cao Y, Xiao G, Greten FR, Krahn G, Bonizzi G, et al. Activation by IKKalpha of a second, evolutionary conserved, NF-kappa B signaling pathway. Science (New York, NY). 2001;293(5534):1495-9.

93. Kuratani T, Nagata K, Kukita T, Hotokebuchi T, Nakasima A, Iijima T. Induction of abundant osteoclast-like multinucleated giant cells in adjuvant arthritic rats with accompanying disordered high bone turnover. Histology and histopathology. 1998;13(3):751-9.

94. Cantley MD, Haynes DR, Marino V, Bartold PM. Pre-existing periodontitis exacerbates experimental arthritis in a mouse model. Journal of clinical periodontology. 2011;38(6):532-41.

95. Gravallese EM, Harada Y, Wang JT, Gorn AH, Thornhill TS, Goldring SR. Identification of cell types responsible for bone resorption in rheumatoid arthritis and juvenile rheumatoid arthritis. The American journal of pathology. 1998;152(4):943-51.

96. Clohisy JC, Roy BC, Biondo C, Frazier E, Willis D, Teitelbaum SL, et al. Direct inhibition of NF-kappa B blocks bone erosion associated with inflammatory arthritis. Journal of immunology (Baltimore, Md : 1950). 2003;171(10):5547-53.

97. Brown KD, Claudio E, Siebenlist U. The roles of the classical and alternative nuclear factor-kappaB pathways: potential implications for autoimmunity and rheumatoid arthritis. Arthritis research & therapy. 2008;10(4):212.

98. Larue L, Antos C, Butz S, Huber O, Delmas V, Dominis M, et al. A role for cadherins in tissue formation. Development (Cambridge, England). 1996;122(10):3185-94.

99. Takeichi M. Cadherins: a molecular family important in selective cell-cell adhesion. Annual review of biochemistry. 1990;59:237-52.

100. Ozawa M, Baribault H, Kemler R. The cytoplasmic domain of the cell adhesion molecule uvomorulin associates with three independent proteins structurally related in different species. The EMBO journal. 1989;8(6):1711-7.

101. Marie PJ. Role of N-cadherin in bone formation. Journal of cellular physiology. 2002;190(3):297-305.

102. Wheelock MJ, Johnson KR. Cadherins as modulators of cellular phenotype. Annual review of cell and developmental biology. 2003;19:207-35.

103.   Valencia X, Higgins JM, Kiener HP, Lee DM, Podrebarac TA, Dascher CC, et al. Cadherin-11 provides specific cellular adhesion between fibroblast-like synoviocytes. The Journal of experimental medicine. 2004;200(12):1673-9.

104.   Kiener HP, Lee DM, Agarwal SK, Brenner MB. Cadherin-11 induces rheumatoid arthritis fibroblast-like synoviocytes to form lining layers in vitro. The American journal of pathology. 2006;168(5):1486-99.

105.   Lee DM, Kiener HP, Agarwal SK, Noss EH, Watts GF, Chisaka O, et al. Cadherin-11 in synovial lining formation and pathology in arthritis. Science (New York, NY). 2007;315(5814):1006-10.

106.   Hatta K, Takeichi M. Expression of N-cadherin adhesion molecules associated with early morphogenetic events in chick development. Nature. 1986;320(6061):447-9.

107.   Brand-Saberi B, Gamel AJ, Krenn V, Muller TS, Wilting J, Christ B. N-cadherin is involved in myoblast migration and muscle differentiation in the avian limb bud. Developmental biology. 1996;178(1):160-73.

108.   Radice GL, Rayburn H, Matsunami H, Knudsen KA, Takeichi M, Hynes RO. Developmental defects in mouse embryos lacking N-cadherin. Developmental biology. 1997;181(1):64-78.

109.   Stains JP, Civitelli R. Cell-cell interactions in regulating osteogenesis and osteoblast function. Birth defects research Part C, Embryo today : reviews. 2005;75(1):72-80.

110.   Modarresi R, Lafond T, Roman-Blas JA, Danielson KG, Tuan RS, Seghatoleslami MR. N-cadherin mediated distribution of beta-catenin alters MAP kinase and BMP-2 signaling on chondrogenesis-related gene expression. Journal of cellular biochemistry. 2005;95(1):53-63.

111.   Agarwal SK, Lee DM, Kiener HP, Brenner MB. Coexpression of two mesenchymal cadherins, cadherin 11 and N-cadherin, on murine fibroblast-like synoviocytes. Arthritis and rheumatism. 2008;58(4):1044-54.

112.   Kim JB, Islam S, Kim YJ, Prudoff RS, Sass KM, Wheelock MJ, et al. N-Cadherin extracellular repeat 4 mediates epithelial to mesenchymal transition and increased motility. The Journal of cell biology. 2000;151(6):1193-206.

113.   Rieger-Christ KM, Lee P, Zagha R, Kosakowski M, Moinzadeh A, Stoffel J, et al. Novel expression of N-cadherin elicits in vitro bladder cell invasion via the Akt signaling pathway. Oncogene. 2004;23(27):4745-53.

114. Hemmings BA, Restuccia DF. PI3K-PKB/Akt pathway. Cold Spring Harbor perspectives in biology. 2012;4(9):a011189.

115. DeLise AM, Tuan RS. Alterations in the spatiotemporal expression pattern and function of N-cadherin inhibit cellular condensation and chondrogenesis of limb mesenchymal cells in vitro. Journal of cellular biochemistry. 2002;87(3):342-59.

116. Cho SH, Oh CD, Kim SJ, Kim IC, Chun JS. Retinoic acid inhibits chondrogenesis of mesenchymal cells by sustaining expression of N-cadherin and its associated proteins. Journal of cellular biochemistry. 2003;89(4):837-47.

117. Oberlender SA, Tuan RS. Expression and functional involvement of N-cadherin in embryonic limb chondrogenesis. Development (Cambridge, England). 1994;120(1):177-87.

118. Civitelli R. Cell-cell communication in the osteoblast/osteocyte lineage. Archives of biochemistry and biophysics. 2008;473(2):188-92.

119. Bienz M. beta-Catenin: a pivot between cell adhesion and Wnt signalling. Current biology : CB. 2005;15(2):R64-7.

120. Brembeck FH, Rosario M, Birchmeier W. Balancing cell adhesion and Wnt signaling, the key role of beta-catenin. Current opinion in genetics & development. 2006;16(1):51-9.

121. Di Benedetto A, Watkins M, Grimston S, Salazar V, Donsante C, Mbalaviele G, et al. N-cadherin and cadherin 11 modulate postnatal bone growth and osteoblast differentiation by distinct mechanisms. Journal of cell science. 2010;123(Pt 15):2640-8.

122. Melnyk VO, Shipley GD, Sternfeld MD, Sherman L, Rosenbaum JT. Synoviocytes synthesize, bind, and respond to basic fibroblast growth factor. Arthritis and rheumatism. 1990;33(4):493-500.

123. Manabe N, Oda H, Nakamura K, Kuga Y, Uchida S, Kawaguchi H. Involvement of fibroblast growth factor-2 in joint destruction of rheumatoid arthritis patients. Rheumatology (Oxford, England). 1999;38(8):714-20.

124. Nakano K, Okada Y, Saito K, Tanaka Y. Induction of RANKL expression and osteoclast maturation by the binding of fibroblast growth factor 2 to heparan sulfate proteoglycan on rheumatoid synovial fibroblasts. Arthritis and rheumatism. 2004;50(8):2450-8.

125. Byrd V, Zhao XM, McKeehan WL, Miller GG, Thomas JW. Expression and functional expansion of fibroblast growth factor receptor T cells in rheumatoid

synovium and peripheral blood of patients with rheumatoid arthritis. Arthritis and rheumatism. 1996;39(6):914-22.

126.   Troyanovsky SM. Mechanism of cell-cell adhesion complex assembly. Current opinion in cell biology. 1999;11(5):561-6.

127.   Cheng SL, Lecanda F, Davidson MK, Warlow PM, Zhang SF, Zhang L, et al. Human osteoblasts express a repertoire of cadherins, which are critical for BMP-2-induced osteogenic differentiation. Journal of bone and mineral research : the official journal of the American Society for Bone and Mineral Research. 1998;13(4):633-44.

128.   Tavella S, Raffo P, Tacchetti C, Cancedda R, Castagnola P. N-CAM and N-cadherin expression during in vitro chondrogenesis. Experimental cell research. 1994;215(2):354-62.

129.   Simonneau L, Kitagawa M, Suzuki S, Thiery JP. Cadherin 11 expression marks the mesenchymal phenotype: towards new functions for cadherins? Cell adhesion and communication. 1995;3(2):115-30.

130.   Tuan RS. Cellular signaling in developmental chondrogenesis: N-cadherin, Wnts, and BMP-2. The Journal of bone and joint surgery American volume. 2003;85-A Suppl 2:137-41.

131.   Haas AR, Tuan RS. Chondrogenic differentiation of murine C3H10T1/2 multipotential mesenchymal cells: II. Stimulation by bone morphogenetic protein-2 requires modulation of N-cadherin expression and function. Differentiation; research in biological diversity. 1999;64(2):77-89.

132.   Tuli R, Tuli S, Nandi S, Huang X, Manner PA, Hozack WJ, et al. Transforming growth factor-beta-mediated chondrogenesis of human mesenchymal progenitor cells involves N-cadherin and mitogen-activated protein kinase and Wnt signaling cross-talk. The Journal of biological chemistry. 2003;278(42):41227-36.

133.   Shin CS, Her SJ, Kim JA, Kim DH, Kim SW, Kim SY, et al. Dominant negative N-cadherin inhibits osteoclast differentiation by interfering with beta-catenin regulation of RANKL, independent of cell-cell adhesion. Journal of bone and mineral research : the official journal of the American Society for Bone and Mineral Research. 2005;20(12):2200-12.

134.   Korb A, Pavenstadt H, Pap T. Cell death in rheumatoid arthritis. Apoptosis : an international journal on programmed cell death. 2009;14(4):447-54.

135. Dharmapatni AA, Smith MD, Findlay DM, Holding CA, Evdokiou A, Ahern MJ, et al. Elevated expression of caspase-3 inhibitors, survivin and xIAP correlates with low levels of apoptosis in active rheumatoid synovium. Arthritis research & therapy. 2009;11(1):R13.

136. Metzstein MM, Stanfield GM, Horvitz HR. Genetics of programmed cell death in C. elegans: past, present and future. Trends in genetics : TIG. 1998;14(10):410-6.

137. Williams B, Tsangari E, Stansborough R, Marino V, Cantley M, Dharmapatni A, et al. Mixed effects of caffeic acid phenethyl ester (CAPE) on joint inflammation, bone loss and gastrointestinal inflammation in a murine model of collagen antibody-induced arthritis. Inflammopharmacology. 2017;25(1):55-68.

138. Locksley RM, Killeen N, Lenardo MJ. The TNF and TNF receptor superfamilies: integrating mammalian biology. Cell. 2001;104(4):487-501.

139. Wajant H. The Fas signaling pathway: more than a paradigm. Science (New York, NY). 2002;296(5573):1635-6.

140. Kischkel FC, Hellbardt S, Behrmann I, Germer M, Pawlita M, Krammer PH, et al. Cytotoxicity-dependent APO-1 (Fas/CD95)-associated proteins form a death-inducing signaling complex (DISC) with the receptor. The EMBO journal. 1995;14(22):5579-88.

141. Elmore S. Apoptosis: a review of programmed cell death. Toxicologic pathology. 2007;35(4):495-516.

142. Saelens X, Festjens N, Vande Walle L, van Gurp M, van Loo G, Vandenabeele P. Toxic proteins released from mitochondria in cell death. Oncogene. 2004;23(16):2861-74.

143. Hill MM, Adrain C, Duriez PJ, Creagh EM, Martin SJ. Analysis of the composition, assembly kinetics and activity of native Apaf-1 apoptosomes. The EMBO journal. 2004;23(10):2134-45.

144. Esposti MD. The roles of Bid. Apoptosis : an international journal on programmed cell death. 2002;7(5):433-40.

145. Zha J, Harada H, Yang E, Jockel J, Korsmeyer SJ. Serine phosphorylation of death agonist BAD in response to survival factor results in binding to 14-3-3 not BCL-X(L). Cell. 1996;87(4):619-28.

146. Schimmer AD. Inhibitor of apoptosis proteins: translating basic knowledge into clinical practice. Cancer research. 2004;64(20):7183-90.

147. Joza N, Susin SA, Daugas E, Stanford WL, Cho SK, Li CY, et al. Essential role of the mitochondrial apoptosis-inducing factor in programmed cell death. Nature. 2001;410(6828):549-54.

148. Enari M, Sakahira H, Yokoyama H, Okawa K, Iwamatsu A, Nagata S. A caspase-activated DNase that degrades DNA during apoptosis, and its inhibitor ICAD. Nature. 1998;391(6662):43-50.

149. Slee EA, Adrain C, Martin SJ. Executioner caspase-3, -6, and -7 perform distinct, non-redundant roles during the demolition phase of apoptosis. The Journal of biological chemistry. 2001;276(10):7320-6.

150. King KL, Cidlowski JA. Cell cycle regulation and apoptosis. Annual review of physiology. 1998;60:601-17.

151. Li CJ, Friedman DJ, Wang C, Metelev V, Pardee AB. Induction of apoptosis in uninfected lymphocytes by HIV-1 Tat protein. Science (New York, NY). 1995;268(5209):429-31.

152. Ethell DW, Buhler LA. Fas ligand-mediated apoptosis in degenerative disorders of the brain. Journal of clinical immunology. 2003;23(6):439-46.

153. Pope RM. Apoptosis as a therapeutic tool in rheumatoid arthritis. Nature reviews Immunology. 2002;2(7):527-35.

154. Firestein GS, Yeo M, Zvaifler NJ. Apoptosis in rheumatoid arthritis synovium. The Journal of clinical investigation. 1995;96(3):1631-8.

155. Pagliari LJ, Perlman H, Liu H, Pope RM. Macrophages require constitutive NF-kappaB activation to maintain A1 expression and mitochondrial homeostasis. Molecular and cellular biology. 2000;20(23):8855-65.

156. Perlman H, Pagliari LJ, Liu H, Koch AE, Haines GK, 3rd, Pope RM. Rheumatoid arthritis synovial macrophages express the Fas-associated death domain-like interleukin-1beta-converting enzyme-inhibitory protein and are refractory to Fas-mediated apoptosis. Arthritis and rheumatism. 2001;44(1):21-30.

157. Perlman H, Georganas C, Pagliari LJ, Koch AE, Haines K, 3rd, Pope RM. Bcl-2 expression in synovial fibroblasts is essential for maintaining mitochondrial homeostasis and cell viability. Journal of immunology (Baltimore, Md : 1950). 2000;164(10):5227-35.

158. Franz JK, Pap T, Hummel KM, Nawrath M, Aicher WK, Shigeyama Y, et al. Expression of sentrin, a novel antiapoptotic molecule, at sites of synovial invasion in rheumatoid arthritis. Arthritis and rheumatism. 2000;43(3):599-607.

159. Perlman H, Liu H, Georganas C, Koch AE, Shamiyeh E, Haines GK, 3rd, et al. Differential expression pattern of the antiapoptotic proteins, Bcl-2 and FLIP, in experimental arthritis. Arthritis and rheumatism. 2001;44(12):2899-908.

160. Catrina AI, Ulfgren AK, Lindblad S, Grondal L, Klareskog L. Low levels of apoptosis and high FLIP expression in early rheumatoid arthritis synovium. Annals of the rheumatic diseases. 2002;61(10):934-6.

161. Newmeyer DD, Bossy-Wetzel E, Kluck RM, Wolf BB, Beere HM, Green DR. Bcl-xL does not inhibit the function of Apaf-1. Cell death and differentiation. 2000;7(4):402-7.

162. Lee SY, Kwok SK, Son HJ, Ryu JG, Kim EK, Oh HJ, et al. IL-17-mediated Bcl-2 expression regulates survival of fibroblast-like synoviocytes in rheumatoid arthritis through STAT3 activation. Arthritis research & therapy. 2013;15(1):R31.

163. Zhang Q, Badell IR, Schwarz EM, Boulukos KE, Yao Z, Boyce BF, et al. Tumor necrosis factor prevents alendronate-induced osteoclast apoptosis in vivo by stimulating Bcl-xL expression through Ets-2. Arthritis and rheumatism. 2005;52(9):2708-18.

164. Hong S, Kim EJ, Lee EJ, San Koo B, Min Ahn S, Bae SH, et al. TNF-alpha confers resistance to Fas-mediated apoptosis in rheumatoid arthritis through the induction of soluble Fas. Life sciences. 2015;122:37-41.

165. Li F. Survivin study: what is the next wave? Journal of cellular physiology. 2003;197(1):8-29.

166. Ahn JK, Oh JM, Lee J, Bae EK, Ahn KS, Cha HS, et al. Increased extracellular survivin in the synovial fluid of rheumatoid arthritis patients: fibroblast-like synoviocytes as a potential source of extracellular survivin. Inflammation. 2010;33(6):381-8.

167. Salvesen GS, Duckett CS. IAP proteins: blocking the road to death's door. Nature reviews Molecular cell biology. 2002;3(6):401-10.

168. Harlin H, Reffey SB, Duckett CS, Lindsten T, Thompson CB. Characterization of XIAP-deficient mice. Molecular and cellular biology. 2001;21(10):3604-8.

169. Bai S, Liu H, Chen KH, Eksarko P, Perlman H, Moore TL, et al. NF-kappaB-regulated expression of cellular FLIP protects rheumatoid arthritis synovial fibroblasts from tumor necrosis factor alpha-mediated apoptosis. Arthritis and rheumatism. 2004;50(12):3844-55.

170. Levine B, Mizushima N, Virgin HW. Autophagy in immunity and inflammation. Nature. 2011;469(7330):323-35.

171. Amaravadi RK, Yu D, Lum JJ, Bui T, Christophorou MA, Evan GI, et al. Autophagy inhibition enhances therapy-induced apoptosis in a Myc-induced model of lymphoma. The Journal of clinical investigation. 2007;117(2):326-36.

172. Lin NY, Beyer C, Giessl A, Kireva T, Scholtysek C, Uderhardt S, et al. Autophagy regulates TNFalpha-mediated joint destruction in experimental arthritis. Annals of the rheumatic diseases. 2013;72(5):761-8.

173. Maiuri MC, Zalckvar E, Kimchi A, Kroemer G. Self-eating and self-killing: crosstalk between autophagy and apoptosis. Nature reviews Molecular cell biology. 2007;8(9):741-52.

174. Xu K, Xu P, Yao JF, Zhang YG, Hou WK, Lu SM. Reduced apoptosis correlates with enhanced autophagy in synovial tissues of rheumatoid arthritis. Inflammation research : official journal of the European Histamine Research Society [et al]. 2013;62(2):229-37.

175. Chen L, Deng H, Cui H, Fang J, Zuo Z, Deng J, et al. Inflammatory responses and inflammation-associated diseases in organs. Oncotarget. 2018;9(6):7204-18.

176. Kannan K, Ortmann RA, Kimpel D. Animal models of rheumatoid arthritis and their relevance to human disease. Pathophysiology : the official journal of the International Society for Pathophysiology. 2005;12(3):167-81.

177. Asquith DL, Miller AM, McInnes IB, Liew FY. Animal models of rheumatoid arthritis. European journal of immunology. 2009;39(8):2040-4.

178. Caplazi P, Baca M, Barck K, Carano RA, DeVoss J, Lee WP, et al. Mouse Models of Rheumatoid Arthritis. Veterinary pathology. 2015;52(5):819-26.

179. van Eden W, Thole JE, van der Zee R, Noordzij A, van Embden JD, Hensen EJ, et al. Cloning of the mycobacterial epitope recognized by T lymphocytes in adjuvant arthritis. Nature. 1988;331(6152):171-3.

180. Holmdahl R, Andersson ME, Goldschmidt TJ, Jansson L, Karlsson M, Malmstrom V, et al. Collagen induced arthritis as an experimental model for rheumatoid arthritis. Immunogenetics, pathogenesis and autoimmunity. APMIS : acta pathologica, microbiologica, et immunologica Scandinavica. 1989;97(7):575-84.

181. Trentham DE. Collagen arthritis as a relevant model for rheumatoid arthritis. Arthritis and rheumatism. 1982;25(8):911-6.

182. Brackertz D, Mitchell GF, Mackay IR. Antigen-induced arthritis in mice. I. Induction of arthritis in various strains of mice. Arthritis and rheumatism. 1977;20(3):841-50.

183. Kouskoff V, Korganow AS, Duchatelle V, Degott C, Benoist C, Mathis D. Organ-specific disease provoked by systemic autoimmunity. Cell. 1996;87(5):811-22.

184. Bevaart L, Vervoordeldonk MJ, Tak PP. Evaluation of therapeutic targets in animal models of arthritis: how does it relate to rheumatoid arthritis? Arthritis and rheumatism. 2010;62(8):2192-205.

185. Bolon B, Stolina M, King C, Middleton S, Gasser J, Zack D, et al. Rodent preclinical models for developing novel antiarthritic molecules: comparative biology and preferred methods for evaluating efficacy. Journal of biomedicine & biotechnology. 2011;2011:569068.

186. McNamee K, Williams R, Seed M. Animal models of rheumatoid arthritis: How informative are they? European journal of pharmacology. 2015;759:278-86.

187. Sardar S, Andersson A. Old and new therapeutics for Rheumatoid Arthritis: in vivo models and drug development. Immunopharmacology and immunotoxicology. 2016;38(1):2-13.

188. Fischer BD, Adeyemo A, O'Leary ME, Bottaro A. Animal models of rheumatoid pain: experimental systems and insights. Arthritis research & therapy. 2017;19(1):146.

189. Nandakumar KS, Svensson L, Holmdahl R. Collagen type II-specific monoclonal antibody-induced arthritis in mice: description of the disease and the influence of age, sex, and genes. The American journal of pathology. 2003;163(5):1827-37.

190. Khachigian LM. Collagen antibody-induced arthritis. Nature protocols. 2006;1(5):2512-6.

191. Nandakumar KS, Holmdahl R. Collagen antibody induced arthritis. Methods in molecular medicine. 2007;136:215-23.

192. Staines NA, Wooley PH. Collagen arthritis--what can it teach us? British journal of rheumatology. 1994;33(9):798-807.

193. Bas DB, Su J, Wigerblad G, Svensson CI. Pain in rheumatoid arthritis: models and mechanisms. Pain management. 2016;6(3):265-84.

194. Muley MM, Krustev E, McDougall JJ. Preclinical Assessment of Inflammatory Pain. CNS neuroscience & therapeutics. 2016;22(2):88-101.

195.   Colebatch AN, Edwards CJ, Ostergaard M, van der Heijde D, Balint PV, D'Agostino MA, et al. EULAR recommendations for the use of imaging of the joints in the clinical management of rheumatoid arthritis. Annals of the rheumatic diseases. 2013;72(6):804-14.

196.   Sudol-Szopinska I, Jans L, Teh J. Rheumatoid arthritis: what do MRI and ultrasound show. Journal of ultrasonography. 2017;17(68):5-16.

197.   Boutry N, Morel M, Flipo RM, Demondion X, Cotten A. Early rheumatoid arthritis: a review of MRI and sonographic findings. AJR American journal of roentgenology. 2007;189(6):1502-9.

198.   Freeston JE, Bird P, Conaghan PG. The role of MRI in rheumatoid arthritis: research and clinical issues. Current opinion in rheumatology. 2009;21(2):95-101.

199.   Ellegaard K, Christensen R, Torp-Pedersen S, Terslev L, Holm CC, Konig MJ, et al. Ultrasound Doppler measurements predict success of treatment with anti-TNF-α drug in patients with rheumatoid arthritis: a prospective cohort study. Rheumatology (Oxford, England). 2011;50(3):506-12.

200.   D'Agostino MA, Wakefield RJ, Berner-Hammer H, Vittecoq O, Filippou G, Balint P, et al. Value of ultrasonography as a marker of early response to abatacept in patients with rheumatoid arthritis and an inadequate response to methotrexate: results from the APPRAISE study. Annals of the rheumatic diseases. 2016;75(10):1763-9.

201.   Sugimoto H, Takeda A, Masuyama J, Furuse M. Early-stage rheumatoid arthritis: diagnostic accuracy of MR imaging. Radiology. 1996;198(1):185-92.

202.   Sugimoto H, Takeda A, Hyodoh K. Early-stage rheumatoid arthritis: prospective study of the effectiveness of MR imaging for diagnosis. Radiology. 2000;216(2):569-75.

203.   Machado PM, Koevoets R, Bombardier C, van der Heijde DM. The value of magnetic resonance imaging and ultrasound in undifferentiated arthritis: a systematic review. The Journal of rheumatology Supplement. 2011;87:31-7.

204.   Ostergaard M, Hansen M, Stoltenberg M, Jensen KE, Szkudlarek M, Pedersen-Zbinden B, et al. New radiographic bone erosions in the wrists of patients with rheumatoid arthritis are detectable with magnetic resonance imaging a median of two years earlier. Arthritis and rheumatism. 2003;48(8):2128-31.

205.   Conaghan PG, O'Connor P, McGonagle D, Astin P, Wakefield RJ, Gibbon WW, et al. Elucidation of the relationship between synovitis and bone damage: a

randomized magnetic resonance imaging study of individual joints in patients with early rheumatoid arthritis. Arthritis and rheumatism. 2003;48(1):64-71.

206. Dohn UM, Ejbjerg BJ, Court-Payen M, Hasselquist M, Narvestad E, Szkudlarek M, et al. Are bone erosions detected by magnetic resonance imaging and ultrasonography true erosions? A comparison with computed tomography in rheumatoid arthritis metacarpophalangeal joints. Arthritis research & therapy. 2006;8(4):R110.

207. Goldbach-Mansky R, Woodburn J, Yao L, Lipsky PE. Magnetic resonance imaging in the evaluation of bone damage in rheumatoid arthritis: a more precise image or just a more expensive one? Arthritis and rheumatism. 2003;48(3):585-9.

208. Perry D, Stewart N, Benton N, Robinson E, Yeoman S, Crabbe J, et al. Detection of erosions in the rheumatoid hand; a comparative study of multidetector computerized tomography versus magnetic resonance scanning. The Journal of rheumatology. 2005;32(2):256-67.

209. Ford-Hutchinson AF, Cooper DM, Hallgrimsson B, Jirik FR. Imaging skeletal pathology in mutant mice by microcomputed tomography. The Journal of rheumatology. 2003;30(12):2659-65.

210. Silva MD, Savinainen A, Kapadia R, Ruan J, Siebert E, Avitahl N, et al. Quantitative analysis of micro-CT imaging and histopathological signatures of experimental arthritis in rats. Molecular imaging. 2004;3(4):312-8.

211. Nishida S, Tsurukami H, Sakai A, Sakata T, Ikeda S, Tanaka M, et al. Stage-dependent changes in trabecular bone turnover and osteogenic capacity of marrow cells during development of type II collagen-induced arthritis in mice. Bone. 2002;30(6):872-9.

212. Chen XX, Baum W, Dwyer D, Stock M, Schwabe K, Ke HZ, et al. Sclerostin inhibition reverses systemic, periarticular and local bone loss in arthritis. Annals of the rheumatic diseases. 2013;72(10):1732-6.

213. Koo V, Hamilton PW, Williamson K. Non-invasive in vivo imaging in small animal research. Cellular oncology : the official journal of the International Society for Cellular Oncology. 2006;28(4):127-39.

214. Perilli E, Cantley M, Marino V, Crotti TN, Smith MD, Haynes DR, et al. Quantifying not only bone loss, but also soft tissue swelling, in a murine

inflammatory arthritis model using micro-computed tomography. Scandinavian journal of immunology. 2015;81(2):142-50.

215. Dharmapatni AA, Cantley MD, Marino V, Perilli E, Crotti TN, Smith MD, et al. The X-Linked Inhibitor of Apoptosis Protein Inhibitor Embelin Suppresses Inflammation and Bone Erosion in Collagen Antibody Induced Arthritis Mice. Mediators Inflamm. 2015;2015:564042.

216. Nandakumar KS, Andren M, Martinsson P, Bajtner E, Hellstrom S, Holmdahl R, et al. Induction of arthritis by single monoclonal IgG anti-collagen type II antibodies and enhancement of arthritis in mice lacking inhibitory FcgammaRIIB. European journal of immunology. 2003;33(8):2269-77.

217. Lange F, Bajtner E, Rintisch C, Nandakumar KS, Sack U, Holmdahl R. Methotrexate ameliorates T cell dependent autoimmune arthritis and encephalomyelitis but not antibody induced or fibroblast induced arthritis. Annals of the rheumatic diseases. 2005;64(4):599-605.

218. Garcia S, Bodano A, Gonzalez A, Forteza J, Gomez-Reino JJ, Conde C. Partial protection against collagen antibody-induced arthritis in PARP-1 deficient mice. Arthritis research & therapy. 2006;8(1):R14.

219. Garcia S, Forteza J, Lopez-Otin C, Gomez-Reino JJ, Gonzalez A, Conde C. Matrix metalloproteinase-8 deficiency increases joint inflammation and bone erosion in the K/BxN serum-transfer arthritis model. Arthritis research & therapy. 2010;12(6):R224.

220. Singh JA, Saag KG, Bridges SL, Jr., Akl EA, Bannuru RR, Sullivan MC, et al. 2015 American College of Rheumatology Guideline for the Treatment of Rheumatoid Arthritis. Arthritis care & research. 2016;68(1):1-25.

221. Smolen JS, Landewe R, Bijlsma J, Burmester G, Chatzidionysiou K, Dougados M, et al. EULAR recommendations for the management of rheumatoid arthritis with synthetic and biological disease-modifying antirheumatic drugs: 2016 update. Annals of the rheumatic diseases. 2017;76(6):960-77.

222. Burmester GR, Bijlsma JWJ, Cutolo M, McInnes IB. Managing rheumatic and musculoskeletal diseases - past, present and future. Nature reviews Rheumatology. 2017;13(7):443-8.

223. Chatzidionysiou K, Emamikia S, Nam J, Ramiro S, Smolen J, van der Heijde D, et al. Efficacy of glucocorticoids, conventional and targeted synthetic disease-modifying antirheumatic drugs: a systematic literature review informing the 2016

update of the EULAR recommendations for the management of rheumatoid arthritis. Annals of the rheumatic diseases. 2017;76(6):1102-7.

224.   Doan T, Massarotti E. Rheumatoid arthritis: an overview of new and emerging therapies. Journal of clinical pharmacology. 2005;45(7):751-62.

225.   Schett G, Stach C, Zwerina J, Voll R, Manger B. How antirheumatic drugs protect joints from damage in rheumatoid arthritis. Arthritis and rheumatism. 2008;58(10):2936-48.

226.   Choy EH, Kingsley GH, Khoshaba B, Pipitone N, Scott DL. A two year randomised controlled trial of intramuscular depot steroids in patients with established rheumatoid arthritis who have shown an incomplete response to disease modifying antirheumatic drugs. Annals of the rheumatic diseases. 2005;64(9):1288-93.

227.   Donahue KE, Gartlehner G, Jonas DE, Lux LJ, Thieda P, Jonas BL, et al. Systematic review: comparative effectiveness and harms of disease-modifying medications for rheumatoid arthritis. Annals of internal medicine. 2008;148(2):124-34.

228.   Fleishmann RM. Safety of anakinra, a recombinant interleukin-1 receptor antagonist (r-metHuIL-1ra), in patients with rheumatoid arthritis and comparison to anti-TNF-alpha agents. Clinical and experimental rheumatology. 2002;20(5 Suppl 27):S35-41.

229.   Strand V, Sokolove J. Randomized controlled trial design in rheumatoid arthritis: the past decade. Arthritis research & therapy. 2009;11(1):205.

230.   Smith MD, Kraan MC, Slavotinek J, Au V, Weedon H, Parker A, et al. Treatment-induced remission in rheumatoid arthritis patients is characterized by a reduction in macrophage content of synovial biopsies. Rheumatology (Oxford, England). 2001;40(4):367-74.

231.   Nakazawa F, Matsuno H, Yudoh K, Katayama R, Sawai T, Uzuki M, et al. Methotrexate inhibits rheumatoid synovitis by inducing apoptosis. The Journal of rheumatology. 2001;28(8):1800-8.

232.   Weinblatt ME. Methotrexate in rheumatoid arthritis: a quarter century of development. Transactions of the American Clinical and Climatological Association. 2013;124:16-25.

233.   Cronstein BN. Low-dose methotrexate: a mainstay in the treatment of rheumatoid arthritis. Pharmacological reviews. 2005;57(2):163-72.

234. Barton JL. Patient preferences and satisfaction in the treatment of rheumatoid arthritis with biologic therapy. Patient preference and adherence. 2009;3:335-44.

235. Moreland LW, O'Dell JR, Paulus HE, Curtis JR, Bathon JM, St Clair EW, et al. A randomized comparative effectiveness study of oral triple therapy versus etanercept plus methotrexate in early aggressive rheumatoid arthritis: the treatment of Early Aggressive Rheumatoid Arthritis Trial. Arthritis and rheumatism. 2012;64(9):2824-35.

236. O'Dell JR, Mikuls TR, Taylor TH, Ahluwalia V, Brophy M, Warren SR, et al. Therapies for active rheumatoid arthritis after methotrexate failure. The New England journal of medicine. 2013;369(4):307-18.

237. van Vollenhoven RF, Ernestam S, Geborek P, Petersson IF, Coster L, Waltbrand E, et al. Addition of infliximab compared with addition of sulfasalazine and hydroxychloroquine to methotrexate in patients with early rheumatoid arthritis (Swefot trial): 1-year results of a randomised trial. Lancet (London, England). 2009;374(9688):459-66.

238. Herman S, Kronke G, Schett G. Molecular mechanisms of inflammatory bone damage: emerging targets for therapy. Trends in molecular medicine. 2008;14(6):245-53.

239. Heiberg MS, Koldingsnes W, Mikkelsen K, Rodevand E, Kaufmann C, Mowinckel P, et al. The comparative one-year performance of anti-tumor necrosis factor alpha drugs in patients with rheumatoid arthritis, psoriatic arthritis, and ankylosing spondylitis: results from a longitudinal, observational, multicenter study. Arthritis and rheumatism. 2008;59(2):234-40.

240. Hoff M, Haugeberg G, Odegard S, Syversen S, Landewe R, van der Heijde D, et al. Cortical hand bone loss after 1 year in early rheumatoid arthritis predicts radiographic hand joint damage at 5-year and 10-year follow-up. Annals of the rheumatic diseases. 2009;68(3):324-9.

241. Emery P, Breedveld F, van der Heijde D, Ferraccioli G, Dougados M, Robertson D, et al. Two-year clinical and radiographic results with combination etanercept-methotrexate therapy versus monotherapy in early rheumatoid arthritis: a two-year, double-blind, randomized study. Arthritis and rheumatism. 2010;62(3):674-82.

242. Hazlewood GS, Barnabe C, Tomlinson G, Marshall D, Devoe D, Bombardier C. Methotrexate monotherapy and methotrexate combination therapy with

traditional and biologic disease modifying antirheumatic drugs for rheumatoid arthritis: abridged Cochrane systematic review and network meta-analysis. BMJ (Clinical research ed). 2016;353:i1777.

243. Dekkers JS, Schoones JW, Huizinga TW, Toes RE, van der Helm-van Mil AH. Possibilities for preventive treatment in rheumatoid arthritis? Lessons from experimental animal models of arthritis: a systematic literature review and meta-analysis. Annals of the rheumatic diseases. 2017;76(2):458-67.

244. Kahlenberg JM, Fox DA. Advances in the medical treatment of rheumatoid arthritis. Hand clinics. 2011;27(1):11-20.

245. Curtis JR, Singh JA. Use of biologics in rheumatoid arthritis: current and emerging paradigms of care. Clinical therapeutics. 2011;33(6):679-707.

246. Deveraux QL, Takahashi R, Salvesen GS, Reed JC. X-linked IAP is a direct inhibitor of cell-death proteases. Nature. 1997;388(6639):300-4.

247. Deveraux QL, Roy N, Stennicke HR, Van Arsdale T, Zhou Q, Srinivasula SM, et al. IAPs block apoptotic events induced by caspase-8 and cytochrome c by direct inhibition of distinct caspases. The EMBO journal. 1998;17(8):2215-23.

248. Carter BZ, Mak DH, Morris SJ, Borthakur G, Estey E, Byrd AL, et al. XIAP antisense oligonucleotide (AEG35156) achieves target knockdown and induces apoptosis preferentially in CD34+38- cells in a phase 1/2 study of patients with relapsed/refractory AML. Apoptosis : an international journal on programmed cell death. 2011;16(1):67-74.

249. Mahadevan D, Chalasani P, Rensvold D, Kurtin S, Pretzinger C, Jolivet J, et al. Phase I trial of AEG35156 an antisense oligonucleotide to XIAP plus gemcitabine in patients with metastatic pancreatic ductal adenocarcinoma. American journal of clinical oncology. 2013;36(3):239-43.

250. Mahendran S, Badami S, Ravi S, Thippeswamy BS, Veerapur VP. Synthesis and evaluation of analgesic and anti-inflammatory activities of most active free radical scavenging derivatives of embelin-A structure-activity relationship. Chemical & pharmaceutical bulletin. 2011;59(8):913-9.

251. Nikolovska-Coleska Z, Xu L, Hu Z, Tomita Y, Li P, Roller PP, et al. Discovery of embelin as a cell-permeable, small-molecular weight inhibitor of XIAP through structure-based computational screening of a traditional herbal medicine three-dimensional structure database. Journal of medicinal chemistry. 2004;47(10):2430-40.

252. Chen J, Nikolovska-Coleska Z, Wang G, Qiu S, Wang S. Design, synthesis, and characterization of new embelin derivatives as potent inhibitors of X-linked inhibitor of apoptosis protein. Bioorganic & medicinal chemistry letters. 2006;16(22):5805-8.

253. Xu M, Cui J, Fu H, Proksch P, Lin W, Li M. Embelin derivatives and their anticancer activity through microtubule disassembly. Planta medica. 2005;71(10):944-8.

254. Williams B, Dharmapatni A, Crotti T. Intracellular apoptotic pathways: a potential target for reducing joint damage in rheumatoid arthritis. Inflammation research : official journal of the European Histamine Research Society [et al]. 2018;67(3):219-31.

255. Park N, Baek HS, Chun YJ. Embelin-Induced Apoptosis of Human Prostate Cancer Cells Is Mediated through Modulation of Akt and beta-Catenin Signaling. PloS one. 2015;10(8):e0134760.

256. Peng M, Huang B, Zhang Q, Fu S, Wang D, Cheng X, et al. Embelin inhibits pancreatic cancer progression by directly inducing cancer cell apoptosis and indirectly restricting IL-6 associated inflammatory and immune suppressive cells. Cancer letters. 2014;354(2):407-16.

257. Hu R, Yang Y, Liu Z, Jiang H, Zhu K, Li J, et al. The XIAP inhibitor Embelin enhances TRAIL-induced apoptosis in human leukemia cells by DR4 and DR5 upregulation. Tumour biology : the journal of the International Society for Oncodevelopmental Biology and Medicine. 2015;36(2):769-77.

258. Wang DG, Sun YB, Ye F, Li W, Kharbuja P, Gao L, et al. Anti-tumor activity of the X-linked inhibitor of apoptosis (XIAP) inhibitor embelin in gastric cancer cells. Molecular and cellular biochemistry. 2014;386(1-2):143-52.

259. Park SY, Lim SL, Jang HJ, Lee JH, Um JY, Kim SH, et al. Embelin induces apoptosis in human glioma cells through inactivating NF-kappaB. Journal of pharmacological sciences. 2013;121(3):192-9.

260. Davis LS. A question of transformation: the synovial fibroblast in rheumatoid arthritis. The American journal of pathology. 2003;162(5):1399-402.

261. Reuter S, Prasad S, Phromnoi K, Kannappan R, Yadav VR, Aggarwal BB. Embelin suppresses osteoclastogenesis induced by receptor activator of NF-kappaB ligand and tumor cells in vitro through inhibition of the NF-kappaB cell signaling pathway. Molecular cancer research : MCR. 2010;8(10):1425-36.

262. Singh B, Guru SK, Sharma R, Bharate SS, Khan IA, Bhushan S, et al. Synthesis and anti-proliferative activities of new derivatives of embelin. Bioorganic & medicinal chemistry letters. 2014;24(20):4865-70.

263. Lu H, Wang J, Wang Y, Qiao L, Zhou Y. Embelin and Its Role in Chronic Diseases. Advances in experimental medicine and biology. 2016;928:397-418.

264. Zou W, Amcheslavsky A, Takeshita S, Drissi H, Bar-Shavit Z. TNF-alpha expression is transcriptionally regulated by RANK ligand. Journal of cellular physiology. 2005;202(2):371-8.

265. Bharti AC, Takada Y, Aggarwal BB. Curcumin (diferuloylmethane) inhibits receptor activator of NF-kappa B ligand-induced NF-kappa B activation in osteoclast precursors and suppresses osteoclastogenesis. Journal of immunology (Baltimore, Md : 1950). 2004;172(10):5940-7.

266. Dai S, Hirayama T, Abbas S, Abu-Amer Y. The IkappaB kinase (IKK) inhibitor, NEMO-binding domain peptide, blocks osteoclastogenesis and bone erosion in inflammatory arthritis. The Journal of biological chemistry. 2004;279(36):37219-22.

267. Bork PM, Schmitz ML, Kuhnt M, Escher C, Heinrich M. Sesquiterpene lactone containing Mexican Indian medicinal plants and pure sesquiterpene lactones as potent inhibitors of transcription factor NF-kappaB. FEBS letters. 1997;402(1):85-90.

268. Hall IH, Lee KH, Starnes CO, Sumida Y, Wu RY, Waddell TG, et al. Anti-inflammatory activity of sesquiterpene lactones and related compounds. Journal of pharmaceutical sciences. 1979;68(5):537-42.

269. Mathema VB, Koh YS, Thakuri BC, Sillanpaa M. Parthenolide, a sesquiterpene lactone, expresses multiple anti-cancer and anti-inflammatory activities. Inflammation. 2012;35(2):560-5.

270. Hehner SP, Heinrich M, Bork PM, Vogt M, Ratter F, Lehmann V, et al. Sesquiterpene lactones specifically inhibit activation of NF-kappa B by preventing the degradation of I kappa B-alpha and I kappa B-beta. The Journal of biological chemistry. 1998;273(3):1288-97.

271. Hehner SP, Hofmann TG, Droge W, Schmitz ML. The antiinflammatory sesquiterpene lactone parthenolide inhibits NF-kappa B by targeting the I kappa B kinase complex. Journal of immunology (Baltimore, Md : 1950). 1999;163(10):5617-23.

272. Yip KH, Zheng MH, Feng HT, Steer JH, Joyce DA, Xu J. Sesquiterpene lactone parthenolide blocks lipopolysaccharide-induced osteolysis through the suppression of NF-kappaB activity. Journal of bone and mineral research : the official journal of the American Society for Bone and Mineral Research. 2004;19(11):1905-16.

273. Idris AI, Krishnan M, Simic P, Landao-Bassonga E, Mollat P, Vukicevic S, et al. Small molecule inhibitors of IkappaB kinase signaling inhibit osteoclast formation in vitro and prevent ovariectomy-induced bone loss in vivo. FASEB journal : official publication of the Federation of American Societies for Experimental Biology. 2010;24(11):4545-55.

274. King TJ, Georgiou KR, Cool JC, Scherer MA, Ang ES, Foster BK, et al. Methotrexate chemotherapy promotes osteoclast formation in the long bone of rats via increased pro-inflammatory cytokines and enhanced NF-kappaB activation. The American journal of pathology. 2012;181(1):121-9.

275. Liu Q, Zhao J, Tan R, Zhou H, Lin Z, Zheng M, et al. Parthenolide inhibits pro-inflammatory cytokine production and exhibits protective effects on progression of collagen-induced arthritis in a rat model. Scandinavian journal of rheumatology. 2015;44(3):182-91.

CHAPTER 2: PHARMACOLOGICAL MODULATION OF AUTOPHAGY AND APOPTOSIS IN PBMC-DERIVED OSTEOCLASTS AND A MOUSE MODEL OF INFLAMMATORY ARTHRITIS

B. Williams, H. Kamitakahara, K. Algate, F. Najimi, E. Tsangari, S. Chaudary, E. Perilli, D.R. Haynes, T.N. Crotti, A. Dharmapatni

Chapter Summary:

The aim of most pharmacological therapies in RA is to resolve inflammation. Whilst having positive effects on disease activity, bone erosion persists. Recent research has associated the chronic accumulation of inflammatory cells and osteoclasts in RA synovial joints, with a decrease in apoptosis, increasing the longevity of the disease processes. Thus, there is immense therapeutic potential in modulating both cell proliferation and death in RA synovial joints. As such, in this study, the effects of the apoptosis inducer Embelin and the autophagy inhibitor Hydroxychloroquine were assessed in both human osteoclastic cells in isolation and in a mild murine model of inflammatory arthritis.

Chapter 2 has been submitted to Bone for publication and is currently under review.

2.1. Abstract

Increased inflammatory cell survival and activity during rheumatoid arthritis (RA) enhances bone destruction. This study aims to target the mechanisms involved in prolonged cell survival by pharmacological induction of apoptosis with Embelin and inhibition of autophagy with hydroxychloroquine (HCQ) in TNF-α stimulated PBMC derived osteoclasts *in vitro* and in a murine model of collagen antibody-induced arthritis (CAIA). *In vitro,* Embelin and HCQ treatment reduced expression of autophagy genes beclin-1 and LC3, and expression of osteoclast gene NFATc1. Embelin and HCQ treatments significantly reduced TRAP positive osteoclast formation and dentine resorption. Embelin significantly reduced paw inflammation by day 5 in CAIA mice compared to treatment with a combination of Embelin and HCQ ($p < 0.05$). At end point, the combination of Embelin and HCQ had reduced paw volume, cellular infiltration and cartilage and bone degradation as assessed histologically in CAIA mice. These mice also had significantly higher TUNEL positive cells compared to CAIA untreated mice ($p < 0.05$). CAIA mice expressed a significantly higher proportion of LC3 positive cells in the articular cartilage compared to healthy mice ($p < 0.005$). These results provide pharmacological evidence of the association between autophagy and apoptosis in human osteoclastic cells, whilst identifying a possible mechanism and intervention for the pathological processes of experimental arthritis.

2.2. Statement of Authorship

Statement of Authorship

Title of Paper	Pharmacological modulation of autophagy and apoptosis in PBMC-derived osteoclasts and a mouse model of inflammatory arthritis.
Publication Status	☐ Published ☐ Accepted for Publication ☑ Submitted for Publication ☐ Unpublished and Unsubmitted work written in manuscript style
Publication Details	Submitted for publication to Bone. Currently under review.

Principal Author

Name of Principal Author (Candidate)	Bonnie Williams
Contribution to the Paper	First author and main contributor. Concept and methodological design, investigation, project administration, data curation and analysis, formulation of primary draft, in addition to reviewing and incorporating co-author comments and suggestions
Overall percentage (%)	90%
Certification:	This paper reports on original research I conducted during the period of my Higher Degree by Research candidature and is not subject to any obligations or contractual agreements with a third party that would constrain its inclusion in this thesis. I am the primary author of this paper
Signature	Date 14/3/19

Co-Author Contributions

By signing the Statement of Authorship, each author certifies that:

    i.   the candidate's stated contribution to the publication is accurate (as detailed above);

    ii.   permission is granted for the candidate in include the publication in the thesis; and

    iii.   the sum of all co-author contributions is equal to 100% less the candidate's stated contribution.

Name of Co-Author	Hanna Karnitakahara
Contribution to the Paper	Methodology and *in vitro* technical support.
Signature	Signed in lieu of Date 1/3/19

Name of Co-Author	Kent Algate
Contribution to the Paper	Investigation, methodology, data interpretation and review of manuscript.
Signature	Date 18/02/2019

Name of Co-Author	Furtutan Najimi		
Contribution to the Paper	Methodology and *in vitro* technical support.		
Signature		Date	27/02/.2019

Name of Co-Author	Eleni Tsangari		
Contribution to the Paper	Methodology and *in vivo* technical support.		
Signature		Date	18/2/19

Name of Co-Author	Sidrah Chaudary		
Contribution to the Paper	Methodology and immunohistochemistry technical support.		
Signature		Date	30.01.2019

Name of Co-Author	Egon Perilli		
Contribution to the Paper	Methodology support, supervision and manuscript review.		
Signature		Date	01.03.19

Name of Co-Author	David Haynes		
Contribution to the Paper	Conceptualisation and manuscript review.		
Signature		Date	7/2/19

Name of Co-Author	Tania Crotti		
Contribution to the Paper	Conceptualisation, methodology, supervision and manuscript review.		
Signature		Date	22/2/19

Name of Co-Author	Anak Dharmapatni		
Contribution to the Paper	Investigation, funding acquisition, methodology, conceptualisation, supervision and review of manuscript.		
Signature		Date	22/2/19

2.3. Introduction

Rheumatoid arthritis (RA) is a systemic, chronic autoimmune inflammatory disorder affecting 1% of individuals worldwide (1). Characteristic features of RA pathogenesis include; synovial hyperplasia, inflammatory cell infiltration, articular inflammation and invasion of the synovium into the adjacent bone and cartilage (2). The chronic accumulation of inflammatory cells and bone resorbing osteoclasts within the RA joint is associated with a decrease in apoptosis, increasing the intensity and longevity of disease processes (3, 4).

Apoptosis is a form of programmed cell death, eliminating damaged cells via extrinsic and/or intrinsic pathways, to maintain cell turnover and homeostatic functioning of the body (5). Interestingly, apoptotic cells are rarely found in synovial tissue from clinical or experimental rheumatic joints (4, 6). Furthermore, low levels of terminal deoxynucleotidyl transferase nick-end labelling (TUNEL) positive cells have been identified in osteoclasts differentiated from blood monocytes of RA patients (7). Decreased apoptosis in the RA synovium is associated with increased expression of X linked inhibitory apoptosis protein (XIAP), a potent inhibitor of apoptosis (4, 8). Subsequently, successful treatment with disease modifying anti-rheumatic drugs (DMARDs) is reported to result in decreased XIAP expression in RA synovial tissue, restoring apoptosis (9). Additionally, we have recently observed a reduction in inflammation and bone erosion in response to XIAP inhibition in a collagen antibody-induced arthritis (CAIA) mouse model (10).

Embelin (2,5-dihydroxy-3-undecyl-1,4-benzoquinone) is a cell permeable, non-peptide small molecule inhibitor of XIAP and produces anti-inflammatory, anti-tumour and analgesic effects (11-13). Extensive oncological research has identified the induction of apoptotic pathways in human cancer cells by Embelin (14-16). In addition to inducing apoptosis through XIAP inhibition, Embelin has also been reported to produce anti-inflammatory effects through the suppression of CD4+ T-cell infiltration and macrophage activity (17). Pertinent to this study, Embelin has been shown to suppress RANKL induced osteoclastogenesis *in vitro* in RAW 264.7 cells (18).

We have recently demonstrated beneficial outcomes with Embelin treatment in a CAIA mouse model (10). In that study, Embelin at 30 mg/kg/day suppressed inflammation with a significant reduction in the number of inflammatory cells, cartilage and bone degradation, and pannus formation in the paws of CAIA mice (10). These mice also showed significantly increased numbers of TUNEL positive apoptotic cells compared to untreated mice (10). Although not significant, mice treated with Embelin exhibited less bone erosion compared to CAIA untreated mice (10). This suggests induction of apoptosis by Embelin may prove effective in reducing bone damage at the joint while reducing inflammation in RA.

Counteracting and opposing apoptosis is the cell survival mechanism known as autophagy (19-21). Autophagy is a cellular process in which damaged cytoplasmic contents are degraded, and the resulting macromolecular constituents are recycled, maintaining homeostasis in normal physiological conditions (22). Autophagy is characterised by the formation of double membrane vesicles (phagophores) and the subsequent formation of autophagosomes that fuse with a lysosome forming a single membrane autophagolysosome. Lysosomal enzymes then initiate degradation of sequestered substances without further cell damage (23, 24).

Autophagy is regulated by the complex interaction of autophagy genes with various signalling pathways, and proteins beclin-1 and LC3 are reported to be central to the autophagy process (22, 25). P62, an adaptor molecule, contains binding sites for LC3 and initiates the incorporation of cellular components into the autophagosome (26). The inverse relationship between autophagy and apoptosis in RA has been supported by several conflicting studies showing an increase in autophagy proteins, beclin-1 and LC3, and a decrease in apoptosis within the synovial lining layers (27). In contrast, a decrease in autophagy and an increase in apoptosis has been observed *in vitro* in RA T-cells (28). The contradictory conclusions drawn in these studies justifies the necessity for further elucidation of this relationship in human osteoclasts and in RA.

Autophagy has been shown to support tumour necrosis factor-α (TNF-α) induced bone resorption in experimental RA (29). In this study, the upregulation of beclin-1 expression

in human osteoclasts was found to result in induction of osteoclast specific genes including, nuclear factor of activated T cells cytoplasmic 1 (NFATc1), osteoclast-associated receptor (OSCAR), tartrate resistant acid phosphatase (TRAP) and calcitonin receptor (CTR) (29, 30). LC3 is also known to be essential for ruffled border formation in the osteoclast, thus regulating osteoclast secretions and bone resorption *in vitro* and *in vivo* (31). Reduced apoptosis in the RA synovia has been extensively reported (32), however a regulatory role for autophagy and its effect on apoptosis in RA, specifically in osteoclasts, is yet to be characterised.

Hydroxychloroquine (HCQ), a traditional and well tolerated DMARD used for decades to treat RA, has been shown to suppress the autophagy process (33). However, the molecular pathway of autophagy inhibition by HCQ has not been fully defined. A recent study by Han *et al.* 2018, found HCQ to reduce the occurrence and severity of inflammatory arthritis in a collagen-induced arthritis (CIA) murine model via the inhibition of T-follicular helper cells (34). This study further elucidates the mechanisms involved in the suppression of inflammatory arthritis by HCQ and provides greater evidence of the beneficial effect of HCQ treatment in the initial stages of RA. However, the effectiveness of HCQ is limited by its slow onset of action to prevent the progression of bone erosion in RA (33). HCQ has been shown to repress osteoclast formation *in vitro* significantly reducing bone resorption through mechanisms distinct from apoptosis (35). Thus, we propose a combination of HCQ and Embelin will enhance the effectiveness in reducing bone erosion by repressing further osteoclast formation and inducing mature osteoclast apoptosis.

We hypothesize that regulating autophagy and apoptotic mechanisms in RA will benefit current treatments targeting joint destruction and inflammation. To the best of our knowledge, there are currently no reports on the association between autophagy and apoptosis in human osteoclasts. To date, the combination of HCQ and Embelin and the simultaneous autophagy apoptosis readouts have not been investigated, although each of the drugs have been investigated as individual treatments previously. This study aimed to investigate the effects of HCQ and Embelin in osteoclasts derived from human peripheral blood mononuclear cells (PBMC) stimulated by the inflammatory cytokine TNF-α. Further to this, the effects of HCQ and Embelin, separately and in combination, were

examined in a CAIA mouse model to identify the autophagy/apoptosis pathway as a possible novel target for reducing inflammation and joint destruction in RA.

2.4. Methods

Ethics approval was obtained from the University of Adelaide Human Research Ethics Committee (H-350-2001), in accordance with National Health and Medical Research Council of Australia guidelines. Informed consent was obtained from all patients. Ethics approval was also obtained from the Animal Ethics Committee of the University of Adelaide (M-2015-263) in compliance with the National Health and Research Council (Australia) Code of Practice for Animal Care in Research and Training. Mice were housed in approved conditions on a 12-hour light/dark cycle. Food and water were provided ad libitum.

2.4.1. In vitro osteoclastogenesis assay

Based on previously established methods (36), PBMCs were isolated from 15 ml human blood buffy coat (n = 4; Australian Red Cross Blood Service) by Ficoll gradient centrifugation. Monocyte isolates were resuspended in alpha-minimum essential medium (α-MEM) containing 10% FCS, 2 mM L-glutamine, 50 µg/ml Penicillin and 50 µg/ml Streptomycin (Invitrogen, ThermoFisher Scientific, California, USA) and seeded at 2 x 10^6 cells/ml. After 24 hours, non-adherent cells were removed by 2 x 5-minute washes in fresh media leaving a population rich of monocytes. Monocytes were treated with 25 ng/ml recombinant human (rh) M-CSF (Chemicon International Inc. Millipore, MA) and cultured for five days prior to the induction of osteoclast differentiation by supplementing media with rhRANKL (50 ng/ml; day 10; Chemicon International Inc. Millipore, MA). After initiation of osteoclastic differentiation, cells were stimulated with the pro-inflammatory cytokine TNF-α (5 ng/ml; day 12) to represent an isolated, TNF-α mediated, inflammatory response *in vitro*. After 24 hours of TNF-α stimulation, cells were treated with either the autophagy inhibitor HCQ (50 µg/ml; (37-39)) or the apoptosis inducer, Embelin (15 µmol/lt; (18)) for 6 or 24 hours. Control cells were differentiated using the standard protocol described above. In the absence of treatment, cells were treated with vehicle Dimethyl sulfoxide (DMSO; 0.01%). Osteoclast formation and function was confirmed by quantification of TRAP positive cells and the presence of

resorption pits in whale dentine (described below), respectively. Dose response curve experiments were performed prior to this report, and experiments were repeated three times.

2.4.2. Quantitative real time polymerase chain reaction (qRT PCR)

Total RNA was extracted and isolated throughout the *in vitro* assay using a TRIzol based method as per manufacturers' direction (Invitrogen, ThermoFisher Scientific, California, USA) and converted to complementary DNA (cDNA) through reverse transcription using the Superscript III kit (Invitrogen, ThermoFisher Scientific, California, USA). Osteoclast genes (NFATc1, OSCAR, CTR and TRAP) were assessed by qRT PCR to confirm osteoclast differentiation after addition of RANKL at day 10 and treatment at day 14. The effect of treatments on osteoclastogenesis, and autophagy and apoptosis associated genes, including beclin-1, P62, LC3 and caspase 3 and 9, were assessed after 6 and 24 hours. Primer sequences were as previously published (27, 40). Changes in the expression of the genes of interest relative to the housekeeping gene hARP were normalised to the expression of the untreated control cells, presented as $2^{-\Delta\Delta ct}$ (fold increase) (41).

2.4.3. Western blot of P62 and LC3

Cells were lysed using RIPA buffer (Life Technologies, CA, USA). Protein was run on a 12% SDS gel and then transferred to PVDF membrane. The membrane was incubated with blocking buffer (PBS/5% BSA, R&D System, MN, USA) and then incubated with mouse anti-human P62 antibody (Ab56416, Abcam, Sapphire Biosciences, NSW, Australia) or rabbit anti-human LC3 antibody (Ab58610, Abcam, Sapphire Biosciences, NSW, Australia), as well as beta actin loading control (Ab8226, Abcam, Sapphire Biosciences, NSW, Australia) overnight. The membrane was then incubated with secondary antibody goat anti-mouse or anti-rabbit IgG, respectively (H&L), DyLight 800 4X PEG conjugated (SA5-35521, Life Technologies). Bands were visualised using LI-COR Odyssey system (LI-COR Biotechnology, Lincoln, NE, USA).

2.4.4. Immunofluorescent staining of beclin-1, LC3 and P62

Fixed cells were permeabilised with PBS/0.1% Triton X and then incubated overnight with, rabbit anti-human beclin-1 antibody (20 µg/ml, Ab 16998, Abcam, Sapphire Biosciences, NSW, Australia), rabbit anti-human LC3 antibody (4 µg/ml, Ab 58610, Abcam, Sapphire Biosciences, NSW, Australia) or mouse anti-human P62 antibody (10 µg/ml, Ab 56416, Abcam, Sapphire Biosciences, NSW, Australia). Donkey anti-rabbit Cy5 or goat anti-mouse Alexa 488 (Jackson Immunoresearch) was then added for 30 minutes and Hoechst (Roche Diagnostics, NSW, Australia) was used for nuclear counter staining. Fluorescence was visualised using a Leica TCS SP5 confocal microscope (Adelaide Microscopy, University of Adelaide, Australia).

Following immunofluorescent detection of beclin-1 or LC3, cells were incubated with TUNEL solution (TUNEL Click it, Roche Diagnostics, NSW, Australia), following manufacturer instructions. Triple staining was also performed using LC3 and P62 antibodies and Hoechst counterstaining (Roche Diagnostics, NSW, Australia) to evaluate co-localisation between LC3 and P62.

2.4.5. Viability assay

Cells grown at 2×10^5 cells/well in 96 well plates and pre-treated/treated with modulators as above, were then incubated with WST-1 solution (Roche Applied Science, NSW, Australia) according to manufacturer instructions. Optical density was read at absorbance 440 nm using an ELISA plate reader (KC4, BioTek Instruments, Winooski, VT, USA) and results extrapolated from a standard curve.

2.4.6. Tartrate-resistant acid phosphatase (TRAP) staining

Cells grown at 2×10^5 cells/well in 16 well chamber slides were pre-treated/treated as above and TRAP staining was used to identify pre-osteoclasts/osteoclasts, as previously published (42). Three regions were captured with a camera attached to a microscope (Nikon, Japan) and TRAP positive cells with three or more nuclei were counted.

2.4.7. Dentine resorption assay

Cells grown at 2×10^5 cells/well on dentine in 96 well plates were pre-treated/treated as above. Cells were detached from dentine slices with 0.5% trypsin/0.25% EDTA, dentine was washed with PBS, air-dried and carbon coated for scanning electron microscopy (SEM XL-30, Adelaide Microscopy, University of Adelaide, Australia). Surface dentine resorption was quantified using Image J V1.47 (National Institutes of Health) (43).

2.4.8. Live cell imaging and transmission electron microscope (TEM)

Immediately following incubation with pharmacological modulators, cells were visualised under a Nikon Ti E Live Cell microscope (40x objective magnification, Adelaide Microscopy, University of Adelaide, Australia). Images were captured every 10 minutes for 24 hours. The change in cell size was quantified in four cells from each group on collated images at 0, 6, 12, 18 and 24 hours using Adobe Photoshop 6 (San Jose, CA, US) and Image J V1.47.

To identify autophagy vesicles a subset of cells were stained with cyto ID (Enzo Life Sciences, ENZ 51031-0050), 18-20 hours following treatment, according to manufacturer instructions (44). Cells were visualised with live cell imaging at 10x objective magnification. Images were captured every 10 minutes for 2 hours.

Autophagic vesicle formation and morphological apoptotic cell changes following 24 hours of treatment were evaluated using TEM. Cells were fixed in buffered glutaraldehyde and then embedded in Epon after routine procedures. Ultrathin sections were photographed using a Philips CM 10 electron microscope (45). Autophagosomes were identified when a double membrane vesicle was present, while autolysosomes were distinguished as being single-membrane vesicles containing remnants of the damaged organelles (46).

2.4.9. Collagen antibody-induced arthritis mouse model

Thirty female Balb/c mice aged six to eight weeks were obtained from the University of Adelaide Laboratory Animal Services and randomly allocated to five groups (n = 6 per group): Control (no arthritis), CAIA (arthritis with no treatment), CAIA + Embelin (arthritis treated with 30 mg/kg/day Embelin), CAIA + HCQ (arthritis treated with 40

mg/kg/day HCQ) and CAIA + Embelin + HCQ (arthritis treated with a combination of 30 mg/kg/day Embelin and 40 mg/kg/day HCQ).

Arthritis was induced in mice by an intravenous injection (via the tail vein) with 150 µl (1.5 mg/mouse) of a cocktail of anti-type II collagen monoclonal antibodies (Arthrogen-CIAs Arthritogenic Monoclonal Antibodies, Chondrex Inc., Redwood, WA, USA). Followed by an intraperitoneal injection of 20 µl (10 µg/mouse) of *E.coli* lipopolysaccharide (LPS) on day 3, as previously described (10, 47). Control animals were injected with PBS alone at both time points. 100 µl of Embelin in 1 % DMSO and/or 100 µl of HCQ in PBS was administered in treatment groups via oral gavage, daily, from day 4 to10.

2.4.10. Clinical analysis of local paw swelling.

Mice were monitored daily using an approved clinical record sheet for arthritis studies to assess body weight and factors of general health. To assess clinical paw swelling; individual front and hind paws were examined daily by two observers for the presence of redness, tenderness, swelling and inflammation using a previously described clinical paw scoring method (47). For each paw, a score of 1 was given for each red and inflamed digit and a score from 0-5 was allocated for swelling of the carpal/tarsal and of the wrist/ankle. The maximum score for each paw was 15, giving a possible total of 60 per mouse (47).

2.4.11. Micro-computed tomography analysis

On day 11, mice were humanely killed via cervical dislocation. All paws were collected, skinned and fixed in 10% neutral buffered formalin for 24 hours. Bone changes and swelling of the front paws was assessed using images obtained at 8.5 µm/pixel by a micro-CT scanner (SkyScan 1076, Bruker, Kontich, Belgium) (47, 48). Paws were scanned at a source voltage of 55 kV, current 180 µA, isotropic pixel size of 8.5 µm with a 0.5 mm thick aluminium filter, rotation step of 0.6, frame averaging of 1 and a total scan time of approximately 35 minutes. Cross-sectional images of the front paws were reconstructed using a filtered back projection algorithm (N-Recon software, Bruker, Kontich, Belgium) and saved as 8-bit grey level files (bitmap format). The stack of reconstructed cross-section images of the front paws were re-aligned in 3D with the long axis of the paw aligned along the inferior superior direction of the images (Dataviewer software, Bruker),

as previously described (48). Analysis of each front paw used a standardised cylindrical volume of interest (VOI; 4.5 mm diameter and 2.4 mm length), starting 200 cross-sections distal and extending to 80 cross-sections proximal to the lower epiphyseal growth plate of the radiocarpal joint (280 consecutive cross-sections in total, corresponding to a VOI length of 2.4 mm).

Image thresholding and calculation of bone volume and paw volume:

On the VOI for the radiocarpal joint specified above, the bone volume (BV, in mm^3) and the paw volume (PV, in mm^3, which includes the soft tissue surrounding the radiocarpal joint), were quantified in 3D using uniform thresholding (CT Analyser software, Bruker). In the grey-level histogram of the reconstructed cross-section images (bitmap format, 256 grey levels, ranging from 0 to 255), the grey level values in the lower range (from 0 to 11) corresponded to air or background, followed in increasing order by values of the soft tissue (ranging from 12 to 134) and bone (from 135 to 255) (48). Two fixed minimum threshold values were applied to the specimens for segmentation. One minimum threshold level was used for segmenting the bone pixels only (from minimum threshold level 135 to maximum 255), leaving air and surrounding soft tissue as background (48-50). The second minimum threshold level was for segmenting the paw, soft tissue and bone together (minimum threshold level 12 to maximum level 255), and leaving air as the background (48-50). By applying the corresponding threshold values to each specimen, automated calculations were performed of BV and PV (CT Analyser software, Bruker). The BV was calculated as the volume occupied by the voxels segmented as bone and the PV was calculated as the volume occupied by the voxels segmented as paw, which included both bone and soft tissue. After segmentation, for PV measurements, loose speckles in the segmented images which originated from noise pixels, having their grey values close to those of soft tissue, were removed. This was completed using a cycle of the software function 'sweep' (CT Analyser software, Bruker) which automatically removes all but the largest object in 3D volume, maintaining the paw as the largest object. BV and PV were then quantified using the marching cubes method (CT Analyser software, Bruker) (51-53).

2.4.12. Histological analysis of the radiocarpal joint

Following decalcification of the front paws using 10% Ethylene diaminetetraacetic acid (EDTA), tissue was processed for paraffin embedding and serial sagittal sections of the radiocarpal joint were cut (5 µm) for histological analysis. Routine haematoxylin and eosin (H&E) staining was conducted and histological evaluation of the radiocarpal joint was carried out by two-blinded observers using a previously described semi-quantitative scoring method (54). The number of inflammatory cells was assessed within the radiocarpal joint; normal tissue (< 5% inflammatory cells) was scored as 0, mild inflammation (6-20% inflammatory cells) was scored as 1, moderate inflammation (21-50% inflammatory cells) was scored as 2 and severe inflammation (> 51% inflammatory cells) was scored as 3. Bone and cartilage destruction was also assessed in these paw sections using a 0-3 scale (0, normal; 1, mild cartilage destruction; 2, evidence of both cartilage and bone destruction; 3, severe cartilage and bone destruction). Pannus formation was scored as either 0, no pannus or 1, pannus formation (55).

TRAP staining was conducted on sagittal sections of the front paws to detect the presence of osteoclasts on the bone surface and pre-osteoclasts in the surrounding soft tissue. Sections were incubated with TRAP solution at 37˚C for 45 minutes and counterstained with haematoxylin, as previously described (42, 56). The number of multinucleated TRAP positive cells (> 3 nuclei) were counted by two blinded observers in a consistent region of interest (2.16 mm^2), to include cells found on the bone surface (54) and within the surrounding soft tissue of the radiocarpal joint (47).

TUNEL staining was performed on sagittal sections of the front paws using a TUNEL POD detection kit (Roche Diagnostic, NSW, Australia), as previously published (10). Tissue sections were incubated with TUNEL solution (enzyme plus label solution). TUNEL solution (label solution only) was added in the presence of 20 µg/ml DNA-ase for the positive control to identify the presence of fragmented DNA. Colour was developed using AEC (Vector Laboratories, CA, USA) and counterstained with haematoxylin and lithium carbonate. The number of TUNEL positive cells in the radiocarpal joint (2.16 mm^2) was scored by two-blinded observers. A score of 0 was allocated to < 10% positive cells, 1; 11-25% positive cells, 2; 26-50% positive cells, 3; 51-75% positive cells and a score of 4 if > 75% positive cells.

Immunohistochemistry staining was also performed on sagittal sections of the front paws to identify the autophagy molecule LC3 using a Vectastain *Elite* ABC HRP kit (Peroxidase, cat no. PK-62000; Vector Laboratories, CA, USA). Tissue was incubated overnight with LC3 primary antibody (0.65 µg/ml; Cell Signalling Technology, Danvers, Massachusetts, USA), followed by biotinylated universal secondary antibody and HRP conjugated Avidin-Biotin complex. Colour was developed using AEC (Vector Laboratories, CA, USA) and counterstained with haematoxylin and lithium carbonate. As the pattern of LC3 staining is diffuse within the articular cartilage and LC3 was exclusively observed in CAIA mice, analysis carried out was based on the presence (positive) or absence (negative) of LC3 staining.

2.4.13. Statistical Analysis

Statistical analysis was performed using GraphPad Prism® software (V 7.03; GraphPad Software, La Jolla, CA, USA) and SPSS (version 20; Chicago, USA). Differences between treatments were analysed using the non-parametric Kruskal-Wallis test. If significant, differences between two groups were analysed using the Mann-Whitney U test. Analysis of *in vitro* qRT PCR data involved repeated measures one-way ANOVA followed by Tukey's post hoc test to incorporate donor matching across treatments. A chi squared test was used to analyse the proportion of positive and negative LC3 stained paws. A p-value less than 0.05 was considered statistically significant.

2.5. Results

2.5.1. HCQ and Embelin alter autophagy related genes beclin-1, P62 and LC3 and suppress NFATc1 expression in human osteoclasts

Human osteoclasts grown in an inflammatory state induced by TNF-α, were treated with Embelin and HCQ to assess the effects on autophagy and apoptosis associated genes. HCQ significantly reduced expression of the autophagy genes beclin-1 ($p = 0.003$) and LC3 ($p < 0.0001$) at 6 and 24 hours post treatment, respectively, whereas P62 expression was induced at 24 hours ($p = 0.0293$; Figure 2.1 and Figure 2.2A). Analysis of protein by western blot confirms the reduction in LC3 I and the induction of P62 by HCQ (Figure 2.2B). Expression of the genes associated with apoptosis (caspases 3 and 9) were unchanged by HCQ ($p > 0.05$). Further to this, a significant reduction in expression of the

key osteoclast transcription factor, NFATc1, was observed after 6 hours of HCQ treatment (p = 0.0027). Unexpectedly, TRAP expression increased after 24 hours of HCQ (p < 0.0093) when compared to untreated cells (Figure 2.1).
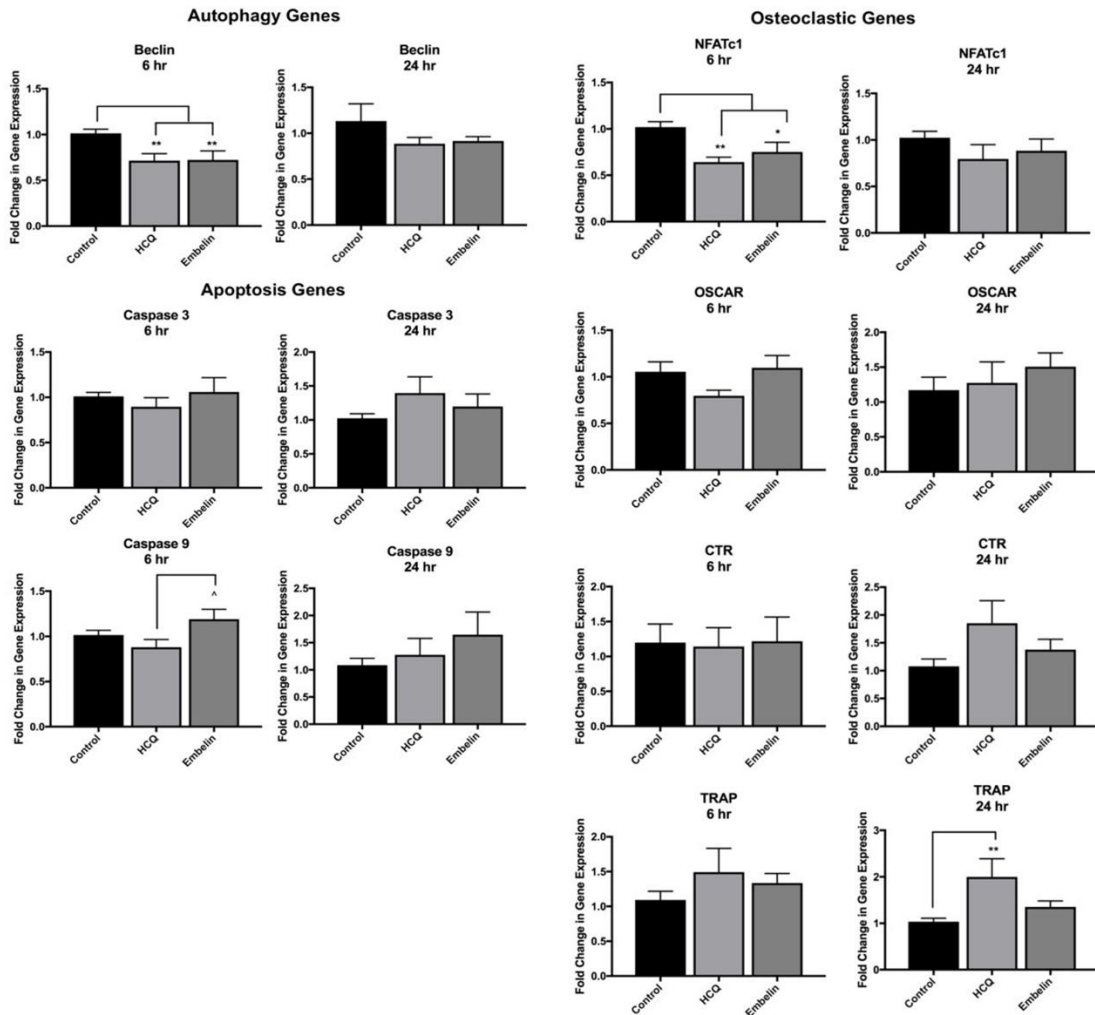
Figure 2.1. The expression of autophagy, apoptosis and osteoclast genes following 6 and 24 hours of treatment. Expression of autophagy gene beclin-1, apoptosis genes caspase 3 and 9 and osteoclast genes NFATc1, OSCAR, CTR and TRAP following 6 and 24 hours of treatment of PBMC-derived osteoclasts with HCQ or Embelin. Control = cells with no treatment added. Error bars represent standard error of mean (SEM; n = 4 donors, * p < 0.05, ** p < 0.0001 compared to control, ^ p < 0.05 compared to Embelin).

Embelin produced similar effects to HCQ, as Embelin significantly suppressed beclin-1 ($p = 0.0038$) and LC3 ($p < 0.0001$) expression at 6 and 24 hours post treatment, respectively, and induced P62 at 24 hours both at the mRNA ($p = 0.0084$) and protein level (Figure 2.1 and Figure 2.2A and B). Embelin also significantly suppressed NFATc1 expression after 6 hours of treatment ($p = 0.0335$). Embelin did not induce a significant increase in the expression of apoptotic factors, caspase 3 and 9, after both 6 and 24 hours of treatment, when compared to untreated cells (Figure 2.1). However, Embelin significantly increased caspase 9 mRNA compared to HCQ following 6 hours of treatment.
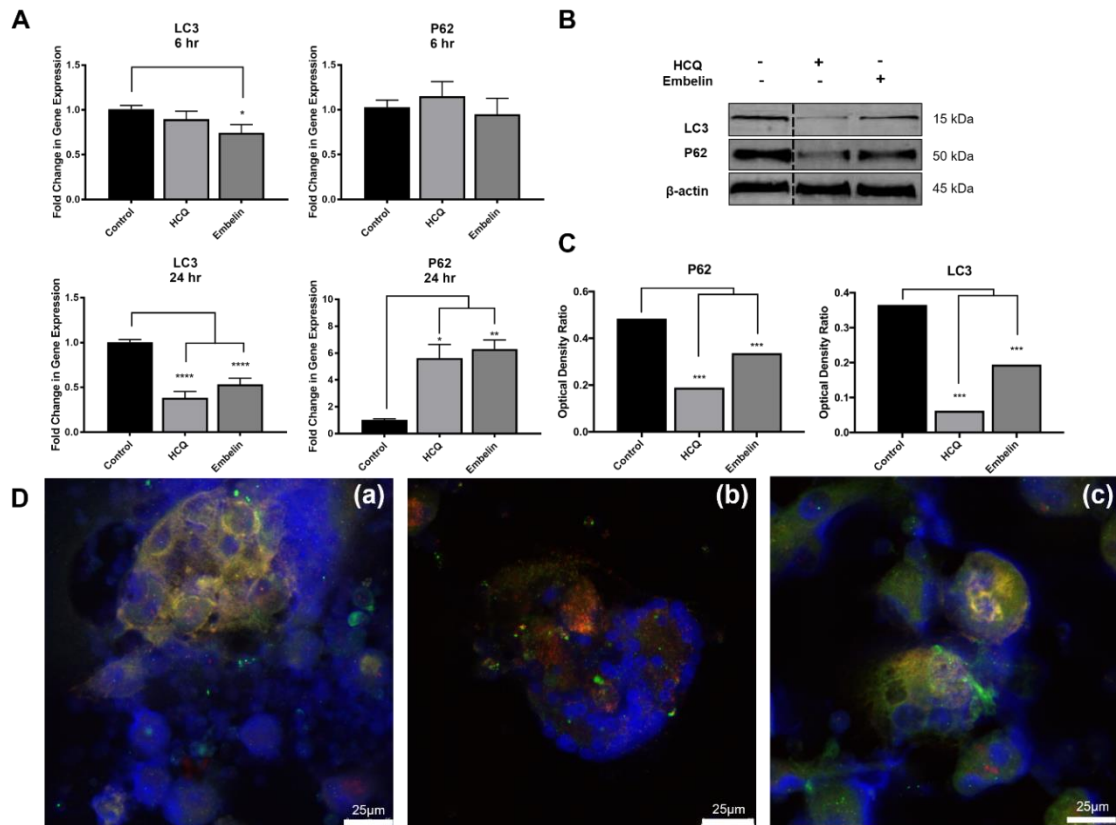
Figure 2.2. The effect of HCQ and Embelin on P62 and LC3 in PBMC-derived osteoclasts. A. Expression of autophagy genes P62 and LC3 following 6 and 24 hours of treatment of PBMC-derived osteoclasts with HCQ or Embelin. B. Western blot analysis of LC3 (upper panel) and P62 (middle panel) protein following 24 hours of treatment with HCQ or Embelin. β-actin (lower panel) is shown as the loading control, band at 45 kDa. Display of cropped gels is presented for clarity; dotted line delineates cropped location. C. Optical density of the western blots were quantified. D. Triple staining of LC3 (red), P62 (green) and Hoescht counterstaining (blue) following treatment with HCQ and Embelin on day 14 of PBMC-derived osteoclasts; (a) control, (b) HCQ and (c) Embelin. Control = cells with no treatment added. Error bars represent SEM (n = 4 donors, * p < 0.05, ** p < 0.005, **** p < 0.0001 compared to control).

2.5.2. HCQ and Embelin reduced beclin-1 and LC3 protein expression and increased the number of cells positive for TUNEL

Beclin-1, was detected in the cytoplasm of osteoclastogenic cells by immunofluorescence. Cells treated with either HCQ or Embelin for 24 hours had decreased fluorescent signal intensity and expression of beclin-1 compared to control (Figure 2.3A, B & C). Coinciding with this observation, TUNEL positive cells were greater in HCQ and Embelin treated cells when compared to untreated cells (Figure 2.3). Dual staining of beclin-1 and TUNEL (Figure 2.3A, B & C) further depict this inverse relationship between markers of apoptosis and autophagy in response to the induction of apoptosis with Embelin or the suppression of autophagy with HCQ.

Similar to beclin-1, the expression of cytosolic LC3, was greatly reduced by HCQ or Embelin compared to control (Figure 2.3D, E & F). Dual staining for LC3 and TUNEL also demonstrates an inverse relationship between autophagy and apoptosis in cells treated with either Embelin or HCQ (Figure 2.3D, E & F). Further to this, the adapter molecule, P62, co-localised with LC3 in osteoclastogenic control cells (Figure 2.2D). P62-LC3 co-localisation was also observed in HCQ or Embelin treated cells (Figure 2.2D).
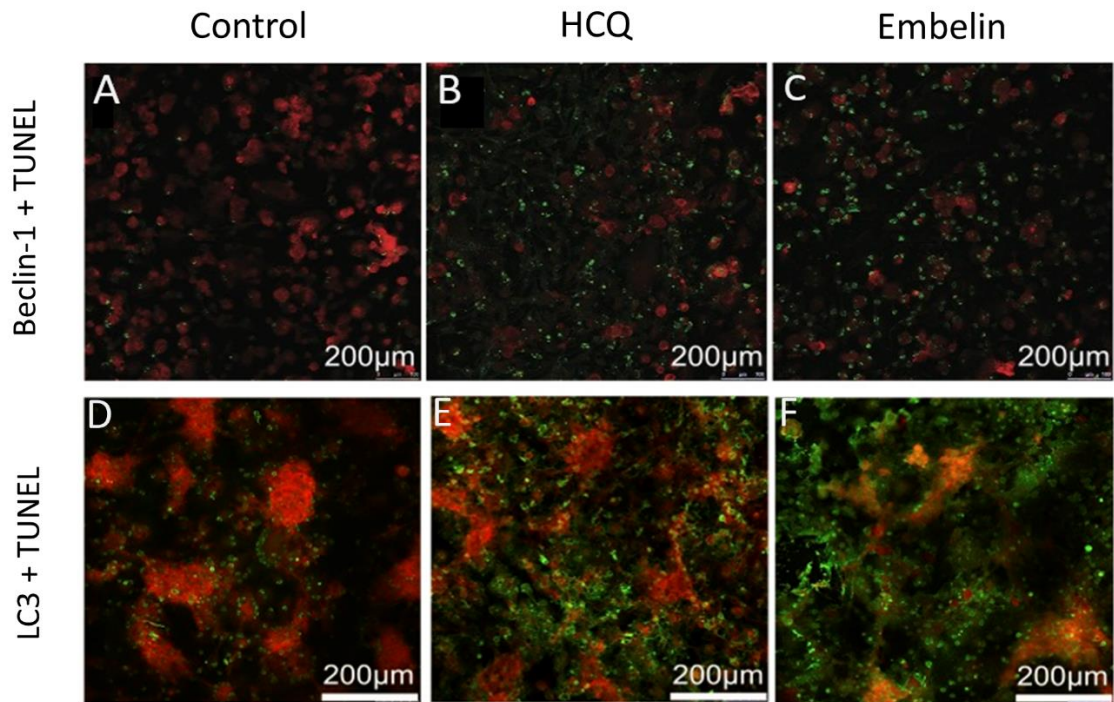
Figure 2.3. Dual staining of beclin-1 and TUNEL, and dual staining of LC3 and TUNEL on PBMC-derived osteoclasts on day 14. Dual staining of Beclin-1 (red) and TUNEL (green; A-C) and LC3 (red) and TUNEL (green; D-F) following treatment on day 14 of PBMC-derived osteoclasts with HCQ or Embelin.

2.5.3. HCQ or Embelin reduced the number of TRAP positive cells and dentine resorption

HCQ or Embelin significantly reduced the number of TRAP positive osteoclastic cells forming *in vitro* compared to untreated cells ($p = 0.0036$ and $p = 0.0047$ respectively; Figure 2.4A and B). Further to this, the area of surface resorption of dentine by osteoclasts was greatly diminished in HCQ or Embelin treated cells ($p = 0.0242$ and $p = 0.0098$ respectively; Figure 2.4A and C).

Total cell viability following treatment was assessed by the WST-1 assay. Response to HCQ and Embelin ($p = 0.0052$; Figure 2.4D) varied but did not differ statistically from untreated controls.
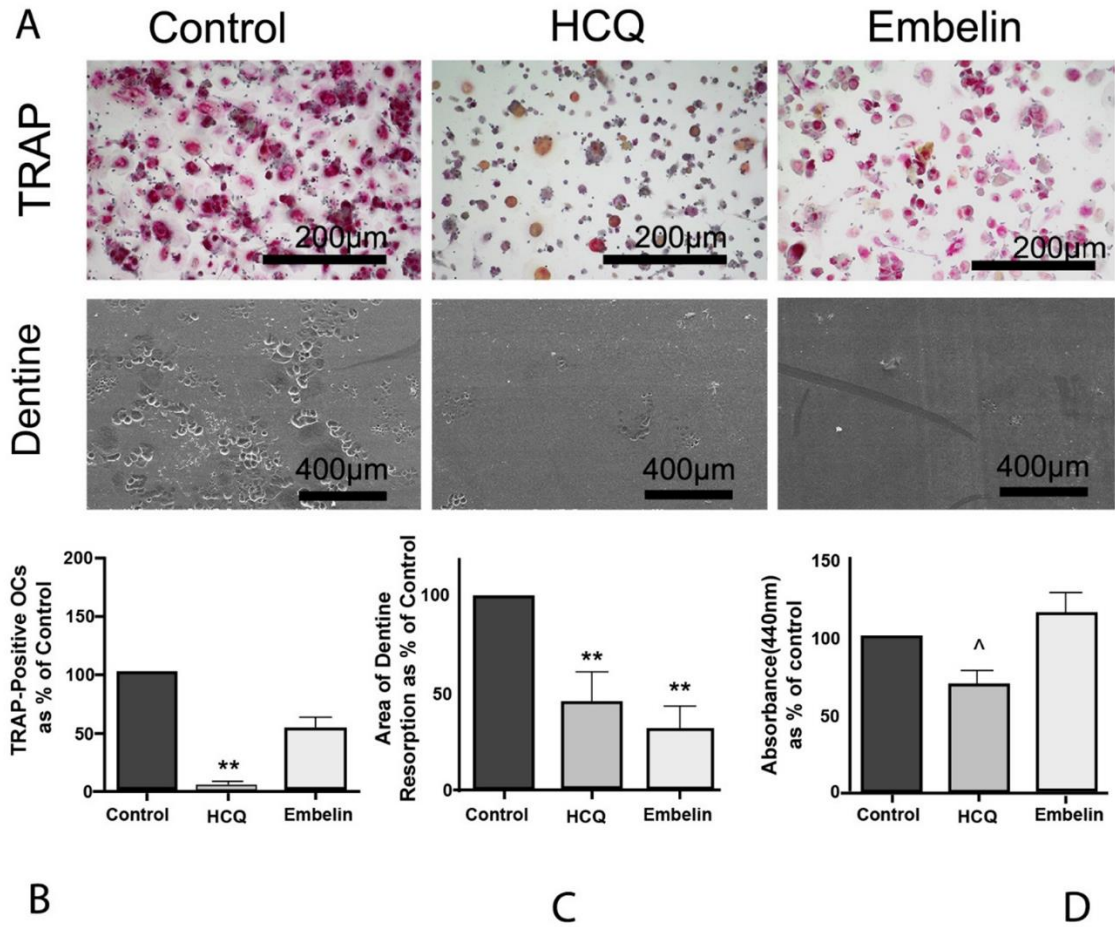
Figure 2.4. TRAP staining, dentine resorption and WST-1 assay 24 hours post-treatment. A. TRAP staining and dentine resorption visualised on scanning electron microscope post 24 hours of treatment of human osteoclasts with HCQ or Embelin. B. Quantitation of TRAP positive cells. C. Quantitation of dentine resorption area. D. WST-1 assay. Control = cells with no treatment added. Error bars represent SEM. (n = 4 donors; * p < 0.005 compared to control, ^ p < 0.05 compared to Embelin).

2.5.4. 24 hours of HCQ or Embelin treatment induced cells with apoptotic morphology

Embelin induced morphological changes consistent with apoptosis at 24 hours as observed by TEM. This was characterised by the presence of nuclear fragmentation, chromatin condensation and cell shrinkage (Figure 2.5A). Although HCQ induced apoptotic changes in some cells (Figure 2.5C), a cell subset with no characteristic apoptotic changes demonstrated an accumulation of autophagy vesicles (Figure 2.5B).
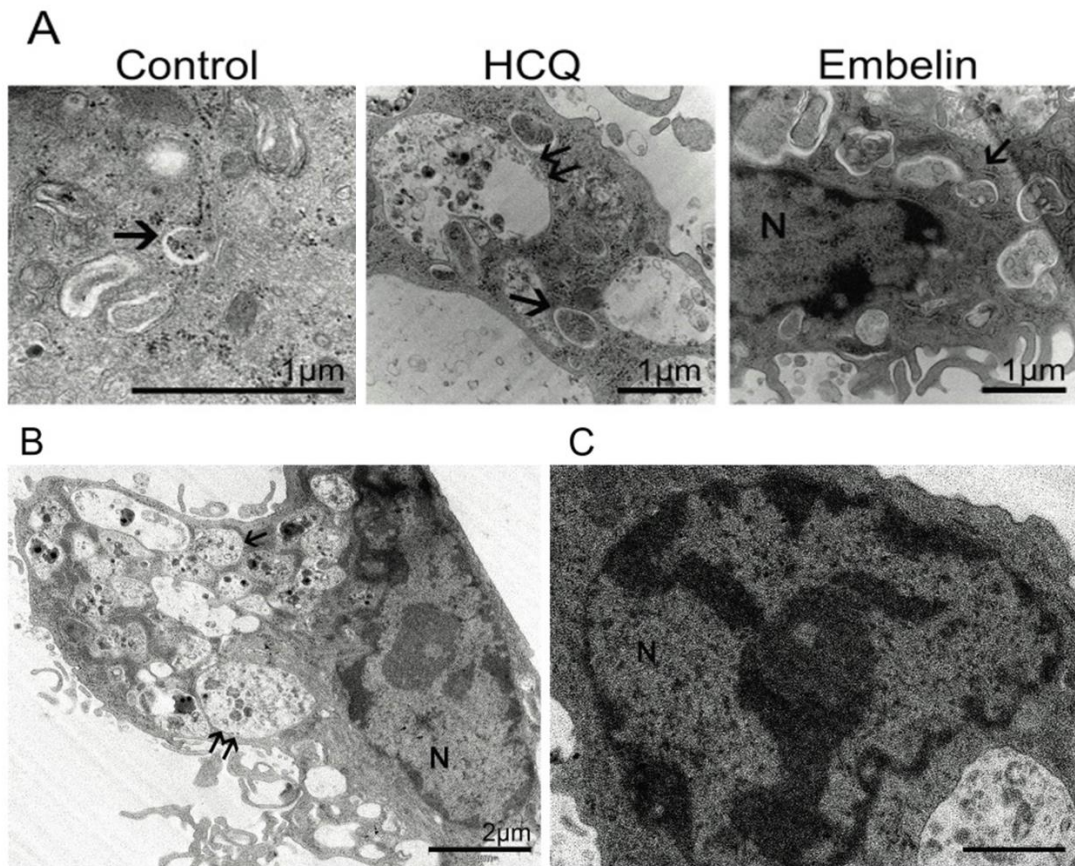
Figure 2.5. Transmission electron microscope (TEM) images of PBMC-derived osteoclasts following 24 hours of treatment. A. Ultrastructural features of PBMC-derived osteoclasts following treatment with HCQ and Embelin for 24 hours visualised using TEM. B. Accumulation of autolysosome following treatment with HCQ. C. Chromatin condensation following HCQ treatment. Single arrows indicate double membrane autophagosomes, double arrows indicate single membrane autolysosomes and N indicates nucleus.

2.5.5. Accumulation of autophagy vesicles and morphological characteristics of apoptosis following HCQ treatment observed in live cell imaging

Live cell imaging showed that HCQ induced cell shrinkage and cell death in most osteoclasts at 24 hours (Figure 2.6A). Quantification of percent change in mean cell size overtime confirmed a reduction in osteoclast size following HCQ or Embelin treatment, as compared to control cells (Figure 2.6B). In cells stained with cyto ID, there was a significant increase in the number of autophagy vesicles in HCQ treated cells ($p < 0.05$) (Figure 2.6C & D).
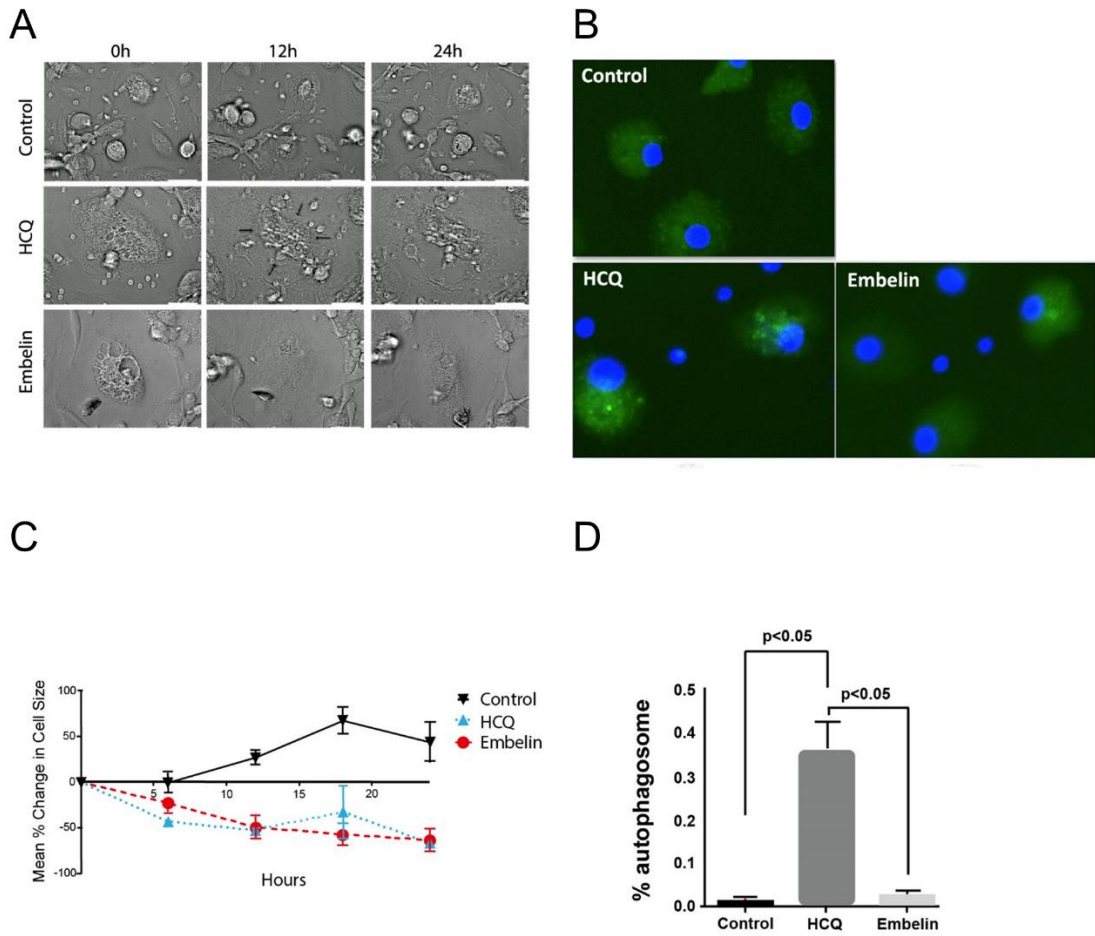
Figure 2.6. Serial measurements of cell size and autophagy vesicle detection using live cell imaging post-treatment. A. Representative images from live cell imaging at 0, 12 and 24 hours following treatment. B. Average percent change in cell size over 24 hours. C. PBMC-derived osteoclasts at day 14 stained with cyto ID post-treatment to visualise autophagy vesicles (green dots in cell cytoplasm). D. Percentage of cells that demonstrate autophagy vesicles following treatment. Error bars represent SEM.

2.5.6. Clinical evaluation of local inflammation in mouse paws

Induction of CAIA resulted in significant redness, tenderness and inflammation in the front and hind paws of Balb/c mice (Figure 2.7A). This was evident from day 5 following LPS administration. On day 5, CAIA mice treated with Embelin had a significantly lower paw score compared to CAIA mice treated with both HCQ and Embelin ($p < 0.05$; Figure 2.7B). Following day 5, the paw scores for treated CAIA groups did not significantly differ among each other and compared to CAIA untreated mice, whereas they were all significantly higher than control mice.
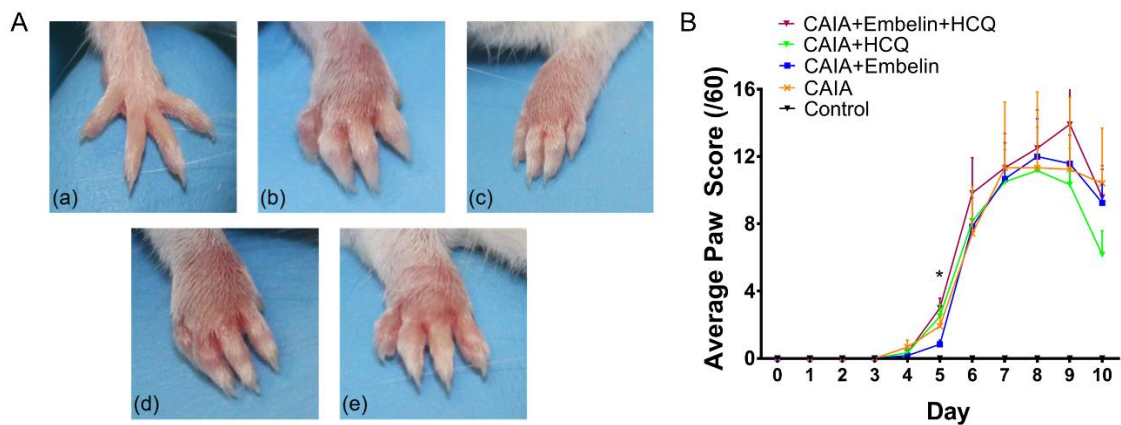
Figure 2.7. Clinical evaluation of local inflammation. A. Macroscopic appearance of the front paws; (a) control, (b) CAIA, (c) CAIA + Embelin, (d) CAIA + HCQ and (e) CAIA + Embelin + HCQ. Paws were imaged at day 7 post-arthritis induction. B. Average clinical paw scores of each group over 10 days. Error bars represent SEM (n = 6 mice per group, * $p < 0.05$ CAIA + Embelin compared to CAIA + Embelin + HCQ).

2.5.7. Micro-CT analysis of bone volume and paw volume

Representative reconstructed 3D images of the radiocarpal joint, including bone and soft tissue are shown in Figure 2.8A. The BV measured in the radiocarpal joints did not differ significantly among groups (Figure 2.8B). Consistent with the clinical evaluation of local inflammation, diseased mice had a significantly greater PV (up to 44%) compared to control mice ($p = 0.008$). However, PV did not significantly differ between CAIA and CAIA treated mice (Figure 2.8C). Although not significant, CAIA mice treated with Embelin and HCQ exhibited a smaller PV compared to CAIA alone and to the other CAIA treated mice (Figure 2.8C).
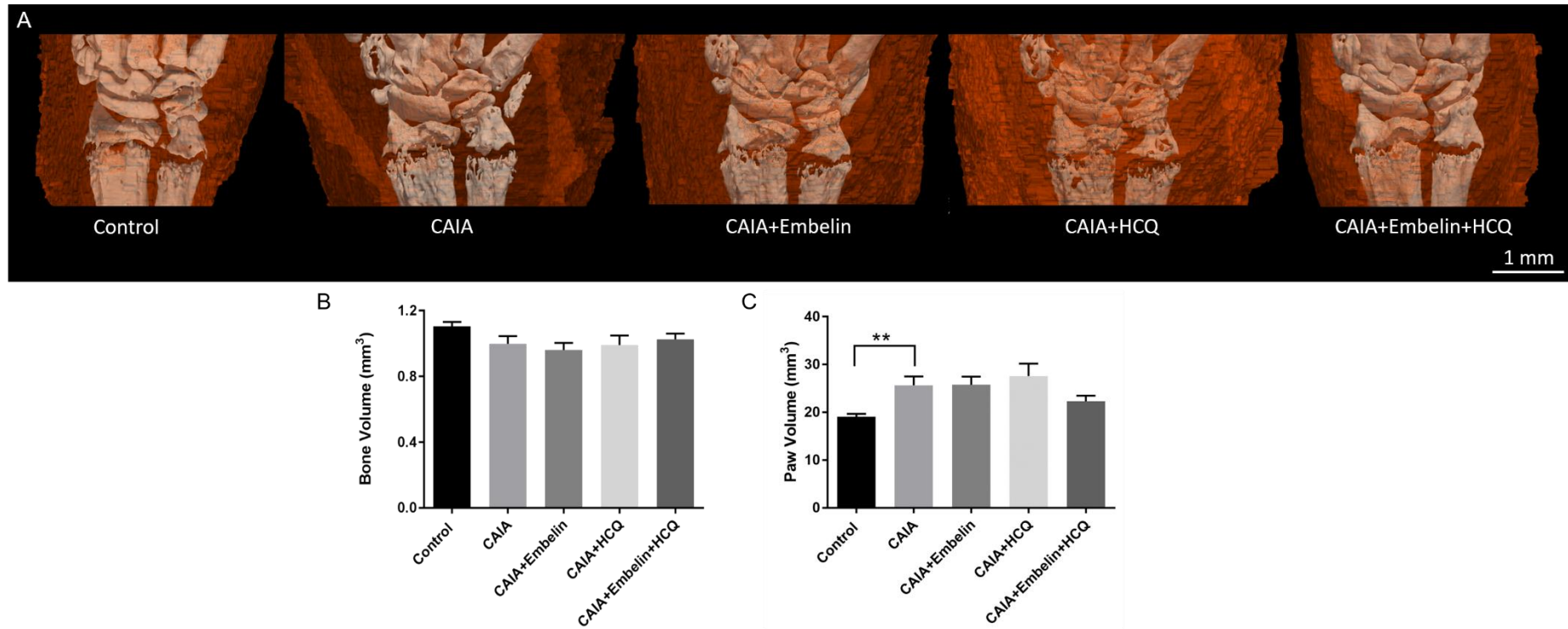
Figure 2.8. Effect of CAIA, Embelin and/or HCQ on bone volume (BV) and soft tissue swelling (PV) of the radiocarpal joint assessed by high resolution micro-CT. A. Three-dimensional micro-CT models of the radiocarpal joint and surrounding soft tissue (indicated in red) in the right paw. Mean BV (B) and PV (C) expressed in mm^3 in the radiocarpal joint as assessed by micro-CT analysis at day 11. Error bars represent SEM (n = 6 per group, * p < 0.05).

2.5.8. Histological evaluation of inflammation and bone erosion in the radiocarpal joint

Histogical evaluation of sagittal sections of the radiocarpal joint (representative images in Figure 2.9A and B) showed that CAIA untreated mice had significantly greater scores for cellular infiltration, cartilage and bone degradation and pannus formation compared to control mice ($p < 0.05$; Figure 2.9C). As expected, CAIA + Embelin + HCQ mice exhibited reduced scores for cellular infiltration, cartilage and bone degradation and pannus formation compared to CAIA alone and CAIA mice treated with Embelin and HCQ individually, however not significantly so (Figure 2.9C). There was no significant difference in the number of TRAP positive multinucleated cells on the bone surface and within the surrounding soft tissue between all groups (Figure 2.9D & E).
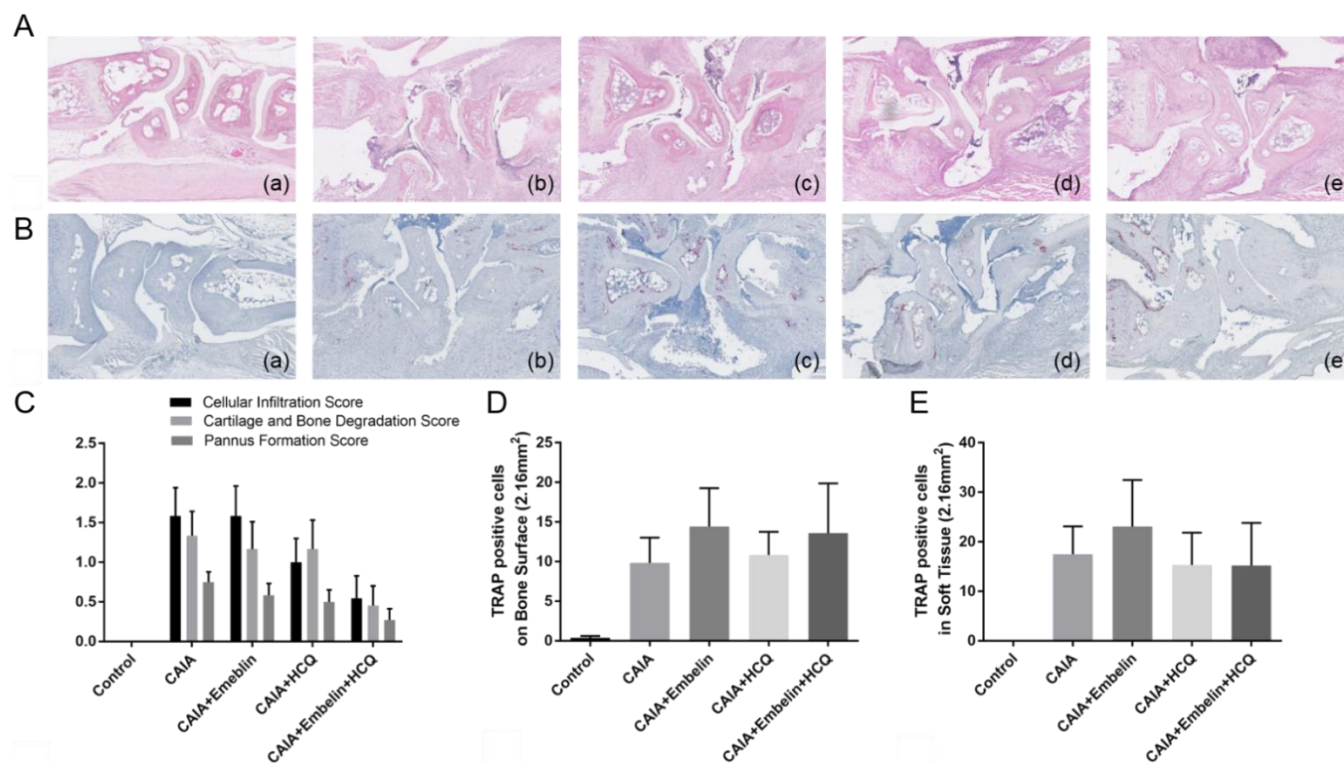
Figure 2.9. Histological assessment of inflammation and bone loss in the radiocarpal joint. Representative images of sagittal sections of the radiocarpal joint stained with haematoxylin and eosin (H&E; A, 10x magnification) and tartrate resistant acid phosphatase (TRAP; indicated in red) with haematoxylin counterstaining (B; 10x magnification); (a) control, (b) CAIA, (c) CAIA + Embelin, (d) CAIA + HCQ and (e) CAIA + Embelin + HCQ. C. Histological scores of H&E stained sagittal sections of the radiocarpal joint. Average values of TRAP positive multinucleated cells in each group on the bone surface (D) and within the surrounding soft tissue (E) in a 2.16 mm^2 area of the radiocarpal joint. Error bar represents SEM (n = 12 paws per group).

2.5.9. Apoptosis and LC3 detection in the radiocarpal joint

TUNEL and LC3 staining was performed on sagittal sections of the front paws to identify the number of apoptotic cells and the expression of the autophagy molecule LC3, within the radiocarpal joint (representative images in Figure 2.10A and 2.10B). CAIA mice treated with Embelin, HCQ and a combination of Embelin and HCQ had a significantly greater number of TUNEL positive cells compared to CAIA untreated mice in the radiocarpal joint (p = 0.003, p = 0.0004 and p = 0.001, respectively; Figure 2.10C). No significant difference was identified in the number of TUNEL positive cells between all treatment groups (Figure 2.10C).

LC3 expression was observed on the surface of the articular cartilage and cartilage of the epiphyseal growth plate (Figure 2.10B) and the proportion of LC3 positive staining was significantly higher (p < 0.005) in all CAIA groups compared to control mice (see Appendix I, Supplementa1 Table 1 & 2). However, there was no statistically significant difference in the proportion of positive LC3 staining between all disease and treatment groups.
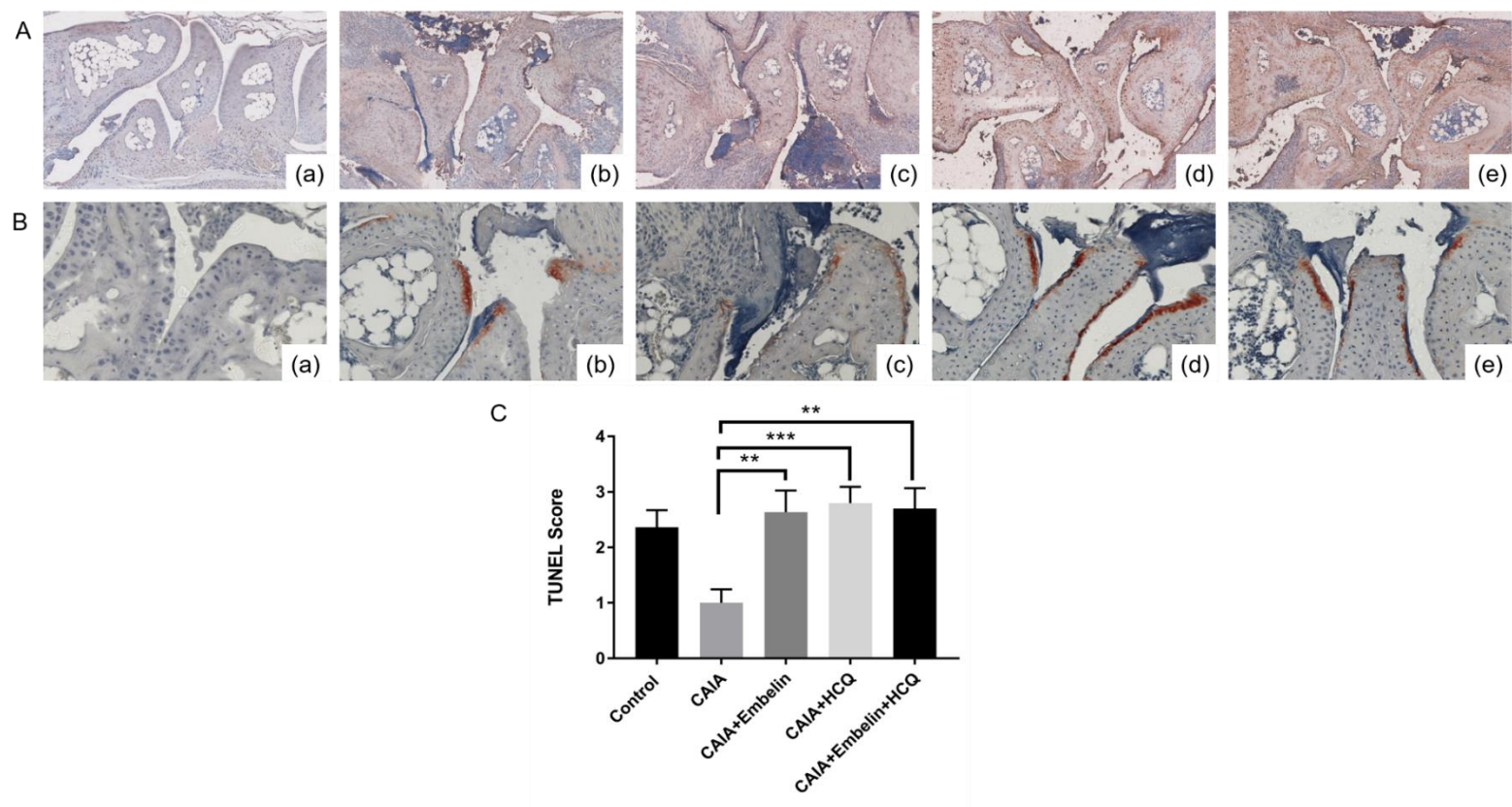
Figure 2.10. Histological assessment of apoptosis and autophagy molecules in the radiocarpal joint. Representative images of sagittal sections of the radiocarpal joint stained with TUNEL (indicated in red) with haematoxylin counterstaining (A; 10x magnification) and LC3 protein expression (indicated in red) with haematoxylin counterstaining (B; 40x magnification); (a) control, (b) CAIA, (c) CAIA + Embelin, (d) CAIA + HCQ and (e) CAIA + Embelin + HCQ. C. Semi-quantitative scores of TUNEL positive cells in sagittal sections of the radiocarpal joint at day 11. Error bars represent SEM (n = 12 paws per group; ** $p < 0.01$, ***$p < 0.0004$, compared to CAIA).

2.6. Discussion

The results of this study suggest a complex relationship between autophagy and apoptosis during inflammatory processes *in vitro* and *in vivo*. Embelin, a small non-peptide inhibitor of XIAP, was used to assess the effect of inducing apoptosis in osteoclastogenic formation *in vitro* and in inflammatory arthritis *in vivo*. Whereas HCQ, reported to inhibit lysosomal degradation (33), was used to investigate autophagy, hence we can compare these distinct mechanisms. From this, we were able to demonstrate the concurrent regulation and cross talk between these pathways of cell death and survival. In addition, our initial findings investigating Embelin or HCQ in isolation were extended by assessing the effects of combining these treatments on inflammation and bone erosion in the CAIA model.

The inflamed RA joint is an environment conducive to enhanced osteoclastogenesis and bone destruction. RANKL is highly expressed in the RA synovium (57) and is required for the differentiation of precursors into TRAP positive cells and activation into mature, active osteoclasts, capable of resorbing bone both in a physiological and pathological state (3, 58). Inflammatory cytokines, such as TNF-α, are also highly expressed in the RA synovium (59). These cytokines not only induce additional RANKL on synovial fibroblasts and T cells, but have a direct stimulatory effect on osteoclast differentiation and bone resorbing activity (60). The *in vitro* assay utilised in this study represents this active, pathological process in isolation. Osteoclast precursors were exposed to both RANKL and TNF-α to induce cytokine stimulated differentiation of TRAP positive bone resorbing cells. Cells were then treated with Embelin and HCQ to investigate the effects on apoptosis and autophagy mechanisms and the therapeutic potential of suppressing further osteoclast resorption.

The induction of apoptosis using Embelin and the suppression of autophagy with HCQ produced similar effects in PBMC-derived osteoclasts and were strongly indicated in our results by TUNEL assay, protein expression and morphological feature analysis using TEM and live cell imaging. The absence of variations in total cell viability between treatments and control, as assessed by WST-1, could be related to the specific action of the compound in osteoclastic cells *in vitro*, as significant reductions in large TRAP

positive multinucleated cells were observed, despite maintaining a large presence of unaffected viable monocytes.

At the gene level, HCQ inhibited beclin-1 and LC3 mRNA. The key osteoclastic transcription factor, NFATc1 was also suppressed at the mRNA level by Embelin and HCQ. Unexpectedly, an increase in TRAP mRNA by Embelin and HCQ was observed. As the transcription factor NFATc1 directly regulates osteoclastic specific genes, including TRAP, it was expected that mRNA levels of TRAP would also be reduced by Embelin and HCQ. This discrepancy could be attributed to the transcriptional activities of pre-formed NFATc1 at the TRAP promoter region (61), prior to the addition of Embelin and HCQ treatments. Future studies should assess the molecular targets of NFATc1 at later time points in addition to proteomic confirmation. The relationship of autophagy inhibition and apoptosis induction was observed in cells treated with HCQ and Embelin and supported by the observation of reduced belcin-1 and LC3 protein expression, with concomitant increase in the apoptosis marker TUNEL demonstrated in dual staining. As a result, our findings partly support the concept of an inverse relationship between autophagy and apoptosis in human osteoclasts under experimental conditions. Beclin-1 has been shown to regulate bone marrow macrophage differentiation into osteoclasts and is also required for RANKL-induced osteoclast differentiation (30). Beclin-1 knockdown has been shown to suppress RANKL-induced activation of NFATc1 (30). Thus, our study supports these findings, as our data demonstrates the suppression of beclin-1 genes and protein by HCQ and Embelin in mature osteoclasts ultimately leading to a reduction of osteoclast formation and activity.

Analyses of gene expression by RT PCR, though very sensitive, inadequately represents formed protein expression and function, particularly for detecting autophagy flux and end stage apoptosis when cells have undergone cellular morphological changes (5, 62). The investigation of these apoptotic and osteoclast related genes is imperative to the investigation of the molecular pathways of both apoptosis and autophagy. Gene expression was assessed in conjunction with visualisation and assessment of apoptosis and autophagy by TEM, the gold standard of autophagy analysis, and TUNEL staining, which is regarded as a reliable and representative assessment of this stage of apoptosis (63, 64).

Recent studies have identified prominent epigenetic modifications involved with regulating the transcriptional activity of key factors that mediate target gene promoters of autophagy and apoptosis (65, 66). Such modifications may contribute to the discrepancies observed between gene and protein expression. Early gene expression (6 hours) of apoptosis was also investigated in this study, however there were no significant variations between treatments and control. Further studies including gene expression analyses at multiple time points in addition to increasing donor pool to reduce donor variability and isolate the exact stage of altered epigenetic processes and the induction of apoptosis at the mRNA level are warranted.

It is important to also highlight the dose and time dependent induction of autophagy or apoptosis by HCQ. Time dependency is evident in our study, whereby autophagy gene suppression was seen at the earlier time point (6 hours) and apoptosis induction was seen later at 24 hours (as observed by TUNEL assay, morphological features by TEM and live cell imaging). It is also possible that the reduction of beclin-1 is associated with the degradation of beclin-1 by caspase 3, as beclin-1 is a substrate of caspase 3 (67, 68). In CAIA mice, HCQ did not reduce inflammation as shown by clinical paw assessment on days 5 through to 7. However, by day 10 HCQ treatment had reduced inflammation in CAIA mice. This may further indicate that longer treatment duration is needed for HCQ to induce apoptosis *in vivo* and therefore reduce inflammation, consistent with what has been observed in the human application of HCQ (33).

The results of the current study support the recent observations by Both *et al.* 2018, of HCQ actions by reducing TRAP positive osteoclast cell formation and bone resorption *in vitro* (35). However, we did not observe the anti-catabolic actions of HCQ *in vivo,* as reported by Both *et al.* 2018 both *in vitro* and in RA patients. This contradiction may be a result of discrepancies in the pathogenesis or a dose factor and/or longevity of treatment regimens in patients compared to an experimental arthritis murine model. Further to this, serum carboxy-terminal collagen crosslinks (CTX) used by Both *et al.* 2018 (35), as the surrogate marker of bone damage, is highly sensitive in detecting the products of bone turnover at the molecular level, whilst the methods utilised in the current study, such as micro-CT, detect effects on bone at the microscopic level. Previously, Dharmapatni *et al.* 2015, reported a reduction of serum CTX in the absence of a significant increase in bone

volume by micro-CT following Embelin treatment in a CAIA murine model (10). However, this was not replicated in the current murine model as both micro-CT and serum CTX analyses (see Appendix I; Supplemental Figure 1) confirmed no significant variations between healthy mice and those with inflammatory arthritis. Future investigations in experimental RA should complement micro-CT scanning with additional data such as serum CTX levels.

As expected, HCQ induced the accumulation of autophagy vesicles preceding cell death. This was observed in a subset of cells via TEM and cyto ID staining. HCQ is known to inhibit autophagy at the end stage by inhibiting lysosome action, thus HCQ still allows the fusion between the autophagosome and the lysosome. As the lysosome action is suppressed, lysosomal degradation of the cargo is inhibited, leading to a decrease in autophagy flux.

Autophagosome formation involves the recruitment of the P62 adaptor molecule to bind to phosphatidylethanolamine (PE) conjugated LC3II, located within the membrane of autophagosomes and autolysosomes (69). Our findings showed an increase in P62 protein expression and a decrease in cytosolic LC3 expression following HCQ treatment, as observed in western blot analysis and fluorescent immunocytochemistry. This is consistent with increased autophagosome formation observed by cyto ID staining. The decrease in cytosolic LC3 following HCQ treatment observed in this study, thus may result from the conjugation of LC3I, located within the cytoplasm, with PE to form LC3II required for the formation of the autophagosomes observed. Further experiments to assess LC3II expression are warranted to confirm the inhibition of autophagy flux following HCQ treatment.

We observed an intriguing finding *in vivo*, where LC3 expression is observed within the articular cartilage with a significantly higher proportion in CAIA mice compared to healthy mice. There was no difference observed in the expression of LC3 in the articular cartilage between treated and untreated CAIA mice, suggesting that LC3 expression has not been modified by Embelin and/or HCQ *in vivo*. Studies have identified LC3 expression on chondrocytes (70-72), thus the increase in LC3 expression observed in this

current study supports a strong association between LC3 positivity and the occurrence of the disease related to pathological destruction of articular cartilage in RA. Conflicting findings regarding LC3 expression in human OA cartilage has been reported by Chang *et al.* 2013 where an increase in LC3 levels was observed (73). However, Carames *et al.* 2010 observed a reduction in LC3 expression in OA human articular cartilage indicating the need for further investigation on the dual role of LC3 as a cytoprotective or cell-death associated contributor in cartilage degeneration (74).

The autophagy vesicle accumulation following HCQ treatment prior to apoptosis may also indicate type 2 cell death which refers to cell death with autophagic features. However, analysis of both morphological changes and biochemical characteristics support that cell death is most likely by apoptosis. Accumulation of autophagic vacuoles has been reported to precede apoptotic cell death in prolonged nutrient starvation and as a result over-activated autophagy and can result in type 2 cell death (20, 75). HCQ treatment of CAIA mice, resulted in a greater number of TUNEL positive cells in the radiocarpal joint compared to untreated CAIA mice which supports the notion that HCQ can induce apoptosis *in vivo*. The expected synergistic effect of the combined treatment of Embelin and HCQ on apoptosis and bone preservation was not observed *in vivo* compared to untreated CAIA mice. However, future investigations should include dual-staining techniques to identify if specific cell subsets are affected by HCQ and/or Embelin *in vivo* to elucidate targeted effects.

Modulation of autophagy molecules by Embelin has been reported in human umbilical vein endothelial cells. This was associated with reduced cell proliferation and increased conversion of LC3I to LC3II, which may mirror autophagy cell death (76). However, Coutelle *et al.* 2014 proposed that autophagy was not the major mechanism of cell death induced by Embelin as it was not reversed by the addition of the autophagy inhibitor Bafilomycin (76). In contrast to our study, induction of autophagy by Embelin was also reported in the colon carcinoma cell line HCT116 (77). Both studies used greater doses of Embelin than what was assessed in the present study, and thus may influence its efficacy. As apoptosis induction by Embelin is known to be rapid, we propose that inhibition of autophagy by Embelin may occur at a very early stage.

Embelin administered daily at 30 mg/kg in CAIA mice initially suppressed local inflammation, as shown by significantly lower clinical paw scores. However, from day 7 when experimental arthritis is thought to reach its peak severity, Embelin had no significant effect reducing paw inflammation. This contrasts with Dharmapatni *et al.* 2015 who observed a significant reduction in inflammation by day 10 following Embelin treatment (10). The combined treatment of HCQ and Embelin showed lower paw scores from day 8-10, however this was not statistically significant. This was observed in both the PV (volumetric indicator of soft tissue swelling) assessed by high resolution micro-CT and histological assessment of inflammatory cell infiltrate in the radiocarpal joints.

The conflicting findings when compared to past studies may also be a result of the methodology employed to assess paw inflammation. In Dharmapatni *et al.* 2015 paw swelling was assessed using a semi quantitative clinical score and histological analyses (10), while the current study took advantage of the novel method of assessing both bone and soft tissue volume from micro-CT imaging as an additional quantitative technique to assess paw inflammation. In the CAIA model, the joints are also randomly affected due to the systemic administration of monoclonal antibodies targeting type-II collagen (78). Thus, the large mouse variability in response to both disease and treatment may explain the results in the current study. There may also be variability in the absorption and availability of active metabolites of Embelin within the circulation following oral administration which may have affected the results obtained in the two studies. To achieve a more effective result in the complex *in vivo* environment the use of an animal model that targets specific joints through the intra-articular injection of the antigen, as well as the intra-articular administration of Embelin may provide a better strategy for future studies.

The mechanism by which Embelin suppresses bone resorption in pathological conditions is still unknown and has only been investigated *in vivo* in a CAIA mouse model. Dharmapatni *et al.* 2015 found that mice treated with low dose Embelin exhibited less bone erosion compared to CAIA untreated mice (10). This was not statistically significant, however, could be attributed to the small number of paws analysed in that study. Embelin has also been identified to suppress RANKL induced activation of osteoclasts via inhibiting NF-κB in RAW 264.7 cells (18). In the present study, Embelin

effectively suppressed the formation and bone resorbing activity of human osteoclastic cells *in vitro* through mechanisms associated with the induction of apoptosis. However, we identified increased TRAP positive osteoclast like cells in the radiocarpal joint, and although not significant, the lowest BV measurements were observed in CAIA mice treated with 30mg/kg Embelin compared to CAIA mice treated with HCQ alone or in combination with Embelin. In the current study, disease was induced with 1.5 mg of collagen antibodies combined with 10 µg of LPS, based on previous studies in our laboratory (10, 47). This results in a milder inflammatory response and could explain the minimal bone erosion observed in all disease and treatment groups. In contrast, the original study involved induction of a severe form of the disease with 2-4 mg of collagen antibodies combined with 50 µg of LPS (78). There are also conflicting reports on the effects of HCQ on bone turnover. Increased bone mineral density has been reported to be associated with HCQ treatment in patients with systemic lupus erythematosus (79). However, Both *et al.* 2018, reported that HCQ treatment decreases human MSC-derived osteoblast differentiation and mineralisation *in vitro* (80). This further indicates the likelihood of discrepancies between *in vitro* and *in vivo* studies due to *in vitro* studies lacking the systemic factors that stimulate bone turnover. Although conflicting findings were identified throughout the study, these results support the complex mechanisms associated with pathological processes *in vivo* and require further investigation to elucidate other factors associated with cell survival and stimulation. Future studies should investigate varying the dose or means of administration to effectively target the specific cells involved with bone destruction and inflammation in the joints.

2.7. Conclusion

This is the first study to provide functional data on the association between autophagy and apoptosis in human PBMC-derived osteoclasts using pharmacological modulators. The pharmacological approach used in this study increases clinical translatability and provides a foundation for future studies targeting these cellular processes in a more specific way. Our findings indicate that inducing osteoclast apoptosis with Embelin and inhibiting autophagy with HCQ is beneficial in preventing pathological bone loss by TNF-α stimulated osteoclasts *in vitro.* It was proposed that there would be a synergistic action between Embelin and HCQ when used in combination *in vivo,* however based on our findings the synergistic actions on the measured outcomes of this study were not identified. Further investigations involving larger sample number and new strategies are required to elucidate the effectiveness and specificity of these compounds *in vivo*.

2.8. References

1.   Mikuls TR. Co-morbidity in rheumatoid arthritis. Best practice & research Clinical rheumatology. 2003;17(5):729-52.

2.   Romas E, Gillespie MT, Martin TJ. Involvement of receptor activator of NFkappaB ligand and tumor necrosis factor-alpha in bone destruction in rheumatoid arthritis. Bone. 2002;30(2):340-6.

3.   Gravallese EM, Manning C, Tsay A, Naito A, Pan C, Amento E, et al. Synovial tissue in rheumatoid arthritis is a source of osteoclast differentiation factor. Arthritis Rheum. 2000;43(2):250-8.

4.   Dharmapatni AA, Smith MD, Findlay DM, Holding CA, Evdokiou A, Ahern MJ, et al. Elevated expression of caspase-3 inhibitors, survivin and xIAP correlates with low levels of apoptosis in active rheumatoid synovium. Arthritis research & therapy. 2009;11(1):R13.

5.   Elmore S. Apoptosis: a review of programmed cell death. Toxicologic pathology. 2007;35(4):495-516.

6.   Perlman H, Liu H, Georganas C, Koch AE, Shamiyeh E, Haines GK, 3rd, et al. Differential expression pattern of the antiapoptotic proteins, Bcl-2 and FLIP, in experimental arthritis. Arthritis and rheumatism. 2001;44(12):2899-908.

7.   Durand M, Boire G, Komarova SV, Dixon SJ, Sims SM, Harrison RE, et al. The increased in vitro osteoclastogenesis in patients with rheumatoid arthritis is due to increased percentage of precursors and decreased apoptosis - the In Vitro Osteoclast Differentiation in Arthritis (IODA) study. Bone. 2011;48(3):588-96.

8.   Bokarewa M, Lindblad S, Bokarew D, Tarkowski A. Balance between survivin, a key member of the apoptosis inhibitor family, and its specific antibodies determines erosivity in rheumatoid arthritis. Arthritis research & therapy. 2005;7(2):R349-58.

9.   Smith MD, Weedon H, Papangelis V, Walker J, Roberts-Thomson PJ, Ahern MJ. Apoptosis in the rheumatoid arthritis synovial membrane: modulation by disease-modifying anti-rheumatic drug treatment. Rheumatology (Oxford, England). 2010;49(5):862-75.

10.   Dharmapatni AA, Cantley MD, Marino V, Perilli E, Crotti TN, Smith MD, et al. The X-Linked Inhibitor of Apoptosis Protein Inhibitor Embelin Suppresses

Inflammation and Bone Erosion in Collagen Antibody Induced Arthritis Mice. Mediators Inflamm. 2015;2015:564042.

11. Nikolovska-Coleska Z, Xu L, Hu Z, Tomita Y, Li P, Roller PP, et al. Discovery of embelin as a cell-permeable, small-molecular weight inhibitor of XIAP through structure-based computational screening of a traditional herbal medicine three-dimensional structure database. Journal of medicinal chemistry. 2004;47(10):2430-40.

12. Chen J, Nikolovska-Coleska Z, Wang G, Qiu S, Wang S. Design, synthesis, and characterization of new embelin derivatives as potent inhibitors of X-linked inhibitor of apoptosis protein. Bioorganic & medicinal chemistry letters. 2006;16(22):5805-8.

13. Xu M, Cui J, Fu H, Proksch P, Lin W, Li M. Embelin derivatives and their anticancer activity through microtubule disassembly. Planta medica. 2005;71(10):944-8.

14. Chitra M, Sukumar E, Suja V, Devi CS. Antitumor, anti-inflammatory and analgesic property of embelin, a plant product. Chemotherapy. 1994;40(2):109-13.

15. Ahn KS, Sethi G, Aggarwal BB. Embelin, an inhibitor of X chromosome-linked inhibitor-of-apoptosis protein, blocks nuclear factor-kappaB (NF-kappaB) signaling pathway leading to suppression of NF-kappaB-regulated antiapoptotic and metastatic gene products. Molecular pharmacology. 2007;71(1):209-19.

16. Mori T, Doi R, Kida A, Nagai K, Kami K, Ito D, et al. Effect of the XIAP inhibitor Embelin on TRAIL-induced apoptosis of pancreatic cancer cells. The Journal of surgical research. 2007;142(2):281-6.

17. Dai Y, Jiao H, Teng G, Wang W, Zhang R, Wang Y, et al. Embelin reduces colitis-associated tumorigenesis through limiting IL-6/STAT3 signaling. Molecular cancer therapeutics. 2014;13(5):1206-16.

18. Reuter S, Prasad S, Phromnoi K, Kannappan R, Yadav VR, Aggarwal BB. Embelin suppresses osteoclastogenesis induced by receptor activator of NF-kappaB ligand and tumor cells in vitro through inhibition of the NF-kappaB cell signaling pathway. Molecular cancer research : MCR. 2010;8(10):1425-36.

19. Maiuri MC, Zalckvar E, Kimchi A, Kroemer G. Self-eating and self-killing: crosstalk between autophagy and apoptosis. Nature reviews Molecular cell biology. 2007;8(9):741-52.

20. Gonzalez-Polo RA, Boya P, Pauleau AL, Jalil A, Larochette N, Souquere S, et al. The apoptosis/autophagy paradox: autophagic vacuolization before apoptotic death. J Cell Sci. 2005;118(Pt 14):3091-102.

21. Mukhopadhyay S, Panda PK, Sinha N, Das DN, Bhutia SK. Autophagy and apoptosis: where do they meet? Apoptosis. 2014;19(4):555-66.

22. Amaravadi RK, Lippincott-Schwartz J, Yin XM, Weiss WA, Takebe N, Timmer W, et al. Principles and current strategies for targeting autophagy for cancer treatment. Clin Cancer Res. 2011;17(4):654-66.

23. He C, Klionsky DJ. Regulation mechanisms and signaling pathways of autophagy. Annu Rev Genet. 2009;43:67-93.

24. Klionsky DJ, Cuervo AM, Seglen PO. Methods for monitoring autophagy from yeast to human. Autophagy. 2007;3(3):181-206.

25. Liang XH, Jackson S, Seaman M, Brown K, Kempkes B, Hibshoosh H, et al. Induction of autophagy and inhibition of tumorigenesis by beclin 1. Nature. 1999;402(6762):672-6.

26. Klionsky DJ, Abeliovich H, Agostinis P, Agrawal DK, Aliev G, Askew DS, et al. Guidelines for the use and interpretation of assays for monitoring autophagy in higher eukaryotes. Autophagy. 2008;4(2):151-75.

27. Xu K, Xu P, Yao JF, Zhang YG, Hou WK, Lu SM. Reduced apoptosis correlates with enhanced autophagy in synovial tissues of rheumatoid arthritis. Inflammation research : official journal of the European Histamine Research Society [et al]. 2013;62(2):229-37.

28. Yang Z, Fujii H, Mohan SV, Goronzy JJ, Weyand CM. Phosphofructokinase deficiency impairs ATP generation, autophagy, and redox balance in rheumatoid arthritis T cells. The Journal of experimental medicine. 2013;210(10):2119-34.

29. Lin NY, Beyer C, Giessl A, Kireva T, Scholtysek C, Uderhardt S, et al. Autophagy regulates TNFalpha-mediated joint destruction in experimental arthritis. Annals of the rheumatic diseases. 2013;72(5):761-8.

30. Chung YH, Jang Y, Choi B, Song DH, Lee EJ, Kim SM, et al. Beclin-1 Is Required for RANKL-Induced Osteoclast Differentiation. J Cell Physiol. 2014;229(12):1963-71.

31. DeSelm CJ, Miller BC, Zou W, Beatty WL, van Meel E, Takahata Y, et al. Autophagy proteins regulate the secretory component of osteoclastic bone resorption. Dev Cell. 2011;21(5):966-74.

32. Korb A, Pavenstadt H, Pap T. Cell death in rheumatoid arthritis. Apoptosis : an international journal on programmed cell death. 2009;14(4):447-54.

33. Carmichael SJ, Charles B, Tett SE. Population pharmacokinetics of hydroxychloroquine in patients with rheumatoid arthritis. Therapeutic drug monitoring. 2003;25(6):671-81.

34. Han J, Zhou Q, Li X, He J, Han Y, Jie H, et al. Novel function of hydroxychloroquine: Down regulation of T follicular helper cells in collagen-induced arthritis. Biomedicine & pharmacotherapy = Biomedecine & pharmacotherapie. 2018;97:838-43.

35. Both T, Zillikens MC, Schreuders-Koedam M, Vis M, Lam WK, Weel A, et al. Hydroxychloroquine affects bone resorption both in vitro and in vivo. J Cell Physiol. 2018;233(2):1424-33.

36. Cantley MD, Fairlie DP, Bartold PM, Rainsford KD, Le GT, Lucke AJ, et al. Inhibitors of histone deacetylases in class I and class II suppress human osteoclasts in vitro. J Cell Physiol. 2011;226(12):3233-41.

37. Lagneaux L, Delforge A, Carlier S, Massy M, Bernier M, Bron D. Early induction of apoptosis in B-chronic lymphocytic leukaemia cells by hydroxychloroquine: activation of caspase-3 and no protection by survival factors. Br J Haematol. 2001;112(2):344-52.

38. Meng XW, Feller JM, Ziegler JB, Pittman SM, Ireland CM. Induction of apoptosis in peripheral blood lymphocytes following treatment in vitro with hydroxychloroquine. Arthritis Rheum. 1997;40(5):927-35.

39. Kim WU, Yoo SA, Min SY, Park SH, Koh HS, Song SW, et al. Hydroxychloroquine potentiates Fas-mediated apoptosis of rheumatoid synoviocytes. Clin Exp Immunol. 2006;144(3):503-11.

40. Alias E, Dharmapatni AS, Holding AC, Atkins GJ, Findlay DM, Howie DW, et al. Polyethylene particles stimulate expression of ITAM-related molecules in peri-implant tissues and when stimulating osteoclastogenesis in vitro. Acta Biomater. 2012;8(8):3104-12.

41. Livak KJ, Schmittgen TD. Analysis of relative gene expression data using real-time quantitative PCR and the 2(-Delta Delta C(T)) Method. Methods. 2001;25(4):402-8.

42. Burstone MS. Histochemical demonstration of acid phosphatases with naphthol AS-phosphates. J Natl Cancer Inst. 1958;21(3):523-39.

43.   Holding CA, Findlay DM, Stamenkov R, Neale SD, Lucas H, Dharmapatni AS, et al. The correlation of RANK, RANKL and TNFalpha expression with bone loss volume and polyethylene wear debris around hip implants. Biomaterials. 2006;27(30):5212-9.

44.   Chan LL, Shen D, Wilkinson AR, Patton W, Lai N, Chan E, et al. A novel image-based cytometry method for autophagy detection in living cells. Autophagy. 2012;8(9):1371-82.

45.   Elsasser A, Vogt AM, Nef H, Kostin S, Mollmann H, Skwara W, et al. Human hibernating myocardium is jeopardized by apoptotic and autophagic cell death. J Am Coll Cardiol. 2004;43(12):2191-9.

46.   Martinet W, Timmermans JP, De Meyer GR. Methods to assess autophagy in situ--transmission electron microscopy versus immunohistochemistry. Methods in enzymology. 2014;543:89-114.

47.   Williams B, Tsangari E, Stansborough R, Marino V, Cantley M, Dharmapatni A, et al. Mixed effects of caffeic acid phenethyl ester (CAPE) on joint inflammation, bone loss and gastrointestinal inflammation in a murine model of collagen antibody-induced arthritis. Inflammopharmacology. 2017;25(1):55-68.

48.   Perilli E, Cantley M, Marino V, Crotti TN, Smith MD, Haynes DR, et al. Quantifying not only bone loss, but also soft tissue swelling, in a murine inflammatory arthritis model using micro-computed tomography. Scandinavian journal of immunology. 2015;81(2):142-50.

49.   Luu YK, Lublinsky S, Ozcivici E, Capilla E, Pessin JE, Rubin CT, et al. In vivo quantification of subcutaneous and visceral adiposity by micro-computed tomography in a small animal model. Medical engineering & physics. 2009;31(1):34-41.

50.   Perilli E, Baruffaldi F, Visentin M, Bordini B, Traina F, Cappello A, et al. MicroCT examination of human bone specimens: effects of polymethylmethacrylate embedding on structural parameters. Journal of microscopy. 2007;225(Pt 2):192-200.

51.   Lane NE, Thompson JM, Haupt D, Kimmel DB, Modin G, Kinney JH. Acute changes in trabecular bone connectivity and osteoclast activity in the ovariectomized rat in vivo. Journal of bone and mineral research : the official journal of the American Society for Bone and Mineral Research. 1998;13(2):229-36.

52.	Perilli E, Le V, Ma B, Salmon P, Reynolds K, Fazzalari NL. Detecting early bone changes using in vivo micro-CT in ovariectomized, zoledronic acid-treated, and sham-operated rats. Osteoporosis international : a journal established as result of cooperation between the European Foundation for Osteoporosis and the National Osteoporosis Foundation of the USA. 2010;21(8):1371-82.

53.	Perilli E, Briggs AM, Kantor S, Codrington J, Wark JD, Parkinson IH, et al. Failure strength of human vertebrae: prediction using bone mineral density measured by DXA and bone volume by micro-CT. Bone. 2012;50(6):1416-25.

54.	Cantley MD, Fairlie DP, Bartold PM, Marino V, Gupta PK, Haynes DR. Inhibiting histone deacetylase 1 suppresses both inflammation and bone loss in arthritis. Rheumatology (Oxford). 2015;54(9):1713-23.

55.	Deveraux QL, Takahashi R, Salvesen GS, Reed JC. X-linked IAP is a direct inhibitor of cell-death proteases. Nature. 1997;388(6639):300-4.

56.	Gravallese EM, Harada Y, Wang JT, Gorn AH, Thornhill TS, Goldring SR. Identification of cell types responsible for bone resorption in rheumatoid arthritis and juvenile rheumatoid arthritis. The American journal of pathology. 1998;152(4):943-51.

57.	Crotti TN, Smith MD, Weedon H, Ahern MJ, Findlay DM, Kraan M, et al. Receptor activator NF-kappaB ligand (RANKL) expression in synovial tissue from patients with rheumatoid arthritis, spondyloarthropathy, osteoarthritis, and from normal patients: semiquantitative and quantitative analysis. Ann Rheum Dis. 2002;61(12):1047-54.

58.	Takayanagi H, Ogasawara K, Hida S, Chiba T, Murata S, Sato K, et al. T-cell-mediated regulation of osteoclastogenesis by signalling cross-talk between RANKL and IFN-gamma. Nature. 2000;408(6812):600-5.

59.	Saklatvala J. Tumour necrosis factor alpha stimulates resorption and inhibits synthesis of proteoglycan in cartilage. Nature. 1986;322(6079):547-9.

60.	Algate K, Haynes DR, Bartold PM, Crotti TN, Cantley MD. The effects of tumour necrosis factor-alpha on bone cells involved in periodontal alveolar bone loss; osteoclasts, osteoblasts and osteocytes. Journal of periodontal research. 2016;51(5):549-66.

61.	Yu M, Moreno JL, Stains JP, Keegan AD. Complex regulation of tartrate-resistant acid phosphatase (TRAP) expression by interleukin 4 (IL-4): IL-4 indirectly suppresses receptor activator of NF-kappaB ligand (RANKL)-mediated TRAP

expression but modestly induces its expression directly. The Journal of biological chemistry. 2009;284(47):32968-79.

62.   Slee EA, Adrain C, Martin SJ. Executioner caspase-3, -6, and -7 perform distinct, non-redundant roles during the demolition phase of apoptosis. The Journal of biological chemistry. 2001;276(10):7320-6.

63.   Kerr JF, Wyllie AH, Currie AR. Apoptosis: a basic biological phenomenon with wide-ranging implications in tissue kinetics. British journal of cancer. 1972;26(4):239-57.

64.   Taatjes DJ, Sobel BE, Budd RC. Morphological and cytochemical determination of cell death by apoptosis. Histochemistry and cell biology. 2008;129(1):33-43.

65.   Liu WJ, Ye L, Huang WF, Guo LJ, Xu ZG, Wu HL, et al. p62 links the autophagy pathway and the ubiqutin-proteasome system upon ubiquitinated protein degradation. Cellular & molecular biology letters. 2016;21:29.

66.   Artal-Martinez de Narvajas A, Gomez TS, Zhang JS, Mann AO, Taoda Y, Gorman JA, et al. Epigenetic regulation of autophagy by the methyltransferase G9a. Molecular and cellular biology. 2013;33(20):3983-93.

67.   Decuypere JP, Parys JB, Bultynck G. Regulation of the autophagic bcl-2/beclin 1 interaction. Cells. 2012;1(3):284-312.

68.   Jacquel A, Obba S, Solary E, Auberger P. Proper macrophagic differentiation requires both autophagy and caspase activation. Autophagy. 2014;8(7):1141-3.

69.   Mizushima N, Yoshimori T. How to interpret LC3 immunoblotting. Autophagy. 2007;3(6):542-5.

70.   Charlier E, Relic B, Deroyer C, Malaise O, Neuville S, Collee J, et al. Insights on Molecular Mechanisms of Chondrocytes Death in Osteoarthritis. International journal of molecular sciences. 2016;17(12).

71.   Sasaki H, Takayama K, Matsushita T, Ishida K, Kubo S, Matsumoto T, et al. Autophagy modulates osteoarthritis-related gene expression in human chondrocytes. Arthritis Rheum. 2012;64(6):1920-8.

72.   Rosenthal AK, Gohr CM, Mitton-Fitzgerald E, Grewal R, Ninomiya J, Coyne CB, et al. Autophagy modulates articular cartilage vesicle formation in primary articular chondrocytes. The Journal of biological chemistry. 2015;290(21):13028-38.

73. Chang J, Wang W, Zhang H, Hu Y, Wang M, Yin Z. The dual role of autophagy in chondrocyte responses in the pathogenesis of articular cartilage degeneration in osteoarthritis. International journal of molecular medicine. 2013;32(6):1311-8.

74. Carames B, Taniguchi N, Otsuki S, Blanco FJ, Lotz M. Autophagy is a protective mechanism in normal cartilage, and its aging-related loss is linked with cell death and osteoarthritis. Arthritis Rheum. 2010;62(3):791-801.

75. Galluzzi L, Vicencio JM, Kepp O, Tasdemir E, Maiuri MC, Kroemer G. To die or not to die: that is the autophagic question. Curr Mol Med. 2008;8(2):78-91.

76. Coutelle O, Hornig-Do HT, Witt A, Andree M, Schiffmann LM, Piekarek M, et al. Embelin inhibits endothelial mitochondrial respiration and impairs neoangiogenesis during tumor growth and wound healing. EMBO Mol Med. 2014;6(5):624-39.

77. Huang X, Wu Z, Mei Y, Wu M. XIAP inhibits autophagy via XIAP-Mdm2-p53 signalling. EMBO J. 2013;32(16):2204-16.

78. Khachigian LM. Collagen antibody-induced arthritis. Nature protocols. 2006;1(5):2512-6.

79. Lakshminarayanan S, Walsh S, Mohanraj M, Rothfield N. Factors associated with low bone mineral density in female patients with systemic lupus erythematosus. The Journal of rheumatology. 2001;28(1):102-8.

80. Both T, van de Peppel HJ, Zillikens MC, Koedam M, van Leeuwen J, van Hagen PM, et al. Hydroxychloroquine decreases human MSC-derived osteoblast differentiation and mineralization in vitro. Journal of cellular and molecular medicine. 2018;22(2):873-82.

CHAPTER 3: THE EFFECT OF AN N-CADHERIN ANTAGONIST, CRS-066, ON JOINT INFLAMMATION AND BONE LOSS IN A MURINE MODEL OF INFLAMMATORY ARTHRITIS; A PILOT STUDY

B. Williams, E. Tsangari, O. Blaschuk, D.R. Haynes, T.N. Crotti, E. Perilli, A. Dharmapatni

Chapter Summary:

Cell adhesion molecules have recently been identified to play crucial roles in perpetuating inflammatory cell infiltration, pannus formation and overall bone destruction in RA. However, the specific role of cell adhesion molecules, such as N-cadherin, in osteoclast activity *in vitro* and in the context of RA *in vivo* is unknown. Thus, this study aimed to investigate the effect of the N-cadherin antagonist CRS-066 on the development of inflammation and bone loss in a mild murine model of inflammatory arthritis.

3.1. Abstract

The pathogenesis of rheumatoid arthritis (RA) involves the hyperproliferation of fibroblast-like synoviocytes (FLS) and infiltration of inflammatory cells, contributing to pannus formation and the production of inflammatory mediators within affected synovial joints. Cell adhesion molecules, including cadherins, play a crucial role in promoting an interaction between FLS and between FLS and infiltrating inflammatory or bone cells within RA. As such, cadherin antagonists, such as the N-cadherin antagonist CRS-066, have the potential to suppress the chronic inflammation process, and subsequent pannus formation and joint destruction in RA. We propose that topical treatment of collagen antibody-induced arthritis (CAIA) in mice with the compound CRS-066 will abrogate FLS hyperplasia, thereby reducing inflammation and joint damage in the synovial joints.

Twenty female Balb/c mice were allocated to four groups; control (n = 6), CAIA (n = 6), CAIA + DMSO (n = 4) and CAIA + CRS-066 (n = 4). In treatment groups the vehicle, DMSO, or N-cadherin antagonist, CRS-066, was applied topically to the front and hind paws every 12 hours, following arthritis development on day 4. Clinical paw inflammation was scored daily. On day 11, bone volume (BV) and paw volume (PV; inflammation) was assessed in the front and hind paws by *ex vivo* micro-CT. Paw sections were stained with haematoxylin and eosin (H&E) and tartrate-resistant acid phosphatase (TRAP), then assessed for joint inflammation, cartilage and bone damage and osteoclast-like cells.

CAIA + CRS-066 mice had significantly lower paw scores compared to CAIA + DMSO mice ($p < 0.05$) on day 6-9, and paw swelling remained lower compared to all diseased groups until endpoint. There was no difference in BV and PV measurements between the front and hind paws of all disease and treatment groups at endpoint. Although not significant, CAIA + CRS-066 had lower scores for cellular infiltration and cartilage and bone degradation compared to CAIA mice. TRAP positive cell number was reduced on the bone surface and in the surrounding soft tissue of CAIA + CRS-066 joints compared to CAIA and CAIA + DMSO mice, however this was not statistically significant.

The findings of this study identified that CRS-066 reduced paw scores during peak stages of the disease and provides evidence for the further investigation into compounds that target cell adhesion molecules in the synovial joint for the treatment of RA.

3.2. Statement of Authorship

Statement of Authorship

Title of Paper	The effect of an N-cadherin antagonist, CRS-066, on joint inflammation and bone loss in a murine model of inflammatory arthritis; a pilot study.	
Publication Status	☐ Published	☐ Accepted for Publication
	☐ Submitted for Publication	☑ Unpublished and Unsubmitted work written in manuscript style
Publication Details		

Principal Author

Name of Principal Author (Candidate)	Bonnie Williams
Contribution to the Paper	First author and main contributor; Concept and methodological design, investigation, project administration, data curation and analysis, formulation of primary draft, in addition to reviewing and incorporating co-author comments and suggestions.
Overall percentage (%)	90
Certification:	This paper reports on original research I conducted during the period of my Higher Degree by Research candidature and is not subject to any obligations or contractual agreements with a third party that would constrain its inclusion in this thesis. I am the primary author of this paper.
Signature	Date 22/2/19

Co-Author Contributions

By signing the Statement of Authorship, each author certifies that:

i.   the candidate's stated contribution to the publication is accurate (as detailed above);

ii. permission is granted for the candidate in include the publication in the thesis; and

iii. the sum of all co-author contributions is equal to 100% less the candidate's stated contribution.

Name of Co-Author	Eleni Tsangari
Contribution to the Paper	Methodology and technical support.
Signature	Date 18/2/19

Name of Co-Author	Orest Blaschuk
Contribution to the Paper	Formulation, supply and methodological advice for use of N-cadherin antagonist.
Signature	*in lieu of* Date 22/2/19

Name of Co-Author	David Haynes		
Contribution to the Paper	Supply and methodological advice for use of N-cadherin antagonist.		
Signature		Date	7/2/19

Name of Co-Author	Tania Crotti		
Contribution to the Paper	Conceptualisation, methodology, supervision and manuscript review.		
Signature		Date	22/2/19

Name of Co-Author	Egon Perilli		
Contribution to the Paper	Methodology support, supervision and manuscript review.		
Signature		Date	01/03/19

Name of Co-Author	Anak Dharmapatni		
Contribution to the Paper	Investigation, funding acquisition, methodology, conceptualisation, supervision and review of manuscript.		
Signature		Date	22/2/19

3.3. Introduction

Rheumatoid arthritis (RA) is a chronic, systemic autoimmune disease which involves inflammation of the synovial tissue, increased joint destruction and local osteopenia (1, 2). Synovial hyperplasia is a hallmark of RA and is one of the major contributors to the formation of invasive pannus tissue within the synovial joints (3). The synovium in normal healthy joints consists of a lining layer of condensed cells, known as fibroblast-like synoviocytes (FLS), and only 1-3 cells thick (4). In RA this lining becomes hyperplastic and transforms into pannus tissue which drives inflammation, leading to destruction of the articular cartilage and underlying subchondral bone (5). Previous studies have supported the role of FLS in the pathogenesis of RA, as the destructive properties of FLS are enhanced by inflammatory factors, such as tumour necrosis factor-alpha (TNF-α), interleukin-1 beta (IL-1β) and interleukin-6 (IL-6). Activated FLS also further enhance the inflammatory cycle within RA synovial joints by producing these inflammatory factors themselves (3, 6, 7).

Cell adhesion is a fundamental biological property and adhesion molecules play a crucial role in the interaction between synovial cells and infiltrating cells in the bone and soft tissue microenvironment (8, 9). Cadherins are a family of integral transmembrane glycoproteins expressed in tissue-restricted patterns that mediate homophilic adhesion between cells (8). In many tissues, cadherins determine the integrity and architecture of the tissue by modulating cell-cell adhesion and interfering with intracellular signalling (10, 11). Cadherins, including cadherin-11 (CDH11), are expressed in FLS in the synovium and are required for the development and organisation of the synovial lining within a synovial joint (12-14). It is thought that cadherins may contribute to the interaction between synovial cells and infiltrating inflammatory cells within RA synovial joints (8, 9). Interactions between synovial stromal cells and osteoblasts mediated through cadherins, may also be involved in the progression of bone destruction in RA. Thus, it is crucial to precisely understand these changes in cell adhesion molecules and their involvement in RA disease progression to assist in finding alternate pathways that can be targeted by novel therapeutics to supress pannus formation and bone erosion in RA.

CDH11 and N-cadherin (cadherin-2; CDH2) are common cell adhesion molecules that have been shown to mediate cell adhesion in a calcium dependent manner (15). CDH11 is largely restricted to mesenchymal lineage cells, while N-cadherin is highly expressed in blood vessels and in poorly differentiated tumour cells (16). However, high levels of CDH11 and N-cadherin have been shown in osteoblasts, bone marrow stromal cells and FLS (4, 17, 18). Distinct roles of CDH11 and N-cadherin have been identified in the skeletal system from mouse genetics and *in vitro* studies (11). These cadherins are anchored to the actin cytoskeleton via binding to β-catenin in a complex that forms adherent junctions (17, 19).

β-catenin is a key component of the canonical Wnt signalling system which controls osteoblastogenesis and bone formation (20-22). Cadherins can modulate signal transduction via the Wnt/β-catenin pathway (23, 24). As CDH11 and N-cadherin bind to β-catenin, they modulate its cytoplasmic pools and the transcriptional activity of osteoblasts, thus stimulating osteoblastogenesis (Figure 3.1). This has been confirmed in previous studies as overexpression of a dominant-negative N-cadherin mutant in differential osteoblasts leads to β-catenin sequestration at the cell surface and decreased bone formation (25). Deletion of N-cadherin, CDH11 or both also causes a reduction in β-catenin abundance at cell-cell contacts and cell-cell adhesion, with a negative effect on osteoblastogenesis and bone regulation (Figure 3.1) (26). Osteoblast apoptosis has also been induced upon disruption of cell-cell adhesion by an anti-N-cadherin antibody (27). Thus, suggesting N-cadherin also plays a role in osteoblast survival and suppression of osteoblast apoptosis.
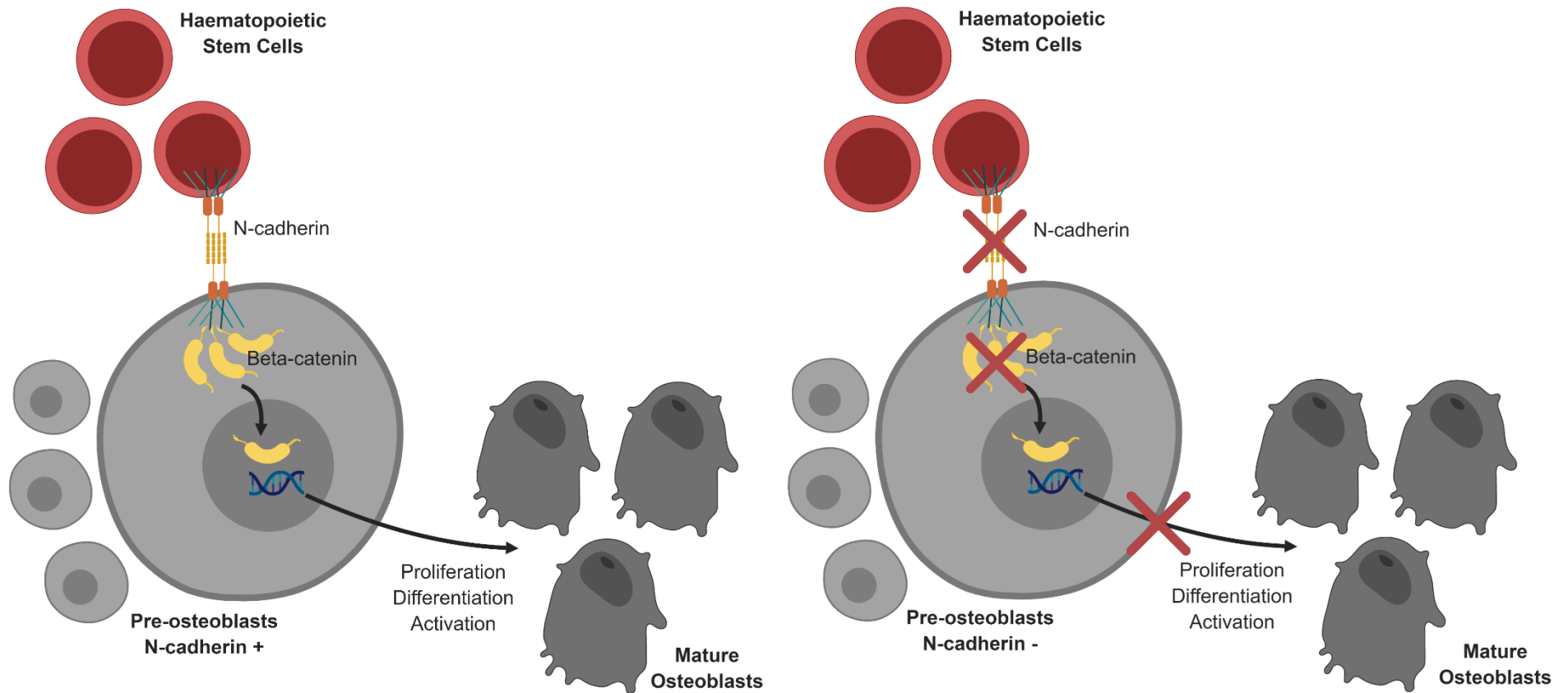
Figure 3.1. Proposed influence of N-cadherin on osteoblastogenesis. N-cadherin is anchored to the cytoskeleton via binding to β-catenin and can therefore modulate signal transduction in osteoblasts via Wnt/β-catenin signalling. N-cadherin is increased with osteogenic commitment and differentiation to pre-osteoblasts (28-30), but is down regulated as pre-osteoblasts become fully differentiated and mature osteoblasts (31). Deletion of N-cadherin reduces β-catenin at cell-cell contacts and cell-cell adhesion with a negative effect on osteoblast differentiation and bone formation.

The role of cadherins in the formation of osteoclasts however is currently not well established. It is believed that cell-cell interactions would be evident between osteoclast precursor cells and osteoblasts due to the close role these cells have in bone regulation (32, 33). During osteoclastogenesis, osteoclast precursor cells interact closely with osteoblasts to allow for the binding of receptor activator of nuclear factor kappa B (RANK) ligand (RANKL) to its receptor RANK resulting in the development of mature and activated osteoclasts (34-36). Thus, cadherins and direct cell-cell interaction should play a role in this highly complicated process. Recently, N-cadherin expression was identified to be increased in a RAW 264.7 cell line, which is a well characterised macrophage cell line that can differentiate into osteoclasts (37). The same study also reported that dominant negative N-cadherin expression in osteogenic cells suppressed osteoclastogenesis via β-catenin dependent regulation of RANKL expression (37). However, the *in vivo* corroboration of the role of cadherins, specifically N-cadherin, in osteoclastogenesis and bone resorption is still unknown.

Although there is little known regarding the role of N-cadherin in osteoclastogenesis, it is well documented that N-cadherin promotes cell growth and survival in most cell types (38). N-cadherin is found to be upregulated in invasive tumours and has consequences on both cellular behaviour and adhesive specificity (38). Numerous studies have shown that aberrant expression of N-cadherin causes tumour cells to lose their polarity, resist apoptosis and become invasive (16, 38). This was confirmed by Hazan *et al.* 2000, who showed that the non-metastatic human breast cancer cell line MCF-7 can be transformed to a metastatic cell line when transfected with N-cadherin (39). In contrast, the disruption of N-cadherin in cultured granulosa cells from human ovarian follicles, using inhibitory antibodies, resulted in the induction of apoptosis within these cells (40). Similarly, endothelial cells which express N-cadherin have been found to undergo apoptosis when treated with the N-cadherin antagonist ADH-1 (41). ADH-1 has also caused apoptosis of multiple myeloma (42), neuroblastoma (43) and pancreatic (44) cancer cells. It is known that apoptotic cells are rarely found within synovial tissue from clinical or experimental rheumatic joints (45, 46). Recently, similarities between malignant cell divisions and FLS hyperproliferation in RA synovial joints have been drawn (14, 47-49). However, it is currently not known if these cells that evade apoptosis or hyperproliferate within RA

synovial joints also express N-cadherin. Thus, it is possible that N-cadherin may be upregulated within these joints promoting cell growth and suppression of apoptosis.

N-cadherin antagonists can modulate a wide variety of biological processes, including metastasis, angiogenesis and apoptosis (16). Recently, small molecule antagonists of N-cadherin, such as ADH-1 (42) and monoclonal antibodies directed against the N-cadherin extracellular domain (50) have been discovered and could potentially be used in the treatment of chronic inflammatory joint diseases such as RA. The effect of N-cadherin antagonists in a murine model of inflammatory arthritis has not yet been investigated. Nor has the arthritic response in hind paws with or without treatment been investigated by high resolution micro-computed tomography (micro-CT). A proprietary small molecule, synthetic, non-peptide N-cadherin antagonist (MW 500), known as CRS-066, has been developed and unlike monoclonal antibodies it has the advantage of topical or oral application. CRS-066 may therefore be the next generation of N-cadherin inhibitors with therapeutic potential. We propose, inhibition of N-cadherin with CRS-066, will disrupt FLS cell adhesion and migration, leading to suppression of overall pannus formation within RA synovial joints. Thus, we propose that CRS-066 treatment will abrogate FLS cell interactions with inflammatory and bone cells, thereby reducing inflammation and joint destruction in a collagen antibody-induced arthritis (CAIA) mouse model. As such, we aim to investigate the effects of CRS-066 as a topical treatment on local inflammation and bone erosion in mice with inflammatory arthritis.

3.4. Methods

Ethics approval was obtained from the University of Adelaide Animal Ethics Committee (M-2015-263A), in accordance with the National Health and Medical Council of Australia Code of Practice for Animal Care in Research Training. Mice were housed in approved conditions on a 12-hour light/dark cycle. Food and water were provided ad libitum.

3.4.1. Collagen antibody-induced arthritis mouse model

Twenty female Balb/c mice aged six to eight weeks were obtained from the University of Adelaide Laboratory Animal Services and randomly allocated into four groups. Control

(no arthritis or treatment; n = 6), CAIA (arthritis with no treatment; n = 6), CAIA + DMSO (arthritis treated with vehicle alone; n = 4), CAIA + CRS-066 (arthritis treated with CRS-066; n = 4). A mild form of inflammatory arthritis was induced on day 0 by intravenous injection of a 150 µl (1.5 mg/mouse) cocktail of anti-type II collagen monoclonal antibodies (Arthrogen-CIAs Arthritogenic Monoclonal Antibodies, Chondrex Inc., Redwood, WA, USA) via the tail vein. This was followed by an intraperitoneal injection with 20 µl (10 µg/mouse) of *E.coli* lipopolysaccharide (LPS) on day 3. Control animals were injected with phosphate buffered saline (PBS) alone at both time points. Treatment was applied topically to the entire surface of the front and hind paws of all mice while under anaesthetic (isoflurane) every 12 hours, for 7 days (day 4-10). A solution of 100% Dimethyl sulfoxide (DMSO) was applied to both the left and right front (40 µl per front paw) and hind (80 µl per hind paw) paws of mice in group 3 (CAIA + DMSO). A solution of 1% CRS-066 in 100% DMSO was applied to the right front (40 µl) and hind (80 µl) paw of mice in group 4 (CAIA + CRS-066) and a solution of 100% DMSO alone was applied to the left front and hind paws of these mice, acting as an internal vehicle control within each mouse. Mice remained in the anaesthetic chamber for 15 minutes following treatment to allow for the solution to be absorbed into the skin.

3.4.2. *Clinical analysis of local paw swelling*

Mice were monitored daily using an approved clinical record sheet for arthritis studies to assess body weight and factors of general health. To assess clinical paw inflammation; front and hind paws were examined daily by two observers for the presence of redness, swelling and tenderness using a method previously described (51, 52). For each paw, a score of 1 was given for each red and inflamed digit and a score from 0-5 was allocated for swelling of the carpal/tarsal and swelling of the wrist/ankle. The maximum score for each paw was 15, giving a possible total of 60 per mouse (51, 52).

3.4.3. *Micro-computed tomography analysis*

At the completion of the study on day 11, paws were collected, skinned and fixed for 24 hours in 10% neutral buffered formalin for further analysis. Following tissue fixation, the front and hind paws were scanned using a micro-CT scanner (SkyScan 1076, Bruker, Kontich, Belgium) to assess changes in bone and the surrounding soft tissue. Paws were

scanned at a source voltage of 55 kV, current 180 µA, isotropic pixel size 8.5 µm with a 0.5 mm thick aluminium filter, rotation step of 0.6, frame averaging of 1 and a total scan time of approximately 35 minutes. Cross sectional images of the front and hind paws were reconstructed using a filtered back projection algorithm (N-Recon software, Bruker micro-CT, Kontich, Belgium). The reconstructed cross-section images were realigned in 3D with the long axis of the paw aligned along the inferior-superior direction of the images (Dataviewer software, Bruker), as previously reported (51, 53).

Selection of volume of interest (VOI) for analysis:

For each front paw, 280 contiguous cross-sections (corresponding to a VOI length of 2.4 mm), starting from 200 cross-sections (1.7 mm) distally to the epiphyseal growth plate of the radiocarpal joint extending through the joint up to 80 cross-sections (0.68 mm) proximally, were used for analysis of both the bone and surrounding soft tissue. A cylindrical VOI (4.5 mm diameter, 2.4 mm length) was used and positioned according to the location of each individual paw in the image (51).

To date, quantification of bone volume and soft tissue swelling using high resolution micro-CT has only been carried out in the front paws of mice using the CAIA mouse model (51, 53, 54). As RA is a systemic disease and the CAIA model also induces joint inflammation in a random manner including in the hind paws, we extended this micro-CT analysis to the hind paws. Thus, a separate volume and region of interest was established to accurately quantify the bone volume in the calcaneus, tarsal and metatarsal bones (Figure 3.2) and soft tissue swelling in the hind paws of the same mice.
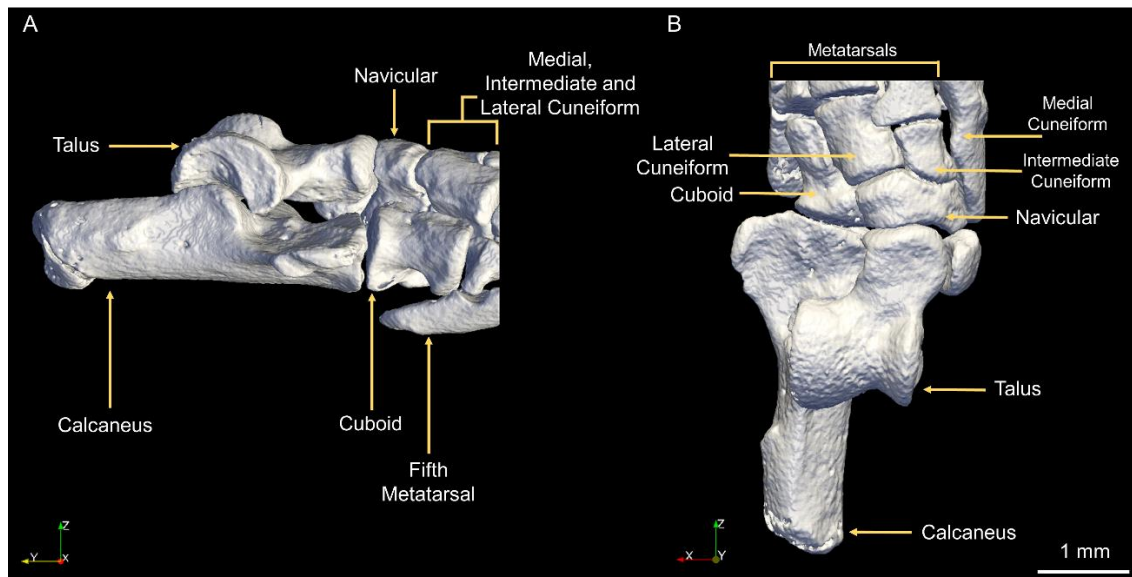
Figure 3.2. 3D micro-CT images of the left hind paw indicating the bones used for quantitative bone volume analysis. A. Lateral view of the left hind paw. B. Top view of the left hind paw. Tibia and fibula have been removed from both images.

In the hind paws, for bone volume, 600 cross-sections (corresponding to a VOI length of 5.1 mm), extending from the posterior surface of the calcaneus through the proximal tarsal and metatarsal bones were used (Figure 3.3). A polygonal region of interest was then traced around the calcaneus, tarsal and metatarsal bones, to exclude the tibia and fibula. Whereas for the soft tissue analysis, 200 cross-sections were used (corresponding to a VOI length of 1.7 mm), extending from the most posterior aspect of the metatarsal bones, excluding the calcaneus and including the cuboid (Figure 3.3). A cylindrical VOI (5.5 mm diameter, 1.7 mm length) was used for paw volume quantification, and positioned according to the location of the individual paws.
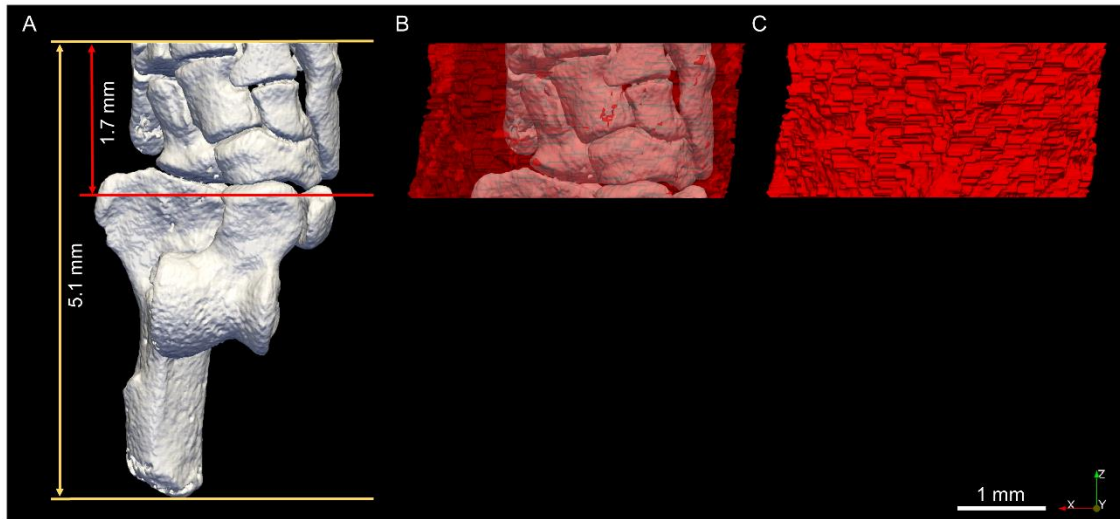
Figure 3.3. 3D micro-CT images of the left hind paw (top view), including calcaneus, tarsal and metatarsal bones for quantitative analysis; bone represented in white colour and soft tissue in red colour. A. The lengths of the volumes of interest (VOIs) used for micro-CT analysis are indicated by the yellow arrows for bone analysis (VOI length of 600 cross sections, corresponding to 5.1 mm) and red arrows for soft tissue analysis (VOI length 200 cross sections, corresponding to 1.7 mm). The 3D rendering of the VOI used for soft tissue analysis is presented in B (bone visible in transparency) and C.

Image thresholding and calculation of bone volume and paw volume:

On the VOIs specified above, the bone volume (BV, in mm^3) and the paw volume (PV, in mm^3, which includes the soft tissue surrounding the radiocarpal joint and tarsal and metatarsal bones), were quantified in 3D using uniform thresholding (CT Analyser software, Bruker). In the grey-level histogram of the reconstructed cross-section images (bitmap format, 256 grey levels, ranging from 0 to 255), the grey-level values in the lower range (from 0 to 11) corresponded to air or background, followed in increasing order by values of the soft tissue (ranging from 12 to 134) and bone (from 135 to 255) (53). Two fixed minimum threshold values were applied to the specimens for segmentation. One minimum threshold level was used for segmenting the bone pixels only (from minimum threshold level 135 to maximum 255), leaving air and surrounding soft tissue as background (53, 55, 56). The second minimum threshold level was for segmenting the paw, soft tissue and bone together (minimum threshold level 12 to maximum level 255),

127

and leaving air as the background (53, 55, 56). By applying the corresponding threshold values to each specimen, automated calculations were performed of BV and PV (CT Analyser software, Bruker). The BV was calculated as the volume occupied by the voxels segmented as bone and the PV was calculated as the volume occupied by the voxels segmented as paw, which included both bone and soft tissue. After segmentation, for PV measurements, loose speckles in the segmented images which originated from noise pixels, having their grey values close to those of soft tissue, were removed. This was completed using a cycle of the software function 'sweep' (CT Analyser software, Bruker) which automatically removes all but the largest object in 3D volume, maintaining the paw as the largest object. BV and PV were then quantified using the marching cubes method (CT Analyser software, Bruker) (57-60).

3.4.4. Histological analysis of the radiocarpal joint

Following micro-CT scanning front paws were decalcified in 10% Ethylene diaminetetraacetic acid (EDTA) and embedded in paraffin wax. Serial sagittal sections of the radiocarpal joint were cut (5 µm) and stained with haematoxylin and eosin (H&E) and then scored for inflammatory cell infiltration, cartilage and bone degradation and pannus formation using a previously described semi-quantitative scoring method (51, 54). Semi-quantitative analysis was carried out by two blinded observers using 40x magnified images on the Nanozoomer Digital Pathology System (NDP Hamamatsu, Hamamatsu City, Japan). Scoring was based on the number of inflammatory cells within the radiocarpal joint. Normal tissue (< 5% inflammatory cells) was scored as 0, mild inflammation (6-20% inflammatory cells) was scored as 1, moderate inflammation (21-50% inflammatory cells) was scored as 2 and severe inflammation (> 51% inflammatory cells) was scored as 3. Bone and cartilage destruction were also assessed using a 0 to 3-point scale (0, normal; 1, mild cartilage destruction; 2, evidence of both cartilage and bone destruction; 3, severe cartilage and bone destruction). Pannus formation was scored as either 0 for no pannus or 1 for pannus formation (61).

Serial sagittal sections of the radiocarpal joint were also stained with tartrate resistant acid phosphatase (TRAP) to identify osteoclasts on the bone surface and pre-osteoclasts in the surrounding soft tissue within the radiocarpal joint (62, 63). Sections were stained as previously described with TRAP solution, left to incubate (37 °C) for 45 minutes and

counterstained with haematoxylin (51, 62, 63). Sections were imaged using the Nanozoomer Digital Pathology System (NDP Hamamatsu, Hamamatsu City, Japan) for analysis at 40x magnification. The number of multinucleated TRAP positive cells (> 3 nuclei) were counted by two blinded observers in a consistent region of interest (2.16 mm^2), to include cells found on the bone surface and within the surrounding soft tissue of the radiocarpal joint (51).

3.4.5. Statistical Analysis

Statistical analysis was performed using the statistical software SAS 9.4 (SAS Institute., Cary, NC, USA). For paw score analysis, a linear mixed-effects model was performed, controlling for clustering on mouse and for repeated measurements over time using a Variance Components covariance structure. Assumptions of a linear model were found to be upheld. An interaction of Group (1 = Control, 2 = CAIA, 3 = CAIA + DMSO and 4 = CAIA + CRS-066) and Day (time) was included with adjustment for paw side (left and right paws).

For micro-CT data 20 mice are assessed on all 4 paws: left front and hind (internal control paw) and right front and hind paw (treatment). As each mouse is assessed in 4 different areas there is clustering on each mouse. To account for clustering a Variance Components covariance structure was used within a linear mixed-effects model for each micro-CT outcome. An interaction term of Group and Side (left and right paw) was included as a predictor.

Assumptions of a linear model were found to be upheld by inspection of histograms and scatter plots of residuals and predicted values, except for the outcome BV which was bimodal. Therefore, two separate linear mixed-effects models were performed for the front and hind paw BV analysis. Assumptions of a linear model were then met. A p value less than 0.05 was considered statistically significant.

3.5. Results

3.5.1. Clinical evaluation of local inflammation in mouse paws

Induction of CAIA resulted in significant redness, tenderness and inflammation in the front and hind paws of all disease mice, following LPS administration on day 3 (Figure 3.4). There is a statistically significant interaction between Day and Group observed for the outcome paw score (interaction p value < 0.0001). From day 6 to day 10 control mice had significantly lower mean paw scores compared to CAIA mice (p value < 0.0001; Table 3.1). At day 7, CAIA mice had a paw score lower than CAIA + DMSO mice (2.83 ± 0.25 and 4.13 ± 0.31, respectively, p = 0.0013; Figure 3.4B). The mean paw scores in CAIA mice remained significantly lower from day 7 to day 10 compared to CAIA + DMSO mice (Table 3.1). At day 7, CAIA + DMSO mice also had a mean paw score greater than CAIA + CRS-066 mice (4.13 ± 0.31 and 2.13 ± 0.31, respectively, p < 0.0001; Figure 3.4B) and remained significantly greater on day 8 and day 9 (3.75 ± 0.31 and 3.72 ± 0.31, respectively; Figure 3.4B and Table 3.1). There was no significant difference observed in mean paw score between CAIA and CAIA + CRS-066 mice throughout the 10 day model. There is also no statistically significant difference in paw score between left and right paws, adjusting for the Group*Day interaction (Global p value = 0.498).
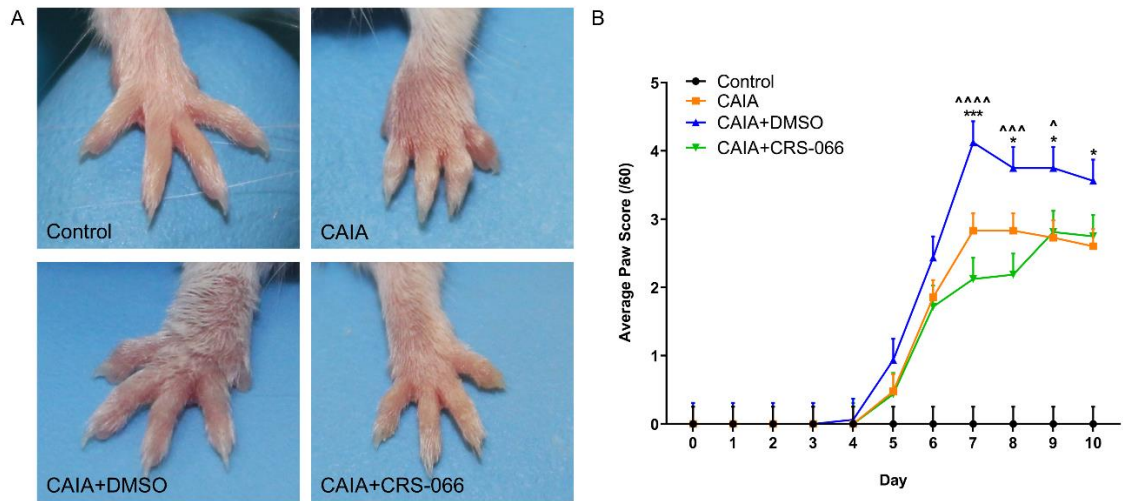
Figure 3.4. Clinical evaluation of local inflammation. A. Macroscopic appearance of the front paws at day 7 post-arthritis induction. B. Average clinical paw scores of each group over 10 days. Error bars represent standard error of mean (SEM; n = 6 per Control and CAIA groups, n = 4 per CAIA + DMSO and CAIA + CRS-066 groups, * p < 0.01 and *** p = 0.001 CAIA vs CAIA + DMSO; ^ p = 0.03, ^^^ p = 0.0004 and ^^^^ p < 0.0001 CAIA + DMSO vs CAIA + CRS-066).

Table 3.1. Linear mixed-effects model of Paw score versus interaction of Day and Group and Side from peak disease (day 6) to the end of the model (day 10): mean differences

Outcome	Interaction	Day	Group Comparison	Difference in Paw Score (95% CI)	Comparison P value	Interaction P value
Paw score	Day*Group	6	1 vs 2	-1.85 (-2.56, -1.15)	**<0.0001**	<0.0001
		6	2 vs 3	-0.58 (-1.37, 0.20)	0.1457	
		6	2 vs 4	0.14 (-0.65, 0.92)	0.7354	
		6	3 vs 4	0.72 (-0.14, 1.58)	0.1018	
		7	1 vs 2	-2.83 (-3.54, -2.13)	**<0.0001**	
		7	2 vs 3	-1.29 (-2.08, -0.51)	**0.0013**	
		7	2 vs 4	0.71 (-0.08, 1.49)	0.0773	
		7	3 vs 4	2.00 (1.14, 2.86)	**<0.0001**	
		8	1 vs 2	-2.83 (-3.54, -2.13)	**<0.0001**	
		8	2 vs 3	-0.92 (-1.70, -0.13)	**0.0224**	
		8	2 vs 4	0.65 (-0.14, 1.43)	0.1072	
		8	3 vs 4	1.56 (0.70, 2.42)	**0.0004**	
		9	1 vs 2	-2.73 (-3.43, -2.03)	**<0.0001**	
		9	2 vs 3	-1.02 (-1.81, -0.23)	**0.0110**	
		9	2 vs 4	-0.08 (-0.87, 0.70)	0.8352	
		9	3 vs 4	0.94 (0.08, 1.80)	**0.0329**	
		10	1 vs 2	-2.60 (-3.31, -1.90)	**<0.0001**	
		10	2 vs 3	-0.96 (-1.74, -0.17)	**0.0170**	
		10	2 vs 4	-0.15 (-0.93, 0.64)	0.7159	
		10	3 vs 4	0.81 (-0.05, 1.67)	0.0644	
	Side		Left vs Right	-0,12 (-0.46, 0.22)		0.4986

Groups: 1 = Control, 2 = CAIA, 3 = CAIA + DMSO and 4 = CAIA + CRS-066

P values less than 0.05 were considered statistically significant.

3.5.2. Micro-CT analysis of bone volume and soft tissue swelling in front and hind paws

<u>Front paws:</u>

Representative reconstructed 3D images of the radiocarpal joint, including both bone and soft tissue are shown in Figure 3.5A. There is a statistically significant interaction between Group and Side for the outcome variable BV, however, only for the front right paw data (interaction p value = 0.0089). For the front right paw, control mice have a mean BV (1.15 ± 0.05 mm^3) significantly greater than CAIA mice (1.00 ± 0.05 mm^3, p = 0.038; Figure 3.5B). There is no significant difference among the other disease and treatment groups for front right paw BV. There is also no significant difference in BV measurements in the left front paw between all groups (Figure 3.5B).

There was no statistically significant interaction between Group and Side for the front paw PV (interaction p value = 0.1530; Figure 3.5C). However, as expected, CAIA mice had a greater PV in both the left (25.98 ± 1.88 mm^3) and right front paws (25.300 ± 1.88 mm^3) when compared to control mice (19.12 ± 1.88 mm^3 for the left paw and 19.06 ± 1.88 mm^3, for the right paw).

<u>Hind Paws:</u>

There was no statistically significant interaction between Group and Side for hind paw BV (interaction p value = 0.0566; Figure 3.5D). Although unexpectedly, in the right hind paws, it was evident that CAIA + CRS-066 mice had a mean BV (3.29 ± 0.13 mm^3) lower than CAIA (3.49 ± 0.10 mm^3) and CAIA + DMSO (3.31 ± 0.13 mm^3) mice, by 0.18 mm^3 and 0.20 mm^3, respectively. In the left hind paws, mean BV was 0.12 mm^3 greater in CAIA + CRS-066 (3.47 ± 0.13 mm^3) mice compared to CAIA (3.35 ± 0.10 mm^3) mice. However, this was not statistically significant (Figure 3.5D).

There is a statistically significant interaction between Group and Side for the hind paw PV (interaction p value = 0.0034; Figure 3.5E). As expected, CAIA mice had a mean PV in the left hind paws (18.80 ± 1.34 mm^3) significantly greater than control mice (12.61 ± 1.47 mm^3), by 6.19 mm^3 (p = 0.0071). However, this increase in PV was not observed in the right hind paws between control and CAIA mice. Unexpectedly, PV in the right hind paw was greater in CAIA + DMSO (21.00 ± 1.64 mm^3) and CAIA + CRS-066 (20.71 ± 1.64 mm^3) mice when compared to the right hind paws of CAIA mice (14.97 ± 1.34 mm^3;

p = 0.0122 and p = 0.016, respectively; Figure 3.5E). Average PV in the right hind paws (20.71 ± 1.64 mm^3) of CAIA + CRS-066 mice was also unexpectedly greater when compared to the left internal control paws (15.20 ± 1.64 mm^3), however not significantly so. There was no significant difference among the disease and treatment groups for left hind paw PV.
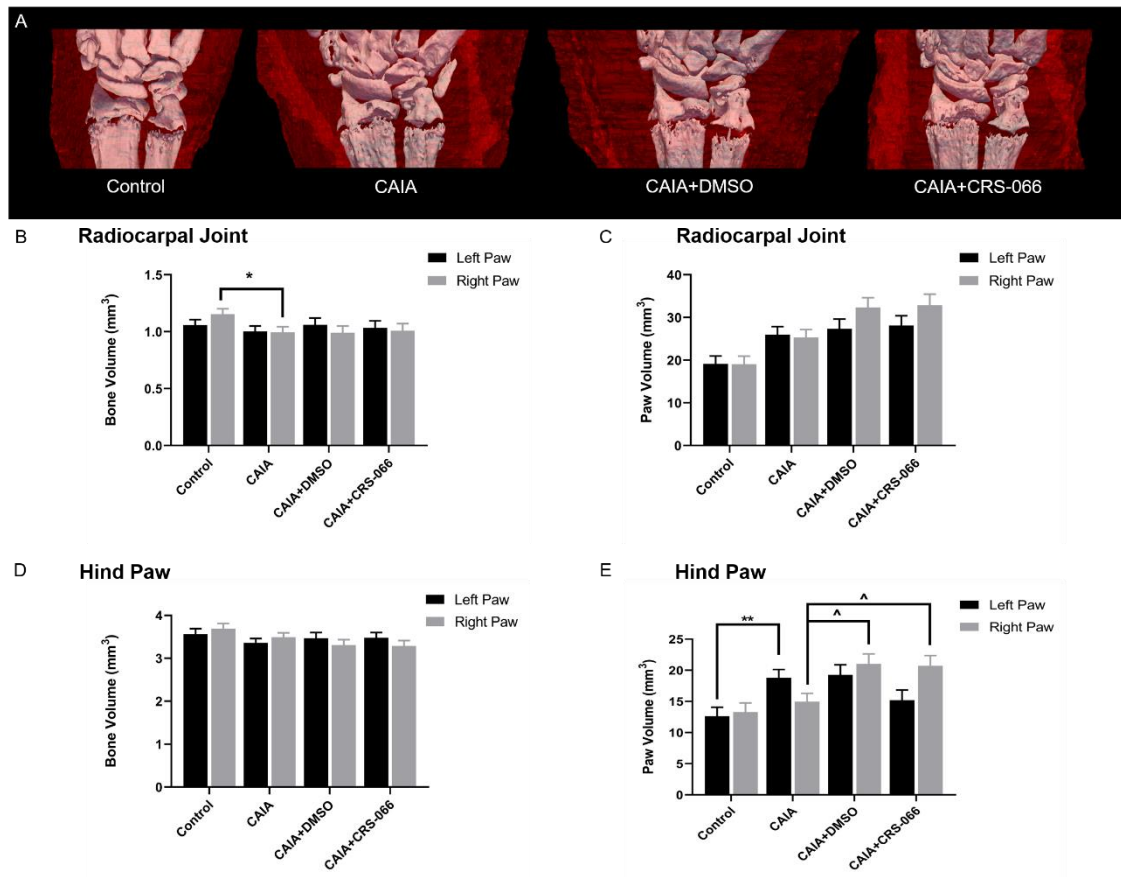
Figure 3.5. Effect of CAIA and CRS-066 on bone volume (BV) and soft tissue swelling (paw volume, PV) of the radiocarpal joint and hind paw assessed by high resolution micro-CT at day 11. A. Three-dimensional micro-CT models of the radiocarpal joint and surrounding soft tissue (indicated in red) in the right paw. Mean BV and PV in the radiocarpal joint (B and C, respectively) and mean BV and PV in the hind paw (D and E, respectively) expressed in mm^3, as assessed by micro-CT analysis at day 11. Error bars represent SEM (n = 12 paws per Control and CAIA and n = 8 paws per CAIA + DMSO and CAIA + CRS-066 groups, * p = 0.03 and ** p< 0.001 Control vs CAIA; ^ p = 0.01 compared to CAIA).

3.5.3. *Histological evaluation of inflammation and bone erosion in the front paws of mice*

Histological evaluation of sagittal sections of the left and right radiocarpal joint showed that CAIA mice and CAIA mice treated with DMSO vehicle alone or CRS-066 had greater scores for cellular infiltration, cartilage and bone degradation and pannus formation compared to control mice (Figure 3.6). CAIA mice treated with CRS-066 had lower inflammatory cell infiltration and cartilage and bone degradation compared to CAIA mice (Figure 3.6A and B). These scores were also lower in the CRS-066 treated right paws, when compared to the vehicle treated left paws of the same mice (Figure 3.6A, B and C). However, there was no statistically significant interaction between Group and Side for inflammatory cell infiltration, cartilage and bone degradation and pannus formation (Interaction p value = 0.8527, 0.8793 and 0.8783, respectively).
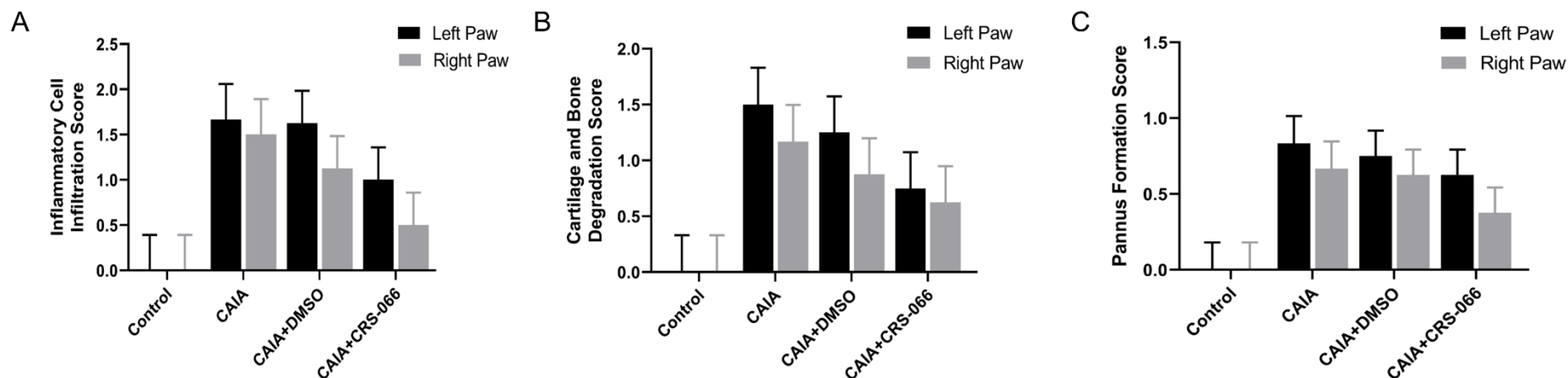
Figure 3.6. Histological assessment of inflammation, cartilage and bone destruction and pannus formation in H&E stained sagittal sections of mouse paws. A. Inflammatory cell infiltration score. B. Cartilage and bone degradation score. C. Pannus formation score. Error bars represent SEM (n = 12 paws per Control and CAIA groups, n = 16 paws per CAIA + DMSO and CAIA + CRS-066 groups).

Representative images of TRAP staining in the radiocarpal joint are presented in Figure 3.7A. A lower number of TRAP positive multinucleated cells were observed on the bone surface of the radiocarpal joint in the left vehicle treated paw (5.25 ± 3.31 cells) of CAIA + CRS-066 mice compared to the left paw of CAIA untreated mice (12.50 ± 3.14 cells; Figure 3.7B). This was not reciprocated in the right paw which found the number of TRAP positive multinucleated cells to be similar between CAIA untreated right paws (7.17 ± 3.14 cells) and CRS-066 treated right paws (7.87 ± 3.31 cells; Figure 3.7B). Unexpectedly, although not significant, the number of TRAP positive multinucleated cells observed on the bone surface in the left vehicle treated paw was lower compared to the right CRS-066 treated paw of CAIA + CRS-066 mice.

Interestingly, within the soft tissue of the radiocarpal joint, a lower number of TRAP positive multinucleated cells were observed in both the left and right front paws of CAIA + CRS-066 mice (3.25 ± 5.64 cells and 5.75 ± 5.64 cells, respectively), compared to CAIA (19.50 ± 6.03 cells and 15.50 ± 6.03 cells, respectively) and CAIA + DMSO mice (10.25 ± 5.64 cells and 25.00 ± 5.64 cells, respectively; Figure 3.7C). However, there was no significant difference in the number of TRAP positive multinucleated cells observed between the left vehicle treated paw (3.25 ± 5.64 cells) and right CRS-066 treated paw (5.75 ± 5.64 cells) of CAIA + CRS-066 mice. There was also no statistically significant interaction between Group and Side for the number of TRAP positive multinucleated cells on the bone surface and within the surrounding soft tissue of the radiocarpal joint (interaction p value = 0.2729 and p = 0.2933, respectively).
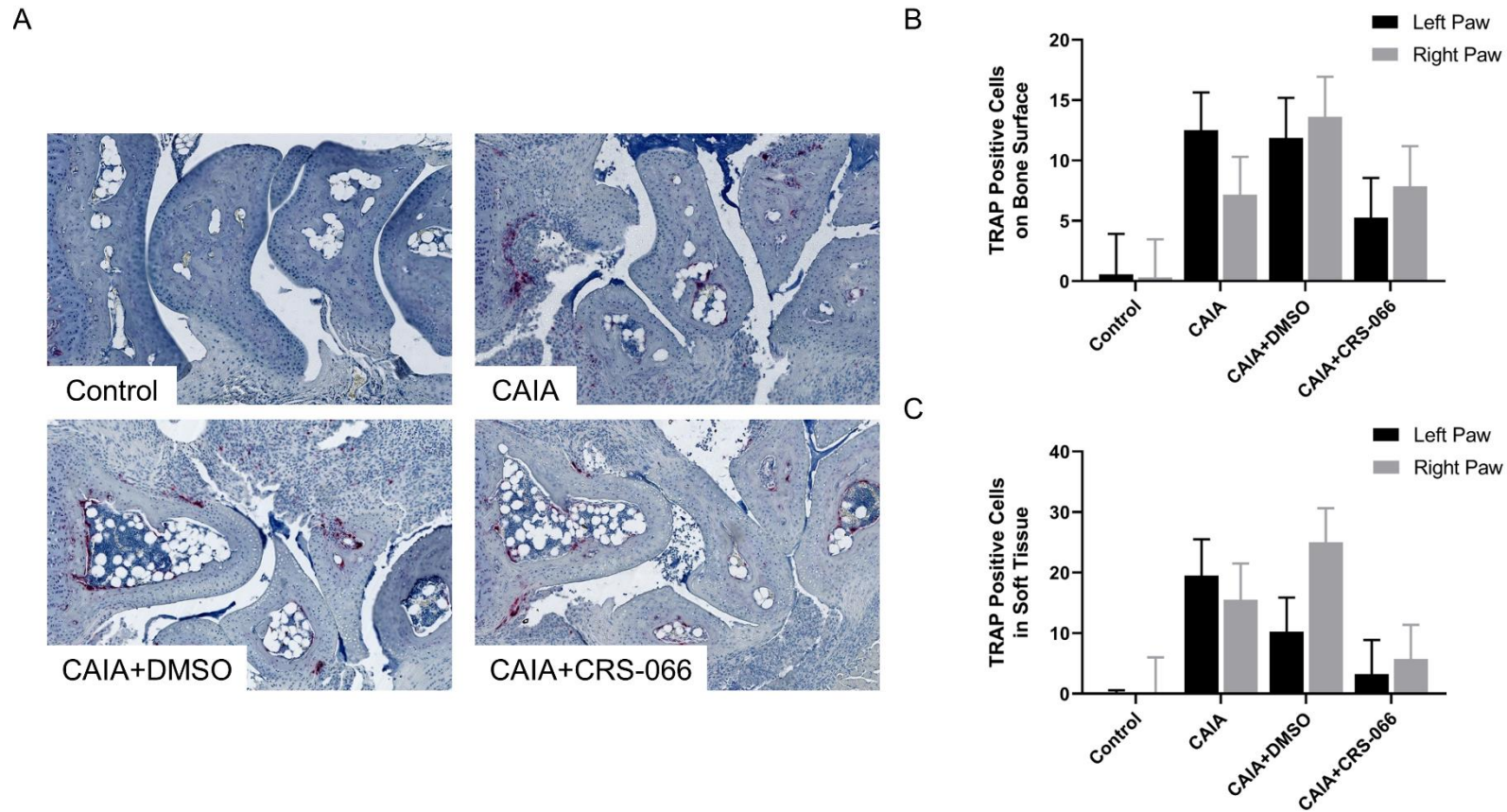
Figure 3.7. Assessment of osteoclasts and pre-osteoclasts in front paws. A. Representative images of sagittal sections of the radiocarpal joint stained with TRAP (indicated in pink) with haematoxylin counterstaining, 20x magnification. Average values of TRAP positive multinucleated cells in each group on the bone surface (B) and in the surrounding soft tissue (C) in a 2.16 mm^2 area of the radiocarpal joint. Error bars represent SEM (n = 12 paws per Control and CAIA groups, n = 16 paws per CAIA + DMSO and CAIA + CRS-066 groups).

3.6. Discussion

The function of cell adhesion molecules, including cadherins has been extensively researched, with a wide range of roles identified in determining the integrity and architecture of different tissues within the body. The destructive influence of FLS in RA, appears to be through the formation of invasive pannus tissue which drives inflammation and the destruction of articular cartilage and underlying subchondral bone (5, 64). It is thought that N-cadherin antagonists may be beneficial in modulating biological processes in RA, such as proliferation of FLS, angiogenesis and apoptosis. Thus, this study utilised the CAIA model as it recapitulates the pathological features of RA in Balb/c mice for the assessment of the novel therapeutic compound CRS-066 designed to suppress the action of N-cadherin.

The results of this study suggest the suppression of N-cadherin using the topical application of CRS-066 may have potential benefit in reducing inflammation and this is particularly supported by the clinical paw scoring and histological analysis. The current study found that CRS-066 applied topically to the right front and hind paws reduced local inflammation in CAIA mice, as evidenced by paw scores from day 7 to 9. This was also supported to a lesser degree by histological analysis of the radiocarpal joints. Although not significant, inflammatory cell infiltration and pannus formation scores were observed to be lower in CRS-066 treated right paws in comparison to the untreated left paws and CAIA untreated mice. In contrast, PV measured at day 11 by high resolution micro-CT was observed to be higher in CRS-066 treated right paws, compared to CAIA untreated mice. This was unexpected and the discrepancy between these results could be attributed to the large variability in animal response to the disease. As CAIA is induced by the systemic administration of anti-type II collagen monoclonal antibodies (65), there is a large variability in which paws are affected and the severity of the disease in each affected paw.

CRS-066 did not have a significant effect on BV in the front and hind paws of CRS-066 treated mice at day 11, and BV in these paws did not appear to change when compared to BV from CAIA untreated or vehicle only treated mice. This is not consistent with the histological analysis of bone and cartilage destruction in the front and hind paws, which

identified CRS-066 treated mice as having a lower histological score for bone and cartilage destruction in the right treated paw, in comparison to the left untreated paw and CAIA untreated mice. A reduced number of multinucleated TRAP positive osteoclast-like cells was also observed on the bone surface and within the surrounding soft tissue in the paws of CRS-066 treated mice, suggesting CRS-066 may play a role in modulating bone turnover. However, the difference in results may be due to the location and size of the volume of interest considered for quantification of BV in the radiocarpal joint and hind paws. Despite high-resolution micro-CT being a sensitive method for quantification of bone, the decrease in BV due to joint destruction may be partially compensated by the larger quantity of bone included in micro-CT analysis. Thus, quantification of BV in the smaller metacarpo-phalangeal joints or individual bones that form the hind paw (e.g. cuboid or navicular) would be beneficial and may provide a more accurate assessment of the effects of CRS-066 on bone erosion in inflammatory arthritis.

The mechanism by which CRS-066 suppresses bone resorption through N-cadherin inhibition in pathological conditions is still unknown and this is the first time the compound has been investigated *in vivo* in a model of inflammatory arthritis. However, it is known that ablation of N-cadherin has a negative effect on osteoblastogenesis and bone growth (26), as β-catenin is reduced and canonical Wnt signalling is impaired (23, 24). CAIA induces significant bone destruction and loss of BV in the joints of mice (51, 54, 65). Further inhibition of osteoblastogenesis through targeting N-cadherin within CAIA mice could thus result in greater disruptions in normal bone turnover and formation. Although a reduction in TRAP positive osteoclast-like cells was observed in CRS-066 treated mice, the bone destruction and slight reduction in BV observed in these mice, in comparison to untreated CAIA mice and healthy controls, may instead be due to a reduction in the number of osteoblasts present within these joints to replace and form new bone. In the current study, the presence of osteoblasts and the activation of Wnt/β-catenin signalling was not directly measured in paw tissue, nor was the expression of N-cadherin. Therefore, it can not be confirmed in this model as to whether CRS-066 is also actively suppressing osteoblast activation and bone formation through N-cadherin inhibition. Future *in vivo* studies could assess the presence of osteoblasts and markers of bone turnover in the radiocarpal joint and hind paws, as well as the expression of N cadherin and β-catenin through immunohistochemical staining to determine if CRS-066

is suppressing bone formation in inflammatory arthritic conditions through inhibition of N-cadherin.

Recent studies have also identified the involvement of N-cadherin in chondrocyte development and the persistence of N-cadherin can prevent the progression of chondrogenic differentiation (66-68). Similar to its implications in osteoblastogenesis, N-cadherin is known to control chondrogenesis through both modulation of cell-cell adhesion and interaction with Wnt and bone morphogenetic protein signalling (66, 69). Thus, inhibiting N-cadherin may have a beneficial effect on preventing the destruction of articular cartilage in RA and may be supported by the slight reduction in the histological cartilage and bone degradation score observed in CRS-066 treated paws of CAIA mice within this study. This highlights another potential target for pharmacological intervention to promote joint repair in RA. However, further investigations are required to confirm this and identify the specific effect of CRS-066 on the differentiation of chondrocytes.

The current study administered 1% CRS-066 topically using 100% DMSO as the vehicle due to the compound not being water soluble. DMSO is a colourless liquid and is a polar aprotic solvent that is capable of dissolving both polar and non-polar compounds (70, 71). DMSO is commonly used as a solvent for water-insoluble drugs. Due to its polar nature, capacity to accept hydrogen bonds and its small and compact structure, DMSO is capable of penetrating living tissues (72). Thus, previous studies have highlighted the beneficial effects of using DMSO as a topical treatment or vehicle, as it greatly enhances the percutaneous penetration and promotes transport into local blood vessels when used in combination with other substances (71, 73). Recent *in vitro* and *in vivo* studies, however, have identified varying cellular and behavioural effects of DMSO depending on the concentration used, including membrane permeability and toxicity (74-77).

The increased PV observed in the CRS-066 treated mice could be attributed to the vehicle the drug was applied with, as using high concentrations of DMSO as a vehicle could result in varying cellular effects and toxicity. This is supported by the DMSO-treated mice which showed a greater PV at day 11, as well as greater local paw swelling, indicated by

significantly higher paw scores compared to all other groups from day 7 to day 10. Recently, studies have highlighted the safety concerns of using low concentrations of DMSO as a solvent for *in vivo* administration and in biological assays (78). DMSO concentrations greater than 10% have been reported to cause cellular toxicity through plasma membrane pore formation and cell death (71, 78). The high concentrations of DMSO used within this study as a vehicle for CRS-066 may have therefore confounded the beneficial effects of CRS-066 and further enhanced the inflammatory response observed in CAIA mice. Thus, resulting in the conflicting findings identified throughout the study. Further investigation is therefore required to identify an appropriate vehicle, for the compound CRS-066, to elucidate if it is beneficial in reducing inflammation and bone destruction in inflammatory arthritis.

3.7.   Conclusion

In conclusion, this is the first study to investigate the effect of topical application of CRS-066, an N-cadherin antagonist, on inflammation and bone erosion *in vivo* in inflammatory arthritis. Our findings indicate the potential beneficial effect of CRS-066 on reducing inflammation in CAIA, however with minimal effect on bone erosion identified. The pharmacological approach used within this study increases clinical translatability, although based on our study, the vehicle, DMSO, could be confounding the beneficial effects of CRS-066 and causing inconsistencies in the results observed. Thus, new strategies of drug administration are required. Further investigations to confirm the expression of N-cadherin in cells within the RA synovium, including FLS, osteoblasts and chondrocytes, is also warranted to elucidate the more specific target of this compound *in vivo*.

3.8. References

1.   Gravallese EM, Manning C, Tsay A, Naito A, Pan C, Amento E, et al. Synovial tissue in rheumatoid arthritis is a source of osteoclast differentiation factor. Arthritis Rheum. 2000;43(2):250-8.

2.   Arnett FC, Edworthy SM, Bloch DA, McShane DJ, Fries JF, Cooper NS, et al. The American Rheumatism Association 1987 revised criteria for the classification of rheumatoid arthritis. Arthritis and rheumatism. 1988;31(3):315-24.

3.   Burmester GR, Feist E, Dorner T. Emerging cell and cytokine targets in rheumatoid arthritis. Nature reviews Rheumatology. 2014;10(2):77-88.

4.   Valencia X, Higgins JM, Kiener HP, Lee DM, Podrebarac TA, Dascher CC, et al. Cadherin-11 provides specific cellular adhesion between fibroblast-like synoviocytes. The Journal of experimental medicine. 2004;200(12):1673-9.

5.   Helder AE, Feltkamp-Vroom TM, Nienhuis RL. Electron and light microscopical observations and serological findings in rheumatoid arthritis. Annals of the rheumatic diseases. 1973;32(6):515-23.

6.   Neumann E, Lefevre S, Zimmermann B, Gay S, Muller-Ladner U. Rheumatoid arthritis progression mediated by activated synovial fibroblasts. Trends in molecular medicine. 2010;16(10):458-68.

7.   Maciejewska Rodrigues H, Jungel A, Gay RE, Gay S. Innate immunity, epigenetics and autoimmunity in rheumatoid arthritis. Molecular immunology. 2009;47(1):12-8.

8.   Lefevre S, Knedla A, Tennie C, Kampmann A, Wunrau C, Dinser R, et al. Synovial fibroblasts spread rheumatoid arthritis to unaffected joints. Nature medicine. 2009;15(12):1414-20.

9.   Lefevre S, Schwarz M, Meier FMP, Zimmermann-Geller B, Tarner IH, Rickert M, et al. Disease-Specific Effects of Matrix and Growth Factors on Adhesion and Migration of Rheumatoid Synovial Fibroblasts. Journal of immunology (Baltimore, Md : 1950). 2017;198(12):4588-95.

10.   Brasch J, Harrison OJ, Honig B, Shapiro L. Thinking outside the cell: how cadherins drive adhesion. Trends in cell biology. 2012;22(6):299-310.

11.   Marie PJ, Hay E, Modrowski D, Revollo L, Mbalaviele G, Civitelli R. Cadherin-mediated cell-cell adhesion and signaling in the skeleton. Calcified tissue international. 2014;94(1):46-54.

12. Chang SK, Gu Z, Brenner MB. Fibroblast-like synoviocytes in inflammatory arthritis pathology: the emerging role of cadherin-11. Immunological reviews. 2010;233(1):256-66.

13. Kiener HP, Lee DM, Agarwal SK, Brenner MB. Cadherin-11 induces rheumatoid arthritis fibroblast-like synoviocytes to form lining layers in vitro. The American journal of pathology. 2006;168(5):1486-99.

14. Lee DM, Kiener HP, Agarwal SK, Noss EH, Watts GF, Chisaka O, et al. Cadherin-11 in synovial lining formation and pathology in arthritis. Science (New York, NY). 2007;315(5814):1006-10.

15. Okazaki M, Takeshita S, Kawai S, Kikuno R, Tsujimura A, Kudo A, et al. Molecular cloning and characterization of OB-cadherin, a new member of cadherin family expressed in osteoblasts. The Journal of biological chemistry. 1994;269(16):12092-8.

16. Blaschuk OW. N-cadherin antagonists as oncology therapeutics. Philosophical transactions of the Royal Society of London Series B, Biological sciences. 2015;370(1661):20140039.

17. Troyanovsky SM. Mechanism of cell-cell adhesion complex assembly. Current opinion in cell biology. 1999;11(5):561-6.

18. Cheng SL, Lecanda F, Davidson MK, Warlow PM, Zhang SF, Zhang L, et al. Human osteoblasts express a repertoire of cadherins, which are critical for BMP-2-induced osteogenic differentiation. Journal of bone and mineral research : the official journal of the American Society for Bone and Mineral Research. 1998;13(4):633-44.

19. Nagafuchi A. Molecular architecture of adherens junctions. Current opinion in cell biology. 2001;13(5):600-3.

20. Bodine PV, Komm BS. Wnt signaling and osteoblastogenesis. Reviews in endocrine & metabolic disorders. 2006;7(1-2):33-9.

21. Krishnan V, Bryant HU, Macdougald OA. Regulation of bone mass by Wnt signaling. The Journal of clinical investigation. 2006;116(5):1202-9.

22. Goltzman D. LRP5, serotonin, and bone: complexity, contradictions, and conundrums. Journal of bone and mineral research : the official journal of the American Society for Bone and Mineral Research. 2011;26(9):1997-2001.

23. Bienz M. beta-Catenin: a pivot between cell adhesion and Wnt signalling. Current biology : CB. 2005;15(2):R64-7.

24.   Brembeck FH, Rosario M, Birchmeier W. Balancing cell adhesion and Wnt signaling, the key role of beta-catenin. Current opinion in genetics & development. 2006;16(1):51-9.

25.   Castro CH, Shin CS, Stains JP, Cheng SL, Sheikh S, Mbalaviele G, et al. Targeted expression of a dominant-negative N-cadherin in vivo delays peak bone mass and increases adipogenesis. Journal of cell science. 2004;117(Pt 13):2853-64.

26.   Di Benedetto A, Watkins M, Grimston S, Salazar V, Donsante C, Mbalaviele G, et al. N-cadherin and cadherin 11 modulate postnatal bone growth and osteoblast differentiation by distinct mechanisms. Journal of cell science. 2010;123(Pt 15):2640-8.

27.   Hunter I, McGregor D, Robins SP. Caspase-dependent cleavage of cadherins and catenins during osteoblast apoptosis. Journal of bone and mineral research : the official journal of the American Society for Bone and Mineral Research. 2001;16(3):466-77.

28.   Hay E, Lemonnier J, Modrowski D, Lomri A, Lasmoles F, Marie PJ. N- and E-cadherin mediate early human calvaria osteoblast differentiation promoted by bone morphogenetic protein-2. Journal of cellular physiology. 2000;183(1):117-28.

29.   Cheng SL, Shin CS, Towler DA, Civitelli R. A dominant negative cadherin inhibits osteoblast differentiation. Journal of bone and mineral research : the official journal of the American Society for Bone and Mineral Research. 2000;15(12):2362-70.

30.   Miron RJ, Hedbom E, Ruggiero S, Bosshardt DD, Zhang Y, Mauth C, et al. Premature osteoblast clustering by enamel matrix proteins induces osteoblast differentiation through up-regulation of connexin 43 and N-cadherin. PloS one. 2011;6(8):e23375.

31.   Greenbaum AM, Revollo LD, Woloszynek JR, Civitelli R, Link DC. N-cadherin in osteolineage cells is not required for maintenance of hematopoietic stem cells. Blood. 2012;120(2):295-302.

32.   Stains JP, Civitelli R. Cell-cell interactions in regulating osteogenesis and osteoblast function. Birth defects research Part C, Embryo today : reviews. 2005;75(1):72-80.

33.   Bennett JH, Moffatt S, Horton M. Cell adhesion molecules in human osteoblasts: structure and function. Histology and histopathology. 2001;16(2):603-11.

34. Xu J, Wu HF, Ang ES, Yip K, Woloszyn M, Zheng MH, et al. NF-kappaB modulators in osteolytic bone diseases. Cytokine & growth factor reviews. 2009;20(1):7-17.

35. Feng X. RANKing intracellular signaling in osteoclasts. IUBMB life. 2005;57(6):389-95.

36. Park-Min KH. Mechanisms involved in normal and pathological osteoclastogenesis. Cellular and molecular life sciences : CMLS. 2018;75(14):2519-28.

37. Shin CS, Her SJ, Kim JA, Kim DH, Kim SW, Kim SY, et al. Dominant negative N-cadherin inhibits osteoclast differentiation by interfering with beta-catenin regulation of RANKL, independent of cell-cell adhesion. Journal of bone and mineral research : the official journal of the American Society for Bone and Mineral Research. 2005;20(12):2200-12.

38. Suyama K, Shapiro I, Guttman M, Hazan RB. A signaling pathway leading to metastasis is controlled by N-cadherin and the FGF receptor. Cancer cell. 2002;2(4):301-14.

39. Hazan RB, Phillips GR, Qiao RF, Norton L, Aaronson SA. Exogenous expression of N-cadherin in breast cancer cells induces cell migration, invasion, and metastasis. The Journal of cell biology. 2000;148(4):779-90.

40. Makrigiannakis A, Coukos G, Christofidou-Solomidou M, Gour BJ, Radice GL, Blaschuk O, et al. N-cadherin-mediated human granulosa cell adhesion prevents apoptosis: a role in follicular atresia and luteolysis? The American journal of pathology. 1999;154(5):1391-406.

41. Erez N, Zamir E, Gour BJ, Blaschuk OW, Geiger B. Induction of apoptosis in cultured endothelial cells by a cadherin antagonist peptide: involvement of fibroblast growth factor receptor-mediated signalling. Experimental cell research. 2004;294(2):366-78.

42. Sadler NM, Harris BR, Metzger BA, Kirshner J. N-cadherin impedes proliferation of the multiple myeloma cancer stem cells. American journal of blood research. 2013;3(4):271-85.

43. Lammens T, Swerts K, Derycke L, De Craemer A, De Brouwer S, De Preter K, et al. N-cadherin in neuroblastoma disease: expression and clinical significance. PloS one. 2012;7(2):e31206.

44.   Shintani Y, Fukumoto Y, Chaika N, Grandgenett PM, Hollingsworth MA, Wheelock MJ, et al. ADH-1 suppresses N-cadherin-dependent pancreatic cancer progression. International journal of cancer. 2008;122(1):71-7.

45.   Dharmapatni AA, Smith MD, Findlay DM, Holding CA, Evdokiou A, Ahern MJ, et al. Elevated expression of caspase-3 inhibitors, survivin and xIAP correlates with low levels of apoptosis in active rheumatoid synovium. Arthritis research & therapy. 2009;11(1):R13.

46.   Perlman H, Pagliari LJ, Liu H, Koch AE, Haines GK, 3rd, Pope RM. Rheumatoid arthritis synovial macrophages express the Fas-associated death domain-like interleukin-1beta-converting enzyme-inhibitory protein and are refractory to Fas-mediated apoptosis. Arthritis and rheumatism. 2001;44(1):21-30.

47.   Davis LS. A question of transformation: the synovial fibroblast in rheumatoid arthritis. The American journal of pathology. 2003;162(5):1399-402.

48.   Bartok B, Firestein GS. Fibroblast-like synoviocytes: key effector cells in rheumatoid arthritis. Immunological reviews. 2010;233(1):233-55.

49.   Chang SK, Noss EH, Chen M, Gu Z, Townsend K, Grenha R, et al. Cadherin-11 regulates fibroblast inflammation. Proceedings of the National Academy of Sciences of the United States of America. 2011;108(20):8402-7.

50.   Tanaka H, Kono E, Tran CP, Miyazaki H, Yamashiro J, Shimomura T, et al. Monoclonal antibody targeting of N-cadherin inhibits prostate cancer growth, metastasis and castration resistance. Nature medicine. 2010;16(12):1414-20.

51.   Williams B, Tsangari E, Stansborough R, Marino V, Cantley M, Dharmapatni A, et al. Mixed effects of caffeic acid phenethyl ester (CAPE) on joint inflammation, bone loss and gastrointestinal inflammation in a murine model of collagen antibody-induced arthritis. Inflammopharmacology. 2017;25(1):55-68.

52.   Nandakumar KS, Svensson L, Holmdahl R. Collagen type II-specific monoclonal antibody-induced arthritis in mice: description of the disease and the influence of age, sex, and genes. The American journal of pathology. 2003;163(5):1827-37.

53.   Perilli E, Cantley M, Marino V, Crotti TN, Smith MD, Haynes DR, et al. Quantifying not only bone loss, but also soft tissue swelling, in a murine inflammatory arthritis model using micro-computed tomography. Scandinavian journal of immunology. 2015;81(2):142-50.

54.   Dharmapatni AA, Cantley MD, Marino V, Perilli E, Crotti TN, Smith MD, et al. The X-Linked Inhibitor of Apoptosis Protein Inhibitor Embelin Suppresses

Inflammation and Bone Erosion in Collagen Antibody Induced Arthritis Mice. Mediators Inflamm. 2015;2015:564042.

55. Luu YK, Lublinsky S, Ozcivici E, Capilla E, Pessin JE, Rubin CT, et al. In vivo quantification of subcutaneous and visceral adiposity by micro-computed tomography in a small animal model. Medical engineering & physics. 2009;31(1):34-41.

56. Perilli E, Baruffaldi F, Visentin M, Bordini B, Traina F, Cappello A, et al. MicroCT examination of human bone specimens: effects of polymethylmethacrylate embedding on structural parameters. Journal of microscopy. 2007;225(Pt 2):192-200.

57. Lane NE, Thompson JM, Haupt D, Kimmel DB, Modin G, Kinney JH. Acute changes in trabecular bone connectivity and osteoclast activity in the ovariectomized rat in vivo. Journal of bone and mineral research : the official journal of the American Society for Bone and Mineral Research. 1998;13(2):229-36.

58. Perilli E, Le V, Ma B, Salmon P, Reynolds K, Fazzalari NL. Detecting early bone changes using in vivo micro-CT in ovariectomized, zoledronic acid-treated, and sham-operated rats. Osteoporosis international : a journal established as result of cooperation between the European Foundation for Osteoporosis and the National Osteoporosis Foundation of the USA. 2010;21(8):1371-82.

59. Perilli E, Briggs AM, Kantor S, Codrington J, Wark JD, Parkinson IH, et al. Failure strength of human vertebrae: prediction using bone mineral density measured by DXA and bone volume by micro-CT. Bone. 2012;50(6):1416-25.

60. Lorensen WE, Cline HE. Marching cubes: a high resolution 3D surface construction algorithm. Comput Graph. 1987;21:163-9.

61. Tak PP, Smeets TJ, Daha MR, Kluin PM, Meijers KA, Brand R, et al. Analysis of the synovial cell infiltrate in early rheumatoid synovial tissue in relation to local disease activity. Arthritis and rheumatism. 1997;40(2):217-25.

62. Gravallese EM, Harada Y, Wang JT, Gorn AH, Thornhill TS, Goldring SR. Identification of cell types responsible for bone resorption in rheumatoid arthritis and juvenile rheumatoid arthritis. The American journal of pathology. 1998;152(4):943-51.

63. Burstone MS. Histochemical demonstration of acid phosphatases with naphthol AS-phosphates. J Natl Cancer Inst. 1958;21(3):523-39.

64.   Barland P, Novikoff AB, Hamerman D. Electron microscopy of the human synovial membrane. The Journal of cell biology. 1962;14:207-20.

65.   Khachigian LM. Collagen antibody-induced arthritis. Nature protocols. 2006;1(5):2512-6.

66.   Tuan RS. Cellular signaling in developmental chondrogenesis: N-cadherin, Wnts, and BMP-2. The Journal of bone and joint surgery American volume. 2003;85-A Suppl 2:137-41.

67.   DeLise AM, Tuan RS. Alterations in the spatiotemporal expression pattern and function of N-cadherin inhibit cellular condensation and chondrogenesis of limb mesenchymal cells in vitro. Journal of cellular biochemistry. 2002;87(3):342-59.

68.   Cho SH, Oh CD, Kim SJ, Kim IC, Chun JS. Retinoic acid inhibits chondrogenesis of mesenchymal cells by sustaining expression of N-cadherin and its associated proteins. Journal of cellular biochemistry. 2003;89(4):837-47.

69.   Delise AM, Tuan RS. Analysis of N-cadherin function in limb mesenchymal chondrogenesis in vitro. Developmental dynamics : an official publication of the American Association of Anatomists. 2002;225(2):195-204.

70.   Hebling J, Bianchi L, Basso FG, Scheffel DL, Soares DG, Carrilho MR, et al. Cytotoxicity of dimethyl sulfoxide (DMSO) in direct contact with odontoblast-like cells. Dental materials : official publication of the Academy of Dental Materials. 2015;31(4):399-405.

71.   Capriotti K, Capriotti JA. Dimethyl sulfoxide: history, chemistry, and clinical utility in dermatology. The Journal of clinical and aesthetic dermatology. 2012;5(9):24-6.

72.   Marren K. Dimethyl sulfoxide: an effective penetration enhancer for topical administration of NSAIDs. The Physician and sportsmedicine. 2011;39(3):75-82.

73.   Goldmann L, Igelman JM, Kitzmiller K. Investigative studies with DMSO in dermatology. Annals of the New York Academy of Sciences. 1967;141(1):428-36.

74.   Santos NC, Figueira-Coelho J, Martins-Silva J, Saldanha C. Multidisciplinary utilization of dimethyl sulfoxide: pharmacological, cellular, and molecular aspects. Biochemical pharmacology. 2003;65(7):1035-41.

75.   Rosenblum WI, Wei EP, Kontos HA. Dimethylsulfoxide and ethanol, commonly used diluents, prevent dilation of pial arterioles by openers of K(ATP) ion channels. European journal of pharmacology. 2001;430(1):101-6.

76.   Morley P, Whitfield JF. The differentiation inducer, dimethyl sulfoxide, transiently increases the intracellular calcium ion concentration in various cell types. Journal of cellular physiology. 1993;156(2):219-25.

77.   Fossum EN, Lisowski MJ, Macey TA, Ingram SL, Morgan MM. Microinjection of the vehicle dimethyl sulfoxide (DMSO) into the periaqueductal gray modulates morphine antinociception. Brain research. 2008;1204:53-8.

78.   Galvao J, Davis B, Tilley M, Normando E, Duchen MR, Cordeiro MF. Unexpected low-dose toxicity of the universal solvent DMSO. FASEB journal : official publication of the Federation of American Societies for Experimental Biology. 2014;28(3):1317-30.

CHAPTER 4: ASSESSMENT OF INFLAMMATION, BONE LOSS AND PAIN-LIKE BEHAVIOUR IN A COLLAGEN ANTIBODY-INDUCED ARTHRITIS MOUSE MODEL FOLLOWING TREATMENT WITH PARTHENOLIDE

B. Williams, F. Lees, E. Perilli, E. Tsangari, A. Dharmapatni, M. Hutchinson, T.N. Crotti

Chapter Summary:

In RA there is a clear link between inflammation and bone loss with elevated expression of RANKL and NF-κB by activated inflammatory cells and FLS. RA specific pain is a major consequence of this inflammation and bone destruction. However, pain can arise prior to disease manifestations and does not correlate with the degree of inflammation or pharmacological modulation. As recent studies have identified a role for NF-κB in the development of neuropathic pain, it is a logical progression to investigate novel therapeutics that target intracellular signalling pathways involved in not only inflammation and bone loss in RA, but in the development of pain as well. Hence, this study aimed to investigate the effect of a novel NF-κB inhibitor on inflammation, bone loss and pain-like behaviour in a mild murine model of inflammatory arthritis.

4.1. Abstract

Rheumatoid arthritis (RA) is a chronic inflammatory disorder characterised by synovial hyperplasia and destruction of bone and cartilage within the joint, leading to severe pain. Nuclear factor-kappa B (NF-κB) intracellular signalling is crucial to T-cell mediated inflammation and osteoclastogenesis in the progression of joint destruction in RA. Thus, this study aims to investigate the effects of NF-κB inhibition by Parthenolide (PAR) on paw inflammation, bone destruction and pain-like behaviour, specifically, mechanical allodynia, in a collagen antibody-induced arthritis (CAIA) mouse model.

Thirty-two Balb/c mice were allocated to four groups (n = 8 per group); Control, CAIA (no treatment), CAIA + PAR 1 mg/kg/day and CAIA + PAR 4 mg/kg/day. Mice were treated daily from day 4 following arthritis development. Paw inflammation was conducted daily, and assessment of mechanical allodynia was conducted on alternate days. At day 11, bone volume (BV) and paw volume (PV) in all paws were assessed *ex vivo* by micro-CT. Sagittal sections of the front and hind paws were stained with haematoxylin and eosin (H&E) and tartrate-resistant acid phosphatase (TRAP) to assess joint inflammation, cartilage and bone damage and the presence of osteoclast-like cells.

Paw scores were significantly lower in CAIA + PAR 4 mg/kg mice compared to CAIA mice at day 8-10 ($p < 0.05$) and in CAIA + PAR 1mg/kg mice compared to CAIA mice at day 10 only ($p = 0.03$). Tactile paw withdrawal thresholds, as a measure of mechanical allodynia, did not show any significant difference between all groups throughout the model. Front and hind paw PV was reduced in CAIA mice treated with 1 mg/kg and 4 mg/kg PAR, however not significantly so. BV measurements did not differ between disease and treatment groups in both front and hind paws. Histological scores for cellular infiltration, cartilage and bone degradation and pannus formation were reduced in front and hind paws of CAIA + PAR 1 mg/kg and CAIA + PAR 4mg/kg mice, but not significantly so. TRAP positive multinucleated cells on the bone surface of the radiocarpal joint and within the surrounding soft tissue of the hind paws were significantly less in CAIA + PAR 4 mg/kg mice compared to CAIA mice ($p < 0.05$ and $p = 0.005$, respectively).

In conclusion, these findings indicate a suppressive effect of both low and moderate dose PAR on paw inflammation and osteoclast presence in mild CAIA. However, significant results may be evident in more long term or severe models of CAIA.

4.2. Statement of Authorship

Statement of Authorship

Title of Paper	Assessment of inflammation, bone loss and pain-like behaviour in a collagen antibody-induced arthritis mouse model following treatment with Parthenolide.
Publication Status	☐ Published ☐ Accepted for Publication ☑ Submitted for Publication ☒ Unpublished and Unsubmitted work written in manuscript style
Publication Details	

Principal Author

Name of Principal Author (Candidate)	Bonnie Williams
Contribution to the Paper	First author and main contributor. Concept and methodological design, investigation, project administration, data curation and analysis, formulation of primary draft, in addition to reviewing and incorporating co-author comments and suggestions.
Overall percentage (%)	
Certification	This paper reports on original research I conducted during the period of my Higher Degree by Research candidature and is not subject to any obligations or contractual agreements with a third party that would constrain its inclusion in this thesis. I am the primary author of this paper.
Signature	Date 22/2/19

Co-Author Contributions

By signing the Statement of Authorship, each author certifies that:

i.   the candidate's stated contribution to the publication is accurate (as detailed above);

ii. permission is granted for the candidate in include the publication in the thesis; and

iii. the sum of all co-author contributions is equal to 100% less the candidate's stated contribution.

Name of Co-Author	Florence Lees
Contribution to the Paper	Methodology and technical support.
Signature	Date 27/2/19

Name of Co-Author	Egon Perilli
Contribution to the Paper	Methodology support, supervision and manuscript review.
Signature	Date 01.03.19

Name of Co-Author	Eleni Tsangari		
Contribution to the Paper	Methodology and technical support.		
Signature		Date	18/2/19

Name of Co-Author	Anak Dharmapatni		
Contribution to the Paper	Supervision and manuscript review.		
Signature		Date	22/2/19

Name of Co-Author	Mark Hutchinson		
Contribution to the Paper	Conceptualisation and data interpretation.		
Signature		Date	20 Feb 2019

Name of Co-Author	Tania Crotti		
Contribution to the Paper	Investigation, funding acquisition, methodology, conceptualisation, supervision and review of manuscript.		
Signature		Date	22/2/19

4.3. Introduction

Rheumatoid arthritis (RA) is a chronic systemic disorder characterised by joint inflammation, synovial hyperplasia and associated destruction of the cartilage and bone. Additionally, pain is associated with this joint destruction and is one of the most debilitating symptoms reported by RA patients (1, 2). Sensitisation of primary afferent nociceptive (pain sensing) neurons is common to inflammatory pain and specifically to RA associated pain (3). This leads to a state of abnormally heightened sensitivity to pain, known as hyperalgesia, where responses to noxious stimuli are enhanced, and mechanical allodynia, where innocuous stimuli produce pain (3). Inflammatory pain and the resulting mechanical allodynia have been identified as a significant problem in RA despite minimal disease activity and effective suppression of inflammation and thus substantially impacts patient quality of life (4-6). The development of mechanical allodynia and hyperalgesia has previously been reported in mice with inflammatory arthritis and is induced by the direct action of pro-inflammatory mediators, such as prostaglandins and pro-inflammatory cytokines, on peripheral nociceptors (7). However, this was observed prior to clinical signs of inflammation, suggesting that the timing of inflammation and pain in RA may not necessarily coincide (7). Given this knowledge, it is a rationale progression to assess mechanical allodynia in RA to enable a complementary and systemic approach to understanding disease progression and the development of new targeted therapeutics.

Pro-inflammatory cytokines including tumour necrosis factor alpha (TNF-α), interleukin-1 beta (IL-1β) and interleukin-6 (IL-6) are significant factors in RA disease progression and the upregulation of these cytokines occurs due to the chronic infiltration of immune cells into the synovial joints of RA patients (8). These cytokines not only prolong the inflammatory response within RA, but their overproduction in the synovial joints promotes bone destruction (9, 10) and sensitisation of peripheral nociceptors, leading to increased pain sensitivity over inflamed joints (11-15).

Recently, research in RA has focussed on nuclear factor-kappa B (NF-κB) signalling and its role in osteoclast mediated bone resorption. NF-κB is a pro-inflammatory transcription factor involved in normal osteoclast differentiation and survival (16) and *in vivo* studies have identified increased NF-κB expression and activity in osteoclasts in the inflamed

joints of arthritic mice (17). NF-κB signalling is stimulated by the binding of receptor activator of nuclear factor kappa B (RANK) ligand (RANKL) to its receptor RANK on pre-osteoclasts and ultimately leads to the differentiation of these cells into mature and active osteoclasts (16, 18). Upregulation of pro-inflammatory cytokines in RA results in the excessive binding of RANKL to RANK, further activating NF-κB signalling and promoting osteoclast recruitment, differentiation and activation. NF-κB is also crucial to T-cell mediated inflammation in RA (8, 19), as well as the pathogenesis of neuropathic pain (20-22), suggesting that NF-κB signalling plays a crucial role in the overall progression of joint destruction and the development of pain in RA.

Previously, direct targeting of osteoclast differentiation by inhibiting RANKL has been shown to arrest bone erosion in several animal models of inflammatory arthritis (16, 23-27). A clinical trial in patients with RA has also shown that blockade of RANKL using a neutralising antibody, denosumab, slows the progression of bone erosion but does not impede inflammation in the synovial joints (28). This shows that suppressing osteoclast formation and activity can protect bone from the consequences of inflammation even in the absence of inhibition of inflammation. However, despite this the destructive consequences of inflammation in the synovial joints persists, resulting in prolonged pain-like behaviour, including mechanical allodynia. Currently, there are limited effective treatments available that collectively target inflammation, bone erosion and pain in RA. Many common disease modifying anti-rheumatic drugs (DMARDs) target inflammation allowing chronic bone erosion to progress and side effects of these treatments can also be attributed to the development of mechanical allodynia in RA (29-31). Thus, inhibition of other intracellular pathways involved concurrently in both T cell mediated inflammation and osteoclastogenesis, such as NF-κB signalling, may be more beneficial in reducing inflammation, bone destruction and overall pain in RA patients.

Parthenolide (PAR) is a sesquiterpene lactone found in the Astercease family of medicinal plants, including FeverFew (32), and is reported to have both anti-inflammatory and anti-tumorigenic actions (33-35). PAR is a potent NF-κB inhibitor and prevents osteoclast formation and RANKL-mediated bone resorption *in vitro* by inhibiting NF-κB activation (36). *In vivo* studies have shown that PAR blocks LPS-induced osteolysis and inhibits

surface bone loss through suppression of NF-κB activity in murine calvarial models (36). High doses (10 mg/kg/day) of PAR have also been reported to inhibit ovariectomy-induced bone loss *in vivo* (37). Recently, PAR was demonstrated to inhibit the effects of IL-1β and TNF-α on cultured human chondrocytes as well as reduce inflammation and pannus formation in the synovial joints of rats with collagen-induced arthritis (CIA) (38), indicating that PAR may directly inhibit pro-inflammatory cytokine release. However, within this study there was no clear reduction of bone erosion or generalised osteopenia beyond the anti-inflammatory effects at the inflamed joint (38). This suggests that when inflammation has reached a maximal level, the mild inhibitory effect of low PAR dosage (1 mg/kg) on inflammation is insufficient to inhibit the subsequent effect inflammation has on bone erosion (38). Further to this, behavioural studies have shown that PAR reduces mechanical allodynia and hyperalgesia in rats after chronic constriction injury to the sciatic nerve (CCI) (39, 40).

It is evident from these studies that PAR is beneficial in reducing inflammation and bone loss, as well as pain in different pathological conditions. However, to date there are no studies which have assessed the effect of NF-κB inhibition on these three key aspects of RA pathogenesis simultaneously. Therefore, the current study aimed to investigate whether PAR would reduce inflammation, bone loss and mechanical allodynia simultaneously in the paws of mice in a mild model of collagen antibody-induced arthritis (CAIA).

4.4. Methods

This study was approved by the Animal Ethics Committee of the University of Adelaide (M-2015-255) and complied with the National Health and Research Council (Australia) Code of Practice for Animal Care in Research and Training (2014). Mice were housed in approved conditions on a 12-hour light-dark cycle. Food and water were provided ad libitum.

4.4.1. Collagen antibody-induced arthritis model

Thirty-two female Balb/c mice aged six to eight weeks were obtained from the University of Adelaide Laboratory Animal Services and randomly divided into four groups (n = 8 per group); Control (no arthritis or treatment), CAIA (arthritis with no treatment), CAIA + PAR 1 mg/kg (arthritis treated with 1 mg/kg PAR) and CAIA + PAR 4 mg/kg (arthritis treated with 4 mg/kg PAR).

To induce arthritis, mice were injected intravenously via the tail vein with 150 µl (1.5 mg/mouse) of a cocktail of anti-type II collagen monoclonal antibodies (Arthrogen-CIAs Arthritogenic Monoclonal Antibodies, Chondrex Inc., Redwood, WA, USA). This was followed by an intraperitoneal injection of 20 µl (10 µg/mouse) of *E. coli* lipopolysaccharide (LPS) on day 3 (Figure 4.1). Control animals were injected with phosphate buffered saline (PBS) alone at both time points. 200 µl of PAR in 10% DMSO for the 1 mg/kg dose (38) and 200 µl of PAR in 0.8% DMSO for 4 mg/kg was administered in the treatment groups via intraperitoneal injections, daily from day 4 to day 10 (Figure 4.1).
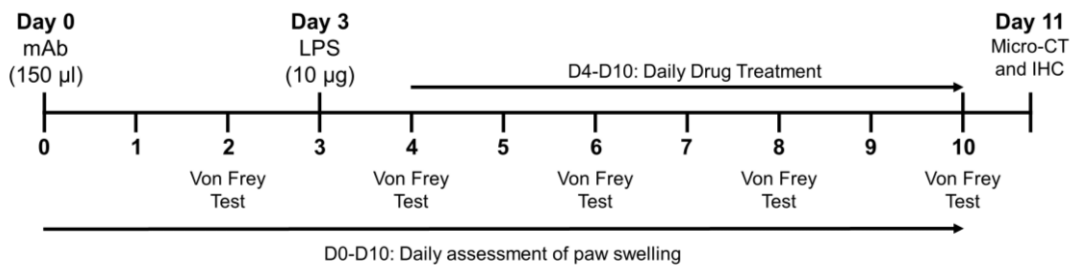
Figure 4.1. Experimental collagen antibody-induced arthritis mouse model timeline. Values represent days. D; Day, IHC; immunohistochemistry, LPS; lipopolysaccharide, mAb; monoclonal antibodies, micro-CT; micro-computed tomography.

4.4.2. Clinical analysis of local paw swelling

Mice were monitored daily using an approved clinical record sheet for arthritis studies to assess body weight and factors of general health. To assess clinical paw swelling; individual paws were examined daily by two observers for the presence of redness, tenderness, swelling and inflammation using a previously described clinical paw scoring

method (41, 42). For each paw, a score of 1 was given for an inflamed digit and a score from 0-5 was allocated for swelling of the carpal/tarsal joint and of the wrist/ankle. The maximum score for each paw was 15, giving a possible total of 60 per mouse (41, 42).

4.4.3. Von Frey paw withdrawal test for the assessment of mechanical allodynia

Mechanical allodynia was assessed in the hind paws of mice using the von Frey paw withdrawal test. As it has been reported that Balb/c mice develop a tolerance to this behavioural test (7), von Frey testing was conducted on alternate days starting on day 2 and ending on day 10 (i.e. testing days were day 2, 4, 6, 8 and 10; Figure 4.1). On testing days mice were placed in a plastic cage with a wire mesh bottom which allows full access to the hind paws and behavioural accommodation was allowed for approximately 15 minutes. Both hind paws were touched with one of a series of seven von Frey filaments with logarithmically incremental stiffness of 0.04, 0.07, 0.16, 0.40, 0.60, 1.00 and 2.00 grams (43). The von Frey filament was presented perpendicular to the hind-plantar surface of the hind paws with sufficient force to cause slight buckling against the paw and held for approximately 6-8 seconds. A positive response was noted if the paw was sharply withdrawn. Flinching immediately upon removal of the hair was also considered a positive response. Ambulation was considered an ambiguous response, and in such cases the stimulus was repeated.

The 50% paw withdrawal threshold was determined using the Dixon up-down method (43). In this method, behavioural testing was initiated with the 0.40 gram filament, in the middle of the series (43). Von Frey filaments were presented in a consecutive fashion, either ascending or descending. In the absence of a positive paw withdrawal response to the initially presented filament a stronger stimulus was presented; in the event of a positive paw withdrawal response, the next weaker stimulus was chosen (43). Stimuli were presented at intervals of several seconds, allowing for apparent resolution of any behavioural responses to previous stimuli. The threshold at which there was a 50% probability of paw withdrawal was then calculated, as previously described (43).

4.4.4. Micro-computed tomography analysis

At the completion of the study on day 11, transcardial perfusions were performed while mice were anaesthetised (175 mg/kg Sodium Pentobarbital). Mice were perfused with 4%

paraformaldehyde prior to the collection of brain and spinal cord tissue, for assessment in ongoing studies. Front and hind paws were then collected and underwent post-fixation for 48 hours.

Bone changes and swelling of the front and hind paws was assessed using images obtained by a micro-computed tomography (micro-CT) scanner (SkyScan 1076, Bruker, Kontich, Belgium), following protocols previously published by our laboratory (42, 44). Paws were scanned at a source voltage of 55 kV, current 180 µA, isotropic pixel size of 8.5 µm with a 0.5 mm thick aluminium filter, rotation step of 0.6, frame averaging of 1 and a total scan time of approximately 35 minutes. Cross-sectional images were reconstructed using a filtered back projection algorithm (N-Recon software, Bruker, Kontich, Belgium) and saved as 8-bit grey level files (bitmap format). The stack of reconstructed cross-section images of the front and hind paws were realigned in 3D with the long axis of the paw aligned along the inferior-superior direction of the images (Dataviewer software, Bruker), as previously described (44).

Selection of volume of interest (VOI) for analysis:

For each front paw, 280 contiguous cross-sections (corresponding to a VOI length of 2.4 mm), starting from 200 cross-sections (1.7 mm) distally to the epiphyseal growth plate of the radiocarpal joint extending through the joint up to 80 cross-sections (0.68 mm) proximally, were used for analysis of both bone and surrounding soft tissue. A cylindrical VOI (4.5 mm diameter, 2.4 mm in length) was used and positioned according to the location of each individual paw in the image (42).

In the hind paws, 600 cross-sections (corresponding to a VOI length of 5.1 mm), extending from the posterior surface of the calcaneus through the proximal tarsal and metatarsal bones, were used for analysis of the bone. A polygonal region of interest was used to trace around the calcaneus, metatarsal and tarsal bones, excluding the tibia and fibula (Figure 4.2). Whereas for the soft tissue analysis, 200 cross-sections were used (corresponding to a length of 1.7 mm), extending from the most posterior aspect of the metatarsal bones, excluding the calcaneus and including the cuboid (Figure 4.2). On these, a standardised cylindrical VOI (5.5 mm diameter, 1.7 mm in length) was selected for quantification.
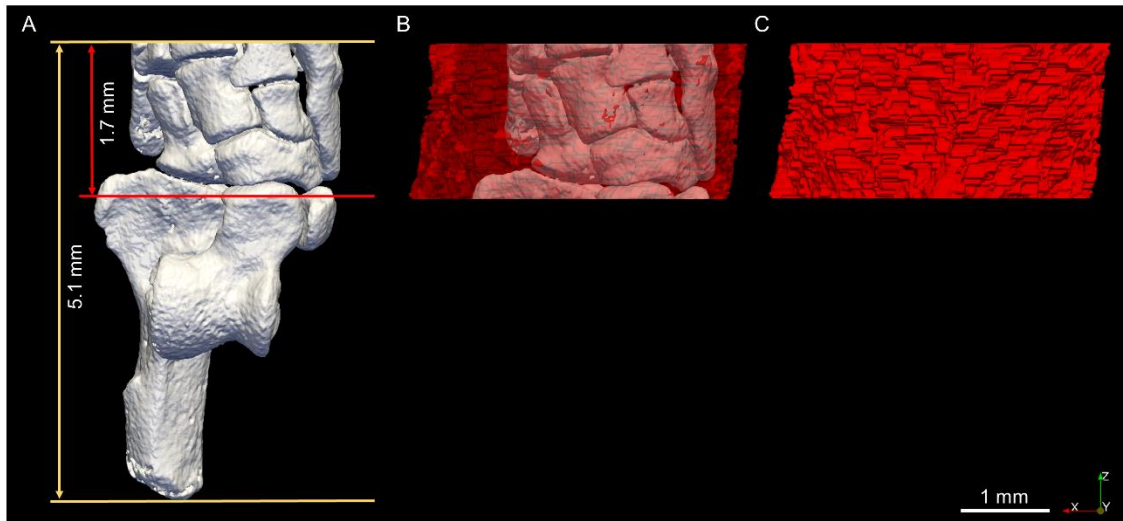
Figure 4.2. 3D micro-CT images of the left hind paw (top view), including calcaneus, tarsal and metatarsal bones for quantitative analysis; bone represented in white colour and soft tissue in red colour. A. The lengths of the volumes of interest (VOIs) used for micro-CT analysis are indicated by the yellow arrows for bone analysis (VOI length of 600 cross sections, corresponding to 5.1 mm) and red arrows for soft tissue analysis (VOI length 200 cross sections, corresponding to 1.7 mm). The 3D rendering of the VOI used for soft tissue analysis is presented in B (bone visible in transparency) and C.

Imaging thresholding and calculation of bone volume and paw volume:

On the VOIs specified above, the bone volume (BV, in mm^3) and the paw volume (PV, in mm^3, which includes the surrounding soft tissue of the radiocarpal, tarsal and metatarsal bones), were quantified in 3D using uniform thresholding (CT Analyser software, Bruker). In the grey-level histogram of the reconstructed cross-section images (bitmap format, 256 grey levels, ranging from 0 to 255), the grey level values in the lower range (from 0 to 11) corresponded to air or background, followed in increasing order by values of the soft tissue (ranging from 12 to 134) and bone (from 135 to 255) (44). Two fixed minimum threshold values were applied to the specimens for segmentation. One minimum threshold level was used for segmenting the bone pixels only (minimum threshold level 135 to maximum level 255), leaving air and surrounding soft tissue as background (44-46). The second minimum threshold level was for segmenting the paw, soft tissue and bone together, (minimum threshold level 12 to maximum level 255) and

leaving air as the background (44-46). By applying the corresponding threshold values to each specimen, automated calculation was performed of BV and PV (CT Analyser software, Bruker). The BV was calculated as the volume occupied by the voxels segmented as bone and the PV was calculated as the volume occupied by the voxels segmented as paw, which included both bone and the surrounding soft tissue. For the PV measurements, loose speckles in the segmented images which originated from noise pixels were removed. This was completed using a cycle of the software function 'sweep' (CT Analyser software, Bruker) which automatically removes all but the largest object in 3D volume, maintaining the paw as the largest object. BV and PV were then quantified using the marching cubes method (CT Analyser software, Bruker) (47-50).

4.4.5. *Histological analysis of the radiocarpal joints and hind paws*

Following decalcification of the front and hind paws using 10% Ethylene diaminetetraacetic acid (EDTA), paws were processed for paraffin embedding and serial sagittal sections were cut (5 µm) for histological analysis. Routine haematoxylin and eosin (H&E) staining was conducted and sections were imaged using the NanoZoomer Digital Pathology System (NDP Hamamatsu, Hamamatsu City, Japan) for semi-quantitative analysis at 40x magnification. Histological evaluation of the radiocarpal joint and hind paw was carried out by two-blinded observers using a previously described scoring method (51). The number of inflammatory cells was assessed within the joints; normal tissue (< 5% inflammatory cells) was scored as 0, mild inflammation (6-20% inflammatory cells) was scored as 1, moderate inflammation (21-50% inflammatory cells) was scored as 2 and severe inflammation (> 51% inflammatory cells) was scored as 3. Cartilage and bone destruction were assessed using a 0 to 3-point scale system (0, normal tissue; 1, mild cartilage destruction; 2, evidence of both cartilage and bone destruction; 3, severe cartilage and bone destruction). Pannus formation was scored as either, 0 no pannus or 1 pannus formation (52).

Tartrate resistant acid phosphatase (TRAP) staining was also conducted on serial sagittal sections of the front and hind paws to identify the presence of osteoclast-like cells on the bone surface and pre-osteoclast-like cells in the surrounding soft tissue of the radiocarpal joints and hind paws. Sections were incubated with TRAP solution at 37 °C for 60 minutes and counterstained with haematoxylin as previously described (53-55). The number of

multinucleated TRAP positive cells (> 3 nuclei) were counted by two blinded observers using 40x magnified images on the NanoZoomer Digital Pathology System (NDP Hamamatsu, Hamamatsu City, Japan). A consistent region of interest (2.16 mm^2) was used for analysis, to include cells found on the bone surface (51) and within the surrounding soft tissue of the radiocarpal joints and hind paws (42).

4.4.6. Statistical analysis

Statistical analysis was performed using GraphPad Prism® software (V 7.03; GraphPad Software, La Jolla, CA, USA) and SPSS Statistics (V 25; IBM SPSS Software, NSW, Australia). For von Frey analysis, a linear mixed-effects model was used, controlling for clustering on mouse and for repeated measurement over time using a Variance Components covariance structure. Assumptions of a linear model were found to be upheld by inspection of histograms and scatter plots of residuals and predicted values. An interaction of Group (1 = Control, 2 = CAIA, 3 = CAIA + PAR 1 mg/kg and 4 = CAIA + PAR 4 mg/kg) and Day (day of test) was included with adjustment for paw side (left and right paws).

For paw score, micro-CT and histology data, differences among groups were analysed using the non-parametric Kruskal-Wallis test and if significant, differences between two groups were analysed using the Mann-Whitney U test. All values shown are mean ± standard error of the mean (SEM). Statistical significance was determined when a p-value of 0.05 or less was identified.

4.5. Results

4.5.1. Assessment of local paw inflammation

Induction of CAIA resulted in significant redness, tenderness and inflammation in the front and/or hind paws of all disease groups following LPS administration on day 3, as evident in the macroscopic images in Figure 4.3A. CAIA mice exhibited significantly greater paw scores compared to control mice from day 5 to day 10 (p < 0.0003; Figure 4.3B). On day 8, 9 and 10, CAIA mice treated with 4 mg/kg PAR had significantly lower paw scores compared to CAIA mice (p = 0.041, p = 0.019 and p = 0.017, respectively; Figure 4.3B). On day 10, CAIA mice treated with 1 mg/kg PAR also had significantly

lower paw scores compared to CAIA mice (p = 0.032). From day 8 to day 10, CAIA mice treated with 4 mg/kg PAR had slightly lower paw scores compared to CAIA mice treated with 1 mg/kg PAR, however this was not statistically significant.
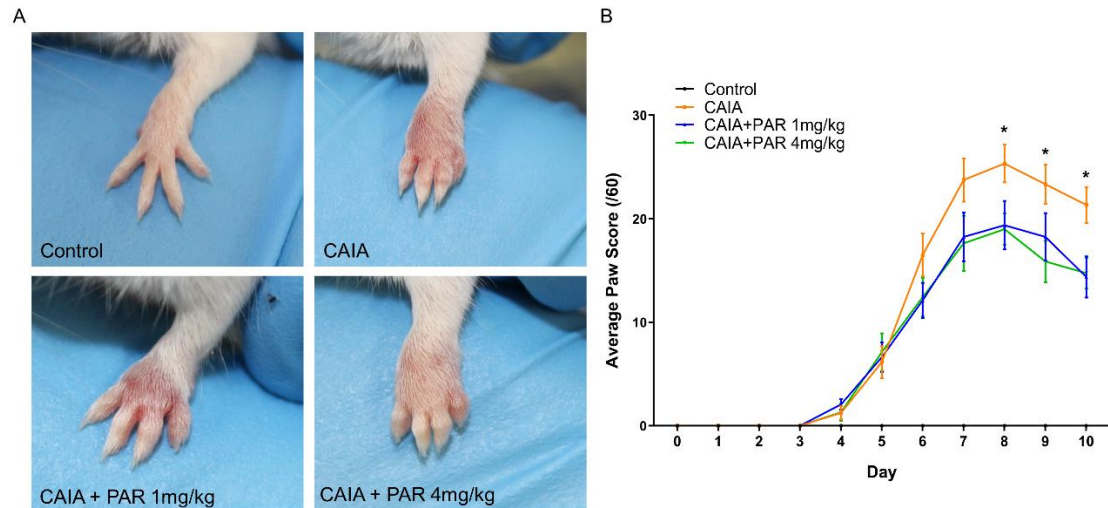
Figure 4.3. Clinical evaluation of local inflammation. A. Representative macroscopic appearance of the front paws at day 7 post-arthritis induction. B. Average paw scores of each group over the 10-day model. Error bars represent SEM (n = 8 mice per Control, CAIA + PAR 1 mg/kg and CAIA + PAR 4 mg/kg; n = 6 mice per CAIA; * p < 0.05 CAIA + PAR 4 mg/kg vs CAIA).

4.5.2. Assessment of mechanical allodynia

There was no statistically significant interaction between Group and Day of Test for the outcome tactile paw withdrawal threshold (g) when controlling for Paw side (interaction p value = 0.903). There was also no statistically significant association between tactile paw withdrawal threshold and Paw side, when controlling for the Group*Day of Test interaction (p = 0.306).

The mean paw withdrawal threshold decreased in control mice from day 4 (1.52 ± 0.13 g) to day 6 (1.29 ± 0.14 g), however this was not statistically significant (Table 4.1 and Figure 4.4). Control mice also had the lowest mean paw withdrawal threshold compared to CAIA and CAIA PAR treated mice throughout the 10 day model (Table 4.1 and 4.2, Figure 4.4). Conversely, the mean paw withdrawal threshold was greatest in CAIA mice

from day 4, when local inflammation is first visible (1.83 ± 0.13 g), to day 8, when local inflammation reaches its peak (1.57 ± 0.17 g, Figure 4.3). Interestingly, when inflammation peaks between day 6 and 8, mean paw withdrawal thresholds decreased in all diseased groups. This was particularly evident in CAIA mice treated with either 1 mg/kg or 4 mg/kg PAR (Figure 4.4). Paw withdrawal thresholds in CAIA mice treated with 1 mg/kg PAR decreased from 1.64 ± 0.14 g on day 6 to 1.37 ± 0.15 g on day 8, while paw withdrawal thresholds in CAIA mice treated with 4 mg/kg PAR decreased from 1.58 ± 0.14 g on day 6 to 1.40 ± 0.15 g on day 8. However, this change was not statistically significant in either group. Again, although not significant, when inflammation subsides from day 8 to 10, there is a slight increase in mean paw withdrawal thresholds observed in CAIA mice treated with either 1 mg/kg (1.37 ± 0.15 g on day 8 to 1.49 ± 0.13 g on day 10) and 4 mg/kg PAR (1.40 ± 0.15 g on day 8 to 1.61 ± 0.13 on day 10, Figure 4.4). Mean paw withdrawals also did not significantly differ between all groups on each day of von Frey testing (Table 4.2).
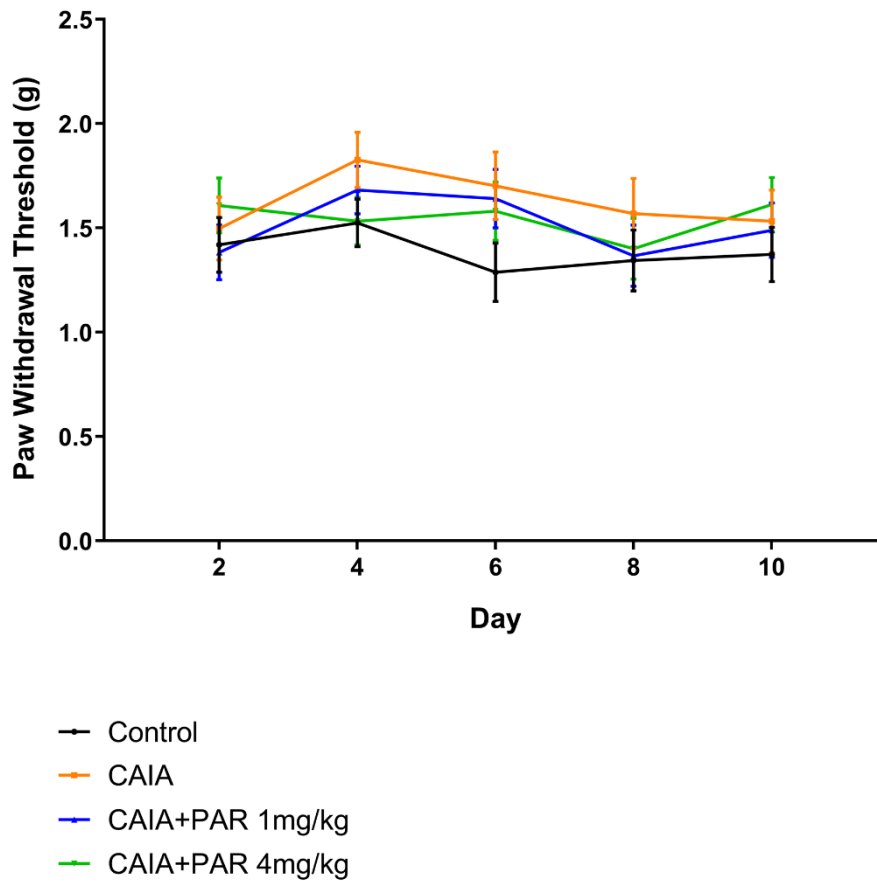
Figure 4.4. Paw withdrawal threshold of the hind paws assessed by application of von Frey filaments. Mean tactile paw withdrawal threshold of each group on alternate days throughout the 10-day model. Error bars represent SEM (n = 8 mice per Control, CAIA + PAR 1 mg/kg and CAIA + PAR 4 mg/kg; n = 6 mice per CAIA).

Table 4.1. Mean and standard error of the mean (SEM) of paw withdrawal threshold (g) in all groups at each day of von Frey testing

Day of Test	Group	Mean	SEM
2	1	1.419	0.131
	2	1.497	0.151
	3	1.383	0.131
	4	1.608	0.131
4	1	1.524	0.114
	2	1.826	0.132
	3	1.682	0.114
	4	1.532	0.114
6	1	1.288	0.140
	2	1.702	0.162
	3	1.640	0.140
	4	1.580	0.140
8	1	1.344	0.146
	2	1.569	0.168
	3	1.367	0.146
	4	1.401	0.146
10	1	1.373	0.130
	2	1.532	0.150
	3	1.489	0.130
	4	1.612	0.130

Groups: 1 = Control, 2 = CAIA, 3 = CAIA + PAR 1 mg/kg and 4 = CAIA + PAR 4 mg/kg

SEM; Standard Error of the Mean

Table 4.2. Linear mixed-effects model of paw withdrawal threshold (g): mean differences

Day of Test	Group Comparison	Difference in paw withdrawal threshold (95% CI)	Comparison P value
2	1 vs 2	-0.08 (-0.48, 0.32)	0.696
	2 vs 3	0.11 (-0.29, 0.51)	0.571
	2 vs 4	-0.11 (-0.511, 0.29)	0.581
	3 vs 4	-0.22 (-0.5.9, 0.15)	0.230
4	1 vs 2	-0.30 (-0.65, 0.05)	0.088
	2 vs 3	0.14 (-0.20, 0.49)	0.413
	2 vs 4	0.29 (-0.05, 0.64)	0.098
	3 vs 4	0.15 (-0.17, 0.47)	0.356
6	1 vs 2	-0.41 (-0.84, 0.01)	0.058
	2 vs 3	0.06 (-0.37, 0.49)	0.773
	2 vs 4	0.12 (-0.31, 0.55)	0.570
	3 vs 4	0.06 (-0.34, 0.46)	0.762
8	1 vs 2	-0.22 (-0.67, 0.22)	0.318
	2 vs 3	0.20 (-0.24, 0.65)	0.370
	2 vs 4	0.17 (-0.28, 0.61)	0.455
	3 vs 4	-0.034 (-0.45, 0.38)	0.870
10	1 vs 2	-0.16 (-0.56, 0.24)	0.432
	2 vs 3	0.04 (-0.36, 0.44)	0.836
	2 vs 4	-0.08 (-0.48, 0.32)	0.685
	3 vs 4	-0.12 (-0.49, 0.25)	0.509

Groups: 1 = Control, 2 = CAIA, 3 = CAIA + PAR 1 mg/kg and 4 = CAIA + PAR 4 mg/kg

P values less than 0.05 were considered to be statistically significant.

4.5.3. Micro-computed tomography analysis of bone volume (BV) and paw volume (PV)

<u>Front Paws:</u>

BV measured in the radiocarpal joints was significantly lower in CAIA mice (1.05 ± 0.05 mm^3) and CAIA mice treated with 1 mg/kg (0.98 ± 0.04 mm^3) and 4 mg/kg PAR (0.93 ± 0.04 mm^3) in comparison to control mice (1.24 ± 0.05 mm^3, p = 0.017, p = 0.0007 and p < 0.0001, respectively; Figure 4.5A). CAIA mice treated with 1 mg/kg and 4 mg/kg PAR tended to have slightly lower BV in the radiocarpal joint compared to CAIA mice, however this was not statistically significant.

PV in the radiocarpal joint was significantly higher in CAIA mice (37.14 ± 2.07 mm^3) and CAIA mice treated with 1 mg/kg (34.74 ± 2.05 mm^3) and 4 mg/kg PAR (34.94 ± 1.75 mm^3) compared to control mice (24.17 ± 0.82 mm^3, p < 0.0001, p = 0.0004 and p < 0.0001, respectively; Figure 4.5B). CAIA mice treated with 1 mg/kg and 4 mg/kg PAR showed lower PV measurements compared to CAIA mice. However, this was not significantly different.
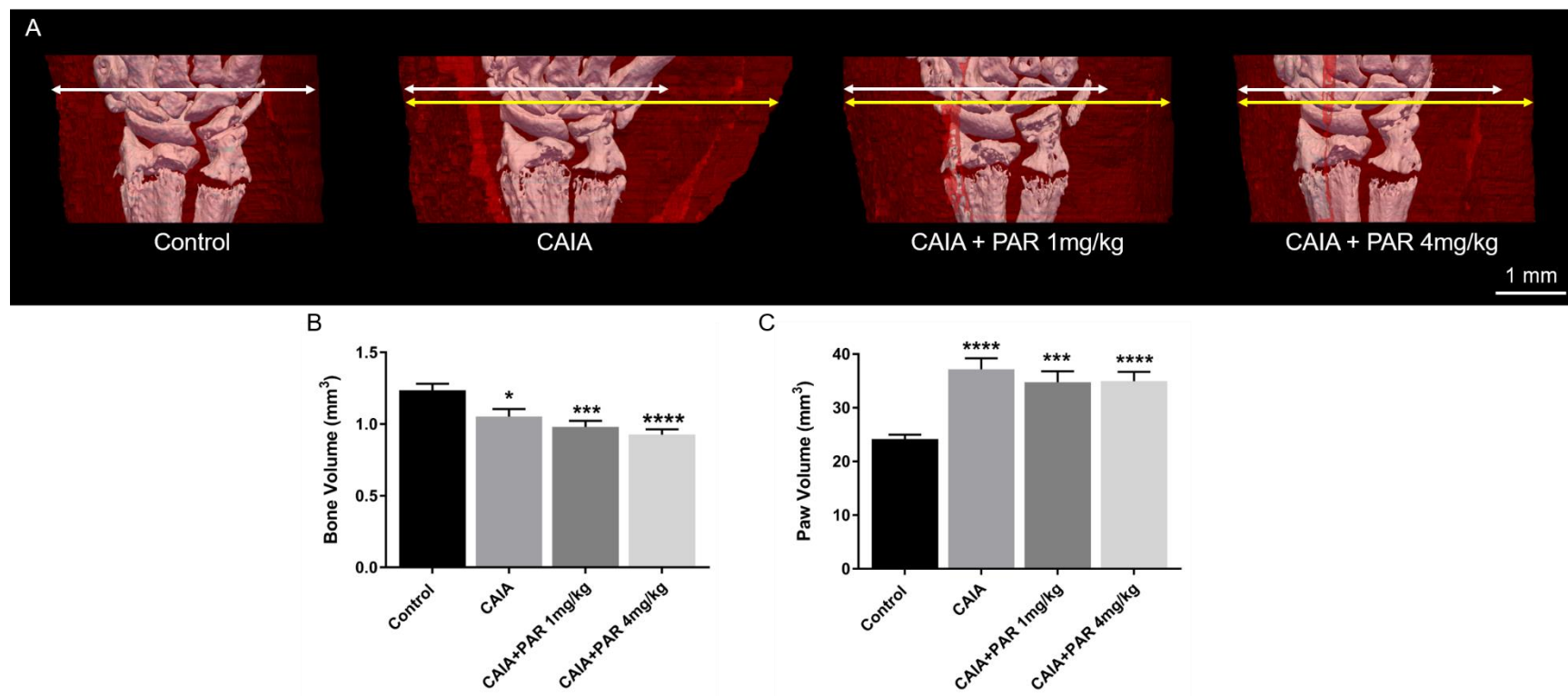
Figure 4.5. Assessment of bone volume (BV) and soft tissue swelling (paw volume, PV) of the radiocarpal joint by high resolution micro-CT at day 11. A. Three-dimensional micro-CT models (length 2.4 mm) of the radiocarpal joint (bone in white colour) and of the surrounding soft tissue (indicated in red colour) in the right paw. White arrows represent the width of the soft tissue volume for controls and yellow arrows for each disease group, highlighting the differences among them. Mean BV (B) and PV (C) expressed in mm^3 in the radiocarpal joint as assessed by micro-CT analysis at day 11. Error bars represent SEM. (n = 16 paws (left and right together) per Control, CAIA + PAR 1 mg/kg and CAIA + PAR 4 mg/kg; n = 12 paws (left and right together) per CAIA; * $p < 0.05$, *** $p < 0.0004$ and **** $p < 0.0001$ vs control).

<u>Hind Paws:</u>

Similar to the front paws, BV measured in the hind paws was significantly lower in CAIA mice (3.64 ± 0.08 mm^3) and CAIA mice treated with 1 mg/kg (3.40 ± 0.07 mm^3) and 4 mg/kg PAR (3.30 ± 0.07 mm^3) compared to control mice (3.98 ± 0.14 mm^3, $p = 0.01$, $p = 0.0004$ and $p = 0.0001$, respectively; Figure 4.6A). CAIA mice treated with 4 mg/kg PAR were also found to have a significantly lower BV compared to CAIA mice in the hind paw ($p = 0.004$).

Despite the difference in BV in the hind paws, between CAIA and CAIA treated groups, there was evidence of bone resorption pits in the 3D images of both the navicular (Figure 4.7) and cuboid (Figure 4.7) of all CAIA groups. However, it was also not conclusive whether these bone resorption pits were reduced following PAR treatment when compared to CAIA untreated mice.

A significant increase in PV was observed in the hind paws of CAIA mice (24.70 ± 0.53 mm^3), and CAIA mice treated with PAR with both 1 mg/kg (25.61 ± 0.57 mm^3) and 4 mg/kg doses (24.65 ± 0.93 mm^3) compared to control mice (13.15 ± 0.33 mm^3; $p < 0.0001$; Figure 4.6B). There was no significant difference in PV measured in the hind paws between CAIA and CAIA treated groups.
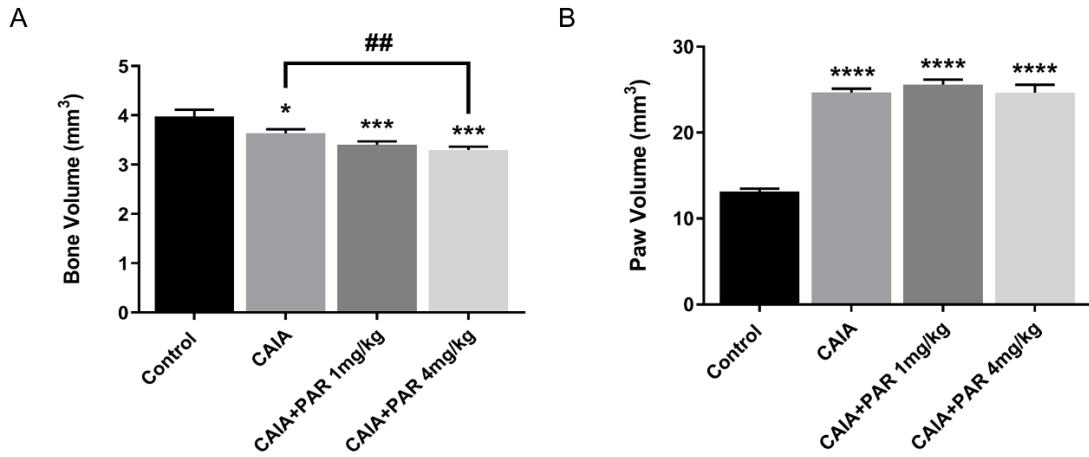
Figure 4.6. Assessment of bone volume (BV) and paw volume (PV) in the hind paw by micro-CT. Mean BV (A) and PV (B) expressed in mm^3 in the hind paw as assessed by micro-CT analysis at day 11. Error bars represent SEM (n = 16 paws (left and right together) per Control, CAIA + PAR 1 mg/kg and CAIA + PAR 4 mg/kg; n = 12 paws (left and right together) per CAIA; * p = 0.01, *** p = 0.0001 and **** p < 0.0001 vs control; ## p = 0.04 vs CAIA).
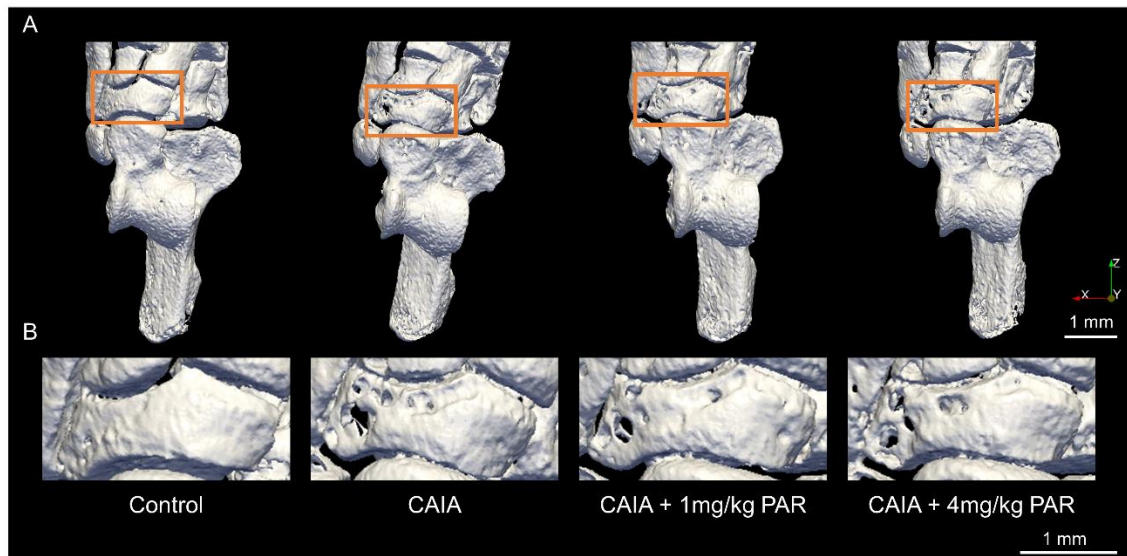
Figure 4.7. Representative three-dimensional models of the right hind paw showing bone resorption pits in the navicular. A. Superior view of right hind paws from the control (First column), CAIA (Second column), CAIA + PAR 1 mg/kg (Third column) and CAIA + PAR 4 mg/kg groups (Fourth column). Orange boxes identify the navicular which is presented at greater magnification (B) to highlight the pitting present in this bone.
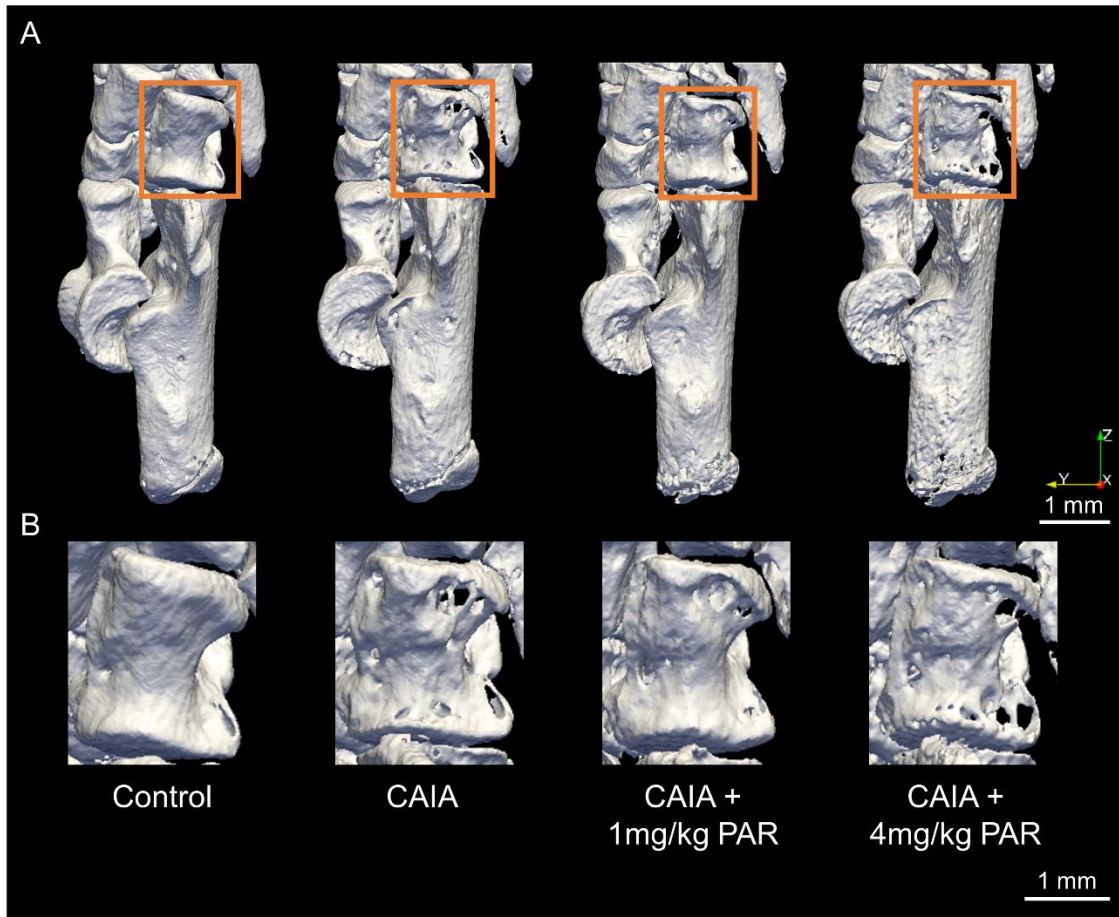
Figure 4.8. Representative three-dimensional models of the right hind paw showing bone resorption pits in the cuboid. A. Lateral view of right hind paw from the control (First column), CAIA (Second column), CAIA + PAR 1 mg/kg (Third column) and CAIA + PAR 4 mg/kg groups (Fourth column). Orange boxes identify the cuboid which is presented at greater magnification (B) to show the pitting present in this bone.

4.5.4. *Histological analysis of the radiocarpal joint*

Representative images of H&E and TRAP staining in the radiocarpal joint are presented in Figure 4.9. Histological evaluation of sagittal sections of the radiocarpal joint showed that CAIA mice had significantly greater scores for cellular infiltration, cartilage and bone degradation and pannus formation compared to control mice ($p = 0.0005$; Figure 4.10). Although CAIA mice treated with PAR at either 1 mg/kg or 4 mg/kg exhibited reduced scores for cellular infiltration, cartilage and bone degradation and pannus formation compared to CAIA mice, this was not statistically significant (Figure 4.10). There was also no significant difference in histological scores between the two treatment groups.
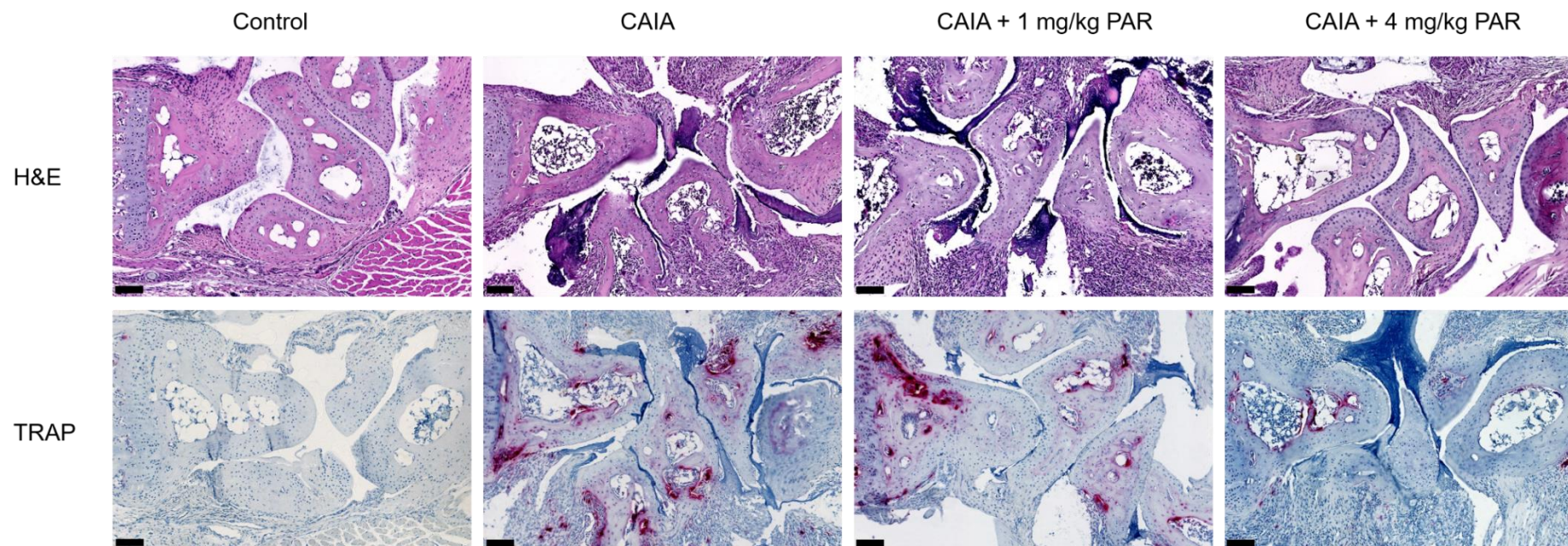
Figure 4.9. Representative immunohistochemical images of the radiocarpal joint (20x magnification) from the Control (First column), CAIA (Second column), CAIA + PAR 1 mg/kg (Third column) and CAIA + PAR 4 mg/kg groups (Fourth column); Top Row (Haematoxylin and Eosin; H&E); Bottom Row (Tartrate Resistant Acid Phosphatase; TRAP). Scale bars represent 100 µm.

Figure 4.10. Semi-quantitative analysis of inflammatory cell infiltration, cartilage and bone degradation and pannus formation in H&E stained sagittal sections of the radiocarpal joint. Error bars represent SEM (n = 16 paws (left and right together) per Control, CAIA + PAR 1 mg/kg and CAIA + PAR 4 mg/kg, n = 12 paws (left and right together) per CAIA; *** p < 0.0005 vs control).

Compared to control mice (0.125 ± 0.125 cells), a significantly greater number of multinucleated TRAP positive cells were observed on the bone surface within the radiocarpal joints of CAIA mice (25.58 ± 5.29 cells, p < 0.0001) and CAIA mice treated with 1 mg/kg (14 ± 4.27 cells, p < 0.0001) or 4 mg/kg PAR (13.13 ± 3.68 cells, p < 0.0001; Figure 4.9 and Figure 4.11A). CAIA mice treated with 4 mg/kg PAR had a significantly lower number of multinucleated TRAP positive cells on the bone surface of the radiocarpal joint compared to CAIA mice (p = 0.04; Figure 4.11A). CAIA mice treated with 4 mg/kg PAR also had a reduced number of multinucleated TRAP positive cells within the surrounding soft tissue of the radiocarpal joint (35.94 ± 13.85 cells) compared to both CAIA mice (64.17 ± 23.64 cells) and CAIA mice treated with 1 mg/kg PAR (44.87 ± 16.05 cells), however this was not statistically significant (Figure 4.11B).

Figure 4.11. Assessment of osteoclasts and pre-osteoclasts within the radiocarpal joint. Average values of TRAP positive multinucleated cells on the bone surface (A) and within the surrounding soft tissue (B) in a 2.16 mm^2 area of the radiocarpal joint. Error bars represent SEM (n = 16 paws (left and right together) per Control, CAIA + PAR 1 mg/kg and CAIA + PAR 4 mg/kg; n= 12 paws (left and right together) per CAIA; **** $p < 0.0001$ vs control, # $p = 0.04$ CAIA + PAR 4 mg/kg vs CAIA).

4.5.5. Histological analysis of the hind paw

Histological evaluation of sagittal sections of the hind paws showed similar results to the radiocarpal joint, as CAIA mice had significantly greater scores for cellular infiltration, cartilage and bone degradation and pannus formation compared to control mice ($p < 0.0001$; Figure 4.12). Similarly, there was no significant difference in the scores for cellular infiltration, cartilage and bone degradation and pannus formation in the hind paws between all CAIA and CAIA treated groups (Figure 4.12).
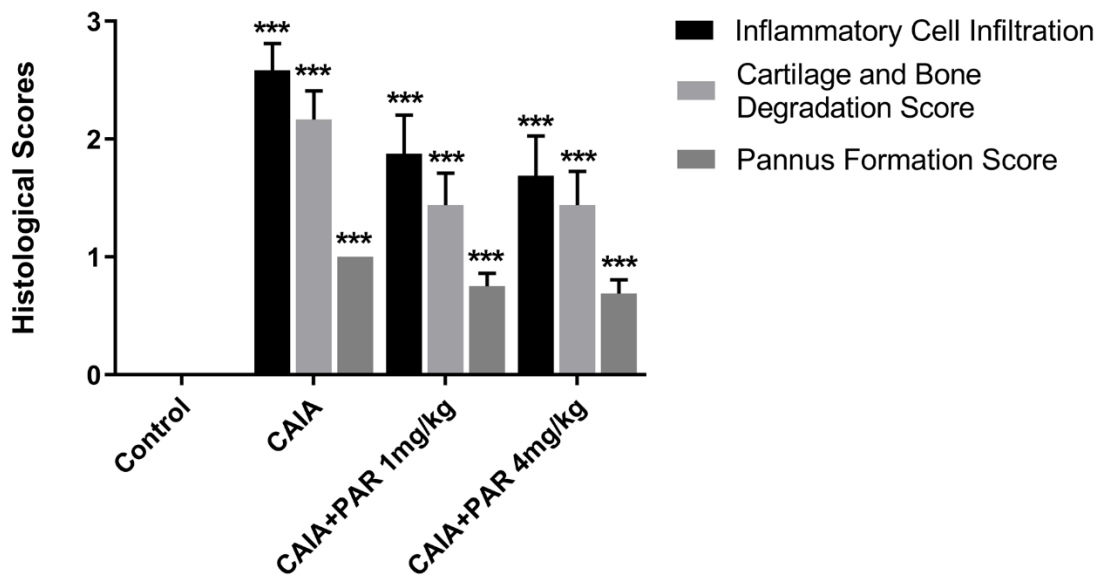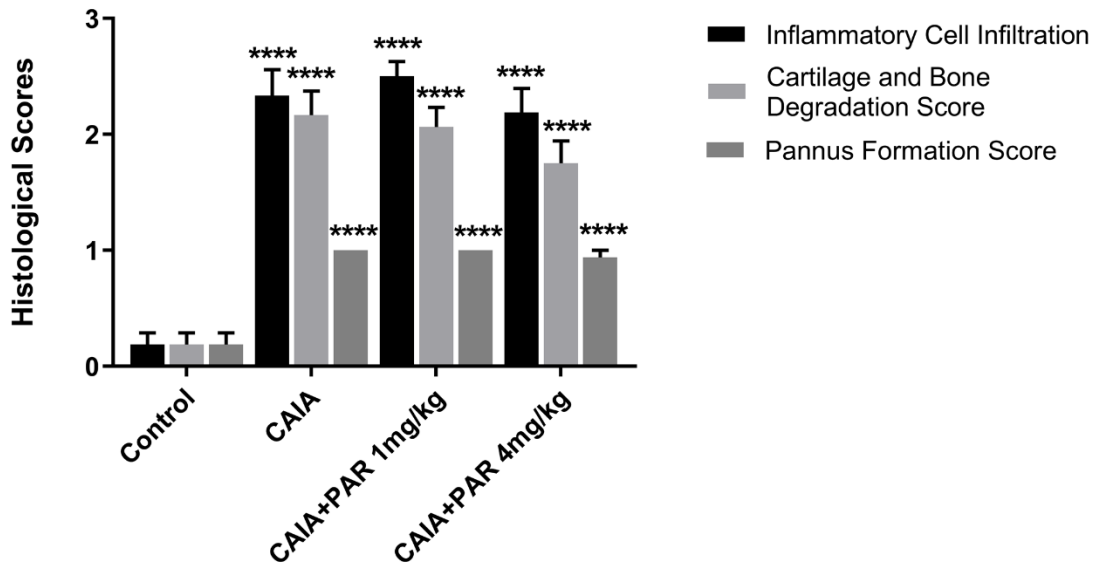
Figure 4.12. Semi-quantitative analysis of inflammatory cell infiltration, cartilage and bone degradation and pannus formation in H&E stained sagittal sections of the hind paw. Error bars represent SEM (n = 16 paws (left and right together) per Control, CAIA + PAR 1 mg/kg and CAIA +PAR 4 mg/kg, n = 12 paws (left and right together) per CAIA; **** $p < 0.0001$ vs control).

In the hind paw, a significantly greater number of multinucleated TRAP positive cells was observed on the bone surface and in the surrounding soft tissue of all CAIA and CAIA treated mice compared to control mice ($p < 0.0001$; Figure 4.13A and 4.13B). Similar to the radiocarpal joint, CAIA mice treated with 4 mg/kg PAR had a lower number of multinucleated TRAP positive cells (5 ± 1.09 cells) on the bone surface of the hind paw compared to CAIA mice treated with 1 mg/kg PAR (6.13 ± 2.36 cells), however this was not statistically significant (Figure 4.13A). Within the surrounding soft tissue of the hind paw, CAIA mice treated with both 1 mg/kg and 4 mg/kg PAR had significantly lower numbers of multinucleated TRAP positive cells (14.31 ± 5.69 cells and 9.31 ± 2.05 cells, respectively) compared to CAIA mice (27.55 ± 5.90 cells, $p = 0.025$ and $p = 0.006$, respectively; Figure 4.13B). However, there was no significant difference between the two treatment groups.
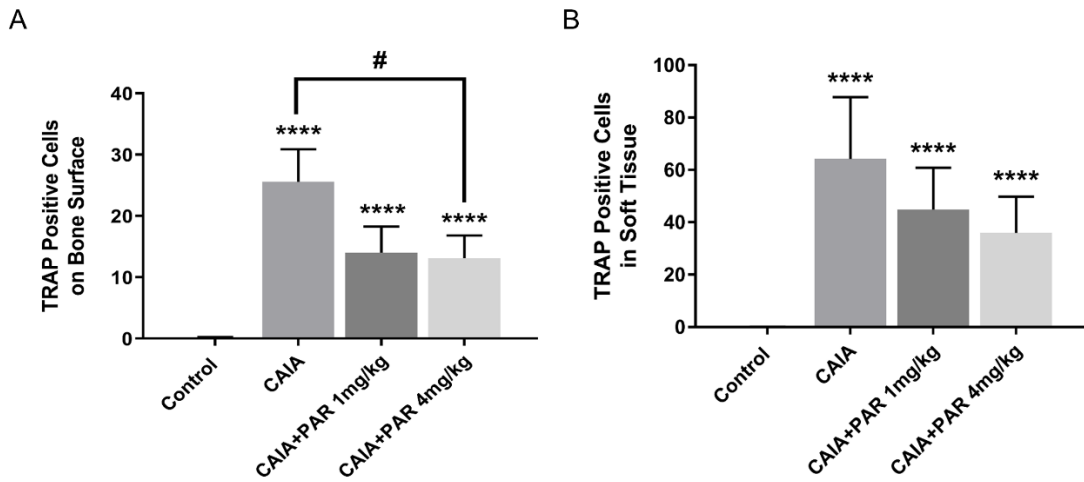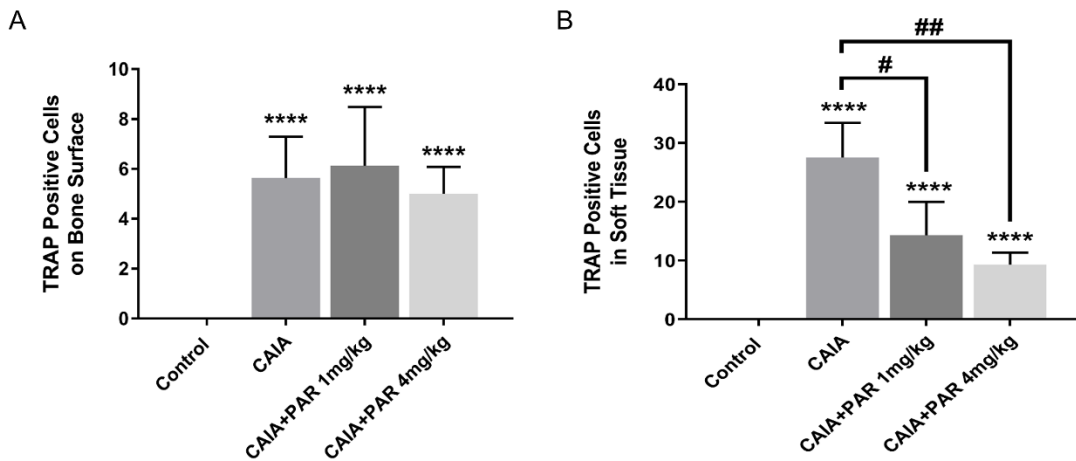
Figure 4.13. Assessment of osteoclasts and pre-osteoclasts within the hind paw. Average values of TRAP positive multinucleated cells on the bone surface (A) and within the surrounding soft tissue (B) in a 2.16 mm^2 area of the hind paw. Error bars represent SEM (n = 16 paws (left and right together) per Control, CAIA + PAR 1 mg/kg and CAIA + PAR 4 mg/kg; n = 12 paws (left and right together) per CAIA; **** p < 0.0001 vs control, # p = 0.025 CAIA + PAR 1 mg/kg vs CAIA, ## p = 0.006 CAIA + PAR 4 mg/kg vs CAIA).

4.6. Discussion

Despite improvements in disease control and remission (6), there are limited effective treatments available that collectively target the key pathogenic features of inflammation, bone destruction and pain in RA. Thus, joint destruction and RA associated pain are still major problems for RA patients. Parthenolide (PAR), an NF-κB inhibitor has been shown to reduce inflammation, bone loss and pain-like behaviour in animal models of different pathological conditions (36-40). However, there are currently no studies which have investigated the effect of PAR on these three key pathogenic features of RA simultaneously. Thus, this study extended previous findings by assessing the effect of PAR treatment at 1 mg/kg and 4 mg/kg on inflammation, bone loss and pain concomitantly in an inflammatory arthritis mouse model.

This study utilised the commercially available and well-established CAIA mouse model which rapidly initiates pathogenic features similar to those found in RA. A mild form of the disease was induced with 150 µl (1.5 mg/mouse) of a cocktail of collagen monoclonal antibodies combined with 10 µg of LPS, based on previous studies within our laboratory (44, 56). Paw inflammation was present in the mild CAIA model, as evidenced by significantly greater paw scores compared to non-diseased controls from day 5 to 10. These paw scores were greatest at day 8, consistent with the previously reported timeline of disease (57). Paws remained inflamed at the conclusion of the model as shown by significantly greater PV when assessed by *ex-vivo* micro-CT. As expected, the mild CAIA model resulted in severe joint destruction and significantly lower BV in the radiocarpal joint and hind paws when compared to non-diseased controls. Previous analysis of the mild CAIA model was extended in this study by analysis of pain-like behaviour in response to disease, as well as analysis of both front and hind paws to enable complete characterisation of disease induction within the CAIA model.

The results of this study suggest that the suppression of NF-κB through PAR treatment, may have potential benefits in reducing inflammation as assessed by clinical paw scoring and high-resolution micro-CT analysis. The current study found that PAR administered at 1 mg/kg and 4 mg/kg significantly reduced local inflammation in CAIA mice, as evidenced by paw scores at day 10. PAR at 4 mg/kg appeared to have a greater effect on

local inflammation as paw scores remained lower compared to CAIA untreated mice from day 6 and were reduced even further from day 8, compared to CAIA mice treated with 1 mg/kg PAR. However, at day 10, following daily treatment, it was evident that levels of local inflammation were the same in both PAR treated groups, despite the dose administered.

Analysis of local inflammation through clinical paw scoring was extended through novel techniques of high-resolution micro-CT previously established within our laboratory (42, 44), to quantitate this inflammation in the front and hind paws. Following micro-CT analysis at endpoint, PV was greater in the front and hind paws of all CAIA groups in comparison to non-diseased controls. Front paw PV was also similar in CAIA mice treated with either 1 mg/kg or 4 mg/kg PAR. Although inflammation was lower at endpoint in the radiocarpal joints of these groups, PV had not been reduced to control levels. Interestingly, PV in the hind paws was also not reduced by PAR treatment and was slightly higher in CAIA mice treated with 1 mg/kg PAR. This contrasts with a previous study which showed reduced local inflammation in the hind paws of rats following treatment with 1 mg/kg PAR at the onset of CIA symptoms. This, however, could be attributed to the large variability in local paw inflammation in response to systemic administration of mild CAIA, as well as the systemic administration of PAR, resulting in difficulty detecting treatment effects within the mild CAIA model.

Histological analysis of the radiocarpal joints and hind paws at endpoint, supports a reduction in local inflammation in CAIA mice treated with either 1 mg/kg or 4 mg/kg PAR. Although not significant, scores for inflammatory cell infiltration and pannus formation were lower in the front paws of PAR treated mice in comparison to CAIA untreated mice. There was also no difference in histological scores for cellular infiltration and pannus formation between both PAR treated groups, consistent with the clinical paw scores observed at day 10. This reduction in histological scores was also not observed in the hind paws. This was again unexpected, as previous studies have shown 1 mg/kg PAR to inhibit the pro-inflammatory effects of TNF-α and IL-1β, resulting in a reduction in inflammation and pannus formation in the synovial joints of CIA rat hind paws (38). PAR has also previously been shown to inhibit fibroblast-like synoviocyte (FLS) proliferation *in vitro* (58). However, along with the presence of pro-inflammatory cytokines, FLS

proliferation in the synovial joints of CAIA mice was not assessed in the current study. Thus, it can not be confirmed if a reduction in pannus formation scores in CAIA PAR treated (1 mg/kg or 4 mg/kg) mice is due to inhibition of FLS production or inflammatory cell infiltration. Future studies could therefore assess the presence and proliferation of FLS and inflammatory cells in synovial joints of CAIA mice following PAR treatment, to identify if PAR is actively suppressing these cells.

The influence of enhanced NF-κB signalling on pain in the complex disease progression of inflammatory arthritis is currently not known. However, previous studies in peripheral nerve injury models, suggest that activation of NF-κB can play a role in the development of neuropathic pain and pain-like behaviours such as mechanical allodynia and hyperalgesia (20-22). In the current study, inhibition of NF-κB through PAR treatment did not reduce mechanical allodynia in CAIA mice, as evidenced by inconsistent paw withdrawal thresholds throughout the model. Paw withdrawal thresholds in CAIA untreated mice remained consistent from day 2 to 8 and did not significantly differ from non-diseased control thresholds despite the presence of mild paw inflammation. This is not consistent with a previous study by Bas *et al.* 2012 using a moderate CAIA model, which displayed robust mechanical allodynia concomitant with the onset of joint inflammation in Balb/c mice (7). This suggests that the milder inflammatory response and limited joint destruction induced within the mild CAIA model did not result in mechanical allodynia which can be detected through the von Frey paw withdrawal test. In the previous study paw withdrawal thresholds did not return to baseline four weeks following the reduction of symptoms (7) and is consistent with current clinical findings of pain-like behaviour in RA patients (5, 59, 60). Increased pain withdrawal thresholds following the reduction of local inflammation, however, was not evident in the current study, as remission stages of the CAIA model were not investigated or extended past 10 days. Future studies in *in vivo* animal models of inflammatory arthritis, should therefore assess the presence of mechanical allodynia prior to the onset of symptoms and during remission stages of the induced model, as it is more clinically relevant and may identify different mechanisms that initiate early pain-like behaviour in RA.

The inconsistencies in paw withdrawal thresholds between groups within this study, particularly between CAIA untreated and non-diseased controls could be attributed to the

von Frey paw withdrawal method implemented to assess mechanical allodynia. The von Frey test is a classical method that has been used widely to examine neuropathic pain in animals (43, 61, 62). However, several disadvantages in the application of the test have recently been identified, highlighting the subjectivity of the test and the varied paw withdrawal behaviours observed in different strains of animals and in different animal models of inflammation (63-66). The manual von Frey technique used, applies the filaments to the inflamed tissue of the animal a high number of times and as a result causes greater discomfort and altered withdrawal behaviour in the mice (67). Studies have also found that Balb/c mice become accustomed to the von Frey testing procedure (7). Despite von Frey testing being carried out on alternate days in the current study, this may contribute to the unexpected paw withdrawal thresholds identified. Future studies should therefore incorporate a range of behavioural tests when assessing pain-like behaviour in animal models of inflammatory arthritis, including electronic von Frey apparatus and automated gait analysis, which have recently been made available and overlap with manual von Frey paw withdrawal analysis.

PAR treatment at both 1 mg/kg and 4 mg/kg did not have an effect on BV in the front and hind paws of CAIA mice at endpoint. Unexpectedly, BV in PAR treated CAIA mice, appeared to decrease when compared to CAIA untreated mice and significantly so for CAIA mice treated with 4 mg/kg PAR. Microscopic analysis of osteoclast-like cells however identified a reduction in TRAP positive multinucleated cells on the bone surface within the radiocarpal joint and hind paws, following PAR treatment, with a greater reduction observed in CAIA mice treated with 4 mg/kg PAR. The presence of osteoclast-like cells was also reflected in 3D models of the hind paws which showed the presence of bone resorption pits on the surface of the navicular and cuboid. It would be expected that these bone resorption pits would decrease in size and number following PAR treatment, however these were not numerically quantified and thus can not be confirmed. This difference in macroscopic and microscopic analysis of bone loss in inflammatory arthritis is consistent with a previous study which showed PAR treatment to have a significant effect on reducing bone surface resorption induced by polyethylene particles in a murine calvarial model of peri-implant osteolysis, with no effect on overall BV (68). Within the current study, it is possible that the surface bone resorption evident through microscopic TRAP analysis and through qualitative observations of bone resorption pits,

are not having a major effect on volumetric reduction in the radiocarpal joints and hind paws. Thus, quantification of bone resorption pits and BV of the smaller individual carpal and tarsal bones in the front and hind paws, respectively, would provide a more accurate analysis of the effects of PAR treatment on bone loss in CAIA mice.

Previous studies have identified that in animal models of inflammatory arthritis, including the common CIA rat model, PAR treatment results in a reduction in inflammation with little effect on overall bone loss (38). This was also evident in the current study which found PAR at 1 mg/kg and 4 mg/kg to reduce local paw inflammation, however with no change in overall BV. This could be attributed to the low dose of PAR used in both treatment groups, as in the complex CAIA model, low dose PAR may be unable to inhibit both local inflammation and the subsequent effect inflammation has on stimulating bone destruction through NF-κB signalling. In the current study, activation of the NF-κB signalling pathway was not directly measured in paw tissues. It was therefore not confirmed if systemic administration of 1 mg/kg or 4 mg/kg PAR reached these areas to actively suppress NF-κB and reduce both inflammation and inflammatory induced bone destruction concurrently. Thus, future studies could assess the phosphorylation of proteins involved in NF-κB signalling and the upregulation of cytokines involved in inflammatory induced osteoclastogenesis, as NF-κB plays a central role in regulating the inflammatory process by controlling expression of these cytokines (34), to identify if PAR actively suppresses NF-κB in inflammatory arthritis.

4.7. Conclusion

In conclusion, the results showed that PAR treatment at both 1 mg/kg and 4 mg/kg reduced local paw inflammation, however with little effect on mechanical allodynia in the CAIA murine model. Furthermore, there is potential that in the presence of inflammation, the low dose of PAR administered, may not be able to prevent inflammatory induced bone loss through inhibition of NF-κB signalling. Future studies will need to confirm the expression of NF-κB in osteoclasts and inflammatory cells, to elucidate the specificity of PAR in the complex *in vivo* environment of inflammatory arthritis. Further investigations involving new strategies to investigate pain-like behaviour in the CAIA mouse model are also warranted, to clarify further the involvement

of NF-κB signalling in RA associated pain and the beneficial effect PAR may have on this key pathogenic feature of RA.

4.8. References

1. Lee YC, Cui J, Lu B, Frits ML, Iannaccone CK, Shadick NA, et al. Pain persists in DAS28 rheumatoid arthritis remission but not in ACR/EULAR remission: a longitudinal observational study. Arthritis research & therapy. 2011;13(3):R83.

2. Heiberg T, Kvien TK. Preferences for improved health examined in 1,024 patients with rheumatoid arthritis: pain has highest priority. Arthritis and rheumatism. 2002;47(4):391-7.

3. McWilliams DF, Walsh DA. Pain mechanisms in rheumatoid arthritis. Clinical and experimental rheumatology. 2017;35 Suppl 107(5):94-101.

4. van Laarhoven AI, Kraaimaat FW, Wilder-Smith OH, van Riel PL, van de Kerkhof PC, Evers AW. Sensitivity to itch and pain in patients with psoriasis and rheumatoid arthritis. Experimental dermatology. 2013;22(8):530-4.

5. Taylor P, Manger B, Alvaro-Gracia J, Johnstone R, Gomez-Reino J, Eberhardt E, et al. Patient perceptions concerning pain management in the treatment of rheumatoid arthritis. The Journal of international medical research. 2010;38(4):1213-24.

6. Wolfe F, Michaud K. Assessment of pain in rheumatoid arthritis: minimal clinically significant difference, predictors, and the effect of anti-tumor necrosis factor therapy. The Journal of rheumatology. 2007;34(8):1674-83.

7. Bas DB, Su J, Sandor K, Agalave NM, Lundberg J, Codeluppi S, et al. Collagen antibody-induced arthritis evokes persistent pain with spinal glial involvement and transient prostaglandin dependency. Arthritis and rheumatism. 2012;64(12):3886-96.

8. Schett G. Erosive arthritis. Arthritis research & therapy. 2007;9 Suppl 1:S2.

9. Gravallese EM, Harada Y, Wang JT, Gorn AH, Thornhill TS, Goldring SR. Identification of cell types responsible for bone resorption in rheumatoid arthritis and juvenile rheumatoid arthritis. The American journal of pathology. 1998;152(4):943-51.

10. Gough A, Sambrook P, Devlin J, Huissoon A, Njeh C, Robbins S, et al. Osteoclastic activation is the principal mechanism leading to secondary osteoporosis in rheumatoid arthritis. The Journal of rheumatology. 1998;25(7):1282-9.

11. Brennan FM, McInnes IB. Evidence that cytokines play a role in rheumatoid arthritis. The Journal of clinical investigation. 2008;118(11):3537-45.

12. Scuri M, Samsell L, Piedimonte G. The role of neurotrophins in inflammation and allergy. Inflammation & allergy drug targets. 2010;9(3):173-80.

13. Antonelli A, Ferrari SM, Giuggioli D, Ferrannini E, Ferri C, Fallahi P. Chemokine (C-X-C motif) ligand (CXCL)10 in autoimmune diseases. Autoimmunity reviews. 2014;13(3):272-80.

14. Edwards RR, Wasan AD, Bingham CO, 3rd, Bathon J, Haythornthwaite JA, Smith MT, et al. Enhanced reactivity to pain in patients with rheumatoid arthritis. Arthritis research & therapy. 2009;11(3):R61.

15. Pollard LC, Ibrahim F, Choy EH, Scott DL. Pain thresholds in rheumatoid arthritis: the effect of tender point counts and disease duration. The Journal of rheumatology. 2012;39(1):28-31.

16. Pettit AR, Ji H, von Stechow D, Muller R, Goldring SR, Choi Y, et al. TRANCE/RANKL knockout mice are protected from bone erosion in a serum transfer model of arthritis. The American journal of pathology. 2001;159(5):1689-99.

17. Clohisy JC, Roy BC, Biondo C, Frazier E, Willis D, Teitelbaum SL, et al. Direct inhibition of NF-kappa B blocks bone erosion associated with inflammatory arthritis. Journal of immunology (Baltimore, Md : 1950). 2003;171(10):5547-53.

18. Park-Min KH. Mechanisms involved in normal and pathological osteoclastogenesis. Cellular and molecular life sciences : CMLS. 2018;75(14):2519-28.

19. Xu J, Wu HF, Ang ES, Yip K, Woloszyn M, Zheng MH, et al. NF-kappaB modulators in osteolytic bone diseases. Cytokine & growth factor reviews. 2009;20(1):7-17.

20. Mika J, Zychowska M, Popiolek-Barczyk K, Rojewska E, Przewlocka B. Importance of glial activation in neuropathic pain. European journal of pharmacology. 2013;716(1-3):106-19.

21. Dominguez E, Rivat C, Pommier B, Mauborgne A, Pohl M. JAK/STAT3 pathway is activated in spinal cord microglia after peripheral nerve injury and contributes to neuropathic pain development in rat. Journal of neurochemistry. 2008;107(1):50-60.

22.   Song XS, Cao JL, Xu YB, He JH, Zhang LC, Zeng YM. Activation of ERK/CREB pathway in spinal cord contributes to chronic constrictive injury-induced neuropathic pain in rats. Acta pharmacologica Sinica. 2005;26(7):789-98.

23.   Kong YY, Feige U, Sarosi I, Bolon B, Tafuri A, Morony S, et al. Activated T cells regulate bone loss and joint destruction in adjuvant arthritis through osteoprotegerin ligand. Nature. 1999;402(6759):304-9.

24.   Romas E, Sims NA, Hards DK, Lindsay M, Quinn JW, Ryan PF, et al. Osteoprotegerin reduces osteoclast numbers and prevents bone erosion in collagen-induced arthritis. The American journal of pathology. 2002;161(4):1419-27.

25.   Lubberts E, Oppers-Walgreen B, Pettit AR, Van Den Bersselaar L, Joosten LA, Goldring SR, et al. Increase in expression of receptor activator of nuclear factor kappaB at sites of bone erosion correlates with progression of inflammation in evolving collagen-induced arthritis. Arthritis and rheumatism. 2002;46(11):3055-64.

26.   Redlich K, Hayer S, Ricci R, David JP, Tohidast-Akrad M, Kollias G, et al. Osteoclasts are essential for TNF-alpha-mediated joint destruction. The Journal of clinical investigation. 2002;110(10):1419-27.

27.   Redlich K, Hayer S, Maier A, Dunstan CR, Tohidast-Akrad M, Lang S, et al. Tumor necrosis factor alpha-mediated joint destruction is inhibited by targeting osteoclasts with osteoprotegerin. Arthritis and rheumatism. 2002;46(3):785-92.

28.   Cohen SB, Dore RK, Lane NE, Ory PA, Peterfy CG, Sharp JT, et al. Denosumab treatment effects on structural damage, bone mineral density, and bone turnover in rheumatoid arthritis: a twelve-month, multicenter, randomized, double-blind, placebo-controlled, phase II clinical trial. Arthritis and rheumatism. 2008;58(5):1299-309.

29.   Roche PA, Klestov AC, Heim HM. Description of stable pain in rheumatoid arthritis: a 6 year study. The Journal of rheumatology. 2003;30(8):1733-8.

30.   Radner H, Ramiro S, Buchbinder R, Landewe RB, van der Heijde D, Aletaha D. Pain management for inflammatory arthritis (rheumatoid arthritis, psoriatic arthritis, ankylosing spondylitis and other spondylarthritis) and gastrointestinal or liver comorbidity. The Cochrane database of systematic reviews. 2012;1:Cd008951.

31.   Richards BL, Whittle SL, Buchbinder R. Antidepressants for pain management in rheumatoid arthritis. The Cochrane database of systematic reviews. 2011(11):Cd008920.

32.   Bork PM, Schmitz ML, Kuhnt M, Escher C, Heinrich M. Sesquiterpene lactone containing Mexican Indian medicinal plants and pure sesquiterpene lactones as potent inhibitors of transcription factor NF-kappaB. FEBS letters. 1997;402(1):85-90.

33.   Hall IH, Lee KH, Starnes CO, Sumida Y, Wu RY, Waddell TG, et al. Anti-inflammatory activity of sesquiterpene lactones and related compounds. Journal of pharmaceutical sciences. 1979;68(5):537-42.

34.   Mathema VB, Koh YS, Thakuri BC, Sillanpaa M. Parthenolide, a sesquiterpene lactone, expresses multiple anti-cancer and anti-inflammatory activities. Inflammation. 2012;35(2):560-5.

35.   Kreuger MR, Grootjans S, Biavatti MW, Vandenabeele P, D'Herde K. Sesquiterpene lactones as drugs with multiple targets in cancer treatment: focus on parthenolide. Anti-cancer drugs. 2012;23(9):883-96.

36.   Yip KH, Zheng MH, Feng HT, Steer JH, Joyce DA, Xu J. Sesquiterpene lactone parthenolide blocks lipopolysaccharide-induced osteolysis through the suppression of NF-kappaB activity. Journal of bone and mineral research : the official journal of the American Society for Bone and Mineral Research. 2004;19(11):1905-16.

37.   Idris AI, Krishnan M, Simic P, Landao-Bassonga E, Mollat P, Vukicevic S, et al. Small molecule inhibitors of IkappaB kinase signaling inhibit osteoclast formation in vitro and prevent ovariectomy-induced bone loss in vivo. FASEB journal : official publication of the Federation of American Societies for Experimental Biology. 2010;24(11):4545-55.

38.   Liu Q, Zhao J, Tan R, Zhou H, Lin Z, Zheng M, et al. Parthenolide inhibits pro-inflammatory cytokine production and exhibits protective effects on progression of collagen-induced arthritis in a rat model. Scandinavian journal of rheumatology. 2015;44(3):182-91.

39.   Popiolek-Barczyk K, Kolosowska N, Piotrowska A, Makuch W, Rojewska E, Jurga AM, et al. Parthenolide Relieves Pain and Promotes M2 Microglia/Macrophage Polarization in Rat Model of Neuropathy. Neural plasticity. 2015;2015:676473.

40.   Popiolek-Barczyk K, Makuch W, Rojewska E, Pilat D, Mika J. Inhibition of intracellular signaling pathways NF-kappaB and MEK1/2 attenuates neuropathic pain development and enhances morphine analgesia. Pharmacological reports : PR. 2014;66(5):845-51.

41.   Nandakumar KS, Svensson L, Holmdahl R. Collagen type II-specific monoclonal antibody-induced arthritis in mice: description of the disease and the influence of age, sex, and genes. The American journal of pathology. 2003;163(5):1827-37.

42.   Williams B, Tsangari E, Stansborough R, Marino V, Cantley M, Dharmapatni A, et al. Mixed effects of caffeic acid phenethyl ester (CAPE) on joint inflammation, bone loss and gastrointestinal inflammation in a murine model of collagen antibody-induced arthritis. Inflammopharmacology. 2017;25(1):55-68.

43.   Chaplan SR, Bach FW, Pogrel JW, Chung JM, Yaksh TL. Quantitative assessment of tactile allodynia in the rat paw. Journal of neuroscience methods. 1994;53(1):55-63.

44.   Perilli E, Cantley M, Marino V, Crotti TN, Smith MD, Haynes DR, et al. Quantifying not only bone loss, but also soft tissue swelling, in a murine inflammatory arthritis model using micro-computed tomography. Scandinavian journal of immunology. 2015;81(2):142-50.

45.   Perilli E, Baruffaldi F, Visentin M, Bordini B, Traina F, Cappello A, et al. MicroCT examination of human bone specimens: effects of polymethylmethacrylate embedding on structural parameters. Journal of microscopy. 2007;225(Pt 2):192-200.

46.   Luu YK, Lublinsky S, Ozcivici E, Capilla E, Pessin JE, Rubin CT, et al. In vivo quantification of subcutaneous and visceral adiposity by micro-computed tomography in a small animal model. Medical engineering & physics. 2009;31(1):34-41.

47.   Lane NE, Thompson JM, Haupt D, Kimmel DB, Modin G, Kinney JH. Acute changes in trabecular bone connectivity and osteoclast activity in the ovariectomized rat in vivo. Journal of bone and mineral research : the official journal of the American Society for Bone and Mineral Research. 1998;13(2):229-36.

48.   Perilli E, Le V, Ma B, Salmon P, Reynolds K, Fazzalari NL. Detecting early bone changes using in vivo micro-CT in ovariectomized, zoledronic acid-treated, and sham-operated rats. Osteoporosis international : a journal established as result of

cooperation between the European Foundation for Osteoporosis and the National Osteoporosis Foundation of the USA. 2010;21(8):1371-82.

49.   Lorensen WE, Cline HE. Marching cubes: a high resolution 3D surface construction algorithm. Comput Graph. 1987;21:163-9.

50.   Perilli E, Briggs AM, Kantor S, Codrington J, Wark JD, Parkinson IH, et al. Failure strength of human vertebrae: prediction using bone mineral density measured by DXA and bone volume by micro-CT. Bone. 2012;50(6):1416-25.

51.   Cantley MD, Fairlie DP, Bartold PM, Marino V, Gupta PK, Haynes DR. Inhibiting histone deacetylase 1 suppresses both inflammation and bone loss in arthritis. Rheumatology (Oxford, England). 2015;54(9):1713-23.

52.   Tak PP, Smeets TJ, Daha MR, Kluin PM, Meijers KA, Brand R, et al. Analysis of the synovial cell infiltrate in early rheumatoid synovial tissue in relation to local disease activity. Arthritis and rheumatism. 1997;40(2):217-25.

53.   Burstone MS. Histochemical demonstration of acid phosphatases with naphthol AS-phosphates. J Natl Cancer Inst. 1958;21(3):523-39.

54.   Angel NZ, Walsh N, Forwood MR, Ostrowski MC, Cassady AI, Hume DA. Transgenic mice overexpressing tartrate-resistant acid phosphatase exhibit an increased rate of bone turnover. Journal of bone and mineral research : the official journal of the American Society for Bone and Mineral Research. 2000;15(1):103-10.

55.   Crotti TN, Dharmapatni AA, Alias E, Zannettino AC, Smith MD, Haynes DR. The immunoreceptor tyrosine-based activation motif (ITAM) -related factors are increased in synovial tissue and vasculature of rheumatoid arthritic joints. Arthritis research & therapy. 2012;14(6):R245.

56.   Dharmapatni AA, Cantley MD, Marino V, Perilli E, Crotti TN, Smith MD, et al. The X-Linked Inhibitor of Apoptosis Protein Inhibitor Embelin Suppresses Inflammation and Bone Erosion in Collagen Antibody Induced Arthritis Mice. Mediators Inflamm. 2015;2015:564042.

57.   Khachigian LM. Collagen antibody-induced arthritis. Nature protocols. 2006;1(5):2512-6.

58.   Parada-Turska J, Mitura A, Brzana W, Jablonski M, Majdan M, Rzeski W. Parthenolide inhibits proliferation of fibroblast-like synoviocytes in vitro. Inflammation. 2008;31(4):281-5.

59.   Koop SM, ten Klooster PM, Vonkeman HE, Steunebrink LM, van de Laar MA. Neuropathic-like pain features and cross-sectional associations in rheumatoid arthritis. Arthritis research & therapy. 2015;17:237.

60.   Boyden SD, Hossain IN, Wohlfahrt A, Lee YC. Non-inflammatory Causes of Pain in Patients with Rheumatoid Arthritis. Current rheumatology reports. 2016;18(6):30.

61.   Dixon WJ. Efficient analysis of experimental observations. Annual review of pharmacology and toxicology. 1980;20:441-62.

62.   Bonin RP, Bories C, De Koninck Y. A simplified up-down method (SUDO) for measuring mechanical nociception in rodents using von Frey filaments. Molecular pain. 2014;10:26.

63.   Massy-Westropp N. The effects of normal human variability and hand activity on sensory testing with the full Semmes-Weinstein monofilaments kit. Journal of hand therapy : official journal of the American Society of Hand Therapists. 2002;15(1):48-52.

64.   Callahan BL, Gil AS, Levesque A, Mogil JS. Modulation of mechanical and thermal nociceptive sensitivity in the laboratory mouse by behavioral state. The journal of pain : official journal of the American Pain Society. 2008;9(2):174-84.

65.   Bradman MJ, Ferrini F, Salio C, Merighi A. Practical mechanical threshold estimation in rodents using von Frey hairs/Semmes-Weinstein monofilaments: Towards a rational method. Journal of neuroscience methods. 2015;255:92-103.

66.   Bove G. Mechanical sensory threshold testing using nylon monofilaments: the pain field's "tin standard". Pain. 2006;124(1-2):13-7.

67.   Martinov T, Mack M, Sykes A, Chatterjea D. Measuring changes in tactile sensitivity in the hind paw of mice using an electronic von Frey apparatus. Journal of visualized experiments : JoVE. 2013(82):e51212.

68.   Zawawi MS, Marino V, Perilli E, Cantley MD, Xu J, Purdue PE, et al. Parthenolide reduces empty lacunae and osteoclastic bone surface resorption induced by polyethylene particles in a murine calvarial model of peri-implant osteolysis. Journal of biomedical materials research Part A. 2015;103(11):3572-9.

CHAPTER 5: EFFECT OF MILD AND MODERATE MONOCLONAL ANTIBODY DOSE ON INFLAMMATION, BONE LOSS AND PAIN WITHDRAWAL IN THE COLLAGEN ANTIBODY-INDUCED ARTHRITIS MOUSE MODEL

B. Williams, E. Tsangari, A. Dharmapatni, E. Perilli, T.N. Crotti

Chapter Summary:

In Chapters 2, 3 and 4 consistent pathogenic features of RA were not induced in the paws of Balb/c mice using the mild subacute CAIA model. As such, large variability in the development of inflammation and severity of the subsequent bone loss was identified in the synovial joints following disease induction. This is consistent with previous findings in our laboratory which were unable to identify changes in bone volume following induction of mild CAIA in Balb/c mice and thus were unable to determine any treatment effects. Thus, this study aimed to optimise the CAIA model to identify if a more moderate model of CAIA would produce clear and consistent pathogenic features detected through clinical paw scoring, histological analysis and high resolution micro-CT, as well as enable the detection of treatment effects without severe joint destruction requiring euthanasia prior to the conclusion of the model.

5.1. Abstract

Animal models are extensively used to elucidate the pathogenesis of rheumatoid arthritis (RA), however limited work evaluates the effect of joint destruction on pain in RA. The collagen antibody-induced arthritis (CAIA) murine model reflects pathogenic features identified in the effector phase of RA. Initial studies induce disease in CAIA models using 2.5-4.0 mg of a cocktail of monoclonal antibodies against type II collagen in combination with *E.coli* lipopolysaccharide (25-50 µg), resulting in severe joint damage, making analysis problematic. We previously induced a mild form of CAIA (1.5 mg monoclonal antibodies with 10 µg LPS), however, with variability in disease prevalence and severity. There are currently no studies comparing different disease severities on resulting joint destruction and pain in the CAIA model. Thus, this study proposes that a greater dose (3 mg) of monoclonal antibodies followed by low dose (10 µg) LPS will lead to greater disease severity and pain in the CAIA model.

Female Balb/c mice were allocated to 3 groups; control (n = 5), mild CAIA (1.5 mg monoclonal antibodies + 10 µg LPS; n = 5) and moderate CAIA (3 mg monoclonal antibodies + 10 µg LPS; n = 8). Assessment of local paw inflammation was conducted daily, whilst mechanical allodynia was assessed in the hind paws on alternate days. At endpoint, bone volume (BV) and paw volume (PV; paw swelling) was assessed in the front and hind paws by micro-CT. Serial histological sections of the front paws were stained with haematoxylin and eosin (H&E) and tartrate-resistant acid phosphatase (TRAP), and assessed for joint inflammation, cartilage and bone damage and osteoclast-like cells.

From day 4-10, moderate CAIA mice had significantly greater paw scores compared to mild CAIA mice (p < 0.01), however mechanical allodynia was not observed in either group. At end point, moderate CAIA mice had significantly greater PV and histological scores for cellular infiltration and pannus formation compared to mild CAIA mice (p < 0.01 and p = 0.02, respectively). However, there was no significant difference in BV or the presence of TRAP positive cells between mild and moderate CAIA mice.

The findings of this study ascertain that a moderate dose of the cocktail of monoclonal antibodies combined with low dose LPS induces greater inflammation and oedema in all paws, with little effect on overall joint destruction, presence of osteoclast-like cells and pain-like behaviour in the CAIA murine model.

195

5.2. Statement of Authorship

Statement of Authorship

Title of Paper	Effect of mild and moderate monoclonal antibody dose on inflammation, bone loss and pain withdrawal in the collagen antibody-induced arthritis mouse model.	
Publication Status	☐ Published ☐ Submitted for Publication	☐ Accepted for Publication ☑ Unpublished and Unsubmitted work written in manuscript style
Publication Details		

Principal Author

Name of Principal Author (Candidate)	Bonnie Williams	
Contribution to the Paper	First author and main contributor. Concept and methodological design, investigation, project administration, data curation and analysis, formulation of primary draft, in addition to reviewing and incorporating co-author comments and suggestions.	
Overall percentage (%)		
Certification	This paper reports on original research I conducted during the period of my Higher Degree by Research candidature and is not subject to any obligations or contractual agreements with a third party that would constrain its inclusion in this thesis. I am the primary author of this paper.	
Signature		Date 22 / 2 / 19

Co-Author Contributions

By signing the Statement of Authorship, each author certifies that:

i.   the candidate's stated contribution to the publication is accurate (as detailed above);

ii.   permission is granted for the candidate in include the publication in the thesis; and

iii.   the sum of all co-author contributions is equal to 100% less the candidate's stated contribution.

Name of Co-Author	Eleni Tsangari	
Contribution to the Paper	Methodology and technical support.	
Signature		Date 18/2/19

Name of Co-Author	Anak Dharmapatni	
Contribution to the Paper	Supervision and manuscript review.	
Signature		Date 22/2/19

Name of Co-Author	Egon Perilli
Contribution to the Paper	Methodology support, supervision and manuscript review.
Signature			Date	01/03/'19

Name of Co-Author	Tania Crotti
Contribution to the Paper	Investigation, funding acquisition, methodology, conceptualisation, supervision and review of manuscript.
Signature			Date	22/2/19

5.3. Introduction

A prerequisite for identifying effective targets for novel therapeutics for rheumatoid arthritis (RA) is to elucidate the disease mechanisms involved. This can only be achieved using animal models, as they provide the opportunity for a detailed analysis of the disease pathways and pathogenesis of RA, as well as the validation of therapeutic targets. Recently, there has been a move away from using traditional murine models of end-stage, chronic disease as there is a growing need to consider the earlier phases of RA pathogenesis as a target for treatment (1). This is beneficial for the study of RA and the development of new therapeutic targets as current therapeutics may take several months to effectively control inflammation in order to restore joint function and pain, thus allowing bone erosion to progress.

RA patients often identify pain as a major symptom and pain often persists despite optimal control of inflammation and disease progression (2-4). RA associated pain is complex and arises from multiple mechanisms involving inflammation, peripheral and central pain processing and structural changes within the joint, and is often associated with neuropathic pain (4-7). Pain is an important indicator of active inflammation in RA, however it is known that non-inflammatory mechanisms contribute to pain and RA associated pain can persist throughout remission (6, 8). Thus, animal models have the potential to provide further insights into the pathology that initiates and maintains pain in RA.

Pain in RA has been widely investigated in rat and mouse models of chronic immune mediated articular inflammation (9-11). However, there are several frequently used models of RA that are not adapted for studies of pain. Recently studies of arthritis-related pain have been performed in the K/BxN serum transfer model (10). In this model peripheral pain was evident at later stages of the disease and resulted in persistent mechanical allodynia, where innocuous stimuli cause pain (10). Similarly, antigen-induced arthritis (AIA) resulted in mechanical hyperalgesia, enhanced pain responses to a noxious stimulus, in ipsilateral and contralateral knees and hind paws of rats (12). Pain-like behaviour in these animal models results from complex interactions between joint destruction, disease longevity and altered pain processing. However, existing evidence is

insufficient to determine whether pain mechanisms differ between acute and chronic models of inflammatory arthritis.

The most widely used animal model for RA is the collagen induced arthritis (CIA) model, which was first developed in rats and later adapted to mice (13-15). This model is reproducible, well defined and has proven useful for the development of new therapies in RA. Pathological features of RA are induced in the CIA model following immunisation with autologous or heterologous type II collagen in complete Freund's adjuvant, with the onset of clinical signs occurring at day 20-30 following immunisation (16, 17). Susceptibility of rodents to the disease is strongly associated with major histocompatibility complex class II genes and results in the development of an acute to subacute, monophasic erosive polyarthritis following immunisation (18). As a result, there is considerable individual variability observed among animals with respect to incidence, synchronicity and distribution of lesions (18, 19). Thus, recent studies have identified a systemically induced, passive immunisation model which is a direct derivative of the CIA model, known as the collagen antibody-induced arthritis (CAIA) model.

Clinical and histological characteristics of CAIA joints are similar to those seen in CIA and mimic the important pathogenic features of human RA, such as inflammatory synovitis, formation of pannus, cartilage degradation and bone remodelling (20). CAIA can be induced by serum transfer from arthritic mice or human RA patients, however it is more practical to use commercially available cocktails of monoclonal antibodies targeted to type II collagen (21, 22). Induction of inflammatory arthritis in the CAIA model is B and T cell independent and susceptibility to CAIA is major histocompatibility complex independent (21, 23). As a result, CAIA doesn't recapitulate the complexity of the immune system and tissue remodelling response which is evident during human RA and the CIA model (24). However, it suggests a regulatory role for these inflammatory cells at the effector level and confirms the pivotal role that pro-inflammatory cytokines have in RA. Similar to RA, inflammation and joint destruction in the CAIA model is predominantly mediated by pro-inflammatory cytokines, including tumour necrosis factor-alpha (TNF-α) and interleukin-1 beta (IL-1β). These cytokines have been reported to be produced in the synovial joints of mice during CAIA induction and are required for

the development of hypersensitivity in ongoing joint inflammation in mice (9, 25, 26). This creates an advantageous murine model of RA as peak disease occurs within 6 days, as opposed to the CIA model, where the first signs of arthritis appear 21-28 days following immunisation (16, 18, 20, 27).

Not all autoantibodies to collagen type II however are capable of inducing arthritis (28-30). This is because the activation of complement on the surface of cartilage requires that multiple antibodies sequestered within cartilage layers are available for this activation as the first step of the inflammatory cascade (28, 29, 31). Due to this Terato *et al.* 1995, identified that bacteria toxins such as E.coli lipopolysaccharide (LPS) have a strong synergistic effect with autoantibodies to collagen type II (21, 32). LPS can therefore be used to reduce the threshold level and number of monoclonal antibodies required for induction of arthritis. This is another major advantage of the CAIA model, as the combination of the monoclonal antibodies with LPS increases the incidence and severity of disease onset (21, 32).

Previous studies have used different doses of monoclonal antibodies (ranging from 1-4 mg/mouse) and LPS (ranging from 5-50 µg/mouse) in the CAIA model (9, 20, 21, 33, 34). Khachigian 2006, recommends a dose of 2-4 mg of monoclonal antibodies in combination with a dose of LPS between 25 µg and 50 µg, to achieve the desired pathological symptoms (20). A high LPS dose of 50 µg produces a florid arthritic reaction and has been used to identify severe cartilage and bone destruction in the paws of mice (20). However, the greater arthritic response causes severe destruction of joint architecture, causing difficulty in histological assessment, the need for earlier euthanasia and can also impede the assessment of co-morbidity factors such as diabetes, periodontal, cardiac diseases and pain (35-37). Thus, a lower dose of LPS (10 µg) in combination with 1.5 mg monoclonal antibodies has been used by our group previously (33, 34, 38). This use of a mild CAIA model still produces the desired arthritic response, which better reflects the current presentation of RA in the clinic, and can be assessed effectively along with co-morbidities.

More recently, CAIA models conducted by our group using this mild model (1.5 mg monoclonal antibodies, 10 µg LPS) and extending to 14 days of disease development, were unable to identify any treatment effects or changes in bone volume assessed by micro-computed tomography (micro-CT), which could be attributed to the arthritic response being too mild (34). It is evident that previous studies have used a variety of timelines and different doses of the monoclonal antibodies and LPS to induce inflammatory arthritis in the CAIA model. There are, however, currently no studies directly comparing different doses of monoclonal antibodies and LPS in regards to clinical paw swelling, histological arthritis and bone changes in mice. Moreover, whereas the CAIA arthritic response has been investigated in the front paws using micro-CT by other groups including ours (33, 34, 38, 39), no study has yet assessed the hind paws with this imaging modality. Assessing front and hind paws will enable a complete characterisation of both inflammation and bone destruction in the CAIA murine model. Further to this the effects of a mild or moderate arthritic response on pain withdrawal have not been investigated at the effector phase of a short-term CAIA murine model. Therefore, this study aimed to identify whether a higher dose (3 mg/mouse) of the cocktail of monoclonal antibodies in combination with the low dose (10 µg) of LPS will produce a more moderate model of inflammatory arthritis in comparison to the mild model (1.5 mg/mouse antibody with 10 µg LPS), over 10 days, which has previously been used by us (33, 34, 38, 39) and in previous studies within this thesis.

5.4. Methods

This study was approved by the Animal Ethics Committee of the University of Adelaide (M-2015-255B) and complied with the National Health and Medical Research Council (Australia) Code of Practice for Animal Care in Research and Training (2014). Mice were housed in approved conditions on a 12 hour light/dark cycle. Food and water were provided ad libitum.

5.4.1. Collagen antibody-induced arthritis

A total of 18 female Balb/c mice aged 6 to 8 weeks were obtained from the University of Adelaide Laboratory Animal Services and randomly divided into 3 groups: control (no

arthritis; n = 5), mild CAIA (CAIA 1.5 mg monoclonal antibodies and 10 µg LPS; n = 5) and moderate CAIA (CAIA 3 mg monoclonal antibodies and 10 µg LPS; n = 8).

To induce arthritis, mice were injected intravenously via the tail vein with a cocktail of anti-type II collagen monoclonal antibodies (Arthrogen-CIAs Arthritogenic Monoclonal Antibodies, Chondrex Inc., Redwood, WA, USA). On day 0, mice in the mild CAIA group received one intravenous injection of 150 µl (total 1.5 mg/mouse) of the cocktail of monoclonal antibodies (33, 34, 38, 39), while the moderate CAIA group received two intravenous injections of 150 µl of the cocktail of monoclonal antibodies (total 3 mg/mouse) approximately 30 minutes apart. This was followed by an intraperitoneal injection of 20 µl (10 µg/mouse) of LPS on day 3 in both groups (Figure 5.1). Control animals were injected with phosphate buffered saline (PBS) alone at both time points.
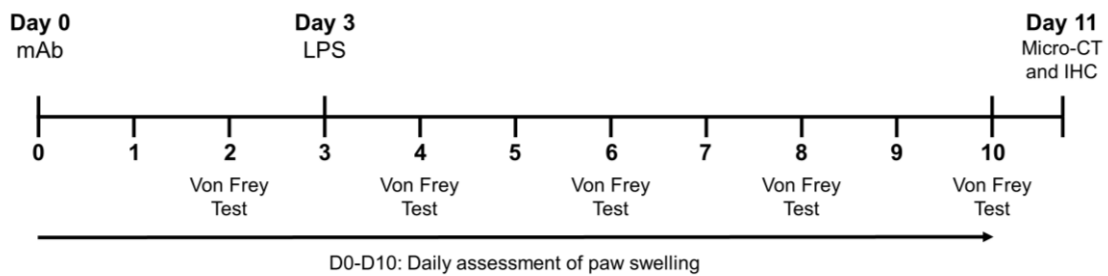
Figure 5.1. Experimental collagen antibody-induced arthritis (CAIA) mouse model timeline. Values represent days. D; Day, IHC; immunohistochemistry, LPS; lipopolysaccharide, mAb; monoclonal antibodies, micro-CT; micro-computed tomography.

5.4.2. *Clinical analysis of local paw swelling*

Mice were monitored daily using an approved clinical record sheet for arthritic studies to assess body weight and factors of general health. To assess clinical paw swelling, individual paws were examined daily for redness, tenderness, swelling and inflammation using a clinical paw scoring method previously described (Figure 5.1) (34). For each paw, a score of 1 was given for an inflamed digit and a score from 0-5 was allocated for swelling of the carpal/tarsal and swelling of the wrist/ankle. The maximum score for each paw was 15, giving a possible total of 60 per mouse (34).

5.4.3. *Von Frey paw withdrawal test for the assessment of mechanical allodynia*

Mechanical allodynia was assessed in mice using the von Frey paw withdrawal test. As it has been reported that Balb/c mice develop a tolerance to this behavioural test (9), von Frey testing was conducted on alternate days from day 0-10 (Figure 5.1). On testing days mice were placed in a plastic cage with a wire mesh bottom which allows full access to the paws and behavioural accommodation was allowed for approximately 15 minutes. The hind paws were touched with one of a series of seven von Frey filaments with logarithmically incremental stiffness of 0.04, 0.07, 0.16, 0.40, 0.60, 1.00 and 2.00 grams (40). The von Frey filaments were presented perpendicular to the hind-plantar surface of the hind paws with sufficient force to cause slight buckling against the paw and held for approximately 6-8 seconds. A positive response was noted if the paw was sharply withdrawn. Flinching immediately upon removal of the hair was also considered a positive response. Ambulation was considered an ambiguous response, and in such cases the stimulus was repeated.

The 50% paw withdrawal threshold was determined using the Dixon up-down method (40). In this method, behavioural testing was initiated with the 0.40 gram filament, in the middle of the series (40). Von Frey filaments were presented in a consecutive fashion, either ascending or descending. In the absence of a positive paw withdrawal response to the initially presented filament a stronger stimulus was presented; in the event of a positive paw withdrawal response, the next weaker stimulus was chosen (40). Stimuli were presented at intervals of several seconds, allowing for apparent resolution of any behavioural responses to previous stimuli. The threshold at which there was a 50% probability of paw withdrawal, was then calculated as previously described (40).

5.4.4. *Micro-computed tomography analysis*

At the completion of the study on day 11, transcardial perfusions were performed while mice were under general anaesthetic (175 mg/kg Sodium Pentobarbital). Mice were perfused with 4% paraformaldehyde prior to the collection of brain and spinal cord tissue, for assessment in ongoing studies. Paw tissues were then collected and underwent post-fixation in 4% paraformaldehyde for 24 hours.

Bone changes and paw swelling of the front and hind paws were assessed using a micro-CT scanner (SkyScan model 1076, Bruker, Kontich, Belgium). Following tissue fixation,

paws were scanned at a source voltage of 55 kV, current 180 µA, isotropic pixel size 8.5 µm with a 0.5 mm thick aluminium filter, rotation step of 0.6, frame averaging of 1 and a total scan time of approximately 35 minutes. The cross-section images were then reconstructed using a filtered back projection algorithm (N-Recon software, Bruker micro-CT, Kontich, Belgium) and saved as 8-bit grey level files (bitmap format). The stack of reconstructed cross-section images of the front and hind paws were realigned in 3D with the long axis of the paw aligned along the inferior-superior direction of the images (Dataviewer software, Bruker), as done previously (34, 39).

Selection of volume of interest (VOI) for analysis:

For each front paw, 280 contiguous cross-sections (corresponding to a VOI length of 2.4 mm), starting from 200 cross-sections (1.7 mm) distally to the epiphyseal growth plate of the radiocarpal joint and extending through the joint up to 80 cross-sections (0.68 mm) proximally, were used for analysis of both the bone and surrounding soft tissue. A cylindrical volume of interest (4.5 mm diameter, 2.4 mm in length) was used and positioned according to the location of each individual paw in the image (34).

In the hind paws, for the bone volume analysis, 600 cross-sections (corresponding to a VOI length of 5.1 mm), extending from the posterior surface of the calcaneus through the proximal tarsal and metatarsal bones were used. A polygonal region of interest was used to trace around the calcaneus, metatarsal and tarsal bones, excluding the tibia and fibula (Figure 5.2). Whereas for the soft tissue analysis, 200 cross-sections were used (corresponding to a VOI length of 1.7 mm), extending from the most posterior aspect of the metatarsal bones, excluding the calcaneus and including the cuboid (Figure 5.2). A standardised cylindrical volume of interest (5.5 mm diameter, 1.7 mm in length) was selected for quantification.
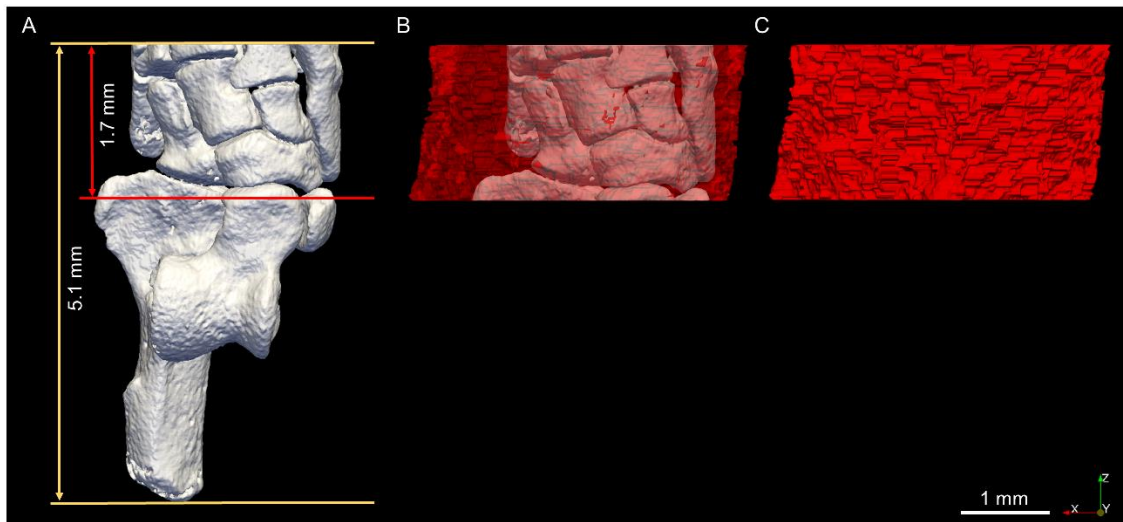
Figure 5.2. 3D micro-CT images of the left hind paw (top view), including calcaneus, tarsal and metatarsal bones for quantitative analysis; bone represented in white colour and soft tissue in red colour. A. The lengths of the volumes of interest (VOIs) used for micro-CT analysis are indicated by the yellow arrows for bone analysis (VOI length of 600 cross sections, corresponding to 5.1 mm) and red arrows for soft tissue analysis (VOI length 200 cross sections, corresponding to 1.7 mm). The 3D rendering of the VOI used for soft tissue analysis is presented in B (bone visible in transparency) and C.

Image thresholding and calculation of bone volume and paw volume:

On the VOIs specified above, the bone volume (BV, in mm^3) and the paw volume (PV, in mm^3, which includes the soft tissue surrounding the radiocarpal joint in the front paws and tarsal and metatarsal bones in the hind paws), were quantified in 3D using uniform thresholding (CT Analyser software, Bruker). In the grey-level histogram of the reconstructed cross-section images (bitmap format, 256 grey levels, ranging from 0 to 255), the grey level values in the lower range (from 0 to 11) corresponded to air or background, followed in increasing order by values of the soft tissue (ranging from 12 to 134) and bone (from 135 to 255) (39). Two fixed minimum threshold values were applied to the specimens for segmentation. One minimum threshold level was used for segmenting the bone pixels only (from minimum threshold level 135 to maximum 255), leaving air and surrounding soft tissue as background (39, 41, 42). The second minimum threshold level was for segmenting the paw, soft tissue and bone together, (minimum

threshold level 12 to maximum level 255) and leaving air as the background (39, 41, 42). By applying the corresponding threshold values to each specimen, automated calculations were performed of BV and PV (CT Analyser software, Bruker). The BV was calculated as the volume occupied by the voxels segmented as bone and the PV was calculated as the volume occupied by the voxels segmented as paw, which included both bone and soft tissue. After segmentation, for PV measurements, loose speckles in the segmented images which originated from noise pixels, having their grey values close to those of soft tissue, were removed. This was completed using a cycle of the software function 'sweep' (CT Analyser software, Bruker) which automatically removes all but the largest object in three-dimensional volume, maintaining the paw as the largest object. BV and PV were then quantified using the marching cubes method (CT Analyser software, Bruker) (43-46).

5.4.5. *Histological analysis of the radiocarpal joint*

Following micro-CT scanning, decalcification of the front paws was carried out for approximately 12 weeks using 10% Ethylene diaminetetraacetic acid (EDTA) solution. The paws were processed for paraffin embedding and serial sagittal sections of the radiocarpal joint were cut (5 µm) for histological analysis. Routine haematoxylin and eosin (H&E) staining was conducted on the front paws and sections were imaged using the Nanozoomer Digital Pathology System (NDP Hamamatsu, Hamamatsu City, Japan) at 40x magnification. Semi-quantitative analysis was carried out by two blinded observers using a previously described scoring method (47). Scoring was based on the number of inflammatory cells within the radiocarpal joint; normal tissue (< 5% inflammatory cells) was scored as 0, mild inflammation (6-20% inflammatory cells) was scored as 1, moderate inflammation (21-50% inflammatory cells) was scored as 2 and severe inflammation (> 51% inflammatory cells) was scored as 3. Bone and cartilage destruction were assessed on a 4-point scale (0, normal; 1, mild cartilage destruction; 2, evidence of both cartilage and bone destruction; 3, severe cartilage and bone destruction). Pannus formation was scored as either 0, no pannus or 1, pannus formation (47).

Tartrate-resistant acid phosphatase (TRAP) staining of the radiocarpal joint was also conducted to detect osteoclasts on the bone surface and pre-osteoclasts in surrounding soft tissue. Slides were stained with TRAP as previously described and left to incubate (37 °C) for 45 minutes then counterstained with haematoxylin (34, 48, 49). The number of TRAP positive cells with 3 or more nuclei were counted by two blinded observers using 40x magnified images on the Nanozoomer Digital Pathology System (NDP Hamamatsu, Hamamatsu City, Japan). Multinucleated TRAP positive cells were counted in a consistent region of interest (2.16 mm^2), which included cells found on the bone surface and within the surrounding soft tissue of the radiocarpal joint (34).

5.4.6. *Statistical Analysis*

Statistical analysis performed in this study utilised GraphPad Prism® software (V 7.03; GraphPad Software, La Jolla, CA, USA). Differences among all groups were first analysed using the non-parametric Kruskal-Wallis test and if significant, differences between two groups were each analysed using the Mann-Whitney U test.

For von Frey data analysis, SPSS Statistics software (V 25; IBM SPSS Software, NSW, Australia) was used to perform a linear mixed-effects model, controlling for clustering on mouse and for repeated measurement over time using a Variance Components covariance structure. Assumptions of a linear model were found to be upheld by inspection of histograms and scatter plots of residuals and predicted values. An interaction of Group (1 = Control, 2 = Mild CAIA and 3 = Moderate CAIA) and Day (day of test) was included with adjustment for paw side (left and right paws).

All values shown are mean ± standard error of the mean (SEM), with a p-value less than 0.05 considered statistically significant.

5.5. Results

5.5.1. *Assessment of paw inflammation and mechanical allodynia*

Induction of CAIA in both disease groups resulted in significant redness, tenderness and inflammation in the front and hind paws of mice following LPS administration on day 3 through to day 10 compared to control mice (Figure 5.3; p < 0.0001). Moderate CAIA mice had significantly greater paw scores compared to mild CAIA mice on days 4 and 6

(p = 0.018 and p = 0.041, respectively; Figure 5.3B). These paw scores remained higher from day 7 to day 10 compared to the mild CAIA mice, however they were not significantly different.

There was no statistically significant interaction between Group and Day of Test for tactile paw withdrawal threshold (g) when controlling for Paw side (interaction p value = 0.70). There was also no statistically significant association between paw withdrawal threshold and Paw side, when controlling for the Group*Day of Test interaction (p = 0.10). However, post-hoc comparisons showed that on day 8, mild CAIA mice had a paw withdrawal threshold greater than control mice (1.99 ± 0.10 g and 1.65 ± 0.10 g, respectively; p = 0.03; Table 5.1). Unexpectedly, moderate CAIA mice also had a significantly greater paw withdrawal threshold (1.94 ± 0.12 g) compared to control mice on day 10 (1.51 ± 0.15 g; p = 0.032; Table 5.1). There was no statistically significant difference in paw withdrawal threshold between the mild and moderate CAIA groups.

Although not significant, the mean paw withdrawal threshold observed in control mice decreased from day 2 (1.83 ± 0.98 g) to day 10 (1.51 ± 0.15 g; Figure 5.3C). A decrease in mean paw withdrawal threshold was also observed in mild CAIA mice from day 2 (2.02 ± 0.98 g) to day 6 (1.7 ± 0.13 g), however, this was not significant and interestingly, increased again at day 8 (1.99 ± 0.11 g; Figure 5.3C) following the peak stage of disease. There was also no statistically significant change in paw withdrawal threshold in moderate CAIA mice throughout the model (Figure 5.3C).
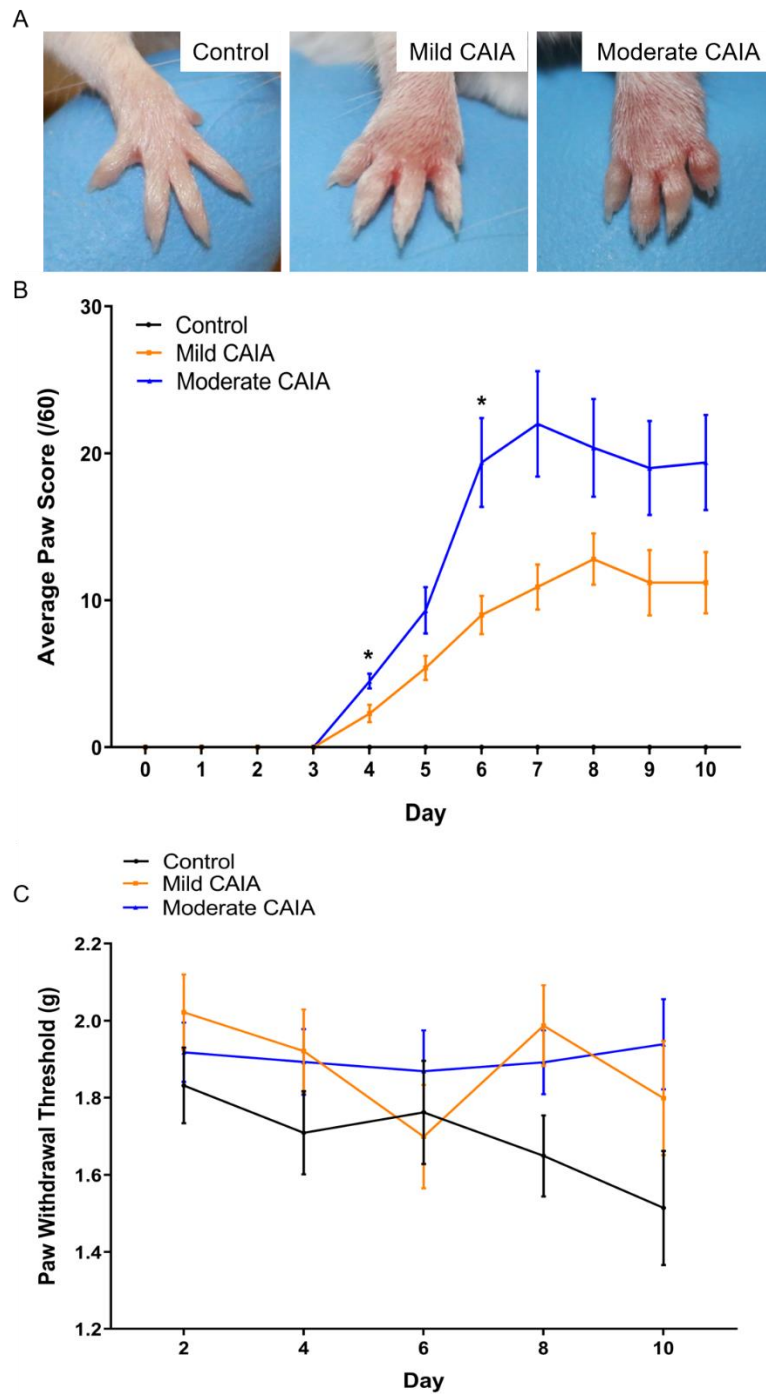
Figure 5.3. Clinical evaluation of local inflammation in all paws and paw withdrawal threshold in the hind paws. A. Representative macroscopic appearance of the front paws at day 7 post-arthritis induction. B. Daily average clinical paw scores of each group throughout the 10-day model. C. Average tactile paw withdrawal threshold of the hind paws on alternate days throughout the 10-day model. Error bars represent SEM (n = 5 mice per control and mild CAIA groups, n = 8 mice per moderate CAIA group, * p < 0.01 mild CAIA vs moderate CAIA).

Table 5.1. Linear mixed-effects model of paw withdrawal threshold: mean differences

Day of Test	Group Comparison	Difference in paw withdrawal threshold (95% CI)	Comparison P value
2	1 vs 2	-0.19 (-0.47, 0.09)	0.178
	1 vs 3	-0.09 (-0.34, 0.17)	0.494
	2 vs 3	0.10 (-0.15, 0.36)	0.409
4	1 vs 2	-0.21 (-0.52, 0.09)	0.174
	1 vs 3	-0.18 (-0.46, 0.09)	0.190
	2 vs 3	0.03 (-0.25, 0.31)	0.840
6	1 vs 2	0.06 (-0.32, -0.45)	0.740
	1 vs 3	-0.11 (-0.45, 0.24)	0.537
	2 vs 3	-0.17 (-0.52, 0.18)	0.327
8	1 vs 2	-0.34 (-0.64, -0.03)	**0.030**
	1 vs 3	-0.24 (-0.52, 0.03)	0.081
	2 vs 3	0.09 (-0.18, 0.37)	0.482
10	1 vs 2	-0.29 (-0.71, 0.14)	0.184
	1 vs 3	-0.43 (-0.81, -0.04)	**0.032**
	2 vs 3	-0.14 (-0.53, 0.25)	0.465

Groups: 1 = Control, 2 = Mild CAIA and 3 = Moderate CAIA

P values less than 0.05 were considered to be statistically significant.

5.5.2. Micro-CT analysis of bone volume and paw volume

<u>Front paws:</u>

Representative reconstructed 3D images of the radiocarpal joint, including bone and soft tissue are shown in Figure 5.3A. Moderate CAIA mice showed a reduced BV in the radiocarpal joint compared to healthy control mice (0.92 ± 0.03 mm^3 and 1.052 ± 0.03 mm^3, respectively; $p = 0.0116$; Figure 5.4B), whereas they showed no significant difference compared to the mild CAIA group. Moderate CAIA mice also had a significantly greater PV (33.31 ± 1.99 mm^3) in the radiocarpal joint compared to both the control (21.7 ± 1.12 mm^3; $p = 0.0003$) and mild CAIA mice (26.86 ± 2.26 mm^3; $p = 0.041$; Figure 5.4C).

<u>Hind paws:</u>

In the hind paw, both the mild and moderate CAIA mice exhibited reduced BV compared to control mice (3.07 ± 0.13 mm^3; $p = 0.027$ and 3.05 ± 0.08 mm^3, respectively; $p = 0.003$; Figure 5.4D), whereas, there was no significant difference in BV between mild and moderate CAIA groups. Similar to the radiocarpal joint, moderate CAIA mice exhibited a significantly greater PV in the hind paw (23.95 ± 1.29 mm^3) compared to both the control (13.08 ± 0.27 mm^3, $p < 0.0001$) and mild CAIA mice (18.82 ± 1.74 mm^3, $p = 0.014$; Figure 5.4E).
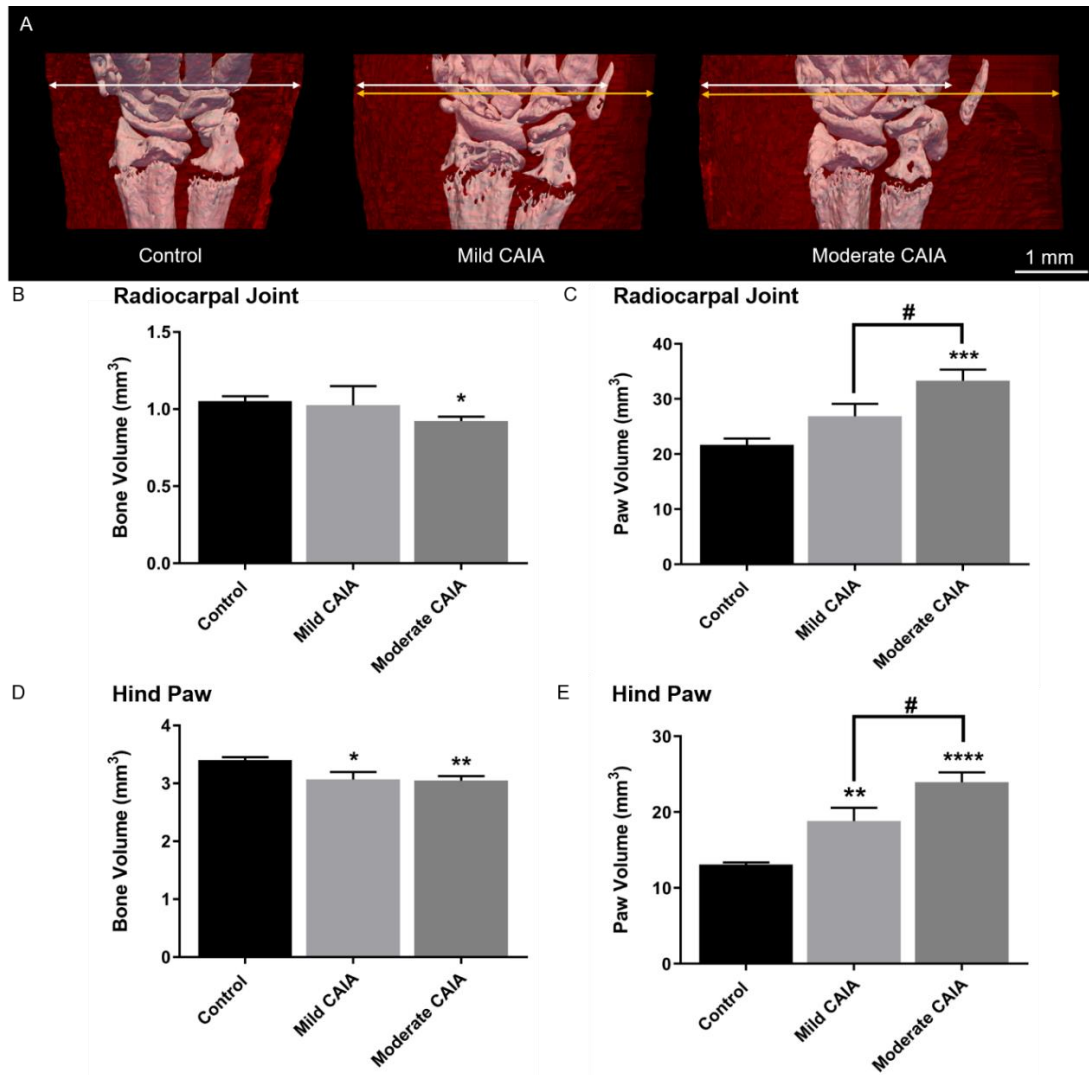
Figure 5.4. Bone volume (BV) and soft tissue swelling (paw volume, PV) of the radiocarpal joint and hind paws of Balb/c mice assessed by high resolution micro-CT at day 11. A. Representative three-dimensional micro-CT models of the radiocarpal joint (in white colour) and surrounding soft tissue (indicated in red) in the right paw. The arrows represent the width of the soft tissue, white arrows for control mice, compared to the yellow arrows for each disease group, highlighting the increase in soft tissue width (and hence paw volume) observed from control to mild and moderate CAIA. Mean BV and PV in the radiocarpal joint (B and C, respectively) and mean BV and PV in the hind paw (D and E, respectively) expressed in mm^3, as assessed by micro-CT analysis at day 11. Error bars represent SEM (n = 10 paws (left and right paws taken together) per control and mild CAIA groups, n = 16 paws (left and right paws taken together) per moderate CAIA group, 1 front paw was removed from the control group for front radiocarpal joint BV analysis due to movement artefacts) * $p < 0.01$, ** $p < 0.003$, *** $p < 0.0003$ and **** $p < 0.0001$ vs control, # $p < 0.01$ vs mild CAIA).

Despite the difference in BV in the hind paws, between mild and moderate CAIA groups, not being statistically significant, bone resorption pits were clearly visible on the surface of the navicular and cuboid bones in both the mild and moderate CAIA groups, as shown by micro-CT 3D images (Figure 5.5). Conversely, control mice exhibited no visible bone resorption pits as of visual examination of micro-CT images on both these bones. In comparison, the number and size of bone resorption pits increased with disease severity. In moderate CAIA mice the cuboid was also observed to have a greater number of pits when compared to the navicular of the same mouse. In comparison to control and mild CAIA mice, bone resorption pits were also observed on other bones within the hind paws of moderate CAIA mice, including the talus and calcaneus (Figure 5.5A and 5.5C).
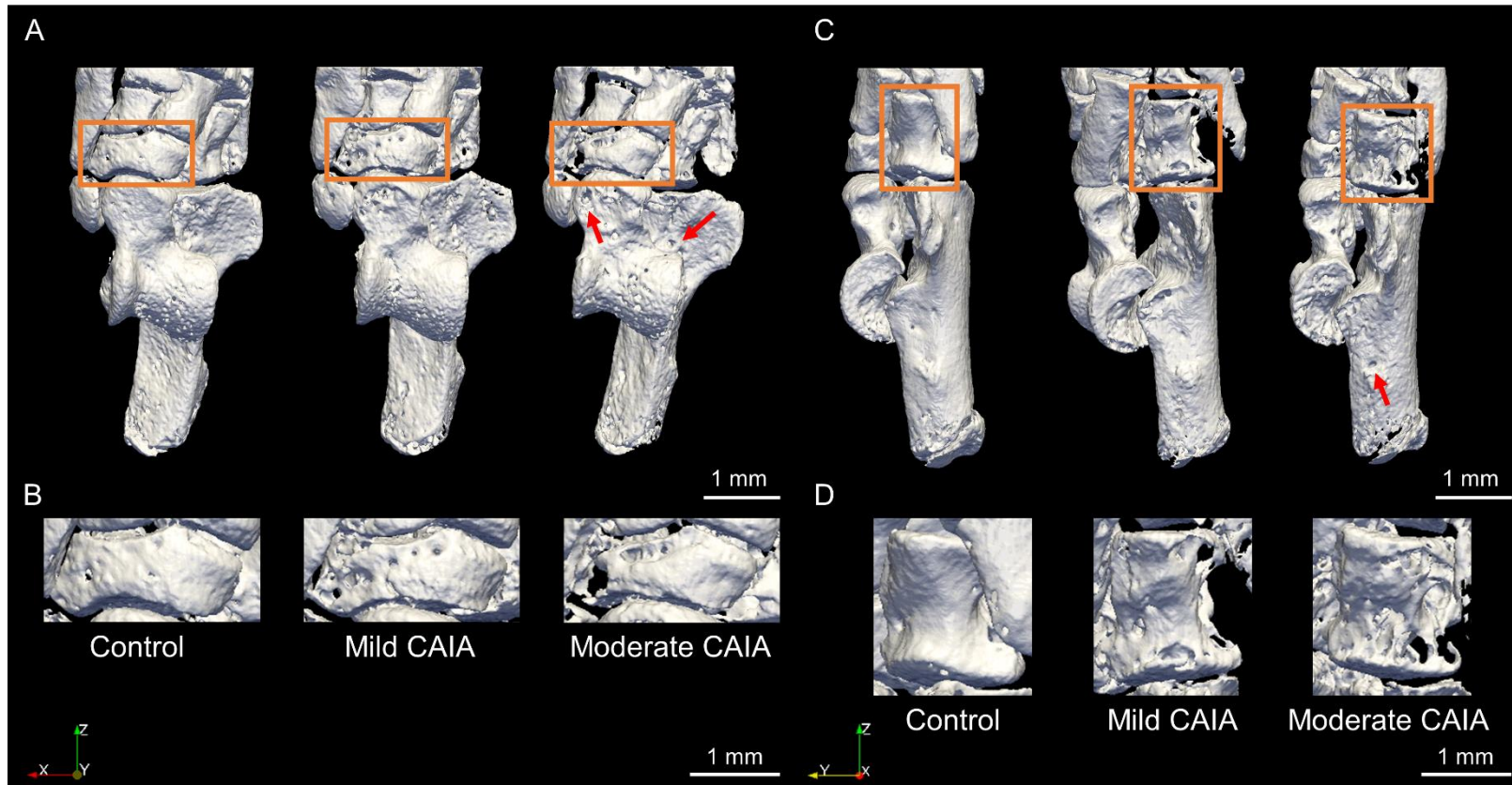
Figure 5.5. Representative three-dimensional models of the right hind paw showing bone resorption pits in the navicular and cuboid. A. Superior view of right hind paw from control, mild CAIA and moderate CAIA mice. Orange boxes identify the navicular which is presented at greater magnification (B) to highlight the pitting present in this bone. C. Lateral view of the right hind paw from control, mild CAIA and moderate CAIA mice. Orange boxes identify the cuboid which is presented at greater magnification (D) to show the pitting present in this bone. Red arrows represent bone resorption pits observed in the talus (A) and calcaneus (C).

5.5.3. *Histological analysis of the radiocarpal joint*

Representative images of H&E and TRAP staining in the radiocarpal joint are presented in Figure 5.6. Histological evaluation of sagittal sections of the radiocarpal joint showed that moderate CAIA mice had significantly greater scores for cellular infiltration, cartilage and bone degradation and pannus formation compared to control mice (p < 0.001; Figure 5.7A). Moderate CAIA mice also had a greater score for cellular infiltration and pannus formation compared to mild CAIA mice (p = 0.02; Figure 5.7A). Cartilage and bone destruction were also scored greater in moderate CAIA mice compared to mild CAIA mice, however this was not statistically significant.

Both mild and moderate CAIA groups had a significantly greater number of TRAP positive multinucleated cells on the bone surface of the radiocarpal joint (8.4 ± 2.42 cells and 15 ± 3.41 cells, respectively) compared to control mice (0.4 ± 0.267 cells; p = 0.0001 and p = 0.001, respectively; Figure 5.7B). A greater number of TRAP positive multinucleated cells were also identified in the surrounding soft tissue of the radiocarpal joint in moderate CAIA mice (44.36 ± 10.3 cells) and mild CAIA mice (32.3 ± 15.91 cells) compared to control mice (0.2 ± 0.2 cells, p = 0.0006 and p = 0.033, respectively; Figure 5.7C). Although moderate CAIA mice appeared to have increased TRAP positive multinucleated cells on both the bone surface and within the surrounding soft tissue compared to mild CAIA mice, there was no significant difference between the two diseased groups.
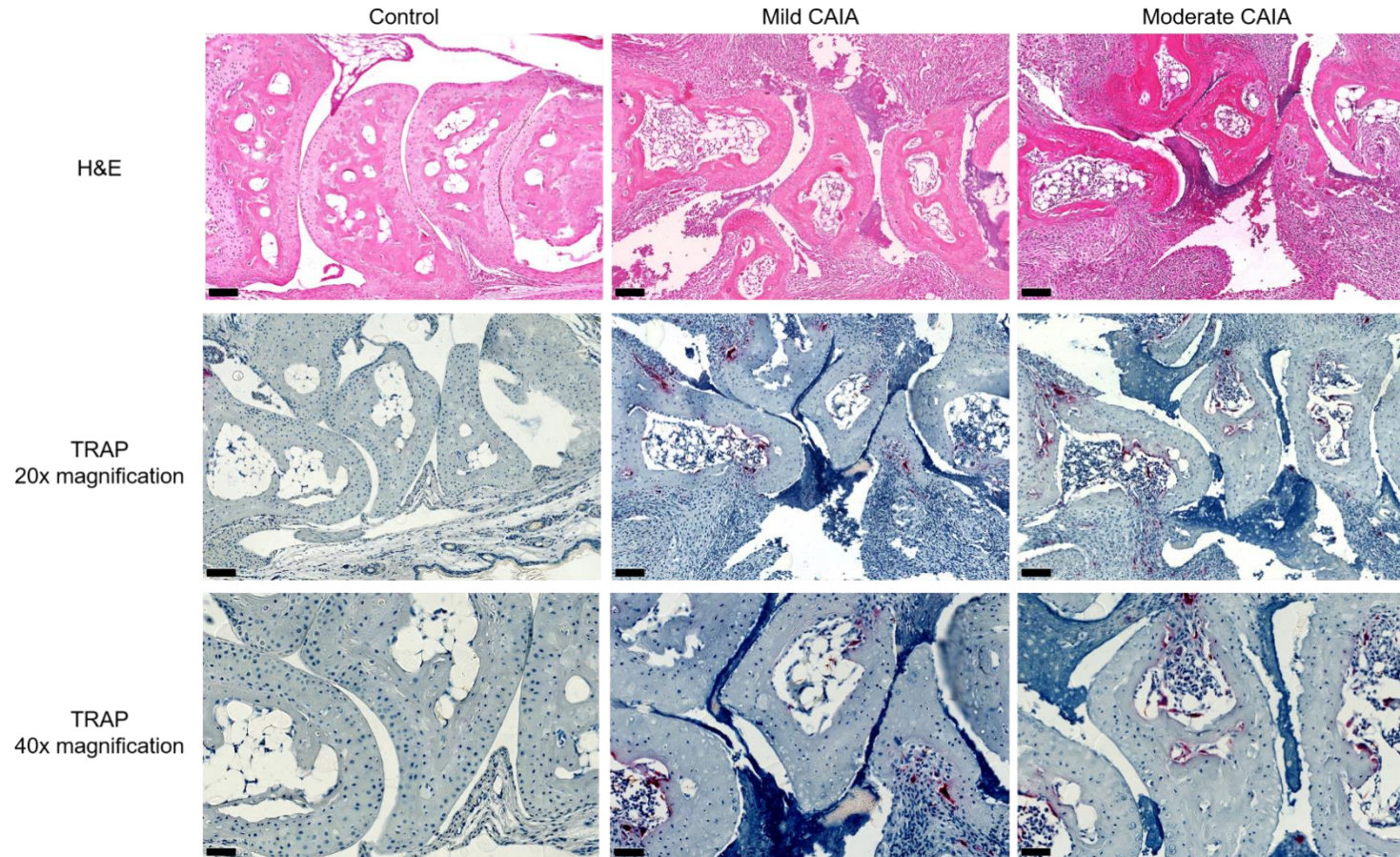
Figure 5.6. Representative immunohistochemical images of bone and inflammatory tissue from mice radiocarpal joints from the Control (left column), mild CAIA (middle column) and moderate CAIA groups (right column); Top row (Haematoxylin and eosin; H&E, 20x magnification); Middle Row (Tartrate Resistant Acid Phosphatase; TRAP, 20x magnification); Bottom Row (TRAP; 40x magnification) Scale bar represents 100 µm for 20x magnification and 50 µm for 40x magnification.
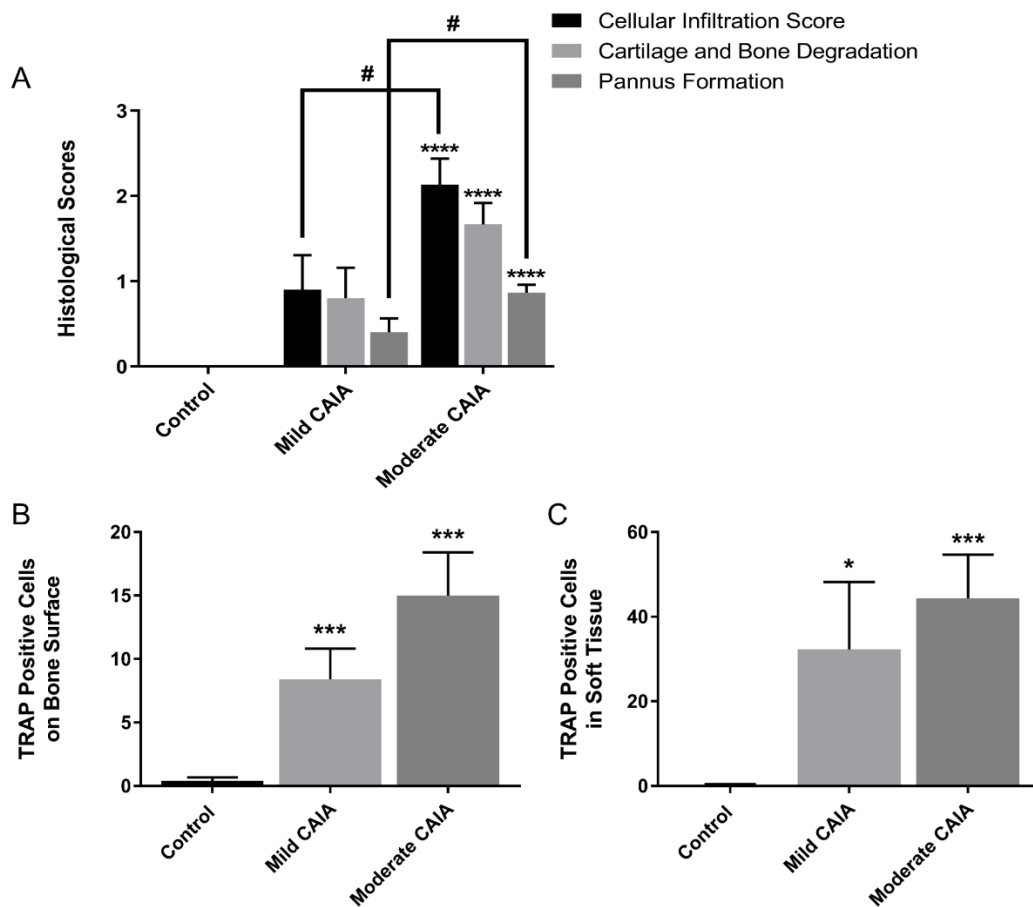
Figure 5.7. Histological assessment of inflammation, cartilage and bone destruction and osteoclast number in the radiocarpal joint. A. Histological scores of H&E stained sagittal sections of the radiocarpal joint. B. Average values of TRAP positive multinucleated cells on the bone surface. C. Average values of TRAP positive multinucleated cells within the surrounding soft tissue of the radiocarpal joint. Error bars represent SEM (n = 10 paws (left and right together) per control and mild CAIA groups and n = 15 paws (left and right together) per moderate CAIA group for histological analysis; n = 10 paws (left and right together) per control and mild CAIA groups and n = 14 (left and right together) paws per moderate CAIA group for TRAP analysis). **** $p < 0.0001$ vs control, # $p = 0.02$ vs mild CAIA; * $p = 0.03$ and *** $p < 0.0001$ vs control).

5.6. Discussion

There are many benefits to using the CAIA murine model in understanding RA disease progression and identifying novel targets for the development of therapeutics. However, there is currently no consistent dose of monoclonal antibodies or LPS used for the induction of disease in the CAIA model. As a result, there is large variability across previous studies in the severity of pathogenic features observed in mice (9, 33, 34, 38, 50). Thus, this study aimed to identify whether a higher dose (3 mg/mouse) of monoclonal antibodies in combination with a low dose (10 µg) of LPS would produce a more moderate model of inflammatory arthritis in comparison to the mild model (1.5 mg/mouse of monoclonal antibodies with 10 µg of LPS), previously used (33, 34, 38).

The results of this study suggest that inducing CAIA with a higher dose of monoclonal antibodies and a reduced dose of LPS induces a moderate inflammatory response within all paws of Balb/c mice. This is evident as moderate CAIA mice were observed to have significantly greater scores for paw inflammation on day 4, when clinical signs of disease are first evident and on day 6 when disease reaches its peak, compared to the paw scores of mild CAIA mice. Although not significant, these paw scores remained elevated compared to mild CAIA mice through to day 10. Despite the onset of joint inflammation in the mild and moderate CAIA mice, these mice did not display robust mechanical allodynia as evidenced by variable and high paw withdrawal thresholds observed throughout the model. This is unexpected, as previous studies in which mice or rats are immunised to produce antibodies against type-II collagen in CIA models or bovine serum albumin in AIA models (11, 51, 52), generate long lasting mechanical allodynia. Within these models the inflammatory process is chronic and thus it is expected that paw withdrawal thresholds will remain low which is consistent to the clinical characteristics in RA patients where pain-like behaviour persists despite remission (51). In contrast, the current CAIA model is based on the systemic injection of a cocktail of monoclonal antibodies and as a result a subacute model is induced and the inflammation resolves within 8-14 days (10, 53, 54). This is evident in our model as paw scores begin to reduce consistently from day 8 until the conclusion of the model at day 10. However, due to the short timeline in the current study, a continued reduction in paw withdrawal threshold is not observed despite resolution of inflammation and thus does not reflect the persistent pain-like behaviour observed in the clinic.

Pain-like behaviour in the CAIA model has previously been confirmed as mice display mechanical allodynia concomitant with the onset of joint inflammation (9). The reduction in paw withdrawal threshold also remains low and does not return to baseline two to four weeks after visible and histologic signs of arthritis have disappeared (9). This was not reflected in the current study and the differences could be attributed to methodology of CAIA induction. Bas *et al.* 2012, induced CAIA with 1.5 mg of a cocktail of monoclonal antibodies followed by a higher dose (25 µg) of LPS on day 5 (9). The model also continued for 45 days post arthritis induction allowing for inflammation to resolve completely and continued pain-like behaviour to be assessed, confirming that pain signalling in RA can be driven by many mechanisms.

Previous studies have shown that systemic and intrathecal injection of LPS alone induces pain-like behaviour (53, 55, 56). In the CAIA model, LPS is injected intraperitoneally three to five days following the injection of monoclonal antibodies, as LPS synchronises the onset of disease and increases the incidence and severity of CAIA (21). The low dose (10 µg) of LPS used in the current study, may therefore not be enough to increase the incidence and severity of inflammation to a level where pain-like behaviour can be assessed in CAIA mice. Previously, Bas *et al.* 2012 assessed LPS alone concurrently with their CAIA model and found 25 µg of LPS alone was not sufficient to alter nociceptive thresholds, however resulted in increased inflammation and mechanical allodynia when in combination with the cocktail of monoclonal antibodies (9). Thus, future studies are needed to identify if 10 µg of LPS alone and in combination with low or high doses of monoclonal antibodies is sufficient to induce both inflammation and pain-like behaviour in the CAIA model.

Assessment of paw inflammation in the CAIA model has previously been based on non-invasive visual assessment methods, including calliper measurements and clinical paw scoring (33, 57, 58). In the current study, the increased paw scores observed at day 10 in moderate CAIA mice were confirmed through increased paw volumes (PV) as assessed using high resolution micro-CT. The moderate CAIA mice had a significantly greater PV in both the radiocarpal joint and hind paw compared to control and mild CAIA mice. This confirms that inflammation of mouse paws in the CAIA model can be enhanced when using a high dose (3 mg/mouse) of monoclonal antibodies in combination with low dose

(10 µg) LPS. This also highlights the relevance of the quantification of soft tissue swelling by high resolution micro-CT as an indicator of disease severity in the CAIA model.

Inflammation in the front paws of moderate CAIA mice is further supported by microscopic histological analysis of the radiocarpal joint. From this analysis it was found that moderate CAIA mice had greater scores for inflammatory cell infiltration and pannus formation compared to control and mild CAIA mice. Though mild CAIA mice were found to have significantly greater paw scores compared to control mice throughout the model, significantly greater histological scores for inflammatory cell infiltration and pannus formation were not observed at end point in mild CAIA mice. This was not expected as we have previously reported significantly greater histological scores in mild CAIA models when compared to control mice (33, 38). The conflicting findings when compared to past studies may be a result of discrepancies in the pathogenesis of CAIA or uptake of the mild form of disease in Balb/c mice as joints are randomly affected due to the systemic administration of the model (20, 21). Thus, it is evident that the higher dose (3 mg/mouse) of monoclonal antibodies achieves a more effective result in producing the desired pathogenic features of RA joint destruction in all paws of Balb/c mice.

The current study used high resolution micro-CT analysis to identify that the moderate CAIA mice showed significantly reduced BV in the radiocarpal joint compared to control mice. However, similar to the histological analysis of inflammation, there was no observable change in BV in the radiocarpal joints of mild CAIA mice when compared to control mice. This limited change in BV is also inconsistent to the significantly greater number of TRAP positive multinucleated cells found on the bone surface and within the surrounding soft tissue of radiocarpal joints in mild CAIA mice compared to control mice. Whereas previously we have reported a significant reduction in BV in the CAIA model when inducing a mild form of the disease (33, 38) (micro-CT analysis conducted at 18 µm/pixel), recently, we were unable to identify changes in BV assessed by micro-CT in mild CAIA (9 µm/pixel micro-CT scans, similar to the present study) (34). This finding is consistent with the current study and could be attributed to the arthritic response being too mild to detect changes in BV at the macroscopic level, despite using high resolution micro-CT analysis. This further corroborates the use of a higher dose of monoclonal

antibodies to induce greater bone erosion in mouse paws that is detected through both micro-CT analysis and histological assessment of osteoclasts.

Micro-CT has proven to be a powerful technique to analyse the detailed 3D micro-architecture of bone in different animal models (50, 59-62). However, there are limited studies which have used high resolution (8.5 µm/pixel) micro-CT to quantitate the change in overall BV in both the radiocarpal joints and hind paws of CAIA mice. Similar to the radiocarpal joint, in this study a significant reduction in BV was observed in the hind paws of moderate CAIA mice compared to control mice. Mild CAIA mice also exhibited significantly reduced BV in the hind paws, however, there was no difference in BV between the two diseased groups. Various studies have used micro-CT to assess BV, BV/tissue volume ratio (BV/TV) and bone structure and density in various bones in rat and mouse models of inflammatory arthritis (50, 63). However, previous studies using the AIA rat model were unable to determine a BV/TV ratio during micro-CT analysis due to severe bone destruction in the talus of vehicle-treated AIA rats (63). This further confirms that inducing a severe arthritic response in animal models causes severe destruction of the joint architecture which is difficult to accurately assess. The current study suggests that inducing moderate pathogenic features of RA in mice allows for a more effective assessment of the hallmark bone changes and offers a potential modification to the CAIA model which could be implemented for the accurate assessment of new therapeutics.

Previous studies have used qualitative methods to identify substantial bone destruction in the tarsal joints of mice induced with CAIA at different severities (50). Although different severities of CAIA were induced in that study, the bone destruction was not compared between these models and there was no quantification of BV (50). Thus, it was so far unclear if inducing a more severe form of the disease also resulted in greater bone destruction and loss of BV. The micro-CT analysis in the current study also extended to qualitative observations of three-dimensional bone models of the hind paws, to investigate the presence of bone resorption pits on the bone surface. An increased number of bone resorption pits was observed on the navicular and cuboid of the hind paw of moderate CAIA mice compared to control and mild CAIA mice. Although not numerically quantified, these resorption pits appeared to be larger in size when compared

to the resorption pits observed on the navicular and cuboid of mild CAIA mice. Although these pits were clearly visible in the 3D micro-CT images on the bone surface when comparing mild to moderate CAIA, these pits were not sufficient to generate detectable BV differences between these two disease groups; this might also be due to the small number of animals per group. As histological analysis of the presence of osteoclasts in the hind paws was not conducted, it cannot be concluded if there is an increase in osteoclast number in the hind paws of moderate CAIA mice compared to mild CAIA. Future studies would benefit from including microscopic analysis of osteoclasts as it would confirm the presence and extent of bone destruction occurring in the hind paws of moderate CAIA mice in comparison to more mild models of CAIA.

5.7. Conclusion

In conclusion, our findings indicate that a higher dose (3 mg/mouse) of the cocktail of monoclonal antibodies in combination with a low dose (10 µg) of LPS in the CAIA murine model produces more desirable and consistent pathogenic features of RA, including greater joint inflammation and bone loss, compared to the mild (1.5 mg/mouse monoclonal antibodies in combination with 10 µg LPS) CAIA murine model. The severity of disease induced in this model had little effect on the development of mechanical allodynia in the hind paws. However, it highlights the complex mechanisms associated with the development of joint destruction and pain-like behaviour *in vivo* in inflammatory arthritis models. Further investigations involving new strategies are required to investigate pain-like behaviour prior to the onset of arthritic symptoms and following the resolution of inflammation in the acute CAIA murine model.

5.8. References

1. Benson RA, McInnes IB, Garside P, Brewer JM. Model answers: Rational application of murine models in Arthritis research. European journal of immunology. 2017.

2. Heiberg T, Kvien TK. Preferences for improved health examined in 1,024 patients with rheumatoid arthritis: pain has highest priority. Arthritis and rheumatism. 2002;47(4):391-7.

3. Lee YC, Cui J, Lu B, Frits ML, Iannaccone CK, Shadick NA, et al. Pain persists in DAS28 rheumatoid arthritis remission but not in ACR/EULAR remission: a longitudinal observational study. Arthritis research & therapy. 2011;13(3):R83.

4. Bas DB, Su J, Wigerblad G, Svensson CI. Pain in rheumatoid arthritis: models and mechanisms. Pain management. 2016;6(3):265-84.

5. Kidd BL, Urban LA. Mechanisms of inflammatory pain. British journal of anaesthesia. 2001;87(1):3-11.

6. Walsh DA, McWilliams DF. Mechanisms, impact and management of pain in rheumatoid arthritis. Nature reviews Rheumatology. 2014;10(10):581-92.

7. Mengshoel AM, Forre O. Pain and fatigue in patients with rheumatic disorders. Clinical rheumatology. 1993;12(4):515-21.

8. Prevoo ML, van 't Hof MA, Kuper HH, van Leeuwen MA, van de Putte LB, van Riel PL. Modified disease activity scores that include twenty-eight-joint counts. Development and validation in a prospective longitudinal study of patients with rheumatoid arthritis. Arthritis and rheumatism. 1995;38(1):44-8.

9. Bas DB, Su J, Sandor K, Agalave NM, Lundberg J, Codeluppi S, et al. Collagen antibody-induced arthritis evokes persistent pain with spinal glial involvement and transient prostaglandin dependency. Arthritis and rheumatism. 2012;64(12):3886-96.

10. Christianson CA, Corr M, Firestein GS, Mobargha A, Yaksh TL, Svensson CI. Characterization of the acute and persistent pain state present in K/BxN serum transfer arthritis. Pain. 2010;151(2):394-403.

11. von Banchet GS, Petrow PK, Brauer R, Schaible HG. Monoarticular antigen-induced arthritis leads to pronounced bilateral upregulation of the expression of neurokinin 1 and bradykinin 2 receptors in dorsal root ganglion neurons of rats. Arthritis research. 2000;2(5):424-7.

12.   Schaible HG, Ebersberger A, Von Banchet GS. Mechanisms of pain in arthritis. Annals of the New York Academy of Sciences. 2002;966:343-54.

13.   Holmdahl R, Jansson L, Larsson E, Rubin K, Klareskog L. Homologous type II collagen induces chronic and progressive arthritis in mice. Arthritis and rheumatism. 1986;29(1):106-13.

14.   Holmdahl R. Primer: comparative genetics of animal models of arthritis--a tool to resolve complexity. Nature clinical practice Rheumatology. 2007;3(2):104-11.

15.   Cordova KN, Willis VC, Haskins K, Holers VM. A citrullinated fibrinogen-specific T cell line enhances autoimmune arthritis in a mouse model of rheumatoid arthritis. Journal of immunology (Baltimore, Md : 1950). 2013;190(4):1457-65.

16.   Williams RO. Collagen-induced arthritis in mice. Methods in molecular medicine. 2007;136:191-9.

17.   Williams RO. Collagen-induced arthritis as a model for rheumatoid arthritis. Methods in molecular medicine. 2004;98:207-16.

18.   Caplazi P, Baca M, Barck K, Carano RA, DeVoss J, Lee WP, et al. Mouse Models of Rheumatoid Arthritis. Veterinary pathology. 2015;52(5):819-26.

19.   Holmdahl R, Bockermann R, Backlund J, Yamada H. The molecular pathogenesis of collagen-induced arthritis in mice--a model for rheumatoid arthritis. Ageing research reviews. 2002;1(1):135-47.

20.   Khachigian LM. Collagen antibody-induced arthritis. Nature protocols. 2006;1(5):2512-6.

21.   Nandakumar KS, Svensson L, Holmdahl R. Collagen type II-specific monoclonal antibody-induced arthritis in mice: description of the disease and the influence of age, sex, and genes. The American journal of pathology. 2003;163(5):1827-37.

22.   Terato K, Hasty KA, Reife RA, Cremer MA, Kang AH, Stuart JM. Induction of arthritis with monoclonal antibodies to collagen. Journal of immunology (Baltimore, Md : 1950). 1992;148(7):2103-8.

23.   Stuart JM, Dixon FJ. Serum transfer of collagen-induced arthritis in mice. The Journal of experimental medicine. 1983;158(2):378-92.

24.   Nandakumar KS, Backlund J, Vestberg M, Holmdahl R. Collagen type II (CII)-specific antibodies induce arthritis in the absence of T or B cells but the arthritis progression is enhanced by CII-reactive T cells. Arthritis research & therapy. 2004;6(6):R544-50.

25.   Marinova-Mutafchieva L, Williams RO, Mason LJ, Mauri C, Feldmann M, Maini RN. Dynamics of proinflammatory cytokine expression in the joints of mice with collagen-induced arthritis (CIA). Clinical and experimental immunology. 1997;107(3):507-12.

26.   Kagari T, Doi H, Shimozato T. The importance of IL-1 beta and TNF-alpha, and the noninvolvement of IL-6, in the development of monoclonal antibody-induced arthritis. Journal of immunology (Baltimore, Md : 1950). 2002;169(3):1459-66.

27.   Brand DD, Latham KA, Rosloniec EF. Collagen-induced arthritis. Nature protocols. 2007;2(5):1269-75.

28.   Watson WC, Townes AS. Genetic susceptibility to murine collagen II autoimmune arthritis. Proposed relationship to the IgG2 autoantibody subclass response, complement C5, major histocompatibility complex (MHC) and non-MHC loci. The Journal of experimental medicine. 1985;162(6):1878-91.

29.   Reife RA, Loutis N, Watson WC, Hasty KA, Stuart JM. SWR mice are resistant to collagen-induced arthritis but produce potentially arthritogenic antibodies. Arthritis and rheumatism. 1991;34(6):776-81.

30.   Hietala MA, Nandakumar KS, Persson L, Fahlen S, Holmdahl R, Pekna M. Complement activation by both classical and alternative pathways is critical for the effector phase of arthritis. European journal of immunology. 2004;34(4):1208-16.

31.   Hutamekalin P, Saito T, Yamaki K, Mizutani N, Brand DD, Waritani T, et al. Collagen antibody-induced arthritis in mice: development of a new arthritogenic 5-clone cocktail of monoclonal anti-type II collagen antibodies. Journal of immunological methods. 2009;343(1):49-55.

32.   Terato K, Harper DS, Griffiths MM, Hasty DL, Ye XJ, Cremer MA, et al. Collagen-induced arthritis in mice: synergistic effect of E. coli lipopolysaccharide bypasses epitope specificity in the induction of arthritis with monoclonal antibodies to type II collagen. Autoimmunity. 1995;22(3):137-47.

33.   Cantley MD, Haynes DR, Marino V, Bartold PM. Pre-existing periodontitis exacerbates experimental arthritis in a mouse model. Journal of clinical periodontology. 2011;38(6):532-41.

34.   Williams B, Tsangari E, Stansborough R, Marino V, Cantley M, Dharmapatni A, et al. Mixed effects of caffeic acid phenethyl ester (CAPE) on joint inflammation,

bone loss and gastrointestinal inflammation in a murine model of collagen antibody-induced arthritis. Inflammopharmacology. 2017;25(1):55-68.

35. Gullick NJ, Scott DL. Co-morbidities in established rheumatoid arthritis. Best practice & research Clinical rheumatology. 2011;25(4):469-83.

36. Humphreys J, Hyrich K, Symmons D. What is the impact of biologic therapies on common co-morbidities in patients with rheumatoid arthritis? Arthritis research & therapy. 2016;18(1):282.

37. Meyer PW, Anderson R, Ker JA, Ally MT. Rheumatoid arthritis and risk of cardiovascular disease. Cardiovascular journal of Africa. 2018;29(5):317-21.

38. Dharmapatni AA, Cantley MD, Marino V, Perilli E, Crotti TN, Smith MD, et al. The X-Linked Inhibitor of Apoptosis Protein Inhibitor Embelin Suppresses Inflammation and Bone Erosion in Collagen Antibody Induced Arthritis Mice. Mediators Inflamm. 2015;2015:564042.

39. Perilli E, Cantley M, Marino V, Crotti TN, Smith MD, Haynes DR, et al. Quantifying not only bone loss, but also soft tissue swelling, in a murine inflammatory arthritis model using micro-computed tomography. Scandinavian journal of immunology. 2015;81(2):142-50.

40. Chaplan SR, Bach FW, Pogrel JW, Chung JM, Yaksh TL. Quantitative assessment of tactile allodynia in the rat paw. Journal of neuroscience methods. 1994;53(1):55-63.

41. Luu YK, Lublinsky S, Ozcivici E, Capilla E, Pessin JE, Rubin CT, et al. In vivo quantification of subcutaneous and visceral adiposity by micro-computed tomography in a small animal model. Medical engineering & physics. 2009;31(1):34-41.

42. Perilli E, Baruffaldi F, Visentin M, Bordini B, Traina F, Cappello A, et al. MicroCT examination of human bone specimens: effects of polymethylmethacrylate embedding on structural parameters. Journal of microscopy. 2007;225(Pt 2):192-200.

43. Lane NE, Thompson JM, Haupt D, Kimmel DB, Modin G, Kinney JH. Acute changes in trabecular bone connectivity and osteoclast activity in the ovariectomized rat in vivo. Journal of bone and mineral research : the official journal of the American Society for Bone and Mineral Research. 1998;13(2):229-36.

44.   Perilli E, Le V, Ma B, Salmon P, Reynolds K, Fazzalari NL. Detecting early bone changes using in vivo micro-CT in ovariectomized, zoledronic acid-treated, and sham-operated rats. Osteoporosis international : a journal established as result of cooperation between the European Foundation for Osteoporosis and the National Osteoporosis Foundation of the USA. 2010;21(8):1371-82.

45.   Lorensen WE, Cline HE. Marching cubes: a high resolution 3D surface construction algorithm. Comput Graph. 1987;21:163-9.

46.   Perilli E, Briggs AM, Kantor S, Codrington J, Wark JD, Parkinson IH, et al. Failure strength of human vertebrae: prediction using bone mineral density measured by DXA and bone volume by micro-CT. Bone. 2012;50(6):1416-25.

47.   Tak PP, Smeets TJ, Daha MR, Kluin PM, Meijers KA, Brand R, et al. Analysis of the synovial cell infiltrate in early rheumatoid synovial tissue in relation to local disease activity. Arthritis and rheumatism. 1997;40(2):217-25.

48.   Burstone MS. Histochemical demonstration of acid phosphatases with naphthol AS-phosphates. J Natl Cancer Inst. 1958;21(3):523-39.

49.   Angel NZ, Walsh N, Forwood MR, Ostrowski MC, Cassady AI, Hume DA. Transgenic mice overexpressing tartrate-resistant acid phosphatase exhibit an increased rate of bone turnover. Journal of bone and mineral research : the official journal of the American Society for Bone and Mineral Research. 2000;15(1):103-10.

50.   Oestergaard S, Rasmussen KE, Doyle N, Varela A, Chouinard L, Smith SY, et al. Evaluation of cartilage and bone degradation in a murine collagen antibody-induced arthritis model. Scandinavian journal of immunology. 2008;67(3):304-12.

51.   Inglis JJ, Notley CA, Essex D, Wilson AW, Feldmann M, Anand P, et al. Collagen-induced arthritis as a model of hyperalgesia: functional and cellular analysis of the analgesic actions of tumor necrosis factor blockade. Arthritis and rheumatism. 2007;56(12):4015-23.

52.   Chillingworth NL, Donaldson LF. Characterisation of a Freund's complete adjuvant-induced model of chronic arthritis in mice. Journal of neuroscience methods. 2003;128(1-2):45-52.

53.   Christianson CA, Dumlao DS, Stokes JA, Dennis EA, Svensson CI, Corr M, et al. Spinal TLR4 mediates the transition to a persistent mechanical hypersensitivity

after the resolution of inflammation in serum-transferred arthritis. Pain. 2011;152(12):2881-91.

54. Nandakumar KS, Holmdahl R. Collagen antibody induced arthritis. Methods in molecular medicine. 2007;136:215-23.

55. Meller ST, Dykstra C, Grzybycki D, Murphy S, Gebhart GF. The possible role of glia in nociceptive processing and hyperalgesia in the spinal cord of the rat. Neuropharmacology. 1994;33(11):1471-8.

56. Maier SF, Wiertelak EP, Martin D, Watkins LR. Interleukin-1 mediates the behavioral hyperalgesia produced by lithium chloride and endotoxin. Brain research. 1993;623(2):321-4.

57. Silva MD, Savinainen A, Kapadia R, Ruan J, Siebert E, Avitahl N, et al. Quantitative analysis of micro-CT imaging and histopathological signatures of experimental arthritis in rats. Molecular imaging. 2004;3(4):312-8.

58. Chao CC, Chen SJ, Adamopoulos IE, Judo M, Asio A, Ayanoglu G, et al. Structural, cellular, and molecular evaluation of bone erosion in experimental models of rheumatoid arthritis: assessment by muCT, histology, and serum biomarkers. Autoimmunity. 2010;43(8):642-53.

59. Sims NA, Green JR, Glatt M, Schlict S, Martin TJ, Gillespie MT, et al. Targeting osteoclasts with zoledronic acid prevents bone destruction in collagen-induced arthritis. Arthritis and rheumatism. 2004;50(7):2338-46.

60. Barck KH, Lee WP, Diehl LJ, Ross J, Gribling P, Zhang Y, et al. Quantification of cortical bone loss and repair for therapeutic evaluation in collagen-induced arthritis, by micro-computed tomography and automated image analysis. Arthritis and rheumatism. 2004;50(10):3377-86.

61. Nishida S, Tsurukami H, Sakai A, Sakata T, Ikeda S, Tanaka M, et al. Stage-dependent changes in trabecular bone turnover and osteogenic capacity of marrow cells during development of type II collagen-induced arthritis in mice. Bone. 2002;30(6):872-9.

62. Kliwinski C, Kukral D, Postelnek J, Krishnan B, Killar L, Lewin A, et al. Prophylactic administration of abatacept prevents disease and bone destruction in a rat model of collagen-induced arthritis. Journal of autoimmunity. 2005;25(3):165-71.

63. Noguchi M, Kimoto A, Sasamata M, Miyata K. Micro-CT imaging analysis for the effect of celecoxib, a cyclooxygenase-2 inhibitor, on inflammatory bone

destruction in adjuvant arthritis rats. Journal of bone and mineral metabolism. 2008;26(5):461-8.

CHAPTER 6: THESIS GENERAL DISCUSSION AND FUTURE CONSIDERATIONS

6.1. Introduction

Bone destruction in the synovial joints and the resulting pain continues to be a major problem for rheumatoid arthritis (RA) disease management, due to the vast array of contributing factors that influence bone remodelling processes in inflammatory conditions. In healthy individuals, bone is continually remodelled by bone forming osteoblasts and bone resorbing osteoclasts and is strictly controlled so that no net change in bone volume (BV) can occur (1). However, in pathological bone loss conditions, including RA, an imbalance between osteoblasts and osteoclasts exists, resulting in extensive bone loss (2). In RA, osteoclasts are stimulated by the chronic activation of the immune system (3). As such there is a clear link between inflammation and bone loss (4-7). Central to this is the elevated expression of receptor activator of nuclear factor kappa B ligand (RANKL), by activated inflammatory cells, specifically fibroblast-like synoviocytes (FLS) and T cells (8-10), as well as the continuous release of pro-inflammatory cytokines (11-16). This in turn promotes the upregulation of osteoclast number, activity and survival rate at the site of local joint inflammation, leading to severe bone erosion (14-16).

RA associated pain is also suggested to be a major consequence of inflammation and bone destruction in the synovial joints (17, 18). However, recent studies have identified that pain can arise prior to disease manifestations and does not necessarily correlate with the degree of inflammation or pharmacological management (19-22). Despite this, many current treatments, including non-steroidal anti-inflammatory drugs (NSAIDs) and disease modifying anti-rheumatic drugs (DMARDs), used to suppress inflammation, have varied effects on bone and RA associated pain (22-25), suggesting the link to inflammation may not be so clear. It is thus imperative to understand the development of RA disease progression in the synovial joints and the specific mechanisms associated with inflammatory induced bone loss using cell culture and *in vivo* models.

Disease progression in RA is complex, and multiple signalling pathways, including the key intracellular inflammatory molecule, nuclear factor-kappa B (NF-κB), has previously been identified as crucial to T-cell mediated inflammation (26, 27) and increased osteoclast production during RA (28). However, despite this knowledge, pharmacological control of bone destruction in RA is still challenging and management of joint pain is often poor despite optimal control of inflammation (19-22, 25). Direct cell to cell interactions are essential for the regulation of cell proliferation and survival in both physiological and pathological conditions and are mediated in part by cell adhesion molecules (29). Recent advances in the understanding of RA disease progression have therefore identified cell adhesion molecules, including N-cadherin, and anti-apoptotic proteins as key regulators of osteoclast formation and migration (30-32). Current research now recognises the immense therapeutic potential of modulating cell proliferation or death, particularly apoptosis, in the synovial joints of RA patients (33-36). However, further *in vitro* and *in vivo* pre-clinical studies are needed to elucidate these intracellular pathways and molecules as potential targets for the development of novel therapeutics to improve disease outcomes in RA.

The overall focus of this thesis involved investigating the therapeutic potential of novel compounds for targeting inflammation, bone resorption and RA specific pain. The overall body of this work was guided by three hypotheses. First, that *targeting autophagy and apoptotic pathways individually and simultaneously through pharmacological modulation will reduce osteoclast activity in vitro and suppress bone resorption in inflammatory arthritis in vivo*. Second, that *topical antagonists targeting N-cadherin will reduce local inflammation and bone erosion in inflammatory arthritis* and finally, that *inhibition of NF-κB will reduce local inflammation and bone erosion in inflammatory arthritis*. Studies were carried out with osteoclasts derived from human peripheral blood mononuclear cells (PBMCs) *in vitro* and *in vivo* using a subacute mild version of the collagen antibody-induced arthritis (CAIA) murine model. For *in vitro* investigations, the addition of the inflammatory cytokine tumour necrosis factor alpha (TNF-α) was used to mimic the inflammatory conditions present in RA.

6.2. Discussion and Future Considerations

6.2.1. An inflammatory arthritis murine model for evaluation of novel compounds in rheumatoid arthritis

The CAIA murine model was used extensively throughout this study (Chapter 2-5), as it is a subacute, simple and versatile murine model of the effector phase of RA. As discussed throughout these studies, pathogenic features of RA are induced in the CAIA model with a combination of monoclonal antibodies targeting type II collagen in combination with *E.coli* lipopolysaccharide (LPS). Previously, studies have modified the dose of autoantibodies and LPS to induce the desired pathogenic features and severity in their research (20, 33, 37, 38). Thus, there is currently large variability in disease onset and the severity of pathogenic features observed in the CAIA model throughout different studies (20, 33, 37, 39, 40). Previously our laboratory has used a mild form of CAIA (1.5 mg monoclonal antibodies in combination with 10 µg LPS) (33, 37, 39). In the current studies (Chapter 2-5) using the same mild model of CAIA, we have identified discrepancies in the uptake of mild disease and the development of arthritic symptoms in the synovial joints of Balb/c mice. This difference in disease uptake was evident across these studies, as although paw inflammation and bone destruction developed in Balb/c mice induced with mild CAIA, there was variability in the severity of inflammation and presence of bone destruction observed within each of the CAIA groups. Changes in BV between healthy control mice and treated or non-treated mild CAIA mice were also unable to be detected in some instances (Chapter 2-4). Given that our findings in these models (Chapter 2-4) were mixed, Chapter 5 further characterised the CAIA model to establish a more moderate disease that is reflective of the clinical setting.

The results of this study (Chapter 5) ascertain that inducing CAIA in mice with a moderate dose of monoclonal antibodies (3 mg/mouse) in combination with low dose LPS (10 µg/mouse) induces greater inflammation and oedema in the front and hind paws of Balb/c mice, compared to the mild (1.5 mg monoclonal antibodies with 10µg LPS) CAIA model. Despite the increased disease severity in the moderate CAIA model, local paw inflammation followed the same pattern of disease development in the mild CAIA model used in this thesis (Chapter 2-4) and in previous studies (37, 38), with peak inflammation observed on day 6 to 8 before reducing through days 8 to 10. Through end point analyses

it was also evident that pathogenic features, including inflammatory cell infiltration and pannus formation were present and significantly greater in the moderate CAIA model in comparison to the mild model. Interestingly, although mild CAIA mice were found to have significantly greater paw scores compared to healthy control mice throughout this study (Chapter 5), greater inflammatory cell infiltration and pannus formation was not observed at end point (day 11), which is consistent with previous findings (Chapter 2-4). This further confirms that the mild CAIA model used in our previous studies is no longer sufficient in inducing significant and consistent enough pathogenic features of RA in Balb/c mice to investigate pathophysiology or treatment effects. As such a more moderate CAIA model may now be a favourable subacute model of the effector phase of RA.

The studies presented in this thesis used high resolution (8.5 µm) micro-computed tomography (micro-CT) to calculate volumetric changes in bone and soft tissue swelling, not only to assess the front paws as is common in other studies (33, 37, 41). In this thesis, micro-CT was further optimised to enable application of this imaging modality to the analysis of hind paws in the CAIA murine model. Although moderate CAIA disease induction resulted in greater inflammation as evidenced by end point micro-CT analysis of soft tissue swelling (Chapter 5), there was little effect on the overall BV detected in the front and hind paws. Unexpectedly, BV analysis in the front and hind paws of moderate CAIA mice were similar to the BV observed in the mild CAIA group. The analysis of the mild CAIA model is consistent with previous CAIA models conducted in this thesis (Chapter 2-4), where the presence of inflammation did not lead to BV changes as detected through micro-CT analysis. This may also be the case with the moderate CAIA model, perhaps suggesting a more chronic disease duration may be required to see volumetric bone changes, and/or a different mode of analysis may also better reflect changes in the bone itself.

Future Directions:

When considering the change in bone throughout the progression of inflammatory arthritis, most studies, including this thesis in the CAIA model, have shown volumetric assessment on bone (33, 37, 39, 41). To our knowledge there is no report of assessing actual surface changes as indicated by bone resorption pits on the surface of individual

bones in the front and hind paws through either quantitative or qualitative assessment. In our studies (Chapter 4 and 5) we used a combination of quantitative BV and qualitative observations of surface bone resorption pits in the hind paws. Previous studies within our laboratory have conducted quantitative analysis of calvarial surface bone resorption using micro-CT derived images (42). We contend that the resorption pits observed in the hind paws (Chapter 4 and 5) are highly important as these better reflect the presence or absence of active osteoclasts. This would also verify the assessment of differentiated and activated osteoclasts currently assessed through histological TRAP analysis (Chapter 2-5). In Chapter 4 and 5, we present qualitative observations of surface bone resorption on the navicular and cuboid, however, these were not measured, nor were bone resorption pits assessed in the front paws. Future studies would benefit by extending the method where by our group quantified bone resorption pits on calvarial surfaces (42) to application in micro-CT derived images of the front and hind paws of CAIA mice to more accurately assess the changes in bone resorption in the CAIA model following disease induction. This may also enable significant changes in bone to be detected in the mild CAIA model following the administration of treatment.

High resolution micro-CT analysis is an important tool to assess volumetric effects of CAIA on bone, however BV calculations and observations of bone resorption pits were only conducted at end point (day 11) and thus comparisons were only made between healthy control and diseased groups throughout all studies (Chapter 2-5). Multiple endpoints could be assessed *ex vivo*, and a prolonged CAIA model may produce detectable changes in BV, however this requires increased animal numbers and further investigation. Previous studies in our laboratory have used high resolution micro-CT to calculate volumetric changes in bone overtime (37, 39) and found on average a 14% reduction in BV 10 days following CAIA induction (39). Future studies could implement a longitudinal study design to assess bone changes in 3D over the course of the CAIA model, using high resolution *in vivo* micro-CT. This study approach would reduce the animal number required to detect RA related changes in bone, as well as strengthen the statistical power as each animal would serve as its own control. Different micro architectural changes in 3D, such as bone density and trabecular or cortical parameters, could also be assessed as few studies have looked at micro architectural changes in *in vivo* preclinical models of RA. Changes in these properties may be better detected in the

CAIA model and more representative of the histological analysis conducted and therefore provide a more accurate reflection of the pathogenic features observed at the joint in this model.

6.2.2. Pain assessment in in vivo models of rheumatoid arthritis

Pain is an active indicator of inflammation and disease progression in RA and is reported as one of the most debilitating symptoms (19, 43). Pain in RA has only recently been investigated in rodent models of chronic immune mediated articular inflammation (20, 44, 45) and is measured through the reduction in intensity of responses to noxious stimuli, as rodents are unable to report pain sensation. Mechanical sensitivity or the response to pressure is therefore often measured in rodents using the von Frey paw withdrawal test (46) or through catwalk gait analysis (47, 48). The most common animal models used for the assessment of RA disease progression, including the CAIA model, are however currently not adapted for studies of RA associated pain. Thus, recent studies utilising the CAIA model (20), including ours (Chapter 4 and 5), have incorporated the von Frey paw withdrawal test in an attempt to assess pain-like behaviour in this model.

A recent study analysing pain-like behaviour in a CAIA model of moderate arthritis (1.5 mg monoclonal antibody in combination with 25 µg LPS) found that mice displayed mechanical allodynia concomitant with the onset of joint inflammation (20). Mechanical allodynia did not subside for two to four weeks after visible and histologic signs of arthritis had disappeared, consistent with pain analysis in the clinical setting (19, 20, 49). In contrast, the current study found mild (1.5 mg monoclonal antibody and 10 µg LPS; Chapter 4 and 5) and moderate (3 mg monoclonal antibody and 10 µg LPS; Chapter 5) CAIA mice to have unexpectedly high paw withdrawal thresholds in comparison to control mice, suggesting mechanical allodynia was not evident. As local paw inflammation reached its peak by day 8 in our model, it was expected that the threshold required to evoke pain in these mice would decrease, with greater reductions in the paw withdrawal threshold observed in the moderate CAIA model.

Future Directions:

The inconsistencies in paw withdrawal thresholds in both chapter 4 and 5, particularly between healthy control and CAIA non-treated mice could be attributed to the von Frey method implemented. Monofilaments are used extensively in the clinical setting to assess pain (50), however, the inaccessibility of perceived pain sensation in non-self-reporting subjects, such as rodents, mandates an indirect approach through observable responses. Recently, strong criticism has been made for the use of von Frey filaments in the study of RA associated pain-like behaviour (51). As such, many disadvantages have been raised, including immense subjectivity and variability due to operator bias (52-54). Although von Frey filaments can deliver a reproducible force, the accuracy of the stimulus can undergo significant alteration when repeatedly applied (55) and the filaments themselves are also subjected to stretching and compression due to ambient temperature and humidity (56-58), impacting the force applied and the responses generated.

Another major concern is that mechanical sensitivity in mice and other rodents can change according to their behaviour (59). The technique also requires rodents to be confined to the von Frey chamber for an extended period, as well as filaments being applied to the inflamed tissue numerous times causing greater discomfort (60). Recent studies have identified certain strains of rodents, including Balb/c mice used in this study (Chapter 4 and 5), can become accustomed to the testing procedure (20), further impacting the responses elicited. Thus, new methods of assessing mechanical sensitivity are required for the future study of pain-like behaviour in animal models of RA. The electronic von Frey apparatus is an extension from the current manual von Frey method used (Chapter 4 and 5) and provides several advantages to the previous technique. The ease and rapidity of the electronic von Frey apparatus allows for a more sensitive, quantitative and objective measure of mechanical sensitivity in rodent models of joint inflammation (61-63). Paw withdrawal response following induction of disease or treatment is also compared to its own individual baseline response (61, 63), creating an internal control, which is not possible when using the traditional manual von Frey method (60). This would add a powerful dimension to the CAIA model to analyse concomitant subacute and chronic pain that underlies the development of local paw inflammation.

Another potential method for future *in vivo* studies of pain in RA is automated gait analysis using the catwalk system (64). This is a developing method which assesses a variety of parameters of walking in freely moving rodents (64-67). It is particularly beneficial for gait analysis in models with lesions that change the gait and behaviour of the animal, such as the severe local paw inflammation present in the CAIA model. However, recent studies suggest that automated gait analysis could be less sensitive to bilaterally elevated pain resulting from systemic changes (64, 65, 68). As RA is a systemic autoimmune disease and CAIA is systemically induced in mice resulting in the greater likelihood of bilateral inflammation of both the front and hind paws, further investigation is needed into the use of automated gait analysis in murine models of inflammatory arthritis and the benefits for assessing pain-like behaviour in RA.

6.2.3. Pharmacological modulation of inflammation, bone loss and pain in a collagen antibody-induced arthritis (CAIA) mouse model

Progression of novel compounds to their application in the clinical setting requires extensive investigation into their mechanism of action, in addition to characterising their broader effects *in vivo*. However, determination of the pharmacodynamics of novel compounds remains a challenge for a range of reasons, including the vast array of potential *in vivo* preclinical models available for the study of RA. The CAIA model has been used extensively to increase our understanding of the pathogenesis of RA, as discussed throughout this thesis. Due to the high reproducibility of the CAIA model and the focus on the effector phase of disease progression, a mild form of the CAIA model was used in these studies (Chapter 2-4) to assess the effect of novel compounds on local inflammation and bone destruction.

6.2.3.1 Inhibition of NF-κB signalling in the mild CAIA mouse model

RANKL and its downstream molecules, including NF-κB, is an important intracellular signalling pathway for osteoclast formation and activity in normal osteoclastogenesis (69-71) and in pathological bone loss (34-36). NF-κB signalling is crucial to enhancing inflammation induced osteoclastogenesis in the progression of RA joint destruction (72-74). Recent studies have investigated several natural compounds that have inhibitory effects on osteoclast formation and bone resorption through suppression of NF-κB

activation (28, 75-79). These include the natural inhibitor Parthenolide (PAR) which was investigated in the current study (Chapter 4). Previous studies have demonstrated the therapeutic potential of PAR in different *in vivo* models of pathological bone loss, including LPS-induced osteolysis, ovariectomy-induced bone loss and collagen-induced arthritis (CIA) models (77, 80, 81). In our murine model of CAIA (Chapter 4), PAR was found to reduce paw inflammation when administered at both 1 mg/kg and 4 mg/kg. However, with no observable difference in the suppression of inflammation between the two doses. Interestingly, PAR treatment did not reduce paw inflammation in the hind paws of CAIA mice. This was unexpected as previous studies have confirmed the anti-inflammatory effects of low dose (1 mg/kg) PAR (81, 82). This could therefore be attributed to the variability in the development of local paw inflammation in response to induction of mild CAIA, as previously discussed throughout this thesis (Chapter 2-5).

Despite reductions in inflammation, Liu *et al.* 2015, found that there was no clear effect on bone erosion at the site of the inflamed joints or on generalised osteopenia following NF-κB suppression by PAR (81). Consistent with this, the present study (Chapter 4) also found PAR to reduce local inflammation with no change in overall BV. This suggests that the mild inhibitory effect of low dose (1-4 mg/kg) PAR on inflammation is insufficient to inhibit the subsequent effect inflammation has on bone erosion. In the current study (Chapter 4), activation of the NF-κB signalling pathway was not directly measured in paw tissue, as such, it was not confirmed in this model as to whether PAR reached the synovial joints to actively suppress NF-κB when delivered via intraperitoneal injection. Further *in vitro* and *in vivo* studies could assess the pharmacodynamics of PAR further, as well as the phosphorylation of proteins involved in the NF-κB pathway to identify if PAR is capable of actively suppressing NF-κB in osteoclasts at the site of local paw inflammation. Additionally, assessment of surface bone resorption pits in the front and hind paws, may yield information around significant effects of PAR treatment on the suppression of bone resorption itself.

6.2.3.2. Inhibition of N-cadherin in the mild CAIA mouse model

Cell adhesion molecules, including N-cadherin, play crucial roles in perpetuating inflammatory cell infiltration, pannus formation and joint destruction in the synovial

joints of RA patients (31, 83-85). The role of cell adhesion molecules, specifically N-cadherin, in osteoclast formation and activity *in vitro* and in the context of RA *in vivo* has not been investigated. This study (Chapter 3) was the first to investigate inhibition of N-cadherin, using the novel N-cadherin antagonist CRS-066 in the CAIA murine model. The results (Chapter 3) suggest suppression of N-cadherin through topical application of CRS-066 may have potential benefit in reducing local inflammation. However, similar to other studies in this thesis (Chapter 2 and 4), suppression of inflammation occurred with no overall effect on BV, when assessed by high resolution micro-CT. In contrast, histological analysis of bone in this study showed a reduction in histologically assessed bone destruction, as well as, reduction in the presence of multinucleated TRAP positive cells in CRS-066 treated paws in comparison to vehicle treated internal-control paws. This suggests inhibition of N-cadherin by CRS-066 may modulate osteoclast formation and activity in synovial joints of CAIA mice. However, the specific effects of CRS-066 on N-cadherin expression was not directly measured in paw tissue. Thus, the penetrance and mechanism of action following topical application could not be confirmed. Further preclinical investigations into the specific role of N-cadherin in osteoclast formation in both normal physiological and pathological conditions, are needed to further elucidate the pharmacodynamic properties of CRS-066 *in vitro* and *in vivo*.

Interestingly, despite CRS-066 reducing local inflammation throughout the CAIA model, paw volume at end point was higher in CRS-066 treated right paws in comparison to the vehicle treated left paw of the same mouse. This could be attributed to factors such as variability in animal response to mild CAIA discussed throughout this thesis (Chapters 2-5), and the small animal number used. CRS-066 (Chapter 3) was administered topically as it is a favoured route for the local delivery of therapeutic compounds, due to its convenience, affordability and direct action at the site of injury (86). However, there are considerable challenges with topical administration of compounds, including achieving optimal concentration of the compound at the site of action and selecting an appropriate soluble drug carrier. As this is the first *in vivo* study investigating CRS-066 there are currently limited known drug carriers for which this compound can be applied. Thus, in this study (Chapter 3), CRS-066 was applied topically using 100% dimethyl sulfoxide (DMSO) as the drug carrier, due to the compound not being water soluble and the beneficial effects of DMSO enhancing the transport and penetration of compounds into

the blood (87, 88). However, recently, *in vitro* and *in vivo* studies have reported safety concerns and toxic effects of DMSO at concentrations greater than 10% (89-91). Thus, the potential effects of CRS-066 on inflammation and the resulting bone destruction may have been confounded using DMSO as the drug carrier. This was further supported by the vehicle treated CAIA group, as inflammation was exacerbated following topical application of DMSO alone. Based on these findings, extensive investigations are required to develop a potential drug delivery system for CRS-066 and other N-cadherin antagonists, aiming to improve its efficacy as well as reducing the confounding effects of DMSO in the complex *in vivo* environment of inflammatory arthritis.

6.2.3.3. Pharmacological modulation of autophagy and apoptosis in in vitro and in vivo models

Numerous studies support the inverse relationship between autophagy and apoptosis in RA (92, 93). However, conflicting evidence (92, 93) justifies the need for further elucidation of this relationship to identify autophagy and apoptosis as novel targets in the treatment of RA. The results of this study (Chapter 2) support a complex relationship between autophagy and apoptosis during inflammatory processes *in vitro*. Initial findings in the studies presented here investigated the effect of the apoptosis inducer Embelin and autophagy inhibitor HCQ in isolation in PBMC-derived osteoclasts. Findings confirmed that inhibition of autophagy through beclin-1 and LC3 suppression, following HCQ treatment, results in reduction of osteoclast formation and activity, in comparison to untreated PBMC-derived osteoclasts. Embelin treatment produced similar effects to HCQ in PBMC-derived osteoclasts *in vitro*, suppressing autophagy and osteoclast related protein expression simultaneously.

Investigation of apoptotic genes is imperative to the investigation of the molecular pathway of both apoptosis and autophagy in RA. Unexpectedly, in this study (Chapter 2) Embelin did not increase the expression of apoptotic factors at the gene level. Analysis of gene expression by real-time polymerase chain reaction (RT PCR), although sensitive, is inadequate for detecting end stage apoptosis when cells have undergone morphological changes (94). Therefore, in combination to RT PCR analysis, terminal deoxynucleotidyl transferase nick-end labelling (TUNEL) staining was conducted as a reliable and

representative assessment of apoptosis (95, 96). Thus, in this study (Chapter 2), Embelin treatment increased the number of TUNEL positive PBMC-derived osteoclasts. In conjunction with the suppression of autophagy and osteoclastogenesis, these findings support the inverse relationship between autophagy and apoptosis in PBMC-derived osteoclasts *in vitro*. These initial findings were then extended by assessing Embelin and HCQ as both single and combination therapies *in vivo*. However, pharmacological modulation of these processes did not result in the suppression of local paw inflammation or bone destruction in the mild CAIA mouse model.

The expected synergistic effect of the combined treatment of Embelin (30 mg/kg/day) and HCQ (40 mg/kg/day) on apoptosis was not observed *in vivo* (Chapter 2). Nor were the anti-catabolic actions of HCQ observed in CAIA mice as inflammation and bone destruction was not suppressed following treatment with HCQ. Embelin as a single treatment did not inhibit local paw inflammation or bone destruction in CAIA mice in this study (Chapter 2). Embelin initially reduced local paw inflammation from day 4-5, however when arthritis paw swelling reached peak severity at day 6-8, Embelin had no further effect on paw inflammation and had no observable effect on BV as assessed by end point micro-CT analysis. This was not consistent with our *in vitro* findings nor previous studies within our laboratory, where significant reductions in local paw inflammation were observed following treatment with 30 mg/kg Embelin (33). This could again be attributed to the large mouse variability in response to mild CAIA as discussed throughout this thesis (Chapter 2-5) and the small animal number used.

As previously discussed, the combination of Embelin and HCQ did not suppress inflammation or bone destruction in the mild CAIA model (Chapter 2). However, the combination of Embelin and HCQ did increase the expression of TUNEL positive cells in the radiocarpal joint of CAIA mice. This supports *in vitro* analyses and suggests these treatments can induce apoptosis in cells located in the synovial joints of CAIA mice. However, due to the vast array of cells infiltrating the synovial joints, it could not be confirmed which specific cell population was undergoing apoptosis and thus it can not be assumed that inflammation and bone destruction will resolve following the death of these TUNEL positive cells. Thus, future investigations should include dual-staining

techniques to identify which specific cell subsets are targeted by Embelin and/or HCQ *in vivo* to elucidate their targeted effects further.

In this study (Chapter 2), LC3 expression was observed in the articular cartilage of the radiocarpal joint of CAIA mice, supporting a strong association with LC3 positivity and the occurrence of the disease. Although LC3 expression was reduced following HCQ and Embelin treatment *in vitro* (Chapter 2), there was no change in LC3 expression in the articular cartilage in CAIA mice following single or combination treatment. We were unable to distinguish between cytosolic (LC3 I) and membrane bound (LC3 II) forms of LC3 and thus could not assess the change in autophagy flux following treatment both *in vitro* and *in vivo*. This supports the need for further investigation on the dual role of LC3 as a cytoprotective or cell-death associated contributor in cartilage destruction and osteoclastogenesis during pathological conditions such as RA. Nevertheless, results in this study (Chapter 2), elucidate the complex role of apoptosis and autophagy in the pathogenesis of RA and support further investigations into other novel compounds that may have the potential to target these pathways specifically in osteoclasts and inflammatory cells to suppress inflammation and bone destruction in RA.

6.3. Thesis Conclusion

In summary, the studies presented here confirm the hypothesis that autophagy and apoptosis pathways are key modulators of inflammation and osteoclast activity in RA (Chapter 2), and their selective inhibition may be an effective target for the development of novel compounds. In addition, the results of this thesis suggest that targeting cell adhesion molecules (Chapter 3) and NF-κB intracellular signalling (Chapter 4) have the potential to reduce inflammation and its subsequent bone destruction in models of inflammatory arthritis. However, the results further highlight the complex mechanisms associated with the progression of bone destruction and RA specific pain in murine models of inflammatory arthritis (Chapter 4 and 5). Furthermore, the mild CAIA mouse model did not accurately or consistently recapitulate pathogenic features of RA in Balb/c mice (Chapter 2-5). Therefore, future investigations should utilise a more moderate or severe CAIA model in addition to the findings produced from this thesis, to further elucidate the role of these key factors in the pathogenesis of RA as potential targets for therapeutic intervention in inflammation induced bone loss.

6.4. References

1. Lerner UH. Osteoclast formation and resorption. Matrix biology : journal of the International Society for Matrix Biology. 2000;19(2):107-20.

2. Parfitt AM. Osteonal and hemi-osteonal remodeling: the spatial and temporal framework for signal traffic in adult human bone. Journal of cellular biochemistry. 1994;55(3):273-86.

3. Burmester GR, Feist E, Dorner T. Emerging cell and cytokine targets in rheumatoid arthritis. Nature reviews Rheumatology. 2014;10(2):77-88.

4. Lorenzo J, Horowitz M, Choi Y. Osteoimmunology: interactions of the bone and immune system. Endocrine reviews. 2008;29(4):403-40.

5. Rho J, Takami M, Choi Y. Osteoimmunology: interactions of the immune and skeletal systems. Molecules and cells. 2004;17(1):1-9.

6. Takayanagi H. Osteoimmunology: shared mechanisms and crosstalk between the immune and bone systems. Nature reviews Immunology. 2007;7(4):292-304.

7. Takayanagi H. Mechanistic insight into osteoclast differentiation in osteoimmunology. Journal of molecular medicine (Berlin, Germany). 2005;83(3):170-9.

8. Crotti T, Smith MD, Hirsch R, Soukoulis S, Weedon H, Capone M, et al. Receptor activator NF kappaB ligand (RANKL) and osteoprotegerin (OPG) protein expression in periodontitis. Journal of periodontal research. 2003;38(4):380-7.

9. Crotti TN, Ahern MJ, Lange K, Weedon H, Coleman M, Roberts-Thomson PJ, et al. Variability of RANKL and osteoprotegerin staining in synovial tissue from patients with active rheumatoid arthritis: quantification using color video image analysis. The Journal of rheumatology. 2003;30(11):2319-24.

10. Haynes DR. Emerging and future therapies for the treatment of bone loss associated with chronic inflammation. Inflammopharmacology. 2006;14(5-6):193-7.

11. Romas E, Gillespie MT, Martin TJ. Involvement of receptor activator of NFkappaB ligand and tumor necrosis factor-alpha in bone destruction in rheumatoid arthritis. Bone. 2002;30(2):340-6.

12. Haynes DR, Barg E, Crotti TN, Holding C, Weedon H, Atkins GJ, et al. Osteoprotegerin expression in synovial tissue from patients with rheumatoid

arthritis, spondyloarthropathies and osteoarthritis and normal controls. Rheumatology (Oxford, England). 2003;42(1):123-34.

13. Quinn JM, Horwood NJ, Elliott J, Gillespie MT, Martin TJ. Fibroblastic stromal cells express receptor activator of NF-kappa B ligand and support osteoclast differentiation. Journal of bone and mineral research : the official journal of the American Society for Bone and Mineral Research. 2000;15(8):1459-66.

14. Braun T, Zwerina J. Positive regulators of osteoclastogenesis and bone resorption in rheumatoid arthritis. Arthritis research & therapy. 2011;13(4):235.

15. McInnes IB, Schett G. The pathogenesis of rheumatoid arthritis. The New England journal of medicine. 2011;365(23):2205-19.

16. Redlich K, Smolen JS. Inflammatory bone loss: pathogenesis and therapeutic intervention. Nature reviews Drug discovery. 2012;11(3):234-50.

17. Kidd BL, Urban LA. Mechanisms of inflammatory pain. British journal of anaesthesia. 2001;87(1):3-11.

18. Schaible HG, Ebersberger A, Von Banchet GS. Mechanisms of pain in arthritis. Annals of the New York Academy of Sciences. 2002;966:343-54.

19. Lee YC, Cui J, Lu B, Frits ML, Iannaccone CK, Shadick NA, et al. Pain persists in DAS28 rheumatoid arthritis remission but not in ACR/EULAR remission: a longitudinal observational study. Arthritis research & therapy. 2011;13(3):R83.

20. Bas DB, Su J, Sandor K, Agalave NM, Lundberg J, Codeluppi S, et al. Collagen antibody-induced arthritis evokes persistent pain with spinal glial involvement and transient prostaglandin dependency. Arthritis and rheumatism. 2012;64(12):3886-96.

21. McWilliams DF, Walsh DA. Pain mechanisms in rheumatoid arthritis. Clinical and experimental rheumatology. 2017;35 Suppl 107(5):94-101.

22. Wolfe F, Michaud K. Assessment of pain in rheumatoid arthritis: minimal clinically significant difference, predictors, and the effect of anti-tumor necrosis factor therapy. The Journal of rheumatology. 2007;34(8):1674-83.

23. Doan T, Massarotti E. Rheumatoid arthritis: an overview of new and emerging therapies. Journal of clinical pharmacology. 2005;45(7):751-62.

24. Hoff M, Kvien TK, Kalvesten J, Elden A, Haugeberg G. Adalimumab therapy reduces hand bone loss in early rheumatoid arthritis: explorative analyses from the PREMIER study. Annals of the rheumatic diseases. 2009;68(7):1171-6.

25. Leffler AS, Kosek E, Lerndal T, Nordmark B, Hansson P. Somatosensory perception and function of diffuse noxious inhibitory controls (DNIC) in patients suffering from rheumatoid arthritis. European journal of pain (London, England). 2002;6(2):161-76.

26. Jimi E, Ikebe T, Takahashi N, Hirata M, Suda T, Koga T. Interleukin-1 alpha activates an NF-kappaB-like factor in osteoclast-like cells. The Journal of biological chemistry. 1996;271(9):4605-8.

27. Schett G. Erosive arthritis. Arthritis research & therapy. 2007;9 Suppl 1:S2.

28. Xu J, Wu HF, Ang ES, Yip K, Woloszyn M, Zheng MH, et al. NF-kappaB modulators in osteolytic bone diseases. Cytokine & growth factor reviews. 2009;20(1):7-17.

29. Larue L, Antos C, Butz S, Huber O, Delmas V, Dominis M, et al. A role for cadherins in tissue formation. Development (Cambridge, England). 1996;122(10):3185-94.

30. Dharmapatni AA, Smith MD, Findlay DM, Holding CA, Evdokiou A, Ahern MJ, et al. Elevated expression of caspase-3 inhibitors, survivin and xIAP correlates with low levels of apoptosis in active rheumatoid synovium. Arthritis research & therapy. 2009;11(1):R13.

31. Shin CS, Her SJ, Kim JA, Kim DH, Kim SW, Kim SY, et al. Dominant negative N-cadherin inhibits osteoclast differentiation by interfering with beta-catenin regulation of RANKL, independent of cell-cell adhesion. Journal of bone and mineral research : the official journal of the American Society for Bone and Mineral Research. 2005;20(12):2200-12.

32. Korb A, Pavenstadt H, Pap T. Cell death in rheumatoid arthritis. Apoptosis : an international journal on programmed cell death. 2009;14(4):447-54.

33. Dharmapatni AA, Cantley MD, Marino V, Perilli E, Crotti TN, Smith MD, et al. The X-Linked Inhibitor of Apoptosis Protein Inhibitor Embelin Suppresses Inflammation and Bone Erosion in Collagen Antibody Induced Arthritis Mice. Mediators Inflamm. 2015;2015:564042.

34. Reuter S, Prasad S, Phromnoi K, Kannappan R, Yadav VR, Aggarwal BB. Embelin suppresses osteoclastogenesis induced by receptor activator of NF-kappaB ligand and tumor cells in vitro through inhibition of the NF-kappaB cell signaling pathway. Molecular cancer research : MCR. 2010;8(10):1425-36.

35.   Boyce BF, Xiu Y, Li J, Xing L, Yao Z. NF-kappaB-Mediated Regulation of Osteoclastogenesis. Endocrinology and metabolism (Seoul, Korea). 2015;30(1):35-44.

36.   Lin NY, Beyer C, Giessl A, Kireva T, Scholtysek C, Uderhardt S, et al. Autophagy regulates TNFalpha-mediated joint destruction in experimental arthritis. Annals of the rheumatic diseases. 2013;72(5):761-8.

37.   Williams B, Tsangari E, Stansborough R, Marino V, Cantley M, Dharmapatni A, et al. Mixed effects of caffeic acid phenethyl ester (CAPE) on joint inflammation, bone loss and gastrointestinal inflammation in a murine model of collagen antibody-induced arthritis. Inflammopharmacology. 2017;25(1):55-68.

38.   Khachigian LM. Collagen antibody-induced arthritis. Nature protocols. 2006;1(5):2512-6.

39.   Cantley MD, Haynes DR, Marino V, Bartold PM. Pre-existing periodontitis exacerbates experimental arthritis in a mouse model. Journal of clinical periodontology. 2011;38(6):532-41.

40.   Oestergaard S, Rasmussen KE, Doyle N, Varela A, Chouinard L, Smith SY, et al. Evaluation of cartilage and bone degradation in a murine collagen antibody-induced arthritis model. Scandinavian journal of immunology. 2008;67(3):304-12.

41.   Perilli E, Cantley M, Marino V, Crotti TN, Smith MD, Haynes DR, et al. Quantifying not only bone loss, but also soft tissue swelling, in a murine inflammatory arthritis model using micro-computed tomography. Scandinavian journal of immunology. 2015;81(2):142-50.

42.   Zawawi MS, Marino V, Perilli E, Cantley MD, Xu J, Purdue PE, et al. Parthenolide reduces empty lacunae and osteoclastic bone surface resorption induced by polyethylene particles in a murine calvarial model of peri-implant osteolysis. Journal of biomedical materials research Part A. 2015;103(11):3572-9.

43.   Heiberg T, Kvien TK. Preferences for improved health examined in 1,024 patients with rheumatoid arthritis: pain has highest priority. Arthritis and rheumatism. 2002;47(4):391-7.

44.   Christianson CA, Corr M, Firestein GS, Mobargha A, Yaksh TL, Svensson CI. Characterization of the acute and persistent pain state present in K/BxN serum transfer arthritis. Pain. 2010;151(2):394-403.

45.   von Banchet GS, Petrow PK, Brauer R, Schaible HG. Monoarticular antigen-induced arthritis leads to pronounced bilateral upregulation of the expression of neurokinin 1 and bradykinin 2 receptors in dorsal root ganglion neurons of rats. Arthritis research. 2000;2(5):424-7.

46.   Chaplan SR, Bach FW, Pogrel JW, Chung JM, Yaksh TL. Quantitative assessment of tactile allodynia in the rat paw. Journal of neuroscience methods. 1994;53(1):55-63.

47.   Parvathy SS, Masocha W. Gait analysis of C57BL/6 mice with complete Freund's adjuvant-induced arthritis using the CatWalk system. BMC musculoskeletal disorders. 2013;14:14.

48.   Hoffmann MH, Hopf R, Niederreiter B, Redl H, Smolen JS, Steiner G. Gait changes precede overt arthritis and strongly correlate with symptoms and histopathological events in pristane-induced arthritis. Arthritis research & therapy. 2010;12(2):R41.

49.   Bas DB, Su J, Wigerblad G, Svensson CI. Pain in rheumatoid arthritis: models and mechanisms. Pain management. 2016;6(3):265-84.

50.   Mogil JS. Animal models of pain: progress and challenges. Nature reviews Neuroscience. 2009;10(4):283-94.

51.   Bove G. Mechanical sensory threshold testing using nylon monofilaments: the pain field's "tin standard". Pain. 2006;124(1-2):13-7.

52.   Chesler EJ, Wilson SG, Lariviere WR, Rodriguez-Zas SL, Mogil JS. Identification and ranking of genetic and laboratory environment factors influencing a behavioral trait, thermal nociception, via computational analysis of a large data archive. Neuroscience and biobehavioral reviews. 2002;26(8):907-23.

53.   Bonin RP, Bories C, De Koninck Y. A simplified up-down method (SUDO) for measuring mechanical nociception in rodents using von Frey filaments. Molecular pain. 2014;10:26.

54.   Sorge RE, Martin LJ, Isbester KA, Sotocinal SG, Rosen S, Tuttle AH, et al. Olfactory exposure to males, including men, causes stress and related analgesia in rodents. Nature methods. 2014;11(6):629-32.

55.   Lavery LA, Lavery DE, Lavery DC, Lafontaine J, Bharara M, Najafi B. Accuracy and durability of Semmes-Weinstein monofilaments: what is the useful service life? Diabetes research and clinical practice. 2012;97(3):399-404.

56. Del Valle ME, Cobo T, Cobo JL, Vega JA. Mechanosensory neurons, cutaneous mechanoreceptors, and putative mechanoproteins. Microscopy research and technique. 2012;75(8):1033-43.

57. Andrews K. The effect of changes in temperature and humidity on the accuracy of von Frey hairs. Journal of neuroscience methods. 1993;50(1):91-3.

58. Moller KA, Johansson B, Berge OG. Assessing mechanical allodynia in the rat paw with a new electronic algometer. Journal of neuroscience methods. 1998;84(1-2):41-7.

59. Massy-Westropp N. The effects of normal human variability and hand activity on sensory testing with the full Semmes-Weinstein monofilaments kit. Journal of hand therapy : official journal of the American Society of Hand Therapists. 2002;15(1):48-52.

60. Martinov T, Mack M, Sykes A, Chatterjea D. Measuring changes in tactile sensitivity in the hind paw of mice using an electronic von Frey apparatus. Journal of visualized experiments : JoVE. 2013(82):e51212.

61. Cunha TM, Verri WA, Jr., Vivancos GG, Moreira IF, Reis S, Parada CA, et al. An electronic pressure-meter nociception paw test for mice. Brazilian journal of medical and biological research = Revista brasileira de pesquisas medicas e biologicas. 2004;37(3):401-7.

62. Wallas TR, Winterson BJ, Ransil BJ, Bove GM. Paw withdrawal thresholds and persistent hindlimb flexion in experimental mononeuropathies. The journal of pain : official journal of the American Pain Society. 2003;4(4):222-30.

63. Vivancos GG, Verri WA, Jr., Cunha TM, Schivo IR, Parada CA, Cunha FQ, et al. An electronic pressure-meter nociception paw test for rats. Brazilian journal of medical and biological research = Revista brasileira de pesquisas medicas e biologicas. 2004;37(3):391-9.

64. Vrinten DH, Hamers FF. 'CatWalk' automated quantitative gait analysis as a novel method to assess mechanical allodynia in the rat; a comparison with von Frey testing. Pain. 2003;102(1-2):203-9.

65. Kang DW, Choi JG, Moon JY, Kang SY, Ryu Y, Park JB, et al. Automated Gait Analysis in Mice with Chronic Constriction Injury. Journal of visualized experiments : JoVE. 2017(128).

66.   Lakes EH, Allen KD. Gait analysis methods for rodent models of arthritic disorders: reviews and recommendations. Osteoarthritis and cartilage. 2016;24(11):1837-49.

67.   Angeby Moller K, Svard H, Suominen A, Immonen J, Holappa J, Stenfors C. Gait analysis and weight bearing in pre-clinical joint pain research. Journal of neuroscience methods. 2018;300:92-102.

68.   Bradman MJ, Ferrini F, Salio C, Merighi A. Practical mechanical threshold estimation in rodents using von Frey hairs/Semmes-Weinstein monofilaments: Towards a rational method. Journal of neuroscience methods. 2015;255:92-103.

69.   Hirotani H, Tuohy NA, Woo JT, Stern PH, Clipstone NA. The calcineurin/nuclear factor of activated T cells signaling pathway regulates osteoclastogenesis in RAW264.7 cells. The Journal of biological chemistry. 2004;279(14):13984-92.

70.   Kim N, Takami M, Rho J, Josien R, Choi Y. A novel member of the leukocyte receptor complex regulates osteoclast differentiation. The Journal of experimental medicine. 2002;195(2):201-9.

71.   Blair HC, Robinson LJ, Zaidi M. Osteoclast signalling pathways. Biochemical and biophysical research communications. 2005;328(3):728-38.

72.   Kong YY, Feige U, Sarosi I, Bolon B, Tafuri A, Morony S, et al. Activated T cells regulate bone loss and joint destruction in adjuvant arthritis through osteoprotegerin ligand. Nature. 1999;402(6759):304-9.

73.   Gravallese EM, Harada Y, Wang JT, Gorn AH, Thornhill TS, Goldring SR. Identification of cell types responsible for bone resorption in rheumatoid arthritis and juvenile rheumatoid arthritis. The American journal of pathology. 1998;152(4):943-51.

74.   Clohisy JC, Roy BC, Biondo C, Frazier E, Willis D, Teitelbaum SL, et al. Direct inhibition of NF-kappa B blocks bone erosion associated with inflammatory arthritis. Journal of immunology (Baltimore, Md : 1950). 2003;171(10):5547-53.

75.   Zou W, Amcheslavsky A, Takeshita S, Drissi H, Bar-Shavit Z. TNF-alpha expression is transcriptionally regulated by RANK ligand. Journal of cellular physiology. 2005;202(2):371-8.

76.   Bharti AC, Takada Y, Aggarwal BB. Curcumin (diferuloylmethane) inhibits receptor activator of NF-kappa B ligand-induced NF-kappa B activation in osteoclast precursors and suppresses osteoclastogenesis. Journal of immunology (Baltimore, Md : 1950). 2004;172(10):5940-7.

77.   Yip KH, Zheng MH, Feng HT, Steer JH, Joyce DA, Xu J. Sesquiterpene lactone parthenolide blocks lipopolysaccharide-induced osteolysis through the suppression of NF-kappaB activity. Journal of bone and mineral research : the official journal of the American Society for Bone and Mineral Research. 2004;19(11):1905-16.

78.   Ichikawa H, Takada Y, Shishodia S, Jayaprakasam B, Nair MG, Aggarwal BB. Withanolides potentiate apoptosis, inhibit invasion, and abolish osteoclastogenesis through suppression of nuclear factor-kappaB (NF-kappaB) activation and NF-kappaB-regulated gene expression. Molecular cancer therapeutics. 2006;5(6):1434-45.

79.   Shishodia S, Gutierrez AM, Lotan R, Aggarwal BB. N-(4-hydroxyphenyl)retinamide inhibits invasion, suppresses osteoclastogenesis, and potentiates apoptosis through down-regulation of I(kappa)B(alpha) kinase and nuclear factor-kappaB-regulated gene products. Cancer research. 2005;65(20):9555-65.

80.   Idris AI, Krishnan M, Simic P, Landao-Bassonga E, Mollat P, Vukicevic S, et al. Small molecule inhibitors of IkappaB kinase signaling inhibit osteoclast formation in vitro and prevent ovariectomy-induced bone loss in vivo. FASEB journal : official publication of the Federation of American Societies for Experimental Biology. 2010;24(11):4545-55.

81.   Liu Q, Zhao J, Tan R, Zhou H, Lin Z, Zheng M, et al. Parthenolide inhibits pro-inflammatory cytokine production and exhibits protective effects on progression of collagen-induced arthritis in a rat model. Scandinavian journal of rheumatology. 2015;44(3):182-91.

82.   Parada-Turska J, Mitura A, Brzana W, Jablonski M, Majdan M, Rzeski W. Parthenolide inhibits proliferation of fibroblast-like synoviocytes in vitro. Inflammation. 2008;31(4):281-5.

83.   Marie PJ, Hay E, Modrowski D, Revollo L, Mbalaviele G, Civitelli R. Cadherin-mediated cell-cell adhesion and signaling in the skeleton. Calcified tissue international. 2014;94(1):46-54.

84.   Castro CH, Shin CS, Stains JP, Cheng SL, Sheikh S, Mbalaviele G, et al. Targeted expression of a dominant-negative N-cadherin in vivo delays peak bone mass and increases adipogenesis. Journal of cell science. 2004;117(Pt 13):2853-64.

85.   Di Benedetto A, Watkins M, Grimston S, Salazar V, Donsante C, Mbalaviele G, et al. N-cadherin and cadherin 11 modulate postnatal bone growth and osteoblast differentiation by distinct mechanisms. Journal of cell science. 2010;123(Pt 15):2640-8.

86.   Singh Malik D, Mital N, Kaur G. Topical drug delivery systems: a patent review. Expert opinion on therapeutic patents. 2016;26(2):213-28.

87.   Capriotti K, Capriotti JA. Dimethyl sulfoxide: history, chemistry, and clinical utility in dermatology. The Journal of clinical and aesthetic dermatology. 2012;5(9):24-6.

88.   Marren K. Dimethyl sulfoxide: an effective penetration enhancer for topical administration of NSAIDs. The Physician and sportsmedicine. 2011;39(3):75-82.

89.   Rosenblum WI, Wei EP, Kontos HA. Dimethylsulfoxide and ethanol, commonly used diluents, prevent dilation of pial arterioles by openers of K(ATP) ion channels. European journal of pharmacology. 2001;430(1):101-6.

90.   Fossum EN, Lisowski MJ, Macey TA, Ingram SL, Morgan MM. Microinjection of the vehicle dimethyl sulfoxide (DMSO) into the periaqueductal gray modulates morphine antinociception. Brain research. 2008;1204:53-8.

91.   Galvao J, Davis B, Tilley M, Normando E, Duchen MR, Cordeiro MF. Unexpected low-dose toxicity of the universal solvent DMSO. FASEB journal : official publication of the Federation of American Societies for Experimental Biology. 2014;28(3):1317-30.

92.   Xu K, Xu P, Yao JF, Zhang YG, Hou WK, Lu SM. Reduced apoptosis correlates with enhanced autophagy in synovial tissues of rheumatoid arthritis. Inflamm Res. 2013;62(2):229-37.

93.   Yang Z, Fujii H, Mohan SV, Goronzy JJ, Weyand CM. Phosphofructokinase deficiency impairs ATP generation, autophagy, and redox balance in rheumatoid arthritis T cells. The Journal of experimental medicine. 2013;210(10):2119-34.

94.   Elmore S. Apoptosis: a review of programmed cell death. Toxicologic pathology. 2007;35(4):495-516.

95.   Kerr JF, Wyllie AH, Currie AR. Apoptosis: a basic biological phenomenon with wide-ranging implications in tissue kinetics. British journal of cancer. 1972;26(4):239-57.

96.   Taatjes DJ, Sobel BE, Budd RC. Morphological and cytochemical determination of cell death by apoptosis. Histochemistry and cell biology. 2008;129(1):33-43.

APPENDIX I: CHAPTER 2 SUPPLEMENTAL DATA

Chapter 2: Pharmacological modulation of autophagy and apoptosis in PBMC-derived osteoclasts and a mouse model of inflammatory arthritis

B. Williams, H. Kamiakahara, K. Algate, F. Najimi, E. Tsangari, S. Chaudary, E. Perilli, D.R. Haynes, T.N. Crotti, A. Dharmapatni

Appendix I contains supplemental data that is referred to throughout Chapter 2 and has been included within the manuscript submission for publication in Bone.

Supplemental Table 1. Proportion of positive and negative LC3 stained sections of the radiocarpal joint.

| GROUP	LC3 POSITIVE	LC3 NEGATIVE	TOTAL
CONTROL	1	9	10
CAIA	8	3	11
CAIA+EMBELIN	11	1	12
CAIA+HCQ	9	3	12
CAIA+EMBELIN+HCQ	12	0	12
TOTAL	41	16	57

Supplemental Table 2. Difference in the proportion of positive and negative LC3 stained sections of the radiocarpal joint.

	DF	X^2	P-VALUE
CONTROL VS. CAIA	1	8.01	0.0047
CONTROL VS. CAIA + EMBELIN	1	13.98	0.0002
CONTROL VS. CAIA + HCQ	1	10.31	0.0013
CONTROL VS. CAIA + EMBELIN + HCQ	1	17.40	<0.0001
CAIA VS. CAIA + EMBELIN	1	1.38	0.2402
CAIA VS. CAIA + HCQ	1	0.25	0.6189
CAIA VS. CAIA + EMBELIN+HCQ	1	3.57	0.0590
CAIA + EMBELIN VS. CAIA + HCQ	1	0.48	0.4909
CAIA + EMBELIN VS. CAIA + EMBELIN + HCQ	1	0.96	0.3270
CAIA + HCQ VS. CAIA + EMBELIN + HCQ	1	2.25	0.1335

Chi squared analysis of the proportion of positive LC3 stained sections of the radiocarpal joints in all groups.

A p-value less than 0.05 was considered statistically significant. DF; degree of freedom.

Supplemental Figure 1:
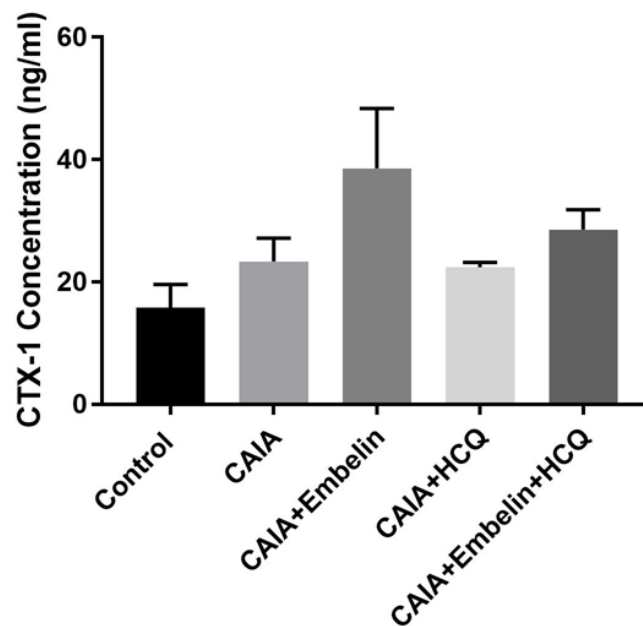
Supplemental Figure 1. Serum CTX-1 (ng/ml) concentration as a measure of systemic bone resorption. Error bars represent standard error of the mean (SEM; n = 6).

C-terminal telopeptide (CTX-1) levels were assessed in serum collected from mice 10 days after arthritis induction as a marker of bone resorption. A RatLaps CTX-1 ELISA kit (Immunodiagnostics Systems, Nordic) was used following the manufacturer's instructions. CTX-1 levels did not differ significantly between groups at day 10. Although not statistically significant, average CTX-1 levels were found to be highest in CAIA + Embelin mice (49.4 ng/ml).

APPENDIX II: PUBLISHED MANUSCRIPTS AS PDFS ARISING FROM THIS THESIS

REVIEW

CrossMark

Intracellular apoptotic pathways: a potential target for reducing joint damage in rheumatoid arthritis

Bonnie Williams[1] · Anak Dharmapatni[1] · Tania Crotti[1]

Abstract

Rheumatoid arthritis (RA) is a chronic autoimmune inflammatory disease that results in both local and systemic bone erosion, causing significant joint deformities and functional disability. The increased number of synovial fibroblasts, inflammatory cells and osteoclasts in RA is associated with reduced apoptosis in these cells. The ability to modulate the cell proliferation or death (particularly apoptosis) is recognised for its immense therapeutic potential. Identifying new therapeutics to assist in stimulating apoptosis within the synovial joints therefore may be beneficial in reducing inflammation and bone loss in RA patients. In this review, the roles of anti-apoptotic proteins that are upregulated in RA synovial joints will be discussed in relation to their actions on bone destruction and inflammation. Evidence recently published suggests that intracellular apoptotic inhibitory molecules can be targeted by current or new therapeutics to reduce joint damage in RA. However, the therapeutics that target these molecules are yet to reach clinical trial stages. Even so it is evident that understanding the upregulation of anti-apoptotic molecules in RA is required to improve treatments currently available for RA patients.

Abbreviations

AIA	Adjuvant-induced arthritis
AIF	Apoptosis-inducing factor
BIR	Baculovirus inhibitor of apoptosis protein repeats
CAIA	Collagen antibody-induced arthritis
DISC	Death-inducing signalling complex
DMARDs	Disease-modifying anti-rheumatic drugs
FADD	Fas-associated death domain
FLS	Fibroblast-like synoviocytes
FLIP	FLICE-like inhibitory protein
IL	Interleukins
IAP	Inhibitor of apoptosis proteins
NF-κB	Nuclear factor-kappa B
PAPR	Poly ADP-ribose polymerase
RA	Rheumatoid arthritis
RANK	Receptor activator of NF-κB
RANKL	Receptor activator of NF-κB ligand
RIP	Receptor-interacting protein
SMAC	Second mitochondrial activator of caspases
TRAIL	Tumour necrosis factor-related apoptosis-inducing ligand
TRAP	Tartrate-resistant acid phosphatase
TNF-α	Tumour necrosis factor alpha
TUNEL	Transferase dUTP nick end labelling
TRADD	TNF receptor type-1 associated death domain
XIAP	X-linked inhibitor of apoptosis protein

✉ Bonnie Williams
bonnie.williams@adelaide.edu.au

Anak Dharmapatni
a.dharmapatni@adelaide.edu.au

Tania Crotti
tania.crotti@adelaide.edu.au

[1] Adelaide Medical School, The University of Adelaide, Adelaide, SA, Australia

Introduction

RA is a chronic autoimmune inflammatory disorder affecting approximately 2% of the Australian population [1]. The disease is characterised by synovial hyperplasia, inflammatory cell infiltration in the synovial tissues, invasion of pannus into the adjacent bone and cartilage and focal marginal bone erosion [2]. Joint destruction is associated with chronic

Springer

inflammation combined with destruction of the surface and extracellular matrix of articular cartilage, and erosion of bone [3]. Collectively, these characteristics lead to painful joint deformities and progressive functional disability. The rapid occurrence of joint destruction therefore originates from a close interaction of the inflamed synovial membrane with the cartilage and subchondral bone [4].

Bone remodelling depends on the balance between bone formation carried out by osteoblasts and bone resorption by osteoclasts and an imbalance between these cells has been linked to the development of joint erosion in RA [5]. Osteoclast and osteoblast balance is modulated by intercellular factors which regulate complex intracellular signalling. The main signalling pathway known to mediate bone erosion in RA involves nuclear factor-kappa B (NF-κB) [6]. NF-κB is a transcription factor involved in normal osteoclast differentiation and survival [7]. NF-κB signalling is stimulated by the binding of receptor activator of NF-κB ligand (RANKL) to its receptor RANK on pre-osteoclasts and this ultimately results in the differentiation and activation of osteoclasts [7].

Inflammatory cytokines such as tumour necrosis factor alpha (TNF-α) and interleukins (IL-1β and IL-6) are also significant factors in RA disease progression. Upregulation of inflammatory cytokines occurs due to the infiltration of immune cells in the synovial joints of RA patients [3]. These cytokines not only prolong the inflammatory response, but they have the potential to further promote osteoclast formation in RA by upregulating RANKL and RANK within the synovial joint [3]. This suggests that pro-inflammatory cytokine-mediated osteoclastogenesis occurs in RA joints and may explain the increased formation and/or function of osteoclasts in the synovial joints [8].

More recently characteristic changes of the inflamed synovium in RA have been linked to an altered apoptotic response of synovial and inflammatory cells [9, 10]. Apoptosis is a form of programmed cell death that plays pivotal roles in embryological cell development as well as in physiological cell turnover and homeostatic functioning of the body. However, an imbalance in apoptosis can be a major factor in the development of many human pathological conditions including cancer, neurodegenerative and autoimmune diseases [11–13]. Thus, current research in RA focuses on the idea that the chronic accumulation of inflammatory cells and osteoclasts in RA synovial joints are due to decreased apoptosis. Proteins involved in the apoptotic pathway have been identified as potential targets to modify the pathogenesis of RA. Additionally, these targets may actually be involved in the actions of existing medications or new therapeutics in RA that have not been fully elucidated [14]. Of note, research thus far has focused primarily on the effect of apoptosis in the immune modulation stages of RA disease development. Therefore, this review explores the mechanisms of apoptosis inhibition involved in the effector phase

of RA, specifically joint damage, and how targeting these molecules could potentially prevent the disease progression in RA patients.

Induction of apoptosis by disease-modifying anti-rheumatic drugs (DMARDs)

Current therapies available for RA include non-steroidal anti-inflammatory drugs, corticosteroids and disease-modifying anti-rheumatic drugs (DMARDs) [15]. DMARDs have been shown to reduce the chronic inflammatory infiltrate in the synovial membrane by suppression of lymphocyte proliferation, suppression of neutrophil chemotaxis and inhibition of vascular endothelial cell proliferation [16, 17]. Findings now suggest this reduction in the chronic inflammatory infiltrate by DMARDs could also be due to the modulation of apoptotic pathways. Smith et al. 2010 reported a significant reduction in the expression of FLICE-like inhibitory protein (FLIP), an anti-apoptotic molecule, and Fas, a proapoptotic molecule in the synovial membrane of RA patients who responded to DMARD treatment [18]. DMARD treatment was confirmed to modulate downstream pro- and anti-apoptotic molecules, including caspase 3 and 8, survivin and X-linked inhibitor of apoptosis protein (XIAP) in the synovial membrane [18]. Despite this, there was no statistically significant difference in apoptosis as measured by terminal deoxynucleotidyl transferase dUTP nick end labelling (TUNEL) and poly ADP-ribose polymerase (PARP) expression at baseline and after conventional DMARD treatment in synovial lining macrophages [18]. Although it is possible that the activation of apoptosis pathways with DMARD treatment causes a reduction in inflammatory cell infiltration, it is also possible that the reduced level in apoptosis inhibitors associated with DMARDs could instead be due to the reduction of inflammatory cell infiltrate. This could explain why Smith et al. 2010 did not detect a significant increase in apoptosis in the synovial membrane following DMARD treatment as assessed by TUNEL expression.

Methotrexate, the most commonly used conventional DMARD has been considerably beneficial as a first-line therapy for RA [19]. Methotrexate has been demonstrated to initiate apoptosis in vitro in proliferating monocytic cells and activated T cells isolated from human peripheral blood, as assessed by TUNEL staining and morphological features of cells confirmed by transmission electron microscopy [20]. However, despite the growing evidence that methotrexate can assist in reducing chronic inflammation and bone erosion through initiating apoptosis and other mechanisms, 50% of RA patients are still nonresponsive to this treatment and do not achieve complete remission [19]. Biologic DMARDs, which are often used for patients who do not respond to conventional DMARDs, are not always a viable option due to adverse effects. Thus,

therapies specifically targeting key molecules in the apoptosis pathway may be a rational approach. As the understanding of apoptosis inhibition in RA synovial tissue grows, inhibitory compounds designed to suppress associated apoptotic molecules are being developed. This review aims to address the role of downstream apoptotic molecules as potential targets for RA treatment and to discuss associated compounds currently available in preclinical stage, which may assist in inhibiting these anti-apoptotic molecules.

Apoptosis pathways

Apoptosis is a highly complex process that involves a cascade of molecular events controlled by different genes and molecular mechanisms [21]. The process of apoptosis occurs through two pathways, the extrinsic, or death receptor pathway and the intrinsic, mitochondrial pathway. These pathways both converge at the execution pathway (Fig. 1). There is now growing evidence that in normal physiology these two pathways are linked and molecules in one pathway can influence the other [22].
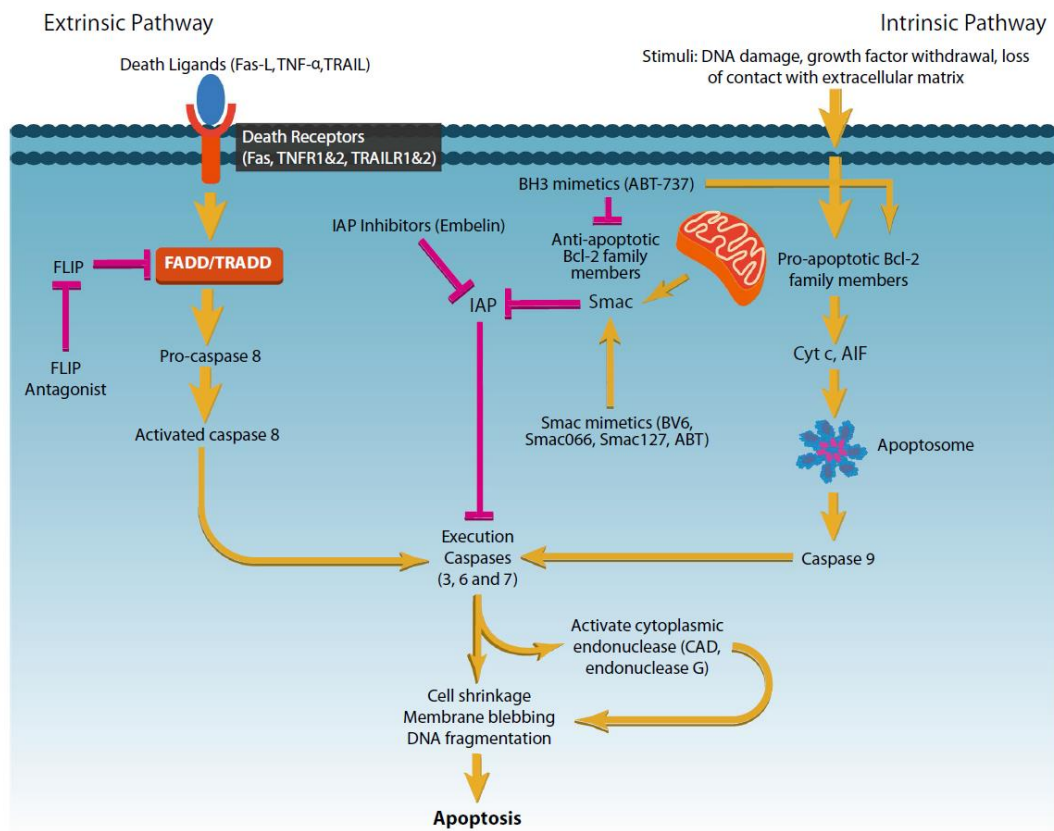

Fig. 1 Proposed influence of antagonists of anti-apoptotic proteins on the extrinsic and intrinsic apoptotic pathways. Schematic diagram of the intrinsic and extrinsic apoptosis pathways. In RA, apoptosis is thought to be inhibited by FLIP, IAP and Bcl-2 proteins. Small molecule forms of these intracellular inhibitory molecules, such as FLIP antagonists, IAP inhibitors, BH3 mimetics and smac mimetics are potential compounds for RA treatment as they can inhibit anti-apoptotic proteins to induce apoptosis. *AIF* apoptosis-inducing factor, *CAD* caspase-activated DNase, *cyt c* cytochrome c, *FADD* Fas-associated death domain, *FasL* Fas ligand, *FLIP* FLICE-like inhibitory protein, *IAP* inhibitor of apoptosis protein, *TNF-α* tumour necrosis factor alpha, *TRADD* TNF receptor type-1 associated death domain protein, *TRAIL* TNF-related apoptosis inducing ligand

Extrinsic pathway of apoptosis

The extrinsic pathway initiates apoptosis through interaction between ligands [such as Fas ligand, TNF-α and tumour necrosis factor-related apoptosis-inducing ligand (TRAIL)] and their transmembrane receptors, which involve death receptors that are members of the TNF receptor gene superfamily (such as Fas, TNFR1 and TRAIL death receptor 1 and 2) [23]. The sequence of events that characterise the extrinsic pathway include clustering of death receptors and binding with a homologous trimeric ligand. As a result, cytoplasmic adapter proteins, which exhibit the corresponding death domains that bind with the death receptors, are recruited. For example, the binding of Fas ligand to Fas receptor results in the binding of Fas-associated death domain (FADD) [24]. FADD then associates with pro-caspase-8 to form a death-inducing signalling complex (DISC) resulting in the activation of pro-caspase-8 [25]. Another example includes the binding of TNF ligand to TNF receptor, which occurs with the recruitment of TNF receptor type 1-associated death domain protein (TRADD) and receptor-interacting protein (RIP) to activate pro-caspase 8 [24]. Following the caspase 8 activation, the execution pathway is activated.

Intrinsic pathway of apoptosis

The intrinsic signalling pathway initiates apoptosis through non-receptor mediated stimuli including DNA damage, growth factor withdrawal or loss of contact with the extracellular matrix. These stimuli produce intracellular signals that act directly in either a positive or negative fashion on specific targets within the cell [22]. Stimulation of this pathway leads to changes in the integrity of the mitochondrial membrane resulting in the loss of mitochondrial transmembrane potential and the release of several pro-apoptotic proteins such as cytochrome c, apoptosis inducing factor (AIF) and second mitochondrial activator of caspases (SMAC) [26]. These proteins activate the caspase-dependent mitochondrial pathway (such as caspase-9) through different mechanisms (Table 1). The control and regulation of these events within the intrinsic pathway is modulated by members of the Bcl-2 family of proteins [27], which regulate cytochrome c release from mitochondria [22].

Execution pathway of apoptosis

The extrinsic and intrinsic signalling pathways converge on the same terminal, known as the execution pathway. This pathway is characterised by the activation of downstream caspases, such as caspase 3, 6 and 7 [28]. Downstream caspases activate cytoplasmic endonuclease (such as caspase-activated DNAse) leads to morphological changes characteristic of apoptosis including; DNA fragmentation, degradation of cytoskeletal and nuclear proteins and formation of apoptotic bodies. The uptake of apoptotic bodies by phagocytic cells is the last step of apoptosis [22].

The role of the intracellular anti-apoptotic molecules for RA pathogenesis

Bcl-2 proteins

Bcl-2 is a family of cytoplasmic proteins that promote cell survival under normal physiological conditions [35]. These proteins are localised to the outer mitochondrial membrane and are essential for preventing apoptosis by maintaining mitochondrial homeostasis [36]. The persistent infiltration of T cells and hyperproliferation of fibroblast-like synoviocytes (FLS) in RA synovium is a hallmark of disease progression. The continuous stimulation of T cells by lymphokines, such as IL-1 or by bi-products of activated fibroblasts can inhibit apoptosis by maintaining high levels of Bcl-2 family proteins specifically Bcl-xL [37]. Increased FLS and inflammatory cell numbers in the RA synovium correlates with an increased expression of the Bcl-2 family of proteins, including Bcl-2, Mcl-1 and Bcl-xL, as well as with synovial lining thickening and the progression of inflammation [38, 39].

The formation of osteoclasts in the RA joint is rapid and triggered by the inflammatory cell influx and continuous

Table 1 Intracellular pro-apoptotic proteins

Protein name	Mechanism to activate intrinsic pathway
Cytochrome C	Binds and activates pro-caspase 9 to form an apoptosome [29]
Bcl-2 family of pro-apoptotic proteins	Regulation of cytochrome c release from the mitochondria
Bcl-10, BAX, BAk, Bid, Bad, Bim, Bik and Blk	Caspase 8 cleavage by Bid to regulate the Fas pathway [30]
	Bad heterodimerize with anti-apoptotic proteins Bcl-xL and Bcl-2 to neutralise their protective effect and promote apoptosis [31]
Second mitochondrial activator of caspase (SMAC)	Promotes apoptosis by inhibiting activity of IAPs [32]
Apoptosis inducing factor (AIF)	DNA fragmentation and condensation of peripheral nuclear chromatin [33]
Caspase-activated DNase (CAD)	Caspase-dependent cleavage of nuclear chromatin to produce oligonucleasomal DNA fragments [34]

production of pro-inflammatory cytokines. Apoptosis in osteoclasts is primarily regulated by the Bcl-2 family of proteins and involves the mitochondrial release of cytochrome c to activate caspase 3 and 9 [22]. As Bcl-xL has been identified to be upregulated in RA synovium and it has been extensively studied in osteoclasts [40]. Zhang et al. 2005 demonstrated that overexpression of Bcl-xL is regulated by NF-κB and this may also contribute to the inhibition of apoptosis in macrophages [41]. The reduction of Bcl-2 proteins led to inhibition of NF-κB and induction of apoptosis in macrophages differentiated in vitro [41]. High Bcl-2 levels have also been detected in ankle joints of an adjuvant-induced arthritis (AIA) rat model and the Bcl-2 expressing osteoclasts correlated with joint erosion [36]. Bcl-2 remained highly expressed at the leading edge of pannus in the ankle joint, but was not detected outside joint erosions [36]. Bcl-2 levels are also elevated in RA synovial tissue compared to synovial tissue from osteoarthritis patients [38]. Despite the exact mechanism of action of Bcl-2 proteins in RA being unknown, it is evident that Bcl-2 and Bcl-xL may play a large role in inhibiting apoptosis of various cell types in the synovial joints of RA patients. Therefore, inhibiting the action of Bcl-2 anti-apoptotic proteins may be beneficial in reducing inflammation and joint erosion in RA patients.

FLICE-like inhibitory protein (FLIP)

FLIP is a naturally endogenous occurring anti-apoptotic protein that inhibits death receptor-mediated apoptosis by binding to pro-caspase 8 and preventing its association with FADD [42]. A high number of synovial cells express Fas, but in contrast low cell numbers show the characteristic morphological signs of apoptosis [43]. RA FLS and cultured FLS are resistant to Fas-mediated apoptosis despite their high expression of Fas [44]. In the AIA model, FLIP expression was upregulated in the synovial lining and pannus of the ankle joints from day 14 and remained in the pannus throughout the disease duration [42]. These studies suggest that in RA synovial joints the extrinsic pathway of apoptosis could be inhibited downstream by FLIP.

Macrophages are essential in maintaining the chronic nature of RA. It is reported that undifferentiated monocytes are highly susceptible to Fas-mediated apoptosis, however, once differentiated into macrophages, the macrophages are resistant to numerous apoptotic stimuli, suggesting an increase of anti-apoptotic protein expression [45, 46]. Perlman et al. 2001 has demonstrated that macrophages in active RA were resistant to Fas-induced apoptosis and showed elevated levels of FLIP [42]. Catrina et al. 2002 also identified FLIP positive cells to be CD68 positive in the sub-lining and lining of the synovium of early RA patients [47].

A study reported that suppressing FLIP expression using an inhibitor of protein kinase-C ameliorated experimental arthritis through the facilitation of Fas-mediated apoptosis [48]. Although this study only assessed the effects of a non-specific FLIP inhibitor and greater investigation is required, it is evident that disrupting FLIP may have a therapeutic potential for targeting RA.

Inhibitory apoptotic proteins (IAP)

The IAP family inhibits both upstream and downstream caspases. They are also involved in other cell processes such as cell cycle regulation, immune function and the activation of immune cells. Eight different IAPs have been identified and include XIAP, ILP-2, cIAP-1, cIAP-2, ML-IAP, NAIP, survivin and apollon [49]. XIAP is the best characterised IAP as it has the most observable biological properties. XIAP has been shown to be a potent inhibitor of apoptosis by binding to active caspase 3, 7 or 9, and therefore can inhibit both extrinsic and intrinsic pathways of apoptosis [50]. This is possible as XIAP has three conserved sequence motifs, the baculovirus IAP repeats (BIR 1–3) which are located at the amino terminal end of the protein and one zinc finger-like RING which is situated at the carboxyl terminus and mediates protein–protein interactions [50]. XIAP can inhibit caspase activity through direct binding and this occurs as BIR3 binds to caspase 9 and BIR2 binds to caspase 3 and 7, [51]. Dharmapatni et al. 2009 found XIAP to be highly expressed in the cytoplasm of cells in active RA [10]. This elevated expression of XIAP was found to correlate with CD68 positive cells in the synovium, suggesting that XIAP is expressed by large numbers of macrophages [10]. This supports the possibility that macrophage apoptosis may also be inhibited by XIAP in active RA synovium.

Survivin acts similarly to XIAP as it directly or indirectly downregulates both extrinsic and intrinsic pathways of apoptosis by inhibiting the activity of caspase 3, 7 and 9 [52]. Normal differentiated human tissues do not express survivin, however, survivin has been shown to be abundantly expressed in most common cancers where apoptosis of cells is inhibited [52]. Survivin has also been reported to be elevated in both the plasma and synovial fluid of RA patients [53]. Consistent with this, Dharmapatni et al. 2009, found survivin to be highly expressed in the cytoplasm of cells within the synovial tissue of active RA patients [10]. Survivin mRNA was also expressed at significantly higher levels in active RA compared to inactive RA [10]. Increased survivin levels were associated with erosive joint disease in both studies [10, 53].

Survivin and XIAP are endogenous inhibitors of caspase 3, thus overexpression of these molecules has a major role in maintaining active RA through contributing to the inhibition of apoptosis of cells within synovial joints. Therefore, modulating molecules of the IAP family may be essential for future treatment of RA.

Therapeutics that target intracellular anti-apoptotic molecules in RA

Promoting apoptosis has been reported to be beneficial in reducing inflammatory cell accumulation, synovial fibroblast proliferation and osteoclast formation in RA. Apoptosis induction can be achieved by stimulating the pro-apoptosis molecules and/or inhibiting the anti-apoptotic molecules. Potential antagonists of anti-apoptotic proteins in RA can take the form of proteins, nucleic acids or small molecule inhibitors. However, further research is required to identify these antagonists and whether they can reduce inflammation and joint destruction in RA. As several intracellular apoptotic inhibitory molecules have been found to be upregulated in RA, research now focuses on small molecule forms of these inhibitors as potential compounds for RA treatment (Fig. 1).

Bcl-2 inhibition using BH3 mimetics for RA treatment

Inhibiting the action of anti-apoptotic Bcl-2 proteins has been suggested for the treatment of RA. Natural and synthetically developed compounds that mimic the function of the Bcl-2 homology (BH) domains have been identified [56]. These compounds specifically target the BH3 domain which is found in all pro-apoptotic Bcl-2 proteins as well as the anti-apoptotic Bcl-xL and Bcl-2 proteins [56]. BH3-only pro-apoptotic proteins act upstream in response to a variety of cellular stimuli to propagate the apoptotic signal and induce activation of the Bcl-2 pro-apoptotic molecules Bax and Bak [57]. BH3 mimetics that have been characterised and are under development for anti-cancer agents include ABT-737, ABT-263 (navotoclax), GX15-070 (obatoclax), gossypol family and AT-101 (enantiomer) [58]. It is possible that these compounds could be beneficial in treating RA as BH3-only pro-apoptotic proteins are thought to have a protective role in RA joint destruction [56].

ABT-737 is a synthetic small molecule BH3-mimetic which is designed to target the BH3 domain of the anti-apoptotic protein Bcl-xL [56]. However, it does not directly initiate apoptosis, but enhances the signals to induce Bax and Bak oligomerisation and subsequent cytochrome c release [56]. ABT-737 has been shown to prevent disease progression in a collagen-induced arthritis (CIA) murine model [57]. In this study, 50 mg/kg of ABT-737 administered daily for 21 days resulted in a reduction of paw swelling, bone and cartilage destruction and total lymphocyte count compared to mice treated with dexamethasone [57]. However, others argue ABT-737 would

not be a good candidate of BH3 mimetics for RA treatment as the anti-apoptotic protein Mcl-1 is a barrier to responsiveness to ABT-737 [39]. Mcl-1 protects against apoptosis by suppressing the activation of Bcl-2 pro-apoptotic molecules including Bak and BH3-only proteins [39]. Mcl-1 overexpression has resistance to ABT-737 confirmed in both in vitro and a mouse lymphoma model, suggesting that ABT-737 may not induce apoptosis in cells with high expression of Mcl-1 [59]. As Bardwell et al. 2009 only assessed lymphocytes in CIA mice, further studies of the effects of ABT-737 on other cell types including macrophages in arthritis mouse models are required [57]. Mcl-1 has emerged as a critical pro-survival factor in several malignancies and in drug resistance [60]. Thus, there is an urgent need for the development of Mcl-1 specific BH3 mimetics to overcome resistance [61, 62]. In a recent review, it is reported that S1 derivatives and polyquinoline derivatives can act as "pan BH3 mimetics" which can bind Bcl-2, Bcl-xL and Mcl-1 with moderate affinity [58]. However, the anti-tumour effects in pre-clinical models are yet to be determined [58].

FLIP antagonists for RA treatment

FLIP (as discussed above, Table 2) is highly expressed in macrophages and in the synovial lining of RA patients [47]. Thus, downregulating the expression of FLIP may induce apoptosis in macrophages and FLS to alleviate or further reduce joint damage. Decreasing the activity of FLIP by at least 25% with FLIP antagonists that have been developed has a significant impact on the pathophysiology of RA [63]. Hurez et al. 2005 found that FLIP antagonists increase apoptosis by impeding FLIPs inhibition of caspase 8 cleavage [63]. Blocking FLIP activity for 6 months in a computer model of a human rheumatic joint, reduced cartilage degradation by 46% and synovial hyperplasia by 63% [63]. Treatment of methotrexate-resistant patients with a FLIP antagonist also reduced cartilage degradation by 28% and synovial hyperplasia by 36% [63]. These results are promising and suggest FLIP antagonists may be beneficial for the treatment of RA. However, to date there are no FLIP antagonists which have been tested on specific cells in vitro or in animal models of RA. Thus, further research is required to identify potential antagonists of FLIP activity and whether they can reduce inflammation and bone destruction in RA.

XIAP inhibition using embelin for RA treatment

XIAP is a potent suppressor of apoptosis via suppression of caspases 3, 7, and 9 directly [64, 65]. It is a new molecular target for the design of novel drugs overcoming the apoptosis resistance of cells. Compounds that have been developed for inhibiting IAP actions are either in the form

Table 2 Intracellular anti-apoptotic proteins that are upregulated in rheumatoid arthritis joints

Anti-apoptotic molecule	Mechanism of apoptosis inhibition	Upregulation in RA
FLIP	Prevents association of pro-caspase 8 with FADD, inhibiting the extrinsic pathway	Macrophages in active RA are resistant to Fas-induced apoptosis and have increased levels of FLIP. FLIP positive cells are predominantly present in the lining and sub-lining of synovium in early RA [36, 47]
Bcl-2 family of anti-apoptotic proteins Bcl-2, Bcl-xl, BAG, Bcl-w, mcl-1	Prevents apoptosis by maintaining mitochondrial homeostasis, inhibiting cytochrome c release and controlling activation of caspase proteases (54)	Increased expression of Bcl-2 in FLS correlates with synovial lining thickening and the progression of inflammation [38] Increased expression of Bcl-xL in osteoclasts prolongs life span in erosive arthritis [55]
XIAP	Prevents apoptosis by binding to active caspase 3, 7 and 9, inhibiting both the extrinsic and intrinsic pathways	XIAP is highly expressed in cytoplasm of CD68 positive cells in synovial joints of RA patients [10]
Survivin	Downregulates directly or indirectly both the intrinsic and extrinsic pathways [52]	Highly expressed in cytoplasm of cells in the synovial tissue of active RA patients [10]

of naturally occurring non-peptide small molecule inhibitors such as embelin or synthetic antisense oligonucleotides and antagonist molecules such as AEG35156, which has been clinically tested for various cancer treatments [66, 67].

Embelin (2,5-dihydroxy-3-undecyl-1,4-benzoquinone) is a naturally occurring alkyl substituted hydroxy benzoquinone and is an active constituent of the fruit Embelia ribes BURM [68]. Embelin is a cell permeable non-peptide small molecule inhibitor of XIAP [69–71]. Embelin has been found to have anti-inflammatory, anti-tumour and analgesic properties; however, the precise mechanism underlying the different properties of embelin is still unclear. Extensive research has identified the benefits of embelin by induction of growth inhibition and apoptosis in various types of human cancer cells [72–75]. Embelin induces apoptosis in T98G glioma cells, pancreatic cancer, PC-3 prostate cancer and human leukemia cell lines with high levels of XIAP and reduced the levels of anti-apoptotic Bcl-2 family proteins [72–74, 76]. As inflammatory cells and FLS in the RA synovium are thought to have similar properties to cancer cells, embelin may also be beneficial for the treatment of RA.

The anti-inflammatory effects of embelin have been investigated in several acute and chronic models of inflammation. Embelin dose dependently inhibited LPS-induced TNF-α production in a mouse model of TPA-induced acute and chronic irritant contact dermatitis [77]. This supports the ability of embelin to resolve existing and persistent inflammation, further supporting the benefits its anti-inflammatory action may have in RA patients. The mechanisms by which embelin suppresses inflammation have also been investigated in acetic acid-induced colitis in rats and dextran sodium sulphate-induced colitis in mice [78, 79]. However, in these models, the animals were treated prior to disease induction or at induction of disease. This may not recapitulate treatment in human RA as inflammation and cartilage and bone destruction may already be established

when diagnosis occurs. Future studies would be required to determine this in murine models of inflammatory arthritis.

There is growing research on the anti-inflammatory and anti-apoptotic properties of embelin in the context of RA, and it is now thought that embelin may be beneficial in reducing chronic inflammation and bone erosion in RA patients. Embelin can suppress RANKL-induced osteoclastogenesis in vitro in RAW 264.7 cells [80]. This was evident as embelin dose dependently decreased the number of tartrate-resistant acid phosphatase (TRAP) positive cells, a marker of osteoclasts with almost complete inhibition at 15 μmol/L on days 3, 4 and 5 [80]. Thus, this study suggests that embelin may be beneficial for reducing the number of osteoclasts present within synovial joints, decreasing overall bone erosion in RA. Reuter et al. 2010 demonstrated that embelin acted at an early stage of osteoclast differentiation as osteoclast formation was inhibited at day 1 and 2 post-RANKL exposure [80]. However, when added at days 3 and 4 post-RANKL, the effect of embelin in preventing osteoclast formation was not as strong [80]. This could be problematic for treatment in RA patients as diagnosis of RA can take several months and by this point bone erosion is already present in the synovial joints. Thus, it is not known whether embelin would have a strong effect on decreasing osteoclast presence through inhibiting proliferation or suppressing osteoclast activity and how this can affect bone formation. Although embelin has many mechanisms of actions, the focus in treatment of RA is to initiate apoptosis in the infiltrating cells in the synovial joints. Reuter et al. 2010 also found embelin to induce apoptosis in mature osteoclasts and this was confirmed by increased activation of caspase 3 [80]. However, it is not clear if apoptosis of osteoclasts is due to the inhibition of NF-kB, thus further research to elucidate the cross talk between NF-κB and the apoptosis pathways is required.

Recently, embelin has been used to treat inflammation and bone erosion in a collagen antibody-induced arthritis

(CAIA) mouse model [81]. In this study, embelin at 30 and 50 mg/kg/day suppressed inflammation clinically and microscopically, with the lower dose of embelin significantly reducing inflammation, cartilage and bone degradation and pannus formation in the front paws of mice [81]. This demonstrates that embelin at a low dose can suppress joint inflammation and bone erosion in an acute inflammatory arthritis mouse model. Dharmapatni et al. 2015 also demonstrated that CAIA mice treated with low-dose embelin had significantly increased numbers of apoptotic cells in the pannus of synovial joints as evident by increased TUNEL staining [81]. These mice had reduced numbers of TRAP positive osteoclasts, suggesting that embelin may be acting to suppress osteoclast activity as well as initiating apoptosis [81]. However, the exact mechanism of action of embelin to reduce bone erosion is still unclear. It is known that embelin specifically inhibits XIAP; however, in this study there was no difference in XIAP protein expression within cells in the pannus, articular cartilage and bone marrow. Thus, it is not conclusive that embelin is completing its action through inhibiting XIAP expression. Although the beneficial effects of embelin have been highlighted in an inflammatory arthritis mouse model, future research will be required to identify its specific mechanism of action and cell targets.

Despite promising research into the anti-inflammatory effects of embelin in RA, pre-clinical efforts of embelin have been hampered due to its poor aqueous solubility which leads to poor bioavailability via oral administration. As a result, new techniques and derivatives of embelin have been trialled to improve solubility [82, 83]. However, further research into these techniques or the use of embelin derivatives for RA treatment and whether they will have the same mechanism of action is required before clinical trials can be conducted. A possible alternative to overcome the poor solubility and bioavailability of embelin is the use of Smac mimetics to target other IAPs for the treatment of joint inflammation and bone erosion in RA.

IAPs inhibition using Smac mimetics for RA treatment

Smac is an endogenous antagonist of IAP proteins XIAP, cIAP-1 and cIAP-2. Smac is released from the mitochondria into the cytosol upon apoptotic stimulation and the 55-residue mitochondria-targeting sequence at its N terminus is proteolytically removed [84]. The cleaved Smac binds to the BIR2 and BIR3 domains of XIAP via an IAP binding motif, resulting in interference with the interaction of XIAP and caspases thus allowing apoptosis to occur [85].

Smac mimetics have primarily been designed and developed for the treatment of cancer following extensive research on their anti-tumour properties. Single agent Smac mimetics, including birinapant (TL32711) have been shown to trigger apoptosis in several cancer cell lines including chronic lymphocyte, acute lymphoblastic and acute myeloid leukemia [86–88]. Several Smac mimetics are also currently being trialled in phase I and II clinical trials in several human cancers and the administration of Smac has proved to be well tolerated [89]. As FLS in RA have a similar phenotype to cancer cells, Smac mimetics may also be beneficial in RA treatment.

Eckhardt, Roesler and Fulda 2013 found that Smac mimetics stimulated NF-κB-mediated expression of TRAIL receptor 1 in glioblastoma cells which eventually led to apoptosis of these cells in a death ligand-independent manner [90]. This suggests that NF-κB stimulation to some extent is important to Smac mimetic-stimulated apoptosis. Smac mimetics also promote TNF-α-dependent apoptosis in a subset of tumour cells and cancer cell lines [89, 91–93]. The secretion of TNF-α is necessary for induction of apoptosis by Smac mimetics and it indicates that additional blockades other than IAP proteins exist for TNF-α-induced apoptosis [94]. In RA, increased TNF-α and NF-κB expression is associated with the upregulation of osteoclastogenesis, which results in greater bone destruction in the synovial joints. Therefore, even though Smac mimetics may be beneficial in stimulating TNF-α-induced apoptosis in some cells in the synovium, the upregulation of NF-κB would be detrimental to bone remodelling in the synovial joints of RA patients as the inflammatory response will be prolonged.

There is growing concern in the clinical development of Smac mimetics as the stimulation of NF-κB activation by Smac mimetics would potentially cause adverse effects to occur in normal tissue due to elevated cytokine levels [89, 94]. This was evident in the first in-human phase I dose escalation study where patients treated with the Smac mimetic LCL161 reported the dose-limiting toxicity of cytokine release syndrome [94]. Thus, it is currently a challenge to maximise the anti-tumour activity of Smac mimetics while minimising potential unwanted effects and this could also become problematic in the treatment of RA.

Despite the promising preclinical research regarding the use of Smac mimetics in cancer treatment, there is still limited research on the presence of Smac in RA patients and currently there are limited studies exploring the use of Smac mimetics in RA treatment. The increased levels of IAPs found in the RA synovial fluid supports the potential use of Smac mimetics compared with XIAP inhibitors as they have the additional mechanism of rapidly degrading cIAP-1, thus would be a more appropriate choice for inducing apoptosis in RA joints. Several Smac mimetics have been investigated in preclinical stages for treatment in RA. However, the possibility of increased cytokine release and inflammatory response in cancer patients due to Smac mimetic treatment may limit the clinical progression and use of Smac mimetic as a therapeutic agent for RA.

BV6 is a Smac mimetic reported to induce apoptosis in human peripheral blood monocytes without affecting dendritic cells, T cells and macrophages [95]. Although BV6 does not induce apoptosis in monocyte-derived immune cells and T cells, inhibition of TNF signalling, CD40L signalling and normal maturation of dendritic cells suggests the suitability of this compound for immunosuppressive therapy [95]. Importantly, a commercially available Smac mimetic ABT (A-4.10099.1) has also been reported to suppress inflammation in an AIA murine model as joint swelling did not develop in the antigen-treated knee after daily treatment [96].

Smac066 is another Smac mimetic which has been reported to significantly inhibit growth of RA FLS in vitro [97]. In contrast, osteoarthritic-derived FLS were not affected by Smac066. Smac066 establishes a novel molecular interaction with XIAP binding site of caspase 3 and caspases 3 and 8 were cleaved after incubating FLS with Smac066 [97]. This supports the posit that Smac066 can induce apoptosis in FLS, indicating a possible use in RA treatment.

Recently, Lattuada et al. 2016, investigated the effect of another Smac mimetic, Smac127 on FLS when cultured in synovial fluid [98]. Smac127 is a more potent analogue than Smac066 as it is more lipophilic and cell permeable, but it has a similar binding potency on BIR3 domains from XIAP and cIAP-1 and 2 [98]. Smac127 induced significant inhibition of cell growth and induced apoptosis in FLS cultured in synovial fluid [98]. Similar to Smac066, Smac127 downregulated cIAP-1 and 2 and XIAP expression, while promoting the proteolytic activation of pro-caspase 3 in the FLS [98]. As there is an imbalance of inflammatory cytokines and RANKL in RA joints, Lattuada et al. 2016 also investigated the influence of Smac127 on these factors [98]. It was reported that Smac127 induced significant inhibition of the secretion of IL-6, which is upregulated in RA. However, Smac127 did not have any effect on the levels of RANKL [98]. Similar to Smac066, Smac127 was effective in inducing apoptosis in FLS and was also beneficial in regulating the expression of pro-inflammatory cytokines. These observations suggest that Smac127 may be a potential therapeutic for controlling inflammation and disease progression in RA, however, further research is required to identify the effect of Smac127 in animal models of inflammatory arthritis. The findings in ongoing early clinical trials and lack of progression for cancer treatment as well as the limited progression of preclinical investigation of Smac mimetics

Table 3 Examples of potential therapeutics for RA that target apoptosis inhibitory molecules

Therapeutic	Mechanism of action	Examples	Effect in RA	Stage
BH3 mimetics	Binds to anti-apoptotic proteins Bcl-xL, Bcl-2 and Bcl-w and initiates apoptosis by inducing pro-apoptotic proteins Bax and Bak to activate cytochrome c release	ABT-737	In vivo: reduces paw swelling and bone and cartilage destruction in a CIA murine model [57](57)	Preclinical CIA murine model
FLIP antagonists	Initiate apoptosis by impeding FLIP inhibition of caspase 8 cleavage		Computer model of human rheumatic joint had decreased cartilage degradation and synovial hyperplasia after exposure to FLIP antagonist for 6 months [63]	
XIAP inhibitors	Target BIR2 and BIR3 domain of XIAP where caspase 3,7 and 9 binds to induce apoptosis	Embelin	In vitro: Dose dependently inhibits LPS-induced TNF-α production [77](77) Suppresses RANKL-induced osteoclastogenesis in RAW 264.7 cells [80](80) In vivo: 30 mg/kg/day embelin significantly reduced inflammation, cartilage and bone degradation and pannus formation in paws of CAIA mice [81](81)	Preclinical CAIA murine model
Smac mimetics	Mimic binding of Smac protein to XIAP and cIAP1/2 to inhibit their anti-apoptotic effects	BV6, ABT, Smac066 and Smac127	In vitro: BV6-induces apoptosis in human peripheral blood monocytes [95](95) Smac066 inhibit growth and induce apoptosis in FLS [97](97) Smac127 inhibit cell growth and induce apoptosis in FLS cultured in synovial fluid [98](98) In vivo: ABT-suppresses inflammation in AIA murine model [96](96)	Preclinical In vitro cell cultures and AIA murine model

for RA treatment perhaps highlight the significant challenges with the development of these agents.

Conclusion

RA is a complex inflammatory disorder with several mechanisms causing synovial hyperplasia, inflammatory cell infiltration and destruction of cartilage and bone. Chronic accumulation of inflammatory cells and osteoclasts in RA synovial joints is due to decreased apoptosis in these cells. Thus, research is currently focusing on identifying treatments to assist in stimulating apoptosis within the synovium through inhibition of intracellular apoptotic inhibitory molecules. There are currently no clinical trials using therapeutics that target apoptosis specifically for RA. However, BH3 mimetics, FLIP antagonists, XIAP inhibitors and Smac mimetics show promising results for the initiation of apoptosis in FLS, inflammatory cells and osteoclasts in vitro or in arthritis animal models (Table 3). XIAP inhibitor embelin and Smac mimetics 066 and 127 have more recently been highlighted as beneficial for reducing inflammation and bone destruction in vitro. However, their progression to preclinical animal studies and clinical trials in human RA may be haltered due to the poor bioavailability and possible adverse effects identified in preclinical and clinical trials in human cancers. Future studies will therefore need to further investigate these complications before their clinical application in RA treatment.

Author contributions BW carried out the literature review, preparing and writing the manuscript with supervision from TC and AD. TC and AD contributed to the writing of the manuscript, discussing the literature and presentation of figures. All authors read and approved the final manuscript.

Compliance with ethical standards

Ethics approval Not applicable.

Consent for publication Not applicable.

Availability of data and material Not applicable.

Conflict of interest The authors declare that they have no competing interests.

References

1. Mikuls TR. Co-morbidity in rheumatoid arthritis. Best Pract Res Clin Rheumatol. 2003;17(5):729–752.
2. Romas E, Gillespie MT, Martin TJ. Involvement of receptor activator of NF-kappaB ligand and tumor necrosis factor-alpha in bone destruction in rheumatoid arthritis. Bone. 2002;30(2):340–6.
3. Schett G. Erosive arthritis. Arthritis Res Ther. 2007;9(Suppl 1):S2.
4. Haynes DR, Barg E, Crotti TN, Holding C, Weedon H, Atkins GJ, et al. Osteoprotegerin expression in synovial tissue from patients with rheumatoid arthritis, spondyloarthropathies and osteoarthritis and normal controls. Rheumatology. 2003;42(1):123–34.
5. Gravallese EM, Harada Y, Wang JT, Gorn AH, Thornhill TS, Goldring SR. Identification of cell types responsible for bone resorption in rheumatoid arthritis and juvenile rheumatoid arthritis. Am J Pathol. 1998;152(4):943–51.
6. Muller-Ladner U, Pap T, Gay RE, Neidhart M, Gay S. Mechanisms of disease: the molecular and cellular basis of joint destruction in rheumatoid arthritis. Nat Clin Pract Rheumatol. 2005;1(2):102–10.
7. Pettit AR, Ji H, von Stechow D, Muller R, Goldring SR, Choi Y, et al. TRANCE/RANKL knockout mice are protected from bone erosion in a serum transfer model of arthritis. Am J Pathol. 2001;159(5):1689–99.
8. Kotake S, Udagawa N, Hakoda M, Mogi M, Yano K, Tsuda E, et al. Activated human T cells directly induce osteoclastogenesis from human monocytes: possible role of T cells in bone destruction in rheumatoid arthritis patients. Arthritis Rheum. 2001;44(5):1003–12.
9. Korb A, Pavenstadt H, Pap T. Cell death in rheumatoid arthritis. Apoptosis. 2009;14(4):447–454.
10. Dharmapatni AA, Smith MD, Findlay DM, Holding CA, Evdokiou A, Ahern MJ, et al. Elevated expression of caspase-3 inhibitors, survivin and xIAP correlates with low levels of apoptosis in active rheumatoid synovium. Arthritis Res Ther. 2009;11(1):R13.
11. King KL, Cidlowski JA. Cell cycle regulation and apoptosis. Annu Rev Physiol. 1998;60:601–17.
12. Li CJ, Friedman DJ, Wang C, Metelev V, Pardee AB. Induction of apoptosis in uninfected lymphocytes by HIV-1 Tat protein. Science. 1995;268(5209):429–31.
13. Ethell DW, Buhler LA. Fas ligand-mediated apoptosis in degenerative disorders of the brain. J Clin Immunol. 2003;23(6):439–46.
14. Pope RM. Apoptosis as a therapeutic tool in rheumatoid arthritis. Nat Rev Immunol. 2002;2(7):527–35.
15. Parida JR, Misra DP, Wakhlu A, Agarwal V. Is non-biological treatment of rheumatoid arthritis as good as biologics? World J Orthop. 2015;6(2):278–83.
16. Smith MD, Kraan MC, Slavotinek J, Au V, Weedon H, Parker A, et al. Treatment-induced remission in rheumatoid arthritis patients is characterized by a reduction in macrophage content of synovial biopsies. Rheumatology. 2001;40(4):367–74.
17. Nakazawa F, Matsuno H, Yudoh K, Katayama R, Sawai T, Uzuki M, et al. Methotrexate inhibits rheumatoid synovitis by inducing apoptosis. J Rheumatol. 2001;28(8):1800–8.
18. Smith MD, Weedon H, Papangelis V, Walker J, Roberts-Thomson PJ, Ahern MJ. Apoptosis in the rheumatoid arthritis synovial membrane: modulation by disease-modifying anti-rheumatic drug treatment. Rheumatology. 2010;49(5):862–75.
19. Weinblatt ME. Methotrexate in rheumatoid arthritis: a quarter century of development. Trans Am Clin Climatol Assoc. 2013;124:16–25.

20. Genestier L, Paillot R, Fournel S, Ferraro C, Miossec P, Revillard JP. Immunosuppressive properties of methotrexate: apoptosis and clonal deletion of activated peripheral T cells. J Clin Invest. 1998;102(2):322–8.

21. Metzstein MM, Stanfield GM, Horvitz HR. Genetics of programmed cell death in C. elegans: past, present and future. Trends Genet. 1998;14(10):410–6.

22. Elmore S. Apoptosis: a review of programmed cell death. Toxicol Pathol. 2007;35(4):495–516.

23. Locksley RM, Killeen N, Lenardo MJ. The TNF and TNF receptor superfamilies: integrating mammalian biology. Cell. 2001;104(4):487–501.

24. Wajant H. The Fas signaling pathway: more than a paradigm. Science. 2002;296(5573):1635–6.

25. Kischkel FC, Hellbardt S, Behrmann I, Germer M, Pawlita M, Krammer PH, et al. Cytotoxicity-dependent APO-1 (Fas/CD95)-associated proteins form a death-inducing signaling complex (DISC) with the receptor. EMBO J. 1995;14(22):5579–88.

26. Saelens X, Festjens N, Vande Walle L, van Gurp M, van Loo G, Vandenabeele P. Toxic proteins released from mitochondria in cell death. Oncogene. 2004;23(16):2861–74.

27. Cory S, Adams JM. The Bcl2 family: regulators of the cellular life-or-death switch. Nat Rev Cancer. 2002;2(9):647–56.

28. Slee EA, Adrain C, Martin SJ. Executioner caspase-3, -6, and -7 perform distinct, non-redundant roles during the demolition phase of apoptosis. J Biol Chem. 2001;276(10):7320–6.

29. Hill MM, Adrain C, Duriez PJ, Creagh EM, Martin SJ. Analysis of the composition, assembly kinetics and activity of native Apaf-1 apoptosomes. EMBO J. 2004;23(10):2134–45.

30. Esposti MD. The roles of Bid Apoptosis. 2002;7(5):433–40.

31. Zha J, Harada H, Yang E, Jockel J, Korsmeyer SJ. Serine phosphorylation of death agonist BAD in response to survival factor results in binding to 14–3–3 not BCL-X(L). Cell. 1996;87(4):619–28.

32. Schimmer AD. Inhibitor of apoptosis proteins: translating basic knowledge into clinical practice. Cancer Res. 2004;64(20):7183–90.

33. Joza N, Susin SA, Daugas E, Stanford WL, Cho SK, Li CY, et al. Essential role of the mitochondrial apoptosis-inducing factor in programmed cell death. Nature. 2001;410(6828):549–54.

34. Enari M, Sakahira H, Yokoyama H, Okawa K, Iwamatsu A, Nagata S. A caspase-activated DNase that degrades DNA during apoptosis, and its inhibitor ICAD. Nature. 1998;391(6662):43–50.

35. Reed JC. Bcl-2 and the regulation of programmed cell death. J Cell Biol. 1994;124(1–2):1–6.

36. Perlman H, Liu H, Georganas C, Koch AE, Shamiyeh E, Haines GK 3rd, et al. Differential expression pattern of the antiapoptotic proteins, Bcl-2 and FLIP, in experimental arthritis. Arthritis Rheum. 2001;44(12):2899–908.

37. Firestein GS, Yeo M, Zvaifler NJ. Apoptosis in rheumatoid arthritis synovium. J Clin Invest. 1995;96(3):1631–8.

38. Perlman H, Georganas C, Pagliari LJ, Koch AE, Haines K 3rd, Pope RM. Bcl-2 expression in synovial fibroblasts is essential for maintaining mitochondrial homeostasis and cell viability. J Immunol. 2000;164(10):5227–35.

39. Liu H, Huang Q, Shi B, Eksarko P, Temkin V, Pope RM. Regulation of Mcl-1 expression in rheumatoid arthritis synovial macrophages. Arthritis Rheum. 2006;54(10):3174–81.

40. Xing L, Boyce BF. Regulation of apoptosis in osteoclasts and osteoblastic cells. Biochem Biophys Res Commun. 2005;328(3):709–20.

41. Pagliari LJ, Perlman H, Liu H, Pope RM. Macrophages require constitutive NF-kappaB activation to maintain A1 expression and mitochondrial homeostasis. Mol Cell Biol. 2000;20(23):8855–65.

42. Perlman H, Pagliari LJ, Liu H, Koch AE, Haines GK 3rd, Pope RM. Rheumatoid arthritis synovial macrophages express the Fas-associated death domain-like interleukin-1beta-converting enzyme-inhibitory protein and are refractory to Fas-mediated apoptosis. Arthritis Rheum. 2001;44(1):21–30.

43. Matsumoto S, Muller-Ladner U, Gay RE, Nishioka K, Gay S. Ultrastructural demonstration of apoptosis, Fas and Bcl-2 expression of rheumatoid synovial fibroblasts. J Rheumatol. 1996;23(8):1345–52.

44. Franz JK, Pap T, Hummel KM, Nawrath M, Aicher WK, Shigeyama Y, et al. Expression of sentrin, a novel antiapoptotic molecule, at sites of synovial invasion in rheumatoid arthritis. Arthritis Rheum. 2000;43(3):599–607.

45. Ma Y, Pope RM. The role of macrophages in rheumatoid arthritis. Curr Pharm Des. 2005;11(5):569–80.

46. Perlman H, Pagliari LJ, Georganas C, Mano T, Walsh K, Pope RM. FLICE-inhibitory protein expression during macrophage differentiation confers resistance to fas-mediated apoptosis. J Exp Med. 1999;190(11):1679–88.

47. Catrina AI, Ulfgren AK, Lindblad S, Grondal L, Klareskog L. Low levels of apoptosis and high FLIP expression in early rheumatoid arthritis synovium. Ann Rheum Dis. 2002;61(10):934–6.

48. Willems F, Amraoui Z, Vanderheyde N, Verhasselt V, Aksoy E, Scaffidi C, et al. Expression of c-FLIP(L) and resistance to CD95-mediated apoptosis of monocyte-derived dendritic cells: inhibition by bisindolylmaleimide. Blood. 2000;95(11):3478–82.

49. Salvesen GS, Duckett CS. IAP proteins: blocking the road to death's door. Nat Rev Mol Cell Biol. 2002;3(6):401–10.

50. Harlin H, Reffey SB, Duckett CS, Lindsten T, Thompson CB. Characterization of XIAP-deficient mice. Mol Cell Biol. 2001;21(10):3604–8.

51. Bai S, Liu H, Chen KH, Eksarko P, Perlman H, Moore TL, et al. NF-kappaB-regulated expression of cellular FLIP protects rheumatoid arthritis synovial fibroblasts from tumor necrosis factor alpha-mediated apoptosis. Arthritis Rheum. 2004;50(12):3844–55.

52. Li F. Survivin study: what is the next wave? J Cell Physiol. 2003;197(1):8–29.

53. Bokarewa M, Lindblad S, Bokarew D, Tarkowski A. Balance between survivin, a key member of the apoptosis inhibitor family, and its specific antibodies determines erosivity in rheumatoid arthritis. Arthritis Res Ther. 2005;7(2):R349–R58.

54. Newmeyer DD, Bossy-Wetzel E, Kluck RM, Wolf BB, Beere HM, Green DR. Bcl-xL does not inhibit the function of Apaf-1. Cell Death Differ. 2000;7(4):402–7.

55. Zhang Q, Badell IR, Schwarz EM, Boulukos KE, Yao Z, Boyce BF, et al. Tumor necrosis factor prevents alendronate-induced osteoclast apoptosis in vivo by stimulating Bcl-xL expression through Ets-2. Arthritis Rheum. 2005;52(9):2708–18.

56. Hutcheson J, Perlman H. BH3-only proteins in rheumatoid arthritis: potential targets for therapeutic intervention. Oncogene. 2008;27(Suppl 1):S168–75.

57. Bardwell PD, Gu J, McCarthy D, Wallace C, Bryant S, Goess C, et al. The Bcl-2 family antagonist ABT-737 significantly inhibits multiple animal models of autoimmunity. J Immunol. 2009;182(12):7482–9.

58. Billard C. BH3 mimetics: status of the field and new developments. Mol Cancer Ther. 2013;12(9):1691–700.

59. van Delft MF, Wei AH, Mason KD, Vandenberg CJ, Chen L, Czabotar PE, et al. The BH3 mimetic ABT-737 targets selective Bcl-2 proteins and efficiently induces apoptosis via Bak/Bax if Mcl-1 is neutralized. Cancer Cell. 2006;10(5):389–99.

60. Beroukhim R, Mermel CH, Porter D, Wei G, Raychaudhuri S, Donovan J, et al. The landscape of somatic copy-number alteration across human cancers. Nature. 2010;463(7283):899–905.

61. Quinn BA, Dash R, Azab B, Sarkar S, Das SK, Kumar S, et al. Targeting Mcl-1 for the therapy of cancer. Expert opinion on investigational drugs. 2011;20(10):1397–411.

62. Billard C. Development of Noxa-like BH3 mimetics for apoptosis-based therapeutic strategy in chronic lymphocytic leukemia. Mol Cancer Res. 2012;10(6):673–6.

63. Hurez VJ, Ramanujan S, Shoda LKM, Wennerberg LG, Michelson SG, Deframoux N. Treatment of rheumatoid arthritis with FLIP antagonists. United States patent application publication. 2005:pp. 1–16.

64. Deveraux QL, Takahashi R, Salvesen GS, Reed JC. X-linked IAP is a direct inhibitor of cell-death proteases. Nature. 1997;388(6639):300–4.

65. Deveraux QL, Roy N, Stennicke HR, Van Arsdale T, Zhou Q, Srinivasula SM, et al. IAPs block apoptotic events induced by caspase-8 and cytochrome c by direct inhibition of distinct caspases. EMBO J. 1998;17(8):2215–23.

66. Carter BZ, Mak DH, Morris SJ, Borthakur G, Estey E, Byrd AL, et al. XIAP antisense oligonucleotide (AEG35156) achieves target knockdown and induces apoptosis preferentially in CD34 + 38-cells in a phase 1/2 study of patients with relapsed/refractory AML. Apoptosis. 2011;16(1):67–74.

67. Mahadevan D, Chalasani P, Rensvold D, Kurtin S, Pretzinger C, Jolivet J, et al. Phase I trial of AEG35156 an antisense oligonucleotide to XIAP plus gemcitabine in patients with metastatic pancreatic ductal adenocarcinoma. Am J Clin Oncol. 2013;36(3):239–43.

68. Mahendran S, Badami S, Ravi S, Thippeswamy BS, Veerapur VP. Synthesis and evaluation of analgesic and anti-inflammatory activities of most active free radical scavenging derivatives of embelin-A structure-activity relationship. Chem Pharm Bull (Tokyo). 2011;59(8):913–9.

69. Nikolovska-Coleska Z, Xu L, Hu Z, Tomita Y, Li P, Roller PP, et al. Discovery of embelin as a cell-permeable, small-molecular weight inhibitor of XIAP through structure-based computational screening of a traditional herbal medicine three-dimensional structure database. J Med Chem. 2004;47(10):2430–40.

70. Chen J, Nikolovska-Coleska Z, Wang G, Qiu S, Wang S. Design, synthesis, and characterization of new embelin derivatives as potent inhibitors of X-linked inhibitor of apoptosis protein. Bioorg Med Chem Lett. 2006;16(22):5805–8.

71. Xu M, Cui J, Fu H, Proksch P, Lin W, Li M. Embelin derivatives and their anticancer activity through microtubule disassembly. Planta Med. 2005;71(10):944–8.

72. Park N, Baek HS, Chun YJ. Embelin-induced apoptosis of human prostate cancer cells is mediated through modulation of akt and beta-catenin signaling. PLoS One. 2015;10(8):e0134760.

73. Peng M, Huang B, Zhang Q, Fu S, Wang D, Cheng X, et al. Embelin inhibits pancreatic cancer progression by directly inducing cancer cell apoptosis and indirectly restricting IL-6 associated inflammatory and immune suppressive cells. Cancer Lett. 2014;354(2):407–16.

74. Hu R, Yang Y, Liu Z, Jiang H, Zhu K, Li J, et al. The XIAP inhibitor Embelin enhances TRAIL-induced apoptosis in human leukemia cells by DR4 and DR5 upregulation. Tumour Biol. 2015;36(2):769–77.

75. Wang DG, Sun YB, Ye F, Li W, Kharbuja P, Gao L, et al. Anti-tumor activity of the X-linked inhibitor of apoptosis (XIAP) inhibitor embelin in gastric cancer cells. Mol Cell Biochem. 2014;386(1–2):143–52.

76. Park SY, Lim SL, Jang HJ, Lee JH, Um JY, Kim SH, et al. Embelin induces apoptosis in human glioma cells through inactivating NF-kappaB. J Pharmacol Sci. 2013;121(3):192–9.

77. Kalyan Kumar G, Dhamotharan R, Kulkarni NM, Mahat MY, Gunasekaran J, Ashfaque M. Embelin reduces cutaneous TNF-alpha level and ameliorates skin edema in acute and chronic model of skin inflammation in mice. Eur J Pharmacol. 2011;662(1–3):63–9.

78. Thippeswamy BS, Mahendran S, Biradar MI, Raj P, Srivastava K, Badami S, et al. Protective effect of embelin against acetic acid induced ulcerative colitis in rats. Eur J Pharmacol. 2011;654(1):100–5.

79. Kumar GK, Dhamotharan R, Kulkarni NM, Honnegowda S, Murugesan S. Embelin ameliorates dextran sodium sulfate-induced colitis in mice. Int Immunopharmacol. 2011;11(6):724–31.

80. Reuter S, Prasad S, Phromnoi K, Kannappan R, Yadav VR, Aggarwal BB. Embelin suppresses osteoclastogenesis induced by receptor activator of NF-kappaB ligand and tumor cells in vitro through inhibition of the NF-kappaB cell signaling pathway. Mol Cancer Res. 2010;8(10):1425–36.

81. Dharmapatni AA, Cantley MD, Marino V, Perilli E, Crotti TN, Smith MD, et al. The X-linked inhibitor of apoptosis protein inhibitor embelin suppresses inflammation and bone erosion in collagen antibody induced arthritis mice. Mediators Inflamm. 2015;2015:564042.

82. Singh B, Guru SK, Sharma R, Bharate SS, Khan IA, Bhushan S, et al. Synthesis and anti-proliferative activities of new derivatives of embelin. Bioorg Med Chem Lett. 2014;24(20):4865–70.

83. Lu H, Wang J, Wang Y, Qiao L, Zhou Y. Embelin and its role in chronic diseases. Adv Exp Med Biol. 2016;928:397–418.

84. Du C, Fang M, Li Y, Li L, Wang X. Smac, a mitochondrial protein that promotes cytochrome c-dependent caspase activation by eliminating IAP inhibition. Cell. 2000;102(1):33–42.

85. Liu Z, Sun C, Olejniczak ET, Meadows RP, Betz SF, Oost T, et al. Structural basis for binding of Smac/DIABLO to the XIAP BIR3 domain. Nature. 2000;408(6815):1004–8.

86. Brumatti G, Ma C, Lalaoui N, Nguyen NY, Navarro M, Tanzer MC, et al. The caspase-8 inhibitor emricasan combines with the SMAC mimetic birinapant to induce necroptosis and treat acute myeloid leukemia. Sci Transl Med. 2016;8(339):339ra69.

87. Lalaoui N, Hanggi K, Brumatti G, Chau D, Nguyen NY, Vasilikos L, et al. Targeting p38 or MK2 Enhances the Anti-Leukemic Activity of Smac-Mimetics. Cancer Cell. 2016;29(2):145–58.

88. Schirmer M, Trentin L, Queudeville M, Seyfried F, Demir S, Tausch E, et al. Intrinsic and chemo-sensitizing activity of SMAC-mimetics on high-risk childhood acute lymphoblastic leukemia. Cell Death Dis. 2016;7:e2052.

89. Infante JR, Dees EC, Olszanski AJ, Dhuria SV, Sen S, Cameron S, et al. Phase I dose-escalation study of LCL161, an oral inhibitor of apoptosis proteins inhibitor, in patients with advanced solid tumors. J Clin Oncol. 2014;32(28):3103–10.

90. Eckhardt I, Roesler S, Fulda S. Identification of DR5 as a critical, NF-kappaB-regulated mediator of Smac-induced apoptosis. Cell Death Dis. 2013;4:e936.

91. Cheung HH, Beug ST, St Jean M, Brewster A, Kelly NL, Wang S, et al. Smac mimetic compounds potentiate interleukin-1beta-mediated cell death. J Biol Chem. 2010;285(52):40612–23.

92. Vince JE, Wong WW, Khan N, Feltham R, Chau D, Ahmed AU, et al. IAP antagonists target cIAP1 to induce TNFalpha-dependent apoptosis. Cell. 2007;131(4):682–93.

93. Lu J, Bai L, Sun H, Nikolovska-Coleska Z, McEachern D, Qiu S, et al. SM-164: a novel, bivalent Smac mimetic that induces apoptosis and tumor regression by concurrent removal of the blockade of cIAP-1/2 and XIAP. Cancer Res. 2008;68(22):9384–93.

94. Bai L, Smith DC, Wang S. Small-molecule SMAC mimetics as new cancer therapeutics. Pharmacol Ther. 2014;144(1):82–95.

95. Muller-Sienerth N, Dietz L, Holtz P, Kapp M, Grigoleit GU, Schmuck C, et al. SMAC mimetic BV6 induces cell death in monocytes and maturation of monocyte-derived dendritic cells. PLoS One. 2011;6(6):e21556.

96. Mayer BA, Rehberg M, Erhardt A, Wolf A, Reichel CA, Kracht M, et al. Inhibitor of apoptosis proteins as novel targets

in inflammatory processes. Arterioscler Thromb Vasc Biol. 2011;31(10):2240–50.

97. Lattuada D, Casnici C, Crotta K, Seneci PF, Corradini C, Truzzi M, et al. Proapoptotic activity of a monomeric smac mimetic on human fibroblast-like synoviocytes from patients with rheumatoid arthritis. Inflammation. 2015;38(1):102–9.

98. Lattuada D, Gualtierotti R, Crotta K, Seneci P, Ingegnoli F, Corradini C, et al. Smac127 has proapoptotic and anti-inflammatory effects on rheumatoid arthritis fibroblast-like synoviocytes. Mediators Inflamm. 2016;2016:6905678.

APPENDIX III: PUBLISHED MANUSCRIPTS AS PDFS ARISING FROM OUTSIDE THIS THESIS

ORIGINAL ARTICLE

CrossMark

Mixed effects of caffeic acid phenethyl ester (CAPE) on joint inflammation, bone loss and gastrointestinal inflammation in a murine model of collagen antibody-induced arthritis

Bonnie Williams[1] · Eleni Tsangari[1] · Romany Stansborough[1] · Victor Marino[2] ·
Melissa Cantley[1] · Anak Dharmapatni[1] · Rachel Gibson[1,3] · Egon Perilli[4] ·
Tania Crotti[1]

Abstract

Objective To investigate the effect of caffeic acid phenethyl ester (CAPE) on local and systemic inflammation and bone loss in collagen antibody-induced arthritis (CAIA) mice.

Methods Four groups of mice ($n = 8$ per group) were allocated; control, CAPE (1 mg/kg), CAIA and CAIA + CAPE (1 mg/kg). Local inflammation and bone loss were evaluated using clinical paw scores, in vivo micro-computed tomography (micro-CT), histological assessment and tartrate-resistant acid phosphatase (TRAP) staining. Serum levels of C-reactive protein (CRP) and C-terminal telopeptide (CTX-1) were measured by ELISA. Jejunum and colon sections were evaluated histopathologically for damage and toxicity.

Results Greater paw scores and percentage change in paw volume were observed in CAIA + CAPE compared to the control groups ($p < 0.05$). Bone volume over time remained unchanged ($p = 0.94$) and the number of multinucleated TRAP-positive cells was greatest in CAIA + CAPE mice ($p < 0.05$). CRP and CTX-1 levels did not differ between groups. CAIA + CAPE mice exhibited lower colon toxicity scores and a reduced percentage of cavitated goblet cells in the colon crypts compared with CAIA mice ($p = 0.026$ and $p = 0.003$, respectively). Histopathology in the jejunum was not altered.

Conclusion CAPE did not reduce paw inflammation or bone loss in CAIA mice. CAPE reduced histopathological changes in the colon of CAIA mice.

Keywords CAIA · CAPE · Gastrointestinal tract · Bone · Micro-CT · Inflammatory arthritis

Abbreviations

CAPE	Caffeic acid phenethyl ester
CAIA	Collagen antibody-induced arthritis
CTX-1	C-terminal telopeptide
RA	Rheumatoid arthritis
NF-κB	Nuclear factor-kappa B
TRAP	Tartrate-resistant acid phosphatase
BV	Bone volume
PV	Paw volume
TNF-α	Tumour necrosis factor alpha
DMARDs	Disease-modifying anti-rheumatic drugs
PE	Polyethylene
micro-CT	Micro-computed tomography
CRP	C-reactive protein

✉ Bonnie Williams
bonnie.williams@adelaide.edu.au

1 Adelaide Medical School, The University of Adelaide, Adelaide, SA, Australia

2 School of Dentistry, The University of Adelaide, Adelaide, SA, Australia

3 Division of Health Sciences, University of South Australia, Adelaide, SA, Australia

4 School of Computer Science, Engineering and Mathematics, Flinders University, Adelaide, SA, Australia

Introduction

Rheumatoid arthritis (RA) is a chronic autoimmune inflammatory disorder affecting approximately 2% of the Australian population (Mikuls 2003). It is characterised by synovial hyperplasia, inflammatory cell infiltration, articular inflammation and invasion of the synovium into the

Springer

adjacent bone and cartilage (Romas et al. 2002). Skeletal complications in RA involve focal bone erosions and generalised bone loss (Romas et al. 2002). Collectively, these characteristics lead to painful joint deformities, progressive functional disability and an increased risk of fractures (Romas et al. 2002). In addition, as RA is a systemic disorder, extra-articular manifestations occur within organs such as the gastrointestinal tract causing additional morbidity (Mikuls 2003).

The chronic inflammatory process in RA results in the increased infiltration of immune cells including macrophages, T and B cells and pro-inflammatory cytokines, including tumour necrosis factor alpha (TNF-α), interleukins (including IL-1 and IL-6) and prostaglandins (including PGE$_2$); which leads to abnormal destruction of joint cartilage and bone (Haynes et al. 2003; Walsh et al. 2005). The destruction of bone is also attributed to the upregulation of receptor activator of nuclear factor-kappa B ligand (RANKL) by T cells, B cells and fibroblastic stromal cells which drives the recruitment, differentiation and activation of bone-resorbing osteoclasts (Quinn et al. 2000). Bone loss is mediated by several intracellular signalling pathways including, nuclear factor-kappa B (NF-κB) signalling. The kallikrein–kinin system can also mediate bone loss in RA, as it involves the upregulation of bradykinin to enhance the production of pro-inflammatory cytokines which stimulate bone resorption (Lerner 1994; Xie et al. 2014). The upregulation of TNF-α, IL-1 and PGE$_2$ in RA results in excessive binding of RANKL to its receptor RANK, which activates the NF-κB pathway (Boyle et al. 2003). A TNF-transgenic RANKL knockout (KO) mouse model has demonstrated that osteoclast differentiation is dependent on RANKL-induced NF-κB activity in osteoclast precursors (Pettit et al. 2001). NF-κB, a pro-inflammatory transcription factor, is also crucial to T cell-mediated inflammation in RA (Schett 2007). Therefore, suppression of NF-κB could potentially downregulate pro-inflammatory cytokines, thus reducing inflammation, osteoclast recruitment, differentiation and activation; and provides a basis for therapeutic intervention in inflammatory arthritis.

A variety of treatments are available for RA; however, disease management relies primarily on disease-modifying anti-rheumatic drugs (DMARDs), such as methotrexate (Parida et al. 2015). Advances in the understanding of the pathogenesis of RA has allowed for the development of biologic DMARDs, including anti-TNF agents; infliximab and adalimumab (Gaffo et al. 2006). Despite having significant benefits in reducing disease activity, biologic DMARDs can have variable effects on bone erosion and can lead to adverse side effects when taken for extended periods of time (Gaffo et al. 2006). Significant time is also

required to establish the correct therapy for individual patients, leading to continued bone erosion (Gaffo et al. 2006). There are currently few effective therapies specifically targeting both inflammation and bone erosion in RA; thus, treatments administered immediately that directly target early bone erosion would be beneficial.

Caffeic acid phenethyl ester (CAPE) is a natural bioactive compound acquired from the propolis of honeybee hives and has both immunomodulatory (Castaldo and Capasso 2002) and anti-inflammatory properties (Michaluart et al. 1999; Borrelli et al. 2002; Marquez et al. 2004) in vivo. Low-dose CAPE (1 mg/kg) has been shown to inhibit polyethylene (PE) particle-induced osteolysis in an in vivo model of peri-prosthetic loosening (Zawawi et al. 2015). In addition, CAPE (0.5 mg/kg) inhibited local bone loss in an ovariectomized murine model of osteolysis (unpublished results from J Xu). In vitro studies have demonstrated that CAPE can suppress NF-κB expression and cell activity in osteoclasts and T cells (Marquez et al. 2004). Despite these findings, the effect of CAPE on bone volume locally and bone resorption systemically within inflammatory arthritis remains unknown. In addition, the effects of inflammatory arthritis in the presence and absence of CAPE on the histopathology of the gastrointestinal tract have not been investigated. The current study aimed to investigate whether CAPE would reduce bone loss and inflammation in a mouse model of inflammatory arthritis. Also, we aimed to assess systemic effects of inflammatory arthritis and CAPE treatment on the gastrointestinal tract by histopathological analysis.

Materials and methods

This study was approved by the Animal Ethics Committee of the University of Adelaide (M-2014-175) and complied with National Health and Research Council (Australia) Code of Practice for Animal Care in Research and Training (2014). Mice were housed in approved conditions on a 12-h light/dark cycle. Food and water were provided ad libitum.

Animals

A total of 32 Balb/c mice aged 6–8 weeks were obtained from the University of Adelaide Laboratory Animal Services and randomly divided into four groups ($n = 8$ animals/group): control (group 1; no arthritis and no treatment), CAPE only (group 2; no arthritis, treated with 1 mg/kg CAPE), CAIA only (group 3; arthritis and no treatment) and CAIA + CAPE (group 4; arthritis treated with 1 mg/kg CAPE).

Collagen antibody-induced arthritis

To induce arthritis, mice were injected intravenously via the tail vein with 150 μL of a cocktail of anti-type II collagen monoclonal antibodies (Arthrogen-CIAs Arthritogenic Monoclonal Antibodies, Chondrex Inc., Redwood, WA, USA). This was followed by an intraperitoneal injection of 20 μL (10 μg) of *E. coli* lipopolysaccharide (LPS) on day 3 (Dharmapatni et al. 2015). Control animals were injected with phosphate-buffered saline (PBS) alone at both time points. Based on the suppression of bone loss by CAPE in a murine PE particle-induced osteolysis model (Zawawi et al. 2015), 200μL of CAPE (Sigma, St. Louis, MO) at 1mg/kg in 0.4% dimethyl sulfoxide (DMSO) was administered subcutaneously in groups 2 and 4 on days 3, 7 and 10. Control groups were subcutaneously injected with 200 μL of PBS in 0.4% DMSO at the same time points.

Mice were monitored daily using an approved clinical record sheet for arthritic studies to assess body weight and factors of general health such as a dull or ruffled coat (Cantley et al. 2011). To assess clinical paw swelling, individual paws were examined daily for redness, tenderness, swelling and inflammation, using a method previously described (Nandakumar et al. 2003). For each paw, a score of 1 was given for an inflamed digit and a score from 0 to 5 was allocated for swelling of the carpal/tarsal and swelling of the wrist/ankle. The maximum score for each paw was 15, giving a possible total of 60 per mouse (Nandakumar et al. 2003).

Live-animal micro-computed tomography

Bone changes and paw swelling of the front paws were assessed using images obtained by a live-animal micro-computed tomography (micro-CT) scanner (SkyScan model 1076, Bruker, Kontich, Belgium). Mice were scanned at a source voltage of 74 kVp, current 136 μA, isotropic pixel size of 9 μm, with a 1-mm-thick aluminium filter, rotation step of 0.8 degrees, frame averaging of 1 and a total scan time of approximately 27 min, as previously published (Zawawi et al. 2015). Scanning was conducted 3 days prior to arthritis induction to obtain baseline measurements and on day 14 at the completion of the study. Prior to scanning, mice were weighed to determine the dose of anaesthetic (0.1 mL per 10 g mouse) and then anaesthetised via intraperitoneal injection (mouse anaesthetic; 1 mL xylazine (20 mg/mL), 2 mL ketamine (100 mg/mL), 17 mL of water). Mice were positioned on the scanner bed with their front paws located within the scanning area. The micro-CT cross-section images were then reconstructed using a filtered back-projection algorithm (N-Recon software, Bruker micro-CT, Kontich,

Belgium) and saved as 8-bit grey-level files (bitmap format). The reconstructed cross-section images of the front paws were realigned in 3D with the long axis of the paw aligned along the inferior–superior direction of the images (software DataViewer, SkyScan), as done previously (Perilli et al. 2015). Then, for each paw, a standardized cylindrical volume of interest of 4.5 mm diameter and of 2.42 mm length, starting from 200 cross-sections distal and extending to 80 cross-sections proximal to the lower epiphyseal growth plate of the radiocarpal joint (280 consecutive cross-sections in total) was used for analysis. For each volume of interest, the bone volume (BV, in mm^3) and the paw volume (PV, mm^3, which includes the soft tissue) were quantified in 3D, using uniform thresholding (CTAn software, Bruker micro-CT, Kontich, Belgium), as previously published (Perilli et al. 2015). Three paws, one from each of three control mice were excluded from the analysis, due to excessive movement throughout the second micro-CT scan and consequent image artefacts not suitable for quantification.

Histological analysis

At the completion of the study, while mice were still under anaesthetic, blood was collected via cardiac puncture, and then, they were humanely killed via cervical dislocation. All paws and heads were collected, skinned and fixed in 10% PBS-buffered formalin for 24 h. Decalcification of the paws was carried out for approximately 12 weeks using 10% EDTA solution. The paws were processed for paraffin embedding and serial sagittal sections were cut (5 μm) for histological analysis. Routine haematoxylin and eosin (H&E) staining was conducted on all paws. Histological sections were imaged with the NanoZoomer™ (Hamamatsu Photonics K.K., Hamamatsu City, Shizuoka Pref., Japan) at 40× magnification. Semi-quantitative analysis was carried out by two blinded observers, using a previously described scoring method (Tak et al. 1997). Scoring was based on the number of inflammatory cells within the wrist/ankle; normal tissue (<5% inflammatory cells) was scored as 0, mild inflammation (6–20% inflammatory cells) was scored as 1, moderate inflammation (21–50% inflammatory cells) was scored as 2 and severe inflammation (>51% inflammatory cells) was scored as 3. Bone and cartilage destruction was assessed on a scale of 0–3 (0, normal; 1, mild cartilage destruction; 2, evidence of both cartilage and bone destruction; 3, severe cartilage and bone destruction). Pannus formation was scored as either 0, no pannus or 1, pannus formation (Tak et al. 1997).

Tartrate-resistant acid phosphatase (TRAP) staining of all paws was conducted to detect osteoclasts on the bone surface and pre-osteoclasts in the surrounding soft tissue (Gravallese et al. 1998). Slides were stained as previously

described with TRAP and left to incubate (37 °C) for 15 min and then counterstained with haematoxylin (Burstone 1958; Gravallese et al. 1998). The number of TRAP-positive cells with three or more nuclei were counted by two blinded observers in a consistent region of interest (2.16 mm^2), to include cells found on the bone surface (Cantley et al. 2015) and within the surrounding soft tissue of the radiocarpal joint.

Histopathological analysis of the gastrointestinal tract

The entire gastrointestinal tract from pyloric sphincter to rectum was dissected and flushed with chilled 1 × PBS (pH 7.4) to remove intestinal contents. Samples (1 cm in length) of the jejunum and colon were fixed in 10% formalin in neutral-buffered saline and embedded into paraffin wax. Tissues were sectioned at 4 μm and mounted onto glass superfrost® microscope slides (Menzel-Gläser, Braunschwerg, Germany). Sections were stained with H&E and Alcian Blue Periodic Acid Schiff's (AB-PAS) as previously described (Yeoh et al. 2005). All slides were scanned using NanoZoomer™ (Hamamatsu Photonics K.K., Hamamatsu City, Shizuoka Pref., Japan) at 40× magnification. Sections were analysed with NanoZoomer™ Digital Pathology view software (Histalim, Montpellier, France).

Tissue sections were assessed by two blind observers using a validated scoring system for the following parameters in the small intestine: disruption of the brush border, crypt loss, disruption of crypt cells, infiltration of neutrophils and lymphocytes, dilatation of lymphatics and capillaries, oedema, and villous blunting and fusion, with a total score of 0–8 (Howarth et al. 1996). The same parameters were also assessed in the colon with the exception of villous blunting and villous fusion with a total score of 0–6 recorded (Howarth et al. 1996). AB–PAS-stained sections were assessed for the number of goblet cells and cavitated goblet cells in 15 well-oriented villi and crypts in the jejunal sections, and 15 well-oriented crypts in the colon sections, as previously described (Barcelo et al. 2000; Stringer et al. 2009a, b). Counts were averaged to give the average number of goblet cells per villi and crypt, and the percentage of cavitated goblet cells was calculated as an indication of mucin secretion.

Enzyme-linked immunosorbent assay (ELISA)

Blood samples were collected from mice under anaesthetic via cardiac puncture prior to cervical dislocation and serum was prepared and stored at −20 °C. Serum C-reactive protein (CRP) levels as a measure of systemic inflammation were assessed using a commercially available mouse CRP ELISA kit (Life Diagnostics, Inc. West Chester, PA,

USA). Samples were diluted 1 in 200 and manufacturer's instructions were followed. Serum C-terminal telopeptide (CTX-1) levels as a measure of systemic bone resorption were also assessed using RatLaps CTX-1 ELISA kit (Immunodiagnostics Systems, Nordic), following the manufacturer's instructions.

Statistics

Statistical analysis was conducted using GraphPad Prism 6. Differences in measured values between the four groups were analysed using the Kruskal–Wallis test, followed by a Mann–Whitney U test for two group comparisons. Comparisons in PV and BV between time points were made using Wilcoxon's signed rank test. For analysis of the GIT goblet cell counts and cavitated goblet cell percentages, a one-way ANOVA was used for multivariate comparisons after normality was confirmed using D'Agostino and Pearson's omnibus normality test. All values shown are mean ± standard error of the mean (SEM), with a p value <0.05 considered statistically significant.

Results

Clinical evaluation of local inflammation

Induction of CAIA resulted in significant redness and inflammation in the paws and was first evident from day 5 following LPS injection (Fig. 1) in both CAIA and CAIA + CAPE mice. The CAIA + CAPE group did not show reduction in arthritis as confirmed by significantly greater paw scores in mice of this group compared to the CAIA group on day 5 ($p < 0.01$). Paw scores did not differ between CAIA and CAIA + CAPE mice from day 9 to day 14, but they were significantly higher compared to the control groups ($p < 0.05$). By day 14, local inflammation had reduced in both CAIA and CAIA + CAPE mice, with no significant difference between the two groups. The macroscopic images of the front paws shown in Fig. 1b are representative of mice at day 10, when disease has been reported to be at a maximum (Khachigian 2006). Severe swelling and redness were predominantly seen in the front paws, with 30% of rear paws being affected.

Micro-CT analysis of soft tissue swelling

Representative three-dimensional micro-CT images of the paw including soft tissue at the radiocarpal joints are shown in Fig. 2a. The PV values increased significantly from baseline to endpoint in the CAIA and CAPE-treated CAIA groups ($p = 0.0002$ and $p = 0.021$, respectively, Fig. 2b), consistent with soft tissue swelling and clinical
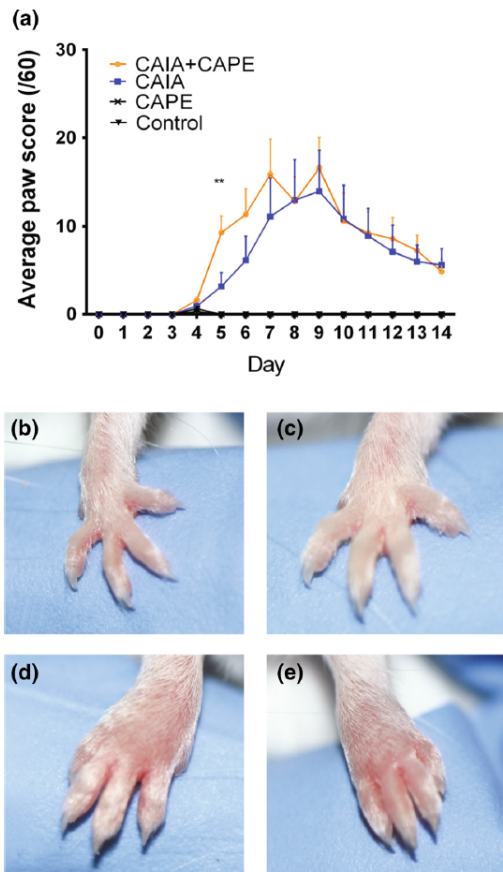
Fig. 1 Clinical evaluation of local inflammation. **a** Average clinical paw scores of each study group over 14 days. *Error bars* represent SEM ($n = 8$ per group; **$p < 0.01$). Macroscopic appearance of the front paws; **b** Control, **c** CAPE, **d** CAIA and **e** CAIA + CAPE. Paws were imaged at day 10 post-arthritis induction

paw scoring. At day 14, PV was significantly higher in both the CAIA (20.81 ± 0.94 mm^3) and CAPE-treated CAIA groups (22.58 ± 1.36 mm^3) compared with control mice (18.39 ± 0.24 mm^3, $p < 0.05$). PV did not differ between the CAIA and CAPE-treated CAIA group ($p = 0.85$). The percentage change in PV over time from baseline to endpoint in CAIA (+18%) and CAPE treated CAIA (+23%) mice was also significantly greater ($p < 0.05$) when compared to the control (1.73%) and the non-diseased CAPE treated mice (1.8%; Fig. 2c).

Micro-CT analysis of bone volume

Live animal micro-CT analysis was used to assess changes in BV over time in the radiocarpal joints. Representative reconstructed three-dimensional images of the radiocarpal joint for each group is shown in Fig. 3a. BV increased significantly over time in the control (+9.1%, $p = 0.039$) and in the non-diseased CAPE treated group (+11.7%, $p = 0.008$; Fig. 3b). The CAIA group showed a non-significant increase in BV over time (+7.4%, $p = 0.1$), whilst BV remained unchanged in the CAPE-treated CAIA group (+0.1%, $p = 0.94$; Fig. 3b). At day 14, the CAPE-treated arthritis group showed lowest BV, with a significant difference compared to the control group ($p = 0.0075$); however, no significant difference was found in BV when compared to the CAPE ($p = 0.0537$) and the CAIA ($p = 0.187$) group. Overall, there was no significant difference in the percentage change in BV over time between groups ($p = 0.255$; Fig. 3c).

Histological evaluation of local inflammation and bone loss

Representative H&E-stained images of the front paws from each group are shown (Fig. 4a). Histological evaluation of all four paws of all mice showed that arthritis and CAPE-treated arthritis mice had greater scores for cellular infiltration, cartilage and bone degradation and pannus formation compared to control mice (Fig. 4c). However, this was not statistically significant. TRAP staining was performed on sagittal sections of all paws to identify the number of pre-osteoclast/osteoclast cells within an area (2.16 mm^2) that included the bones of the wrist/ankle and the surrounding soft tissue. Representative images of TRAP staining in the radiocarpal joint are presented in Fig. 4b. Compared to controls, a significantly greater number of multinucleated TRAP-positive cells were observed on the bone surface within the paws of CAIA (2.3 ± 0.83, $p = 0.029$) and CAPE-treated CAIA mice (4.9 ± 2.3, $p = 0.003$; Fig. 4d). Similarly, there was a significantly greater number of multinucleated TRAP-positive cells found in the soft tissue of CAIA (2.7 ± 1.3; $p = 0.005$) and CAPE-treated CAIA mice (7.5 ± 3.3; $p = 0.024$) compared to control groups (0 ± 0; $p > 0.99$). Although the number of multinucleated TRAP-positive cells on the bone surface and in the soft tissue were greater in CAPE-treated CAIA mice compared to CAIA mice, this was not significantly different ($p = 0.865$ and $p = 0.985$, respectively; Fig. 4d, e).

Serum indicators of systemic inflammation (CRP) and bone resorption (CTX-1)

CRP and CTX-1 levels were assessed in serum collected from mice 14 days after arthritis induction as markers of systemic inflammation and bone resorption (Fig. 5). Both CRP and CTX-1 levels did not significantly differ between
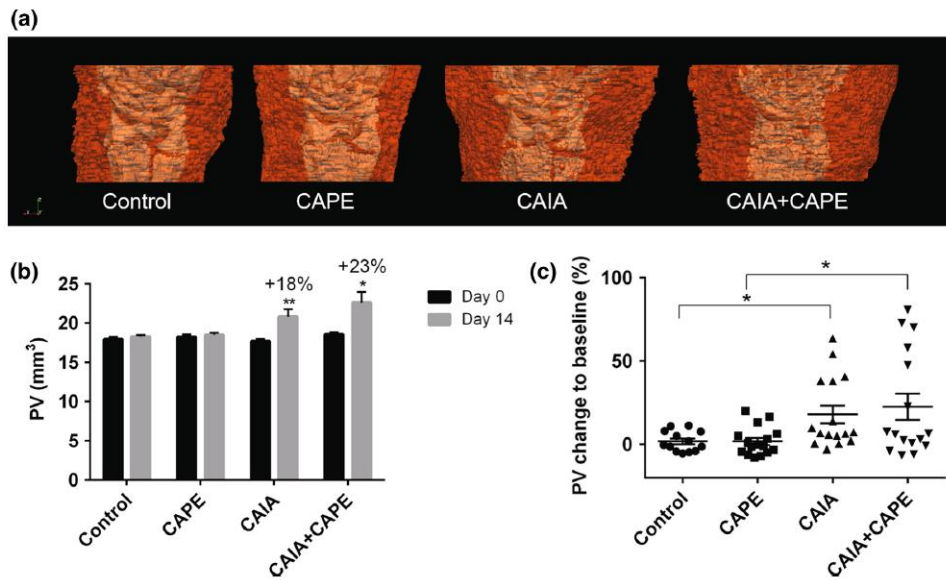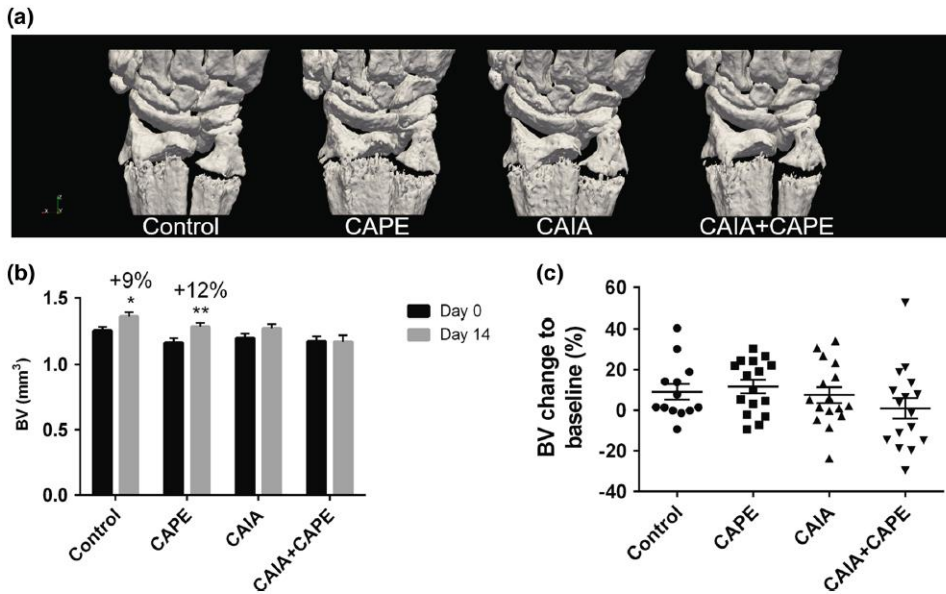
(a)

(b)

(c)

Fig. 2 Effect of CAIA and CAPE treatment on local inflammation assessed by in vivo micro-CT. **a** Three-dimensional micro-CT rendering of the radiocarpal joint in the right paw with bone segmented in white and soft tissue in *red*, at day 14. **b** Mean paw volume (PV) in mm^3 in the radiocarpal joint as assessed by micro-CT analysis at day 0 and day 14. *Error bars* represent SEM (*$p < 0.05$). **c** Percentage change in PV from baseline to endpoint in the radiocarpal joint. Values are presented as mean ± SEM (*$p < 0.05$); $n = 16$ front paws per group

(a)

(b)

(c)

Fig. 3 Effect of CAIA and CAPE treatment on local bone volume assessed by in vivo micro-CT. **a** Three-dimensional micro-CT models of the radiocarpal joint in the right paw at day 14. **b** Mean bone volume (BV, expressed in mm^3), in the radiocarpal joint as assessed by micro-CT analysis at day 0 and day 14. *Error bars* represent SEM ($n = 8$ per group, *$p < 0.05$, **$p < 0.01$). **c** Percentage change in BV of the radiocarpal joint from baseline to endpoint. Values represent mean ± SEM; $n = 16$ front paws per group
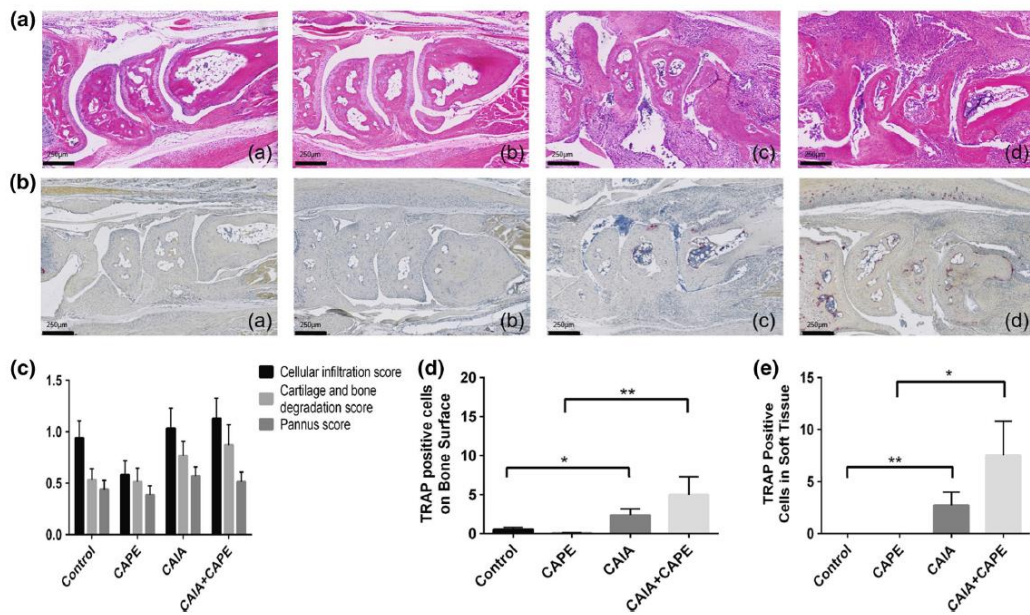
Fig. 4 Effect of CAPE treatment on inflammation and bone loss assessed histologically. **a** Haematoxylin and eosin (H&E)-stained sections of the corresponding radiocarpal joint at ×10 magnification. **b** Tartrate-resistant acid phosphatase-stained (TRAP) images of the corresponding radiocarpal joints at ×10 magnification. **c** Histological score of paw tissues at day 14. *Error bars* represent SEM. **d** Average number of TRAP-positive multinucleated cells on the bone surface in a 2.16-mm^2 area in all paws. Error bars represent SEM ($n = 8$ per group; *$p < 0.05$. **e** Average number of TRAP-positive multinucleated cells in the surrounding soft tissue in a 2.16-mm^2 area in all paws. *Error bars* represent SEM ($n = 8$ per group; *$p < 0.05$, **$p < 0.01$)

Fig. 5 Biochemical analyses of mouse serum in the CAIA model at day 14. **a** Serum CRP concentration (μg/mL) as an indicator of systemic inflammation. **b** Serum CTX-1 (ng/mL) concentration as a measure of systemic bone resorption. Values are presented as mean ± SEM
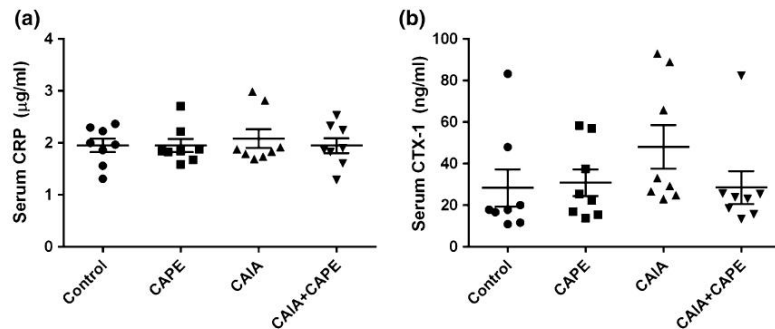
groups at day 14 ($p = 0.94$ and $p = 0.08$, respectively). Average CTX-1 levels were highest in CAIA mice (48.1 ng/mL); however, this was not statistically significant.

Gastrointestinal changes in response to CAIA and CAPE treatment

Neither CAPE treatment nor CAIA affected the jejunum compared to control mice as assessed by the toxicity score (Fig. 6). The goblet cell count per villi and the percentage of cavitated goblet cells per villi did not differ between any of the groups. However, CAPE treatment on CAIA mice significantly reduced the percentage of cavitated goblet cells in the jejunum compared with the control mice ($p = 0.0433$; Fig. 7).

In the colon, both CAPE treatment ($p = 0.0431$) and CAIA ($p = 0.0226$) significantly increased the toxicity score compared to control mice (Fig. 6b). The
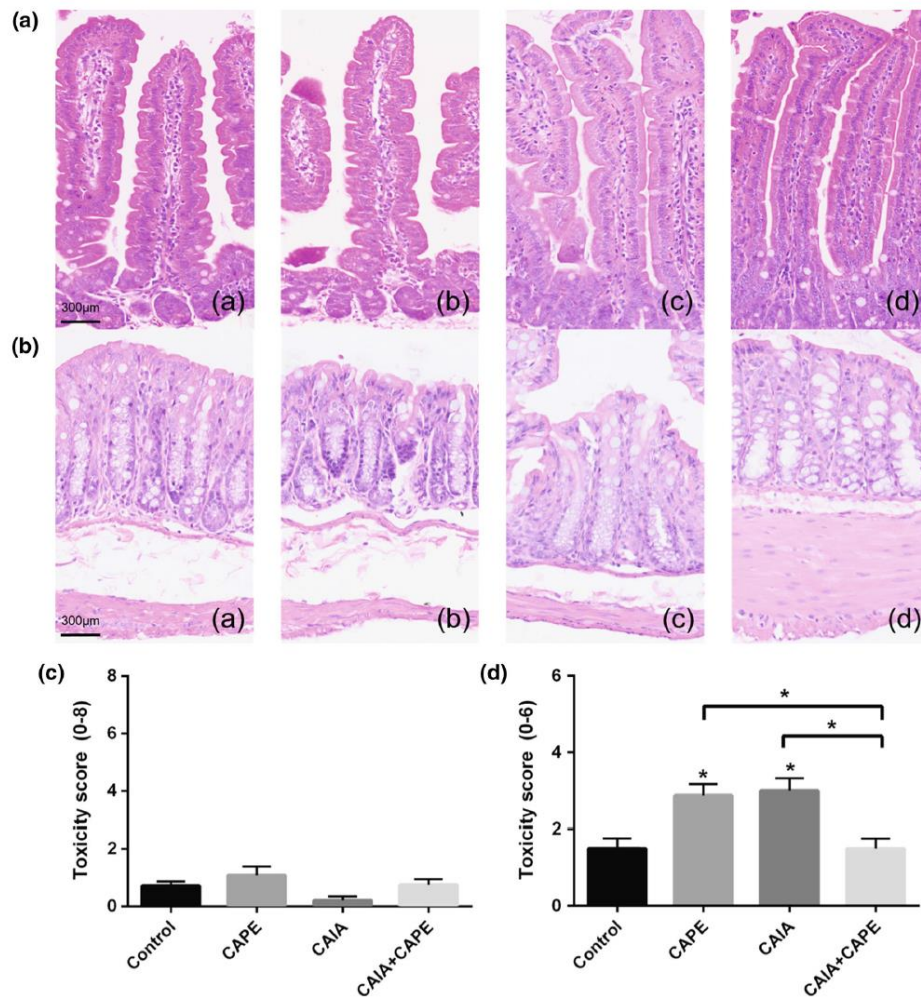
Fig. 6 Toxicity scoring of jejunum and colon. **a** Haematoxylin-and-eosin-stained jejunum; **a** Control, **b** CAPE, **c** CAIA and **d** CAIA + CAPE. ×30 magnification. **b** Haematoxylin-and-eosin-stained colon; **a** Control, **b** CAPE, **c** CAIA and **d** CAIA + CAPE. ×30 original magnification. **c** Jejunum toxicity score. **d** Colon toxicity score. *Error bars* represent SEM ($n = 8$ per group; *$p < 0.05$)

CAIA + CAPE group showed a reduced toxicity score to normal levels compared to CAPE alone ($p = 0.049$) or CAIA alone ($p = 0.026$). There was no difference in the goblet cell count between groups. The cavitated goblet cells in the crypts were significantly increased in the CAPE-treated mice compared to non-diseased mice ($p = 0.002$; Fig. 8). There was no difference between CAIA and control mice. As per the toxicity score in the colon, the combination of CAIA and CAPE treatment reduced the percentage of cavitated goblet cells in the crypt compared with CAPE alone ($p < 0.0001$) or CAIA alone ($p = 0.003$; Fig. 8).

Discussion

This study utilised the commercially available and well-established CAIA mouse model, which focuses on the effector phase of the disease. The CAIA mouse model offers several benefits over other inflammatory arthritis models, such as the collagen-induced arthritis (CIA) model. Systemic administration of monoclonal antibodies targeting type-II collagen in mice, rapidly initiates pathogenic features similar to those found in human RA within only a few days rather than several weeks required for
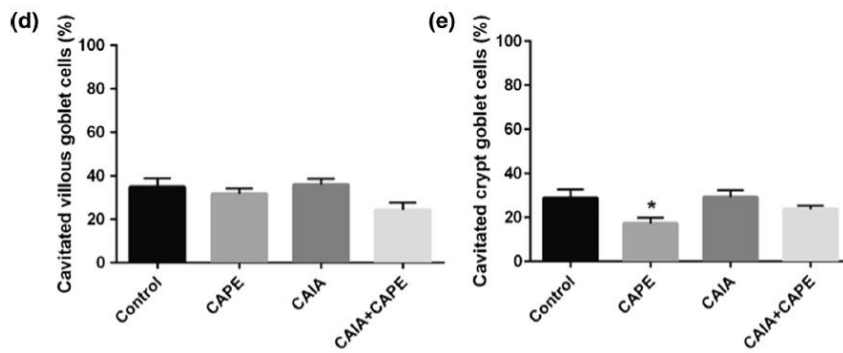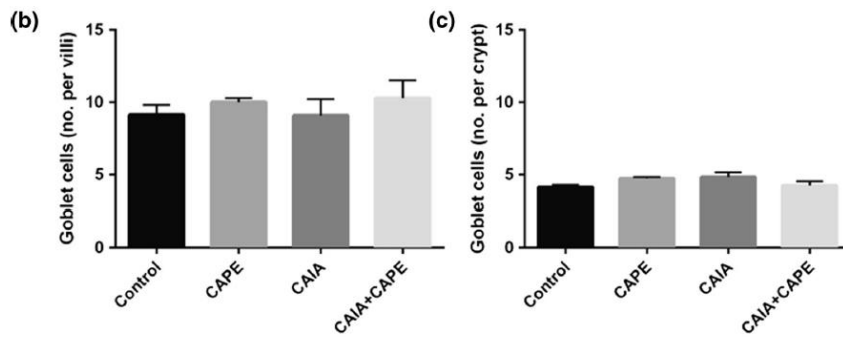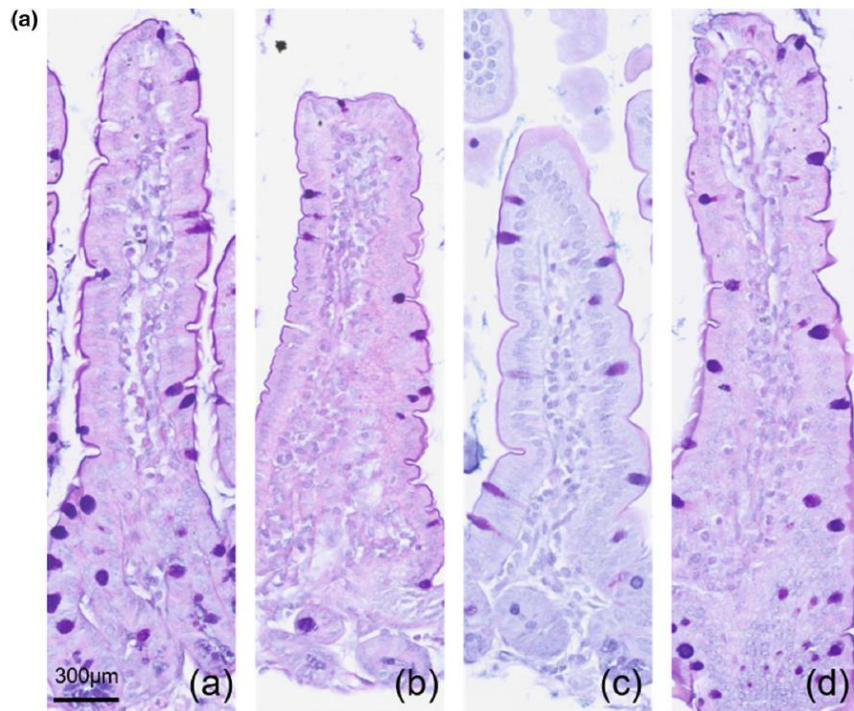
◄**Fig. 7** Jejunal goblet cell counts and percentage of cavitated goblet cells. **a** AB–PAS-stained jejunal villi and crypts; **a** Control, **b** CAPE, **c** CAIA and **d** CAIA + CAPE. ×30 magnification. **b** Average number of goblet cells per villi. *Error bars* represent SEM ($n = 8$ per group). **c** Average number of goblet cells per crypt. *Error bars* represent SEM ($n = 8$ per group). **d** Percentage of cavitated goblet cells per villi. Error bars represent SEM ($n = 8$ per group). **e** Percentage of cavitated goblet cells per crypt. *Error bars* represent SEM ($n = 8$ per group; *$p < 0.05$ compared to control)

arthritis induction in the CIA model (Hutamekalin et al. 2009). A more mild form of the disease was induced with 150 µL of collagen antibodies combined with 10 µg of LPS based on studies within our laboratory (Dharmapatni et al. 2015; Perilli et al. 2015), compared with the original study that induces a severe form of the disease with 200–400 µL of collagen antibodies combined with 50 µg of LPS (Khachigian 2006). The CAIA mouse model has a high uptake rate; thus, paw inflammation was present as

evidenced by significantly greater paw scores than non-diseased controls, which is consistent with previous findings (Dharmapatni et al. 2015). Previous analysis of the CAIA model was extended by analysis of the effect of CAPE on local and systemic inflammation and bone loss in addition to analysis of the gastrointestinal tract in response to disease and treatment with CAPE.

The current study found that CAPE administered at 1 mg/kg did not suppress local inflammation in the CAIA mice, as evidenced by the paw scores over time and PV in the radiocarpal joint at day 14. Although not significant, PV was higher in the CAPE-treated CAIA mice at day 14, compared to untreated mice with CAIA. This was an unexpected finding as in vivo studies report the downregulation of inflammation by CAPE (Orban et al. 2000; Ilhan et al. 2004). Locally administered CAPE at 40 mg/kg has also been shown to induce apoptotic cell death in leukocytes and have anti-inflammatory effects in a rat model of
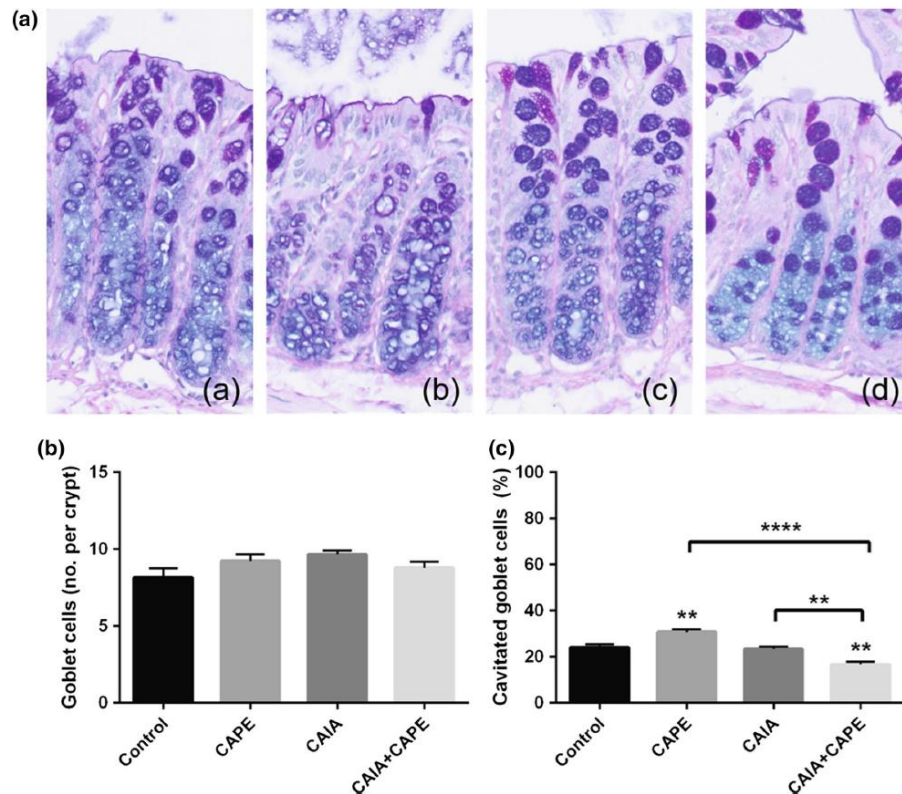

Fig. 8 Colon goblet cell counts and percentage of cavitated goblet cells. **a** AB–PAS-stained colon villi and crypts; **a** Control, **b** CAPE, **c** CAIA and **d** CAIA + CAPE. ×30 magnification. **b** Average number of goblet cells per crypt. *Error bars* represent SEM ($n = 8$ per group). **c** Percentage of cavitated goblet cells per crypt. *Error bars* represent SEM ($n = 8$ per group; **$p < 0.01$, ****$p < 0.0001$)

Ⓐ Springer

carrageenan-induced subcutaneous inflammation (Orban et al. 2000). Anti-inflammatory effects have been reported as induced by intraperitoneal injection of CAPE at 10–100 mg/mL in a rat air pouch model (Michaluart et al. 1999). Of note, when CAPE at 40 mg/kg was administered intravenously, there was no change in apoptosis or inflammatory exudate (Orban et al. 2000). The current study administered 1 mg/kg of CAPE subcutaneously based on the effectiveness of CAPE on bone loss suppression at 1 mg/kg (Zawawi et al. 2015) and the toxicity concerns at higher doses (Fitzpatrick et al. 2001). The increased paw scores and PV at endpoint in the CAPE-treated CAIA mice in this study could be attributed to the rapid systemic clearance of the drug or its penetration to the site of inflammation (Wang et al. 2009).

CAPE has previously been shown to act as a potent and specific inhibitor of NF-κB by preventing its interaction with DNA (Natarajan et al. 1996, Marquez et al. 2004). In vitro studies have demonstrated that the inhibition of NF-κB by CAPE in T cells reduces T cell proliferation and activation (Marquez et al. 2004). In the current study, activation of the NF-κB pathway was not directly measured in paw tissue nor gastrointestinal tract. It was, therefore, not confirmed in this model as to whether CAPE reached these areas to actively suppress NF-κB at 1 mg/kg when delivered subcutaneously. Future in vivo studies could assess induction of MCP-1, the phosphorylation of proteins and upregulation of pro-inflammatory cytokines involved in the NF-κB pathway, including TNF-α, IL-1 and PGE$_2$ to identify if CAPE actively suppresses NF-κB in inflammatory arthritis.

The current study investigated the effect of arthritis on bone by quantifying BV in the radiocarpal joint at baseline and endpoint using in vivo micro-CT. At day 14, CAIA mice did not show significantly lower BV compared to non-diseased mice, whereas we previously reported a significant reduction in BV in the CAIA model assessed at day 10 (Dharmapatni et al. 2015) and an 18% increase in non-diseased mice at day 10 (Cantley et al. 2011). In addition, the present study did not reveal statistically significant BV changes in the CAIA group over time compared to its own baseline. Of note, micro-CT scanning to determine BV was conducted at an earlier stage (10 days) post collagen-antibody injection in our previous studies, rather than at day 14 in the present study. This distinction is supported by the evidence of arthritis symptoms in the CAIA model declining from day 10 onwards (Khachigian 2006). In addition, the micro-CT scans for the current model were conducted at 9 μm/pixel (higher resolution) compared to 18 μm/pixel in previous studies (Cantley et al. 2011, Dharmapatni et al. 2015). The BV values measured in the current study at day 14 could, therefore, be a result of bone growth and repair in response to inflammatory joint

destruction, occurring after day 10 within the CAIA model. Although not significant, the smaller increase of BV over time observed in the CAPE-treated CAIA mice compared to untreated CAIA and controls suggests that treatment did not suppress bone loss.

Histological analysis of local inflammation and bone and cartilage destruction was carried out on all paws. A greater number of multinucleated TRAP-positive osteoclast-like cells were observed in the radiocarpal joints and surrounding soft tissue of CAPE-treated CAIA mice when compared to CAIA mice; however, this was not significant. These findings reflect local bone resorption in the paws and support the results obtained through micro-CT analysis, suggesting that CAPE did not suppress local bone loss in inflammatory arthritis. This is in contrast to a previous study which found CAPE at 1 mg/kg to suppress bone loss in a particle-induced calvarial model of osteolysis (Zawawi et al. 2015). This was evident in that study, as greater BV and a reduced number of multinucleated TRAP-positive cells were observed in the calvariae of CAPE-treated diseased mice when compared to non-diseased mice (Zawawi et al. 2015). Similar to the higher levels of local inflammation found in the current study, the reduced BV observed could be attributed to disease severity, the subcutaneous route of drug administration and the potential that CAPE did not reach the paws. CAPE at 10 vM/kg/day has been found to stimulate PGE$_2$ synthesis in a bleomycin-induced pulmonary fibrosis rat model (Larki-Harchegani et al. 2013). As PGE$_2$ is known to mediate osteoclastogenesis through RANKL stimulation and activation of the NF-κB pathway (Saegusa et al. 2003), the possibility that CAPE increases PGE$_2$ may explain the increase in TRAP-positive osteoclast-like cells in the CAPE-treated CAIA mice. However, as pro-inflammatory cytokines that stimulate the NF-κB pathway were not directly measured, it is not known if PGE$_2$ is upregulated and future studies will need to address this. There is currently limited information about the pharmacokinetics of CAPE; thus, further investigation is required to establish the most appropriate mode of administration of CAPE for paw inflammation. The effects of CAPE on osteoblasts and osteocytes, however, are not known nor are the effects on apoptosis within the joint. Therefore, future in vitro and in vivo studies are required to establish the effect CAPE has on apoptosis of bone cells in a physiological and inflammatory environment.

RA is an autoimmune disease that not only affects the synovial joints as ongoing recurrent inflammation may result in extra-articular tissues and organs being affected (Lefevre et al. 2009). Systemic features in RA are often a reflection of longstanding inflammation (Cojocaru et al. 2010). Serum CRP levels and gastrointestinal changes were

assessed as an indication of the systemic effect of disease induction and treatment with CAPE on inflammation. CRP is a marker of inflammation in both humans and mice and its levels in blood increases when inflammation is present (Black et al. 2004). The current study found no change in serum CRP levels between groups at day 14 and could be attributed to the notion that CRP is only synthesised in trace amounts in mice or low levels of disease activity at this point (Szalai and McCrory 2002). Future studies that investigate serum levels of pro-inflammatory cytokines upregulated by RA may be beneficial to elucidate the systemic effect of disease and treatment in the CAIA model. Furthermore, in the CAIA model, arthritis symptoms have been shown to peak at day 10 with both a 10-µg (Cantley et al. 2011) and 50-µg (Khachigian 2006) LPS boost with the severity of arthritis declining in the following days. Analysis of CRP levels at 10 days has been found to be significantly greater in untreated arthritis mice when compared to non-diseased mice (Cantley et al. 2011), whereas in the current study, CRP levels may have declined by day 14 consistent with a reduction in paw scores.

CTX-1 is a marker of systemic bone resorption as serum levels of CTX-1 are proportional to osteoclastic activity at the time that blood is collected (Rosen et al. 2000). In the current study, CTX-1 levels were found to be higher in the CAIA group compared to non-diseased mice at day 14. Although this was not statistically significant, it suggests that bone resorption was induced. Similar to systemic inflammation, future studies which end the CAIA model at day 10 may be beneficial to identify a change in systemic bone resorption as a result of disease induction and CAPE treatment.

RA is a systemic disorder with extra-articular manifestations occurring within organs including the gastrointestinal tract, leading to additional patient morbidity (Lefevre et al. 2009). Previous reports have documented that nearly 80% of RA patients also report gastrointestinal complications including but not limited to constipation and diarrhoea (Katayama et al. 2011). The gastrointestinal tract is lined by cells that form a barrier between the host organism and the external environment (Gonzalez-Mariscal et al. 2008). Within this barrier are goblet cells that secrete intestinal mucins essentially forming a hydrating gel over the tissue providing a protective barrier from both mechanical and chemical stress (Specian and Oliver 1991; Robbe et al. 2004; Stringer et al. 2007). Although the present study demonstrated no significant changes in histopathology in the jejunum, CAPE treatment did significantly reduce the number of cavitated goblet cells. Previous research has shown that goblet cells and mucous may, in fact, be regulated by interactions with the commensal bacterial (Leiper et al. 2001; Stringer et al.

2009a, b). This offers a new path of investigation for this research.

In contrast to the jejunum, the present study demonstrated that CAPE treatment and disease significantly increased the toxicity score in the colon. In line with this increased toxicity, the combination of CAIA and CAPE treatment reduced the percentage of cavitated goblet cells in the crypt. This suggests that there may be a decrease in the protective mucous layer allowing potential pathogens to damage the tissue. This study was an acute study only lasting 14 days from the onset of RA. Although no clinical signs of gastrointestinal damage including diarrhoea or constipation were seen in our study, it maybe that these develop over time and specific changes occurring in the gastrointestinal tract over a longer duration of disease are worth future analysis.

In conclusion, this study aimed to investigate whether low-dose CAPE would suppress local and systemic inflammation and bone resorption in a murine model of inflammatory arthritis. Results showed that CAPE treatment did not reduce paw inflammation or bone loss in arthritis mice. Furthermore, there is a potential that in the presence of inflammation, CAPE may increase bone resorption through the upregulation of osteoclasts in the radiocarpal joint. Future studies will need to address the mechanism of CAPE in a physiological environment as well as its effect on apoptosis and bone cells in the presence of inflammation. As RA is a systemic disorder, greater analyses of the systemic effects of the disease and CAPE on other organs, such as the gastrointestinal tract are required.

Compliance with ethical standards

Practice for Animal Care in Research and Training (2014). All applicable international, national and/or institutional guidelines for the care and use of animals were followed.

References

Barcelo A, Claustre J, Moro F, Chayvialle JA, Cuber JC, Plaisancie P (2000) Mucin secretion is modulated by luminal factors in the isolated vascularly perfused rat colon. Gut 46:218–224

Black S, Kushner I, Samols D (2004) C-reactive Protein. J Biol Chem 279:48487–48490

Borrelli F, Maffia P, Pinto L, Ianaro A, Russo A, Capasso F, Ialenti A (2002) Phytochemical compounds involved in the anti-inflammatory effect of propolis extract. Fitoterapia 73(Suppl 1):S53–S63

Boyle WJ, Simonet WS, Lacey DL (2003) Osteoclast differentiation and activation. Nature 423:337–342

Burstone MS (1958) Histochemical demonstration of acid phosphatases with naphthol AS-phosphates. J Natl Cancer Inst 21:523–539

Cantley MD, Haynes DR, Marino V, Bartold PM (2011) Pre-existing periodontitis exacerbates experimental arthritis in a mouse model. J Clin Periodontol 38:532–541

Cantley MD, Fairlie DP, Bartold PM, Marino V, Gupta PK, Haynes DR (2015) Inhibiting histone deacetylase 1 suppresses both inflammation and bone loss in arthritis. Rheumatology (Oxford) 54:1713–1723

Castaldo S, Capasso F (2002) Propolis, an old remedy used in modern medicine. Fitoterapia 73(Suppl 1):S1–S6

Cojocaru M, Cojocaru IM, Silosi I, Vrabie CD, Tanasescu R (2010) Extra-articular manifestations in rheumatoid arthritis. Maedica (Buchar) 5:286–291

Dharmapatni AA, Cantley MD, Marino V, Perilli E, Crotti TN, Smith MD, Haynes DR (2015) The X-linked inhibitor of apoptosis protein inhibitor embelin suppresses inflammation and bone erosion in collagen antibody induced arthritis mice. Mediators Inflamm 2015:564042

Fitzpatrick LR, Wang J, Le T (2001) Caffeic acid phenethyl ester, an inhibitor of nuclear factor-kappaB, attenuates bacterial peptidoglycan polysaccharide-induced colitis in rats. J Pharmacol Exp Ther 299:915–920

Gaffo A, Saag KG, Curtis JR (2006) Treatment of rheumatoid arthritis. Am J Health Syst Pharm 63:2451–2465

Gonzalez-Mariscal L, Tapia R, Chamorro D (2008) Crosstalk of tight junction components with signaling pathways. Biochim Biophys Acta 1778:729–756

Gravallese EM, Harada Y, Wang JT, Gorn AH, Thornhill TS, Goldring SR (1998) Identification of cell types responsible for bone resorption in rheumatoid arthritis and juvenile rheumatoid arthritis. Am J Pathol 152:943–951

Haynes DR, Barg E, Crotti TN, Holding C, Weedon H, Atkins GJ, Zannetino A, Ahern MJ, Coleman M, Roberts-Thomson PJ, Kraan M, Tak PP, Smith MD (2003) Osteoprotegerin expression in synovial tissue from patients with rheumatoid arthritis, spondyloarthropathies and osteoarthritis and normal controls. Rheumatology (Oxford) 42:123–134

Howarth GS, Francis GL, Cool JC, Xu X, Byard RW, Read LC (1996) Milk growth factors enriched from cheese whey ameliorate intestinal damage by methotrexate when administered orally to rats. J Nutr 126:2519–2530

Hutamekalin P, Saito T, Yamaki K, Mizutani N, Brand DD, Waritani T, Terato K, Yoshino S (2009) Collagen antibody-induced arthritis in mice: development of a new arthritogenic 5-clone cocktail of monoclonal anti-type II collagen antibodies. J Immunol Methods 343:49–55

Ilhan A, Akyol O, Gurel A, Armutcu F, Iraz M, Oztas E (2004) Protective effects of caffeic acid phenethyl ester against experimental allergic encephalomyelitis-induced oxidative stress in rats. Free Radic Biol Med 37:386–394

Katayama K, Matsuno T, Waritani T, Terato K, Shionoya H (2011) Supplemental treatment of rheumatoid arthritis with natural milk antibodies against enteromicrobes and their toxins: results of an open-labelled pilot study. Nutr J 10:2

Khachigian LM (2006) Collagen antibody-induced arthritis. Nat Protoc 1:2512–2516

Larki-Harchegani A, Hemmati AA, Arzi A, Ghafurian-Boroojerdnia M, Shabib S, Zadkarami MR, Esmaeilzadeh S (2013) Evaluation of the effects of caffeic acid phenethyl ester on prostaglandin E2 and two key cytokines involved in bleomycin-induced pulmonary fibrosis. Iran J Basic Med Sci 16:850–857

Lefevre S, Knedla A, Tennie C, Kampmann A, Wunrau C, Dinser R, Korb A, Schnaker EM, Tarner IH, Robbins PD, Evans CH, Sturz H, Steinmeyer J, Gay S, Scholmerich J, Pap T, Muller-Ladner U, Neumann E (2009) Synovial fibroblasts spread rheumatoid arthritis to unaffected joints. Nat Med 15:1414–1420

Leiper K, Campbell BJ, Jenkinson MD, Milton J, Yu LG, Democratis J, Rhodes JM (2001) Interaction between bacterial peptides, neutrophils and goblet cells: a possible mechanism for neutrophil recruitment and goblet cell depletion in colitis. Clin Sci 101:395–402

Lerner UH (1994) Regulation of bone metabolism by the kallikrein-kinin system, the coagulation cascade, and the acute-phase reactants. Oral Surg Oral Med Oral Pathol 78:481–493

Marquez N, Sancho R, Macho A, Calzado MA, Fiebich BL, Munoz E (2004) Caffeic acid phenethyl ester inhibits T-cell activation by targeting both nuclear factor of activated T-cells and NF-kappaB transcription factors. J Pharmacol Exp Ther 308:993–1001

Michalaurt P, Masferrer JL, Carothers AM, Subbaramaiah K, Zweifel BS, Koboldt C, Mestre JR, Grunberger D, Sacks PG, Tanabe T, Dannenberg AJ (1999) Inhibitory effects of caffeic acid phenethyl ester on the activity and expression of cyclooxygenase-2 in human oral epithelial cells and in a rat model of inflammation. Cancer Res 59:2347–2352

Mikuls TR (2003) Co-morbidity in rheumatoid arthritis. Best Pract Res Clin Rheumatol 17:729–752

Nandakumar KS, Svensson L, Holmdahl R (2003) Collagen type II-specific monoclonal antibody-induced arthritis in mice: description of the disease and the influence of age, sex, and genes. Am J Pathol 163:1827–1837

Natarajan K, Singh S, Burke TR Jr, Grunberger D, Aggarwal BB (1996) Caffeic acid phenethyl ester is a potent and specific inhibitor of activation of nuclear transcription factor NF-kappa B. Proc Natl Acad Sci USA 93:9090–9095

Orban Z, Mitsiades N, Burke TR Jr, Tsokos M, Chrousos GP (2000) Caffeic acid phenethyl ester induces leukocyte apoptosis, modulates nuclear factor-kappa B and suppresses acute inflammation. Neuroimmunomodulation 7:99–105

Parida JR, Misra DP, Wakhlu A, Agarwal V (2015) Is non-biological treatment of rheumatoid arthritis as good as biologics? World J Orthop 6:278–283

Perilli E, Cantley M, Marino V, Crotti TN, Smith MD, Haynes DR, Dharmapatni AA (2015) Quantifying not only bone loss, but also soft tissue swelling, in a murine inflammatory arthritis model

using micro-computed tomography. Scand J Immunol 81:142–150

Pettit AR, Ji H, von Stechow D, Muller R, Goldring SR, Choi Y, Benoist C, Gravallese EM (2001) TRANCE/RANKL knockout mice are protected from bone erosion in a serum transfer model of arthritis. Am J Pathol 159:1689–1699

Quinn JM, Horwood NJ, Elliott J, Gillespie MT, Martin TJ (2000) Fibroblastic stromal cells express receptor activator of NF-kappa B ligand and support osteoclast differentiation. J Bone Miner Res 15:1459–1466

Robbe C, Capon C, Coddeville B, Michalski JC (2004) Structural diversity and specific distribution of O-glycans in normal human mucins along the intestinal tract. Biochem J 384:307–316

Romas E, Gillespie MT, Martin TJ (2002) Involvement of receptor activator of NFkappaB ligand and tumor necrosis factor-alpha in bone destruction in rheumatoid arthritis. Bone 30:340–346

Rosen HN, Moses AC, Garber J, Iloputaife ID, Ross DS, Lee SL, Greenspan SL (2000) Serum CTX: a new marker of bone resorption that shows treatment effect more often than other markers because of low coefficient of variability and large changes with bisphosphonate therapy. Calcif Tissue Int 66:100–103

Saegusa M, Murakami M, Nakatani Y, Yamakawa K, Katagiri M, Matsuda K, Nakamura K, Kudo I, Kawaguchi H (2003) Contribution of membrane-associated prostaglandin E2 synthase to bone resorption. J Cell Physiol 197:348–356

Schett G (2007) Erosive arthritis. Arthritis Res Ther 9(Suppl 1):S2

Specian RD, Oliver MG (1991) Functional biology of intestinal goblet cells. Am J Physiol 260:C183–C193

Stringer AM, Gibson RJ, Bowen JM, Logan RM, Yeoh AS, Keefe DM (2007) Chemotherapy-induced mucositis: the role of gastrointestinal microflora and mucins in the luminal environment. J Support Oncol 5:259–267

Stringer AM, Gibson RJ, Logan RM, Bowen JM, Yeoh AS, Hamilton J, Keefe DM (2009a) Gastrointestinal microflora and mucins

may play a critical role in the development of 5-Fluorouracil-induced gastrointestinal mucositis. Exp Biol Med 234:430–441

Stringer AM, Gibson RJ, Logan RM, Bowen JM, Yeoh AS, Laurence J, Keefe DM (2009b) Irinotecan-induced mucositis is associated with changes in intestinal mucins. Cancer Chemother Pharmacol 64:123–132

Szalai AJ, McCrory MA (2002) Varied biologic functions of C-reactive protein: lessons learned from transgenic mice. Immunol Res 26:279–287

Tak PP, Smeets TJ, Daha MR, Kluin PM, Meijers KA, Brand R, Meinders AE, Breedveld FC (1997) Analysis of the synovial cell infiltrate in early rheumatoid synovial tissue in relation to local disease activity. Arthritis Rheum 40:217–225

Walsh NC, Crotti TN, Goldring SR, Gravallese EM (2005) Rheumatic diseases: the effects of inflammation on bone. Immunol Rev 208:228–251

Wang X, Pang J, Maffucci JA, Pade DS, Newman RA, Kerwin SM, Bowman PD, Stavchansky S (2009) Pharmacokinetics of caffeic acid phenethyl ester and its catechol-ring fluorinated derivative following intravenous administration to rats. Biopharm Drug Dispos 30:221–228

Xie Z, Dai J, Yang A, Wu Y (2014) A role for bradykinin in the development of anti-collagen antibody-induced arthritis. Rheumatology (Oxford) 53:1301–1306

Yeoh AS, Bowen JM, Gibson RJ, Keefe DM (2005) Nuclear factor kappaB (NFkappaB) and cyclooxygenase-2 (Cox-2) expression in the irradiated colorectum is associated with subsequent histopathological changes. Int J Radiat Oncol Biol Phys 63:1295–1303

Zawawi MS, Perilli E, Stansborough RL, Marino V, Cantley MD, Xu J, Dharmapatni AA, Haynes DR, Gibson RJ, Crotti TN (2015) Caffeic acid phenethyl ester abrogates bone resorption in a murine calvarial model of polyethylene particle-induced osteolysis. Calcif Tissue Int 96(6):565–574